Behavior of Intramolecular π-π and Chalcogen-Chalcogen Interactions of the Closed Shell Type, Elucidated with Quantum Theory of Atoms-in-Molecules Dual Functional Analysis

March 2017

Graduate School of Systems Engineering
Wakayama University

Kohei Matsuiwa

閉殻型分子内π-πおよびカルコゲン–カルコゲン相互作用の挙動：

QTAIM 二元関数解析法による解明

平成２９年　３月

和歌山大学大学院システム工学研究科

松岩　浩平

概　要

化学結合や非結合相互作用は、様々な分野において大変重要な役割を果たしている。化学結合は、実験的に結合エネルギーを求めることで、その強さを知ることができる。一方で、非結合相互作用は、非常に弱いものから化学結合程度に強いものまで幅広く存在し、実験的に明らかにできるものは少ない。このような状況下、Bader 氏によって提唱された Atoms-in-Molecules 法 (QTAIM)は、化学結合や相互作用の性質を解明できるものとして大きな期待が寄せられている。

本研究では、理論計算ソフト Gaussian 09 (Gaussian 03)を使用し、様々な相互作用分子の最適化構造を求め、AIM2000 ソフトにより相互作用を解析するファイルを作成し、$H(\boldsymbol{r})$(全電子エネルギー密度)および $V(\boldsymbol{r})$(ポテンシャルエネルギー密度)を得た。種々の相互作用について、$H(\boldsymbol{r})$ vs $H(\boldsymbol{r}) - V(\boldsymbol{r})/2$ をプロットし、さらに摂動構造を加味して解析を行った。解析にはこのプロットを極座標表示にし、θ, θ_p を導出した。この解析法を AIM2 元関数解析法 (QTAIM-DFA)と命名した。この手法によって、同じ水素結合でもはっきりと強さの違いを評価できるようになった。この解析法を用い、様々な相互作用の解析・評価・分類を目指した。

本研究では以下の 3 点に成功した。

1. QTAIM-DFA 解析法で最も重要となる、「摂動構造の作成法」を提案し、van der Waals 力、水素結合、電荷移動相互作用、共有結合などを有すると考えられる 35 種類の化学種に適応して、相互作用の解析・評価・分類に成功した。またこの解析法の有効性を明らかにした。(2 章)

2. 「π–π 相互作用」の解析に適応できることを明らかにした。エテニル基が近い位置にあるような分子からシクロファン類のようにベンゼン環が 3 個積層したような分子まで、それらの分子中の π–π 相互作用の実態を明らかにした。グラファイトの層状構造の解明や、分子間の分子認識の機構の解明、分子内の立体配座の支配因子の解明など、様々な方面で活用されると考えられる。(3–5 章)

3. 「中性分子・ラジカル分子・カチオン分子、アニオン分子」など様々な電子状態の化学種における、「第 16 族元素間の非結合相互作用」に適応できることを明らかにした。これは生体内のサイクルや製薬・医薬品の製造過程における触媒サイクル、有機エレクトロニクス材料の機構の解明などに有益である。(6,7 章)

この解析法を用いれば、理論家のみならず、実験化学者も、自身が着目する結合や非結合相互作用を自在に解析できる。以上のように、分子内および分子間における様々な相互作用を QTAIM-DFA 法により明らかにし、評価・分類に成功した。さらに、その結果を実験化学者に還元することで理論と実験の橋渡しを図った好例となった。

Abstract

Chemical bonds and interactions must be most important concepts in chemical sciences. The quantum theory of atoms-in-molecules (QTAIM) approach, proposed by Bader, is a fine example that enables us to analyze, evaluate, classify, and understand the nature of chemical bonds and interactions.

For understand to various interactions, QTAIM functions were calculated with the Gaussian 09 and/or Gaussian 03 program and analyzed by the AIM2000 program. QTAIM functions are total electron energy densities $H(\boldsymbol{r})$, potential energy densities $V(\boldsymbol{r})$ and others. His research group proposed the QTAIM dual functional analysis(QTAIM-DFA) of weak to strong interactions by plotting $H(\boldsymbol{r})$ versus $H(\boldsymbol{r}) - V(\boldsymbol{r})/2$. Data for the perturbed structures around the fully optimized structures are employed in the plots, in addition to those for the fully optimized ones. The method will help to analyze, evaluate, and classify the nature of chemical bonds and interactions. More complex interaction systems will be analyzed by the QTAIM-DFA, on the basis established in this work.

In this works, he succeeded in the following three points.

1. The dynamic behavior of interactions must be very important, as well as the static one, for the better understanding of interactions in molecules and adducts. Perturbed structures around a fully optimized structure are necessary to evaluate the dynamic nature. Normal coordinates of internal vibrations (NIV) are proposed to generate the perturbed structures in wide range of weak to strong interactions. (Chapter 2)
2. π–π interactions are interested as a factor to control the fine details of structures and to create delicate properties in materials. The behavior of the intramolecular π–π interactions is elucidated, exemplified by diethanodihydronaphthalene/diethenodihydronaphthalene, the derivatives and phenyl moieties in cyclophanes employing QTAIM-DFA. (Chapter 3-5)
3. The nature of the E-∗-E' bonds in neutral, mono-anionic, mono-cationic, and di-cationic forms of HEE'H, MeEE'Me, cyclo-1,2-EE'$(CH_2)_3$ and *cyclo*-E$(CH_2CH_2CH_2)_2$E’ (E, E' = O, S, Se, and Te) is investigated by applying QTAIM-DFA. (Chapter 6-7)

To clarify the nature of the weak interactions must be the first step to control the whole picture of the weak interactions. QTAIM approach, introduced by Bader, enables us to analyze the nature of chemical bonds and interactions. A lot of QTAIM investigations have been reported so far, however, those from a viewpoint of experimental chemists seem not so many. Then such method that enables experimental chemists to analyze their own results, concerning chemical bonds and interactions, by their own image, and proposed QTAIM-DFA, recently. Weak to strong interactions can be analyzed in a unified from with QTAIM-DFA.

Contents

Chapter 1. General Introduction 1

Chapter 2. Applications of Normal Coordinates of Internal Vibrations to Generate Perturbed Structures: Dynamic Behavior of Weak to Strong Interactions Elucidated by Atoms-in-Molecules Dual Functional Analysis 13

Chapter 3. Intramolecular π–π Interactions in Diethanodihydronaphthalene and Derivatives: Dynamic and Static Behavior of the Interactions Elucidated by QTAIM Dual Functional Analysis 41

Chapter 4. Behavior of Intramolecular π–π Interactions with Doubly Degenerated Bond Paths Between Carbon Atoms in Opposite Benzene Rings of Diethenodihydronaphthalene and Derivatives, Elucidated by QTAIM Approach 75

Chapter 5. Behavior of Intramolecular π–π Interactions in [2,2]- and [3,3]Cyclophanes, Elucidated by QTAIM Dual Functional Analysis: Requirements for Appearance of Bond Critical Points Between the Phenyl Moieties 105

Chapter 6. Dynamic and Static Behavior of E–E' Bonds in Neutral and Charged Forms of HEE'H, MeEE'Me, and *cyclo*-1,2-EE'$(CH_2)_3$ (E, E' = O, S, Se, and Te) Elucidated by QTAIM Dual Functional Analysis 135

Chapter 7. Transannular E---E' Interactions in Neutral, Radical Cationic, and Dicationic Forms of *cyclo*-[E$(CH_2CH_2CH_2)_2$E'] (E, E' = S, Se, Te, and O) with Structural Feature: Dynamic and Static Behavior of E---E' Elucidated by QTAIM Dual Functional Analysis 177

Conclusions 217

List of Publications 220

Other Publication 221

List of International Conferences 221

Acknowledgement 222

Chapter 1

General Introduction

Chemical bonds and interactions must be most important concepts in chemical sciences. A great deal of effort has been paid to understand the nature of chemical bonds and interactions in more detail for the development of chemical sciences. The quantum theory of atoms-in-molecules (QTAIM) approach, proposed by Bader,[1–3] is a fine example that enables us to analyze, evaluate, classify, and understand the nature of chemical bonds and interactions.[4–8] The bond critical point[1–3] (BCP; ∗[9]) is an important concept in QTAIM. BCP is a point along the bond path (BP) at the interatomic surface, at which charge density $\rho(\boldsymbol{r})$ reaches a minimum. The $\rho(\boldsymbol{r})$ values at BCPs are described by $\rho_b(\boldsymbol{r}_c)$, so are the QTAIM functions, such as total electron energy densities $H_b(\boldsymbol{r}_c)$, potential energy densities

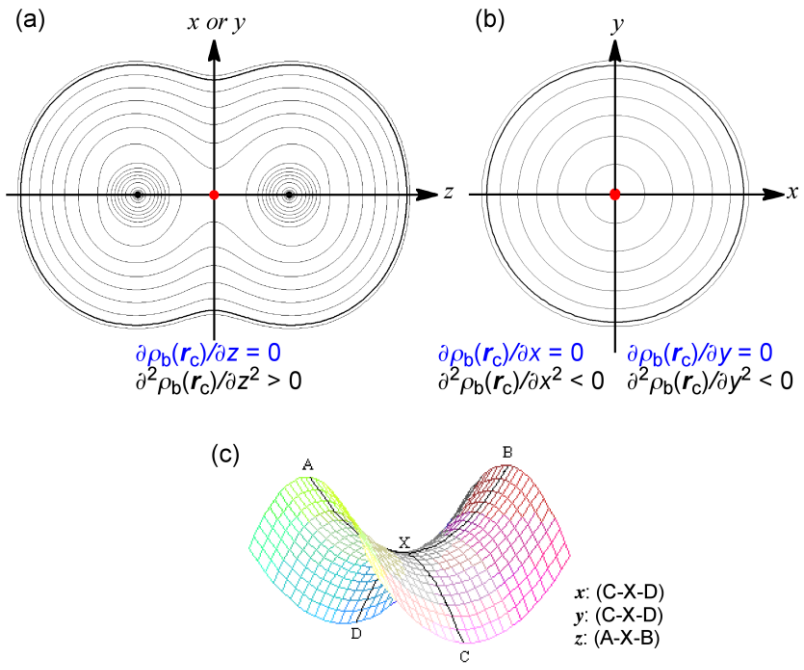

Figure 1-1. Contour plot of $\rho(\boldsymbol{r})$ for Cl-∗-Cl. Drawn on the plane containing the bond direction (z axis) (a), that perpendicular to it (b), and the image for the three dimensional saddle point (c).

$V_b(\boldsymbol{r}_c)$, and kinetic energy densities $G_b(\boldsymbol{r}_c)$ at BCPs. BCP must exist at the three dimensional saddle point of $\rho(\boldsymbol{r})$. Figure 1-1 explains BP and BCP, employing the contour plot of $\rho(\boldsymbol{r})$ for Cl-∗-Cl, together with the image for the three dimensional saddle point of $\rho(\boldsymbol{r})$.

A lot of QTAIM investigations have been reported so far;[1–3,10–18] however, those from a viewpoint of experimental chemists do not seem to be many. Such method is searched for that enables experimental chemists to analyze their own results, concerning chemical bonds and interactions, by their own image. Then, QTAIM dual functional analysis (QTAIM-DFA) was proposed, recently.[19–22] $H_b(\boldsymbol{r}_c)$ are plotted versus $H_b(\boldsymbol{r}_c) - V_b(\boldsymbol{r}_c)/2$ at BCPs in QTAIM-DFA. Data for the perturbed structures around the fully optimized structures are employed in the plots, in addition to those for the fully optimized ones. The concept of dynamic nature of interactions has been proposed based on the data from the perturbed structures, while the data from the fully optimized structures correspond to the static nature.[19–21] Rough criteria are established by applying QTAIM-DFA to typical chemical bonds and interactions,[19a,20,21] which serve as the standard parameters to distinguish the chemical bonds and interactions in question, from others. QTAIM-DFA will provide an excellent possibility to evaluate, classify, characterize, and understand weak to strong interactions in a unified form.[19–21] Scheme 1-1 explains the QTAIM-DFA treatment, by plotting $H_b(\boldsymbol{r}_c)$ versus $H_b(\boldsymbol{r}_c) - V_b(\boldsymbol{r}_c)/2$ for the interactions in question at BCPs. Scheme 1-2 summarizes rough criteria established with QTAIM-DFA.

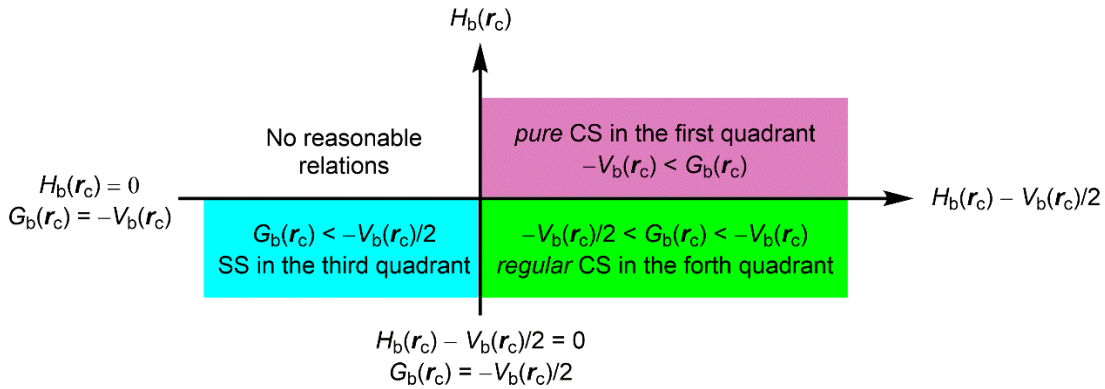

Scheme 1-1. Requirements for the data to appear in certain quadrant in the plots of $H_b(\boldsymbol{r}_c)$ versus $H_b(\boldsymbol{r}_c) - V_b(\boldsymbol{r}_c)/2$, where $H_b(\boldsymbol{r}_c) - V_b(\boldsymbol{r}_c)/2 = (\hbar^2/8m)\nabla^2\rho_b(\boldsymbol{r}_c)$.

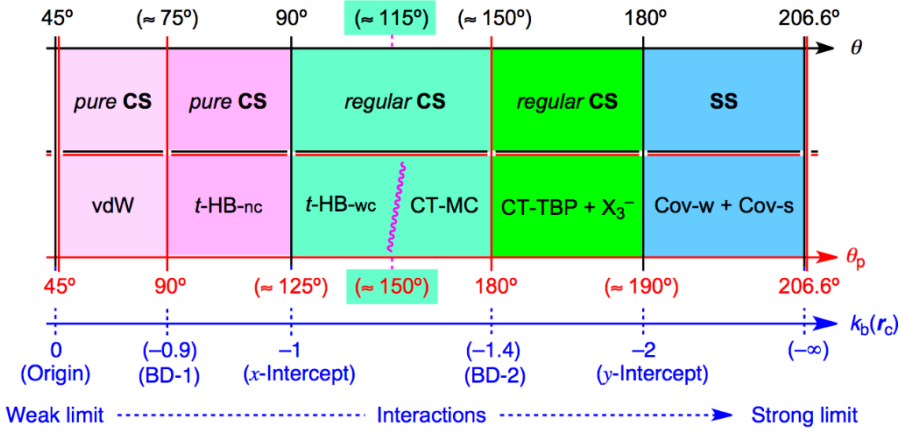

Scheme 1-2. Rough classification of interactions by θ and θ_p, together with $k_b(\boldsymbol{r}_c)$ (= $V_b(\boldsymbol{r}_c)/G_b(\boldsymbol{r}_c)$). The border area between Cov-w and Cov-s seems R of around 0.15 au.

How can the perturbed structures be generated necessary for QTAIM-DFA? A couple of methods are proposed to generate the perturbed structures, which are called POM and NIV. In POM, the perturbed structures are obtained by the partial optimizations with the interaction distances in question being fixed suitably.[19b,20] The perturbed structure with POM must exist at a minimum on the potential energy surface, except for the coordinate of the interaction in question. Therefore, the perturbed structures with POM are related to the thermal process. Normal coordinates of internal vibrations, obtained through the frequency analysis, are employed to generate the perturbed structures in NIV. Therefore, the perturbed structures with NIV are closely related to the adiabatic process.

The predicted dynamic nature of interactions would change depending on the perturbed structures, since the dynamic nature is predicted based on the data from the perturbed structures. How are the differences in the behavior of the interactions in question if the perturbed structures generated with NIV are employed in place of those with POM? The differences in the predicted behavior are examined in Chapter 2.[22] The applicability of POM and NIV is also validated in Chapter 2.[22] QTAIM-DFA and the criteria are explained in Chapter 2, together with the basic concept of the QTAIM approach.

After demonstrating the high applicability of POM and NIV, QTAIM-DFA is applied to elucidate the dynamic and static nature of various interactions.

As the first step to clarify the behavior of weak interactions, the nature of the intramolecular π–π interactions were elucidated, exemplified by diethanodihydronaphthalene (**1**-**1**) and derivatives.[23] The results are discussed in Chapter 3.[23] The intramolecular π–π interactions are demonstrated to be so delicate. The delicate behavior of the interactions would be affected by the slight structural change around the π–π interaction moieties, he wondered, where the properties of the materials should be originated depending on the behavior of π–π interactions. Such consideration led him to examine the behavior of the intramolecular π–π interactions between the ethylene moieties in diethenodihydronaphthalene (**1-2**) and the derivatives (Chart 1-1).[24] The results are discussed in Chapter 4.[24] During the course of the investigations, the doubly degenerated bond paths were detected between the carbon atoms in the opposite phenyl groups in the derivative of **1-2** (**1-3**), where the ethylene moieties are replaced by the benzene moieties.[24] The results are also discussed in Chapter 4.

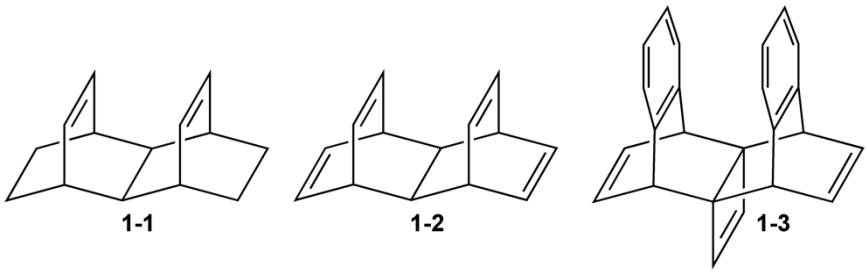

Chart 1-1. Compounds **1-1**–**1-3**

The π system in cyclophanes would be much strained through the alkyl bridgings between the aromatic rings. Therefore, the π system in cyclophanes must provide another intriguing intramolecular π–π interactions. The behavior of the intramolecular π–π interactions in cyclophanes (**1-4**–**1-6**)[25] (Chart 1-2) is clarified by applying QTAIM-DFA. The results are discussed in Chapter 5.[25] BPs between benzene rings are clearly detected in most cases, whereas they are not detected in some cases. The reason is also discussed in Chapter 5.[25]

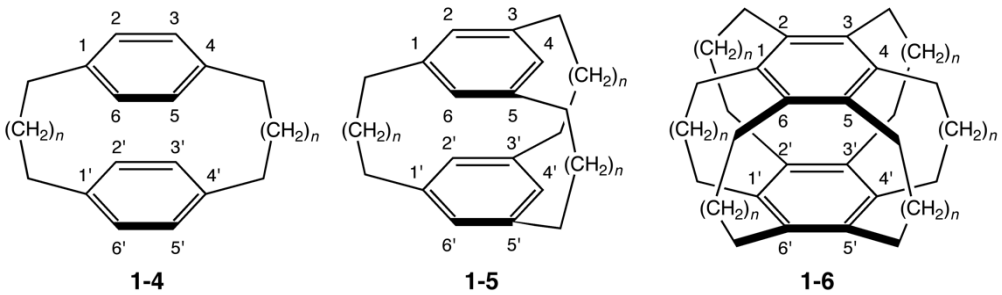

Chart 1-2. Compounds **1-4**–**1-6**

Chalcogen−chalcogen interactions (E−E′ and E···E′: E, E′ = S, Se, and Te, together with O) are of current and continuous interest, not only those of the shared-shell (SS) type (E−E′) but also of the closed-shell (CS) type (E···E′).[26–30] The E− E′ bonds play an important role in all fields of chemical and biological sciences. They maintain peptide structures and biological activities in enzymes, especially for E, E′ = S, Se.[31–35] The E−E′ bonds in dichalcogenides (RE−E′R′) supply low-lying vacant orbitals of the σ-type (σ*(E−E′)), where the E/E′ atoms contain lone pair orbitals of s- and p-types (n_s (E/E′) and n_p (E/E′), respectively) of relatively high energy levels. Consequently, the E−E′ bonds in RE−E′R′ are easily oxidized and reduced, which is important to develop highly functionalized materials. On the other hand, the intermolecular E···E′ interactions of the CS type are often encountered in crystals of organic compounds containing chalcogen atoms, which must be the important driving force to grow the crystals, and they create useful properties of materials. The behavior of the E–E′ bonds seems well described at first glance; however, it is still of highly importance to clarify the causality in the phenomena of the bonds, with physical necessity. Therefore, the behavior of the E–E′ bonds is elucidated for neutral, anionic, monocationic, and dicationic forms of REE′R, exemplified by HEE′H (**1-7**), MeEE′Me (**1-8**), and *cyclo*-1,2-EE′$(CH_2)_3$ (**1-9**) (E, E′ = O, S, Se, and Te) (Chart 1-3). E and E′ are chosen so as to the electronegativity of E (χ_E) is larger than or equal to that of E′ ($\chi_{E'}$)[36]. The results are discussed in Chapter 6.

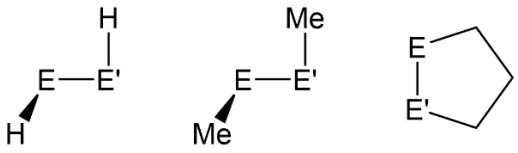

1-7 **1-8** **1-9**

(E, E') = (O, S, Se and Te: $\chi_E \leq \chi_{E'}$)

Chart 1-3. Compounds **1-7**–**1-9**

Cyclic dichalcogenides **1-9** are the example of *cis*-dichalcogenides. Another aim of the analysis is to construct the firm basis to clarify the E–E′ *trans*-annular interactions in *cyclo*-E($CH_2CH_2CH_2$)$_2$E′ (**1-10**) (Chart 1-4), their dications and the dication dimers reported by research groups of Furukawa[37–46] and Glass[47–51]. The dynamic and static nature of the interactions is elucidated, exemplified by 1,8-(dichalcogena)canes, which provide the typical systems for the intramolecular E⋯E′ interactions.[52] The results are discussed in Chapter 7.

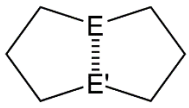

1-10

(E, E') = (O, S, Se and Te: $\chi_E \leq \chi_{E'}$)

Chart 1-4. Compound **1-10**

The results outlined above are discussed in the following chapters in the sequence from weaker to stronger interactions and the conclusive remarks are described in Chapter 8.

Appendix

Abbreviated Words

QTAIM-DFA ・・・・ Quantum theory of Atoms-in-Molecules dual functional analysis

POM ・・・・・・・・ Partial optimization method

NIV ・・・・・・・・ Normal coordinates of internal vibrations

BCP ・・・・・・・・ Bond critical point

RCP ・・・・・・・・ Ring critical point

CCP ・・・・・・・・ Cage critical point

BP ・・・・・・・・ Bond Path

$\rho_b(\boldsymbol{r}_c)$ ・・・・・・・・ Electron densities at BCPs

$\nabla^2\rho_b(\boldsymbol{r}_c)$ ・・・・・・・・ Laplacian $\rho_b(\boldsymbol{r}_c)$; second derivative of $\rho_b(\boldsymbol{r}_c)$;

$(\hbar^2/8m)\nabla^2\rho_b(\boldsymbol{r}_c) = H_b(\boldsymbol{r}_c) - V_b(\boldsymbol{r}_c)/2$

$H_b(\boldsymbol{r}_c)$ ・・・・・・・・ Total electron energy densities at BCPs; $G_b(\boldsymbol{r}_c) + V_b(\boldsymbol{r}_c)$

$G_b(\boldsymbol{r}_c)$ ・・・・・・・・ Kinetic energy densities at BCPs

$V_b(\boldsymbol{r}_c)$ ・・・・・・・・ Potential energy densities at BCPs

SS interaction ・・・・ Shared-shell interaction; $\nabla^2\rho_b(\boldsymbol{r}_c) < 0$

CS interaction ・・・・ Closed-shell interaction; $\nabla^2\rho_b(\boldsymbol{r}_c) > 0$

Pure CS ・・・・・・ CS interaction for $H_b(\boldsymbol{r}_c) > 0$

Regular CS ・・・・・ CS interaction for $\nabla^2\rho_b(\boldsymbol{r}_c) > 0$ and $H_b(\boldsymbol{r}_c) < 0$

vdW ・・・・・・・・ Van der Waals

HB ・・・・・・・・ Hydrogen bond

t-HB-$_{nc}$ ・・・・・・ Typical hydrogen bond no covalency

t-HB-$_{wc}$ ・・・・・・ Typical hydrogen bond with covalency

CT-MC ・・・・・・・ Molecular complexes through charge transfer

X_3^- ・・・・・・・・・ Trihalide ions

CT-TBP ・・・・・・ Trigonal bipyramidal adducts through charge transfer

Cov-w ・・・・・・・・ Classical chemical bonds of weak cases

Cov-s ・・・・・・・・ Classical chemical bonds of strong cases

References

1 *Atoms in Molecules. A Quantum Theory*, ed. by R. F. W. Bader, Oxford University Press, Oxford, UK, **1990**.

2 *At An Introduction to the Quantum Theory of Atoms in Molecules In The Quantum Theory of Atoms in Molecules: From Solid State to DNA and Drug Design*, ed. by C. F. Matta, R. J. Boyd, WILEY-VCH, Weinheim, Germany, **2007**, ch. 1.

3 a) F. Biegler-König, R. F. W. Bader, T. H. Tang, *J. Comput. Chem.* **1982**, *3*, 317–328; b) R. F. W. Bader, T. S. Slee. D. Cremer, E. Kraka, *J. Am. Chem. Soc.* **1983**, *105*, 5061–5068; c) R. F. W. Bader, *Acc. Chem. Res.* **1985**, *18*, 9–15; d) T. H. Tang, R. F. W. Bader, P. MacDougall, *Inorg. Chem.* **1985**, *24*, 2047–2053; e) R. F. W. Bader, *Chem. Res.* **1991**, *91*, 893–926; f) R. F. W. Bader, *J. Phys. Chem. A* **1998**, *102*, 7314–7323; g) F. Biegler-König, J. Schönbohm, D. Bayles, *J. Comput. Chem*. **2001**, *22*, 545–559; h) F. Biegler-König, J. Schönbohm, *J. Comput. Chem.* **2002**, *23*, 1489–1494.

4 J. Molina, J. A. Dobado, *Theor. Chem. Acc.* **2001**, *105*, 328–337.

5 J. A. Dobado, H. Martinez-Garcia, J. Molina, M. R. Sundberg, *J. Am. Chem. Soc.* **2000**, *122*, 1144–1149.

6 S. K. Ignatov, N. H. Rees, B. R. Tyrrell, S. R. Dubberley, A. G. Razuvaev, P. Mountford, G. I. Nikonov, *Chem. Eur. J.* **2004**, *10*, 4991–4999.

7 S. K. Tripathi, U. Patel, D. Roy, R. B. Sunoj, H. B. Singh, G. Wolmershäuser, R. J. Butcher, *J. Org. Chem.* **2005**, *70*, 9237–9247.

8 R. J. Boyd, S. C. Choi, *Chem. Phys. Lett.* **1986**, *129*, 62–65.

9 Dots are usually employed to show BCPs in molecular graphs. Therefore, A-•-B would be more suitable to describe the BP with the BCP. Nevertheless, A-∗-B is employed to emphasize the existence of the BCP on the BP, in question, in his research group case.

10 M. T. Carroll, R. F. W. Bader, *Mol. Phys.* **1988**, *65*, 695–722.

11 E. Espinosa, E. Molins, C. Lecomte, *Chem. Phys. Lett.* **1998**, *285*, 170–173.

12 S. J. Grabowski, *J. Phys. Chem. A* **2001**, *105*, 10739–10746.

13 a) E. Espinosa, I. Alkorta, J. Elguero, E. Molins, *J. Chem. Phys.* **2002**, *117*, 5529–5542; b) I. Rozas, I. Alkorta, J. Elguero, *J. Am. Chem. Soc.* **2000**, *122*, 11154–11161.

14 M. Domagała, S. Grabowski, K. Urbaniak, G. Mloston, *J. Phys. Chem. A* **2003**, *107*, 2730–2736.

15 S. Grabowski, W. A. Sokalski, J. Leszczynski, *J. Phys. Chem. A* **2005**, *109*, 4331–4341.

16 M. Domagala, S. Grabowski, *J. Phys. Chem. A* **2005**, *109*, 5683–5688.

17 R. Parthasarathi, V. Subramanian, N. Sathyamurthy, *J. Phys. Chem. A* **2006**, *110*, 3349–3351.

18 W. Nakanishi, T. Nakamoto, S. Hayashi, T. Sasamori, N. Tokitoh, *Chem. Eur. J.* **2007**, *13*, 255–268.

19 a) W. Nakanishi, S. Hayashi, K. Narahara, *J. Phys. Chem. A* **2009**, *113*, 10050–10057; b) W. Nakanishi, S. Hayashi, K. Narahara, *J. Phys. Chem. A* **2008**, *112*, 13593–13599.

20 W. Nakanishi, S. Hayashi, *Curr. Org. Chem.* **2010**, *14*, 181–197.

21 W. Nakanishi, S. Hayashi, *J. Phys. Chem. A* **2010**, *114*, 7423–7430.

22 W. Nakanishi, S. Hayashi, K. Matsuiwa and M. Kitamoto, *Bull. Chem. Soc. Jpn.* **2012**, *85*, 1293–1305.

23 K. Matsuiwa, S. Hayashi, W. Nakanishi, *ChemistrySelect* **2016**, *1*, 2344–2353.

24 K. Matsuiwa, Y. Sugibayashi, Y. Tsubomoto, S. Hayashi, W. Nakanishi, Submitted.

25 K. Matsuiwa, S. Hayashi, W. Nakanishi, in preparation.

26 a) D. L. Klayman, W. H. H. Günther, Eds. *Organic Selenium Compounds: Their Chemistry and Biology*; Wiley: New York, 1973; b) S. Patai, Z. Rappoport, Eds. *The Chemistry of Organic Selenium and Tellurium Compounds*; John-Wiley and Sons: New York, 1986, Vols. 1 and 2; () D. Liotta, Ed. *Organic Selenium Chemistry*; Wiley-Interscience: New York, 1987; d) T. G. Back, Ed. *Organoselenium Chemistry, A practical Approach*; Oxford University Press: Oxford, 1999; e) T. Wirth, Ed. *Organoselenium Chemistry Modern Developments in Organic Synthesis, Top. Curr. Chem.*; Springer: Berlin, Heidelberg, New York, London, Paris, Tokyo, 2000.

27 K.-y. Akiba, Ed. *Chemistry of Hypervalent Compounds*: Wiley-VCH, New York, 1999.

28 a) W. Nakanishi, In *Handbook of Chalcogen Chemistry: New Perspectives in Sulfur, Selenium and Tellurium*: F. A. Devillanova, Ed. Royal Society of Chemistry, Cambridge, 2006, Chap. 10.3, pp. 644–668; b) W. Nakanishi, S. Hayashi, In *Handbook of Chalcogen Chemistry: New Perspectives in Sulfur, Selenium and Tellurium: 2nd Edition*, F. A. Devillanova, W.-W. du Mont, Eds. Royal Society of Chemistry, Cambridge, 2013, Vol. 2, Chap. 12.3, pp. 335–372.

29 A. J. Mukherjee, S. S. Zade, H. B. Singh, R. B. Sunoj, *Chem. Rev.* **2010**, 110, 4357–4416.

30 a) K. Morihashi, S. Kushihara, Y. Inadomi, O. Kikuchi, *J. Mol. Struct. (Theochem.)* **1997**, *418*, 171–178; b) B. Mueller, T. T. Takaluoma, R. S. Laitinen, K. Seppelt, *Eur. J. Inorg. Chem.* **2011**, 4970–4977; c) B. Mueller, H. Poleschner, K. Seppelt, *Dalton Trans.* **2008**, 4424–4427; d) A. Wakamiya, T. Nishinaga, K. Komatsu, *J. Am. Chem. Soc.* **2002**, *124*, 15038–15050; e) O. Mundt, G. Becker, J. Baumgarten, H. Riffel, A. Simon, *Z. Anorg. Allg. Chem.* **2006**, *632*, 1687–1709.

31 B. J. Bhuyan, D. S. Lamani, G. Mugesh, T. Wirth, In *Handbook of Chalcogen Chemistry: New Perspectives in Sulfur, Selenium and Tellurium: 2nd Edition*, F. A. Devillanova, W.-W. du Mont, Eds. Royal Society of Chemistry, Cambridge, 2013, Vol. 2, Chap. 10.2, pp. 25–46.

32 S. R. Jakka, G. Mugesh, In *Handbook of Chalcogen Chemistry: New Perspectives in Sulfur, Selenium and Tellurium: 2nd Edition*, F. A. Devillanova, W.-W. du Mont, Eds. Royal Society of Chemistry, Cambridge, 2013, Vol. 2, Chap. 10.3, pp. 46–65.

33 S. Patai, Z. Rappoport, Eds. *The Chemistry of Organic Selenium and Tellurium Compounds*; Wiley, New York, 1986, Vol. 1, Chap. 6.

34 Z. Rappoport, Ed. *The Chemistry of Organic Selenium and Tellurium Compounds*; Wiley, New York, 2013, Vol. 4, Chaps. 13–16.

35 a) A. Panda, G. Mugesh, H. B. Singh, R. Butcher, *Organometallics* **1999**, *18*, 1986–1993; b) M. Kulcsar, A. Beleaga, C. Silvestru, A. Nicolescu, C. Deleanu, C. Todasca, A. Silvestru, *Dalton Trans.* **2007**, 2187–2196; c) A. Beleaga, M. Kulcsar, C. Deleanu, A. Nicolescu, C. Silvestru, A. Silvestru, *J. Organomet. Chem.* **2009**, *694*, 1308–1316.

36 The electronegativity proposed by Allred-Rochow was employed to discuss the structure of the

adducts. See a) A. L. Allred, E. G. J. Rochow, *Inorg. Nucl. Chem.* **1958**, *5*, 264–268; b) A. L. Allred, E. G. J. Rochow, *Inorg. Nucl. Chem.* **1958**, *5*, 269–288.

37 a) F. Iwasaki, N. Toyoda, R. Akaishi, H. Fujihara, N. Furukawa, N. *Bull. Chem. Soc. Jpn.* **1988**, *61*, 2563–2567; b) H. Fujihara, A. Kawada, N. Furukawa, *J. Org. Chem.* **1987**, *52*, 4254–4257.

38 a) F. Iwasaki, M. Morimoto, M. Yasui, R. Akaishi, H. Fujihara, N. Furukawa, *Acta Cryst.* **1991**, *C47*, 1463–1466; b) H. Fujihara, N. Furukawa, *Phosphorus, Sulfur Silicon Rel. Elem.* **1992**, *67*, 131–134.

39 a) H. Fujihara, R. Akaishi, T. Erata, N. Furukawa, *Chem. Commun.* **1989**, 1789–1790; b) H. Fujihara, R. Akaishi, N. Furukawa, *Tetrahedron* **1993**, *49*, 1605–1618.

40 H. Fujihara, R. Akaishi, A. Nakamura, N. Furukawa, *Tetrahedron Lett.* **1990**, *31*, 6375–6378.

41 H. Fujihara, M. Yabe, J.-J. Chiu, N. Furukawa, *Tetrahedron Lett.* **1991**, *32*, 4345–4348.

42 H. Fujihara, T. Ninoi, R. Akaishi, T. Erata, N. Furukawa, *Tetrahedron Lett.* **1991**, *32*, 4537–4540.

43 H. Fujihara, Y. Takuguchi, T. Ninoi, T. Erata, N. Furukawa, *J. Chem. Soc., Perkin Trans. 1* **1992**, 2583–2584.

44 H. Fujihara, N. Furukawa, *J. Mol. Struct. (Theochem)* **1989**, *186*, 261–272.

45 N. Nakayama, O. Takahashi, O. Kikuchi, N. Furukawa, *Heteroatom Chem.* **2000**, *11*, 31–41.

46 N. Nakayama, O. Takahashi, O. Kikuchi, N. Furukawa, *J. Mol. Struct. (Theochem.)* **2001**, *542*, 215–226.

47 a) E. Block, E. V. Dikarev, R. S. Glass, J. Jin, B. Li, X. Li, S.-Z. Zhang, *J. Am. Chem. Soc.* **2006**, *128*, 14949–14961; b) E. Block, R. S. Glass, E. V. Dikarev, N. E. Gruhn, J. Jin, B. Li, E. Lorance, U. I. Zakai, S. Z. Zhang, *Heteroatom Chem.* **2007**, *18*, 509–515; c) C. Liao, S.-Z. Zhang, E. Block, E. L. Clennan, *J. Org. Chem.* **2008**, *73*, 8587–8590.

48 a) R. S. Glass, E. Block, E. Lorance, U. I. Zakai, N. E. Gruhn, J. Jin, S.-Z. Zhang, *J. Am. Chem. Soc.* **2006**, *128*, 12685–12692; b) R. S. Glass, E. Block, N. E. Gruhn, J. Jin, E. Lorance, U. I. Zakai, S.-Z. Zhang, *J. Org. Chem.* **2007**, *72*, 8290–8297.

49 a) R. S. Glass, L. Adamowicz, J. L. Broeker, *J. Am. Chem. Soc.* **1991**, *113*, 1065–1072; b) R. S.

Glass, S. W. Andruski, J. L. Broeker, H. Firouzabadi, L. K. Steffen, G. S. Wilson, *J. Am. Chem. Soc.* **1989**, *111*, 4036–4045.

50 D. H. Evans, N. E. Gruhn, J. Jin, B. Li, E. Lorance, N. Okumura, N. A. Macias-Ruvalcaba, U. I. Zakai, S.-Z. Zhang, E. Block, R. S. Glass, *J. Org. Chem.* **2010**, *75*, 1997–2009.

51 R. Stowasser, R. S. Glass, R. Hoffmann, *J. Chem. Soc., Perkin Trans. 2* **1999**, 1559–1561.

52 S. Hayashi, K. Matsuiwa, N. Nishizawa, and W. Nakanishi, *J. Org. Chem.* **2015**, *80*, 11963−11976.

Chapter 2

Applications of Normal Coordinates of Internal Vibrations to Generate Perturbed Structures: Dynamic Behavior of Weak to Strong Interactions Elucidated by Atoms-in-Molecules Dual Functional Analysis

Abstract

Normal coordinates of internal vibrations (NIV) are employed to generate the perturbed structures necessary in the quantum theory of atoms-in-molecules (QTAIM) dual functional analysis for a wide range of weak to strong interactions. $H_b(\boldsymbol{r}_c)$ are plotted versus $H_b(\boldsymbol{r}_c) - V_b(\boldsymbol{r}_c)/2$ [$= (\hbar^2/8m)\nabla^2\rho_b(\boldsymbol{r}_c)$] at bond critical points in the treatment, which incorporates the classification of interactions by signs of $\nabla^2\rho_b(\boldsymbol{r}_c)$ and $H_b(\boldsymbol{r}_c)$. The plots are analyzed using the polar (R, θ) representation. Each plot for an interaction shows a specific curve, which is expressed by (θ_p, κ_p): θ_p corresponds to the tangent line for the plot from the y-direction and κ_p is the curvature. While (R, θ) correspond to the static behavior of interactions at the fully optimized structures, (θ_p, κ_p) exhibit the dynamic nature. The (θ_p, κ_p) values evaluated employing the perturbed structures with NIV are shown to be very close to those obtained using perturbed structures partially optimized with the distances in question being fixed suitably (POM). The magnitudes of differences in θ_p and κ_p between those evaluated with NIV and POM are $\leq 2^o$ and ≤ 2 au^{-1}, respectively, for usual interactions. It is demonstrated that NIV is applicable to wide range of usual interactions, as well as POM.

Introduction

It must be of highly importance to understand the nature of chemical bonds and interactions in detail for the development of chemical sciences. The quantum theory of atoms-in-molecules (QTAIM) method, proposed by Bader,[1,2] enables us to analyze, evaluate, and classify the nature of chemical bonds and interactions.[3–7] Electron densities at bond critical points (BCPs: $\boldsymbol{r}_c$, ∗) of (ω, σ) = (3, –1)[1] ($\rho_b(\boldsymbol{r}_c)$) are strongly related to the binding energies[8–14] and bond orders.[15] The sign of the Laplacian $\rho_b(\boldsymbol{r}_c)$ ($\nabla^2\rho_b(\boldsymbol{r}_c)$) indicates that $\rho_b(\boldsymbol{r}_c)$ is depleted or concentrated with respect to its surroundings, since $\nabla^2\rho_b(\boldsymbol{r}_c)$ is the second derivative of $\rho_b(\boldsymbol{r}_c)$. $\rho_b(\boldsymbol{r}_c)$ is locally concentrated relative to the average distribution around BCPs if $\nabla^2\rho_b(\boldsymbol{r}_c) < 0$, but it is depleted when $\nabla^2\rho_b(\boldsymbol{r}_c) > 0$. On the other hand, total electron energy densities at BCPs ($H_b(\boldsymbol{r}_c)$) must be a more appropriate measure for weak interactions on the energy basis.[1,2,16–20] $H_b(\boldsymbol{r}_c)$ are the sum of kinetic energy densities ($G_b(\boldsymbol{r}_c)$) and potential energy densities ($V_b(\boldsymbol{r}_c)$) at BCPs. Electrons at BCPs are stabilized when $H_b(\boldsymbol{r}_c) < 0$, therefore, interactions exhibit the covalent nature in this region, whereas they exhibit no covalency if $H_b(\boldsymbol{r}_c) > 0$ due to the destabilization of electrons at BCPs under the conditions. Eqs (2-1) and (2-2) represent the relations between $H_b(\boldsymbol{r}_c)$, $G_b(\boldsymbol{r}_c)$, $V_b(\boldsymbol{r}_c)$, and $\nabla^2\rho_b(\boldsymbol{r}_c)$.

$$H_b(\boldsymbol{r}_c) = G_b(\boldsymbol{r}_c) + V_b(\boldsymbol{r}_c) \tag{2-1}$$

$$(\hbar^2/8m)\nabla^2\rho_b(\boldsymbol{r}_c) = H_b(\boldsymbol{r}_c) - V_b(\boldsymbol{r}_c)/2 = G_b(\boldsymbol{r}_c) + V_b(\boldsymbol{r}_c)/2 \tag{2-2}$$

Chemical bonds and interactions are classified by the signs of $\nabla^2\rho_b(\boldsymbol{r}_c)$ and $H_b(\boldsymbol{r}_c)$. Scheme 2-1 summarizes the classification. Interactions in the region of $\nabla^2\rho_b(\boldsymbol{r}_c) < 0$ are called shared-shell (SS) interactions and they are closed-shell (CS) interactions for $\nabla^2\rho_b(\boldsymbol{r}_c) > 0$. $H_b(\boldsymbol{r}_c)$ must be negative when $\nabla^2\rho_b(\boldsymbol{r}_c) < 0$, since $H_b(\boldsymbol{r}_c)$ are larger than $(\hbar^2/8m)\nabla^2\rho_b(\boldsymbol{r}_c)$ by $V_b(\boldsymbol{r}_c)/2$ where $V_b(\boldsymbol{r}_c)$ are negative at all BCPs (eq (2-2)). Consequently, $\nabla^2\rho_b(\boldsymbol{r}_c) < 0$ and $H_b(\boldsymbol{r}_c) < 0$ for the SS interactions. The CS interactions are especially called *pure* CS interactions for $H_b(\boldsymbol{r}_c) > 0$ and $\nabla^2\rho_b(\boldsymbol{r}_c) > 0$, since electrons at BCPs are depleted and destabilized under the conditions.[1] Electrons in the intermediate

region between SS and *pure* CS, which belong to CS, are locally depleted but stabilized at BCPs, since $\nabla^2\rho_b(\boldsymbol{r}_c) > 0$ but $H_b(\boldsymbol{r}_c) < 0$.[11] The redistribution of $\rho_b(\boldsymbol{r}_c)$ occurs between those electronic states in this region. Nakanishi and his coworkers will call the interactions in this region *regular* CS, when it is necessary to distinguish from *pure* CS.[17-19] $\nabla^2\rho_b(\boldsymbol{r}_c)$ can be replaced by $H_b(\boldsymbol{r}_c) - V_b(\boldsymbol{r}_c)/2$ in the classification shown in Scheme 2-1, since $(\hbar^2/8m)\nabla^2\rho_b(\boldsymbol{r}_c) = H_b(\boldsymbol{r}_c) - V_b(\boldsymbol{r}_c)/2$ (eq (2-2)), of which signs necessary for the classification are the same with each other. The classification by the signs of $\nabla^2\rho_b(\boldsymbol{r}_c)$ and $H_b(\boldsymbol{r}_c)$ can be achieved only by one parameter of θ, as shown in Scheme 2-1. The reason will be discussed later.

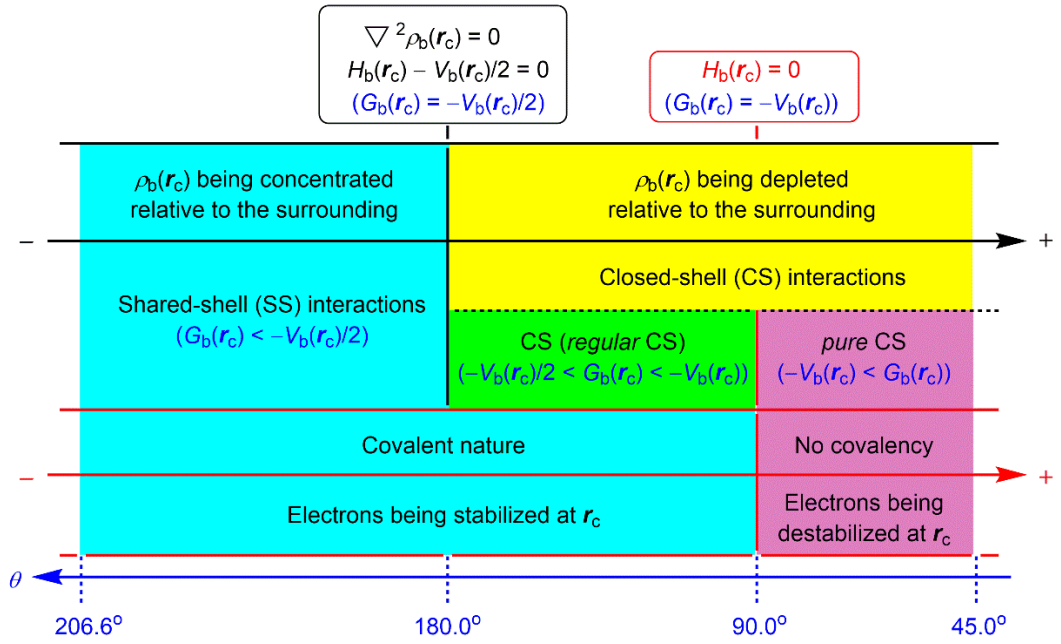

Scheme 2-1. Classification of interactions by QTAIM functions, where $H_b(\boldsymbol{r}_c) - V_b(\boldsymbol{r}_c)/2 = (\hbar^2/8m)\nabla^2\rho_b(\boldsymbol{r}_c)$.

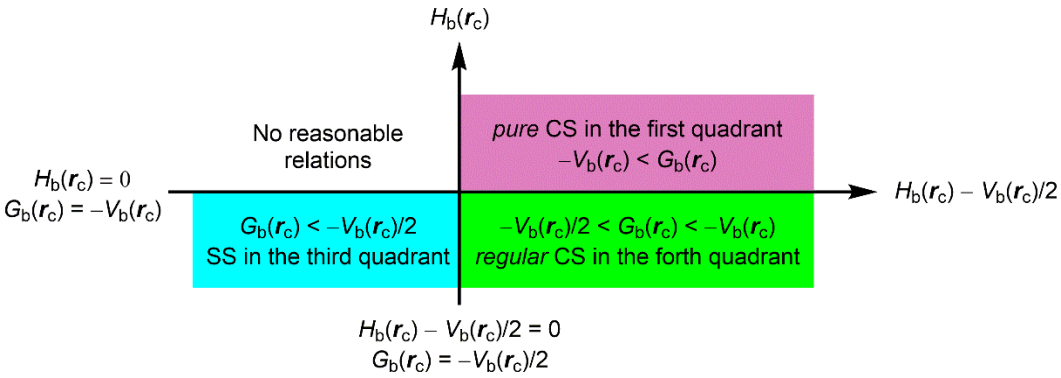

Scheme 2-2. Requirements for the data to appear in certain quadrant in the plots of $H_b(\boldsymbol{r}_c)$ versus $H_b(\boldsymbol{r}_c) - V_b(\boldsymbol{r}_c)/2$, where $H_b(\boldsymbol{r}_c) - V_b(\boldsymbol{r}_c)/2 = (\hbar^2/8m)\nabla^2\rho_b(\boldsymbol{r}_c)$.

It must be of great use if this classification can be incorporated into the QTAIM analysis. This expectation led us to propose the QTAIM dual functional analysis of weak to strong interactions by plotting $H_b(\boldsymbol{r}_c)$ versus $H_b(\boldsymbol{r}_c) - V_b(\boldsymbol{r}_c)/2$,[18] after the proposal of $H_b(\boldsymbol{r}_c)$ versus $\nabla^2\rho_b(\boldsymbol{r}_c)$.[17] Two treatments are essentially the same with each other, which incorporates the classification shown in Scheme 2-1.[21] The former is obtained through reducing the *x*-axis of the latter by 1/8 in atomic unit according to eq (2-2). Scheme 2-2 is the same as Scheme 1-1 that shows the requirements for data to appear in certain quadrant in the proposed plots of $H_b(\boldsymbol{r}_c)$ versus $H_b(\boldsymbol{r}_c) - V_b(\boldsymbol{r}_c)/2$. Data appear in the first quadrant if they are *pure* CS, in the fourth quadrant for the *regular* CS, and those of SS drop in the third quadrant. No data appear in the second quadrant. The results are essentially the same as the classification shown in Scheme 2-1. Both axes in Scheme 2-2 are given in energy unit, therefore, distances on the $(x, y) = (H_b(\boldsymbol{r}_c) - V_b(\boldsymbol{r}_c)/2, H_b(\boldsymbol{r}_c))$ plane can be expressed in energy unit, which provides an analytical development. In his research group treatment, data at BCPs on the interactions in question are also employed for the plots, together with the fully optimized ones (see Figure 2-1), where the atomic distances for the interactions are suitably fixed longer and shorter around those of fully optimized structures (perturbed structures).[18,19,21] The plots for weak to strong interactions show spiral streams. While data for perturbed structures form local streams in the plots, together with fully optimized ones, those for fully optimized structures do an averaged stream, as a whole. His research group proposed the concept of "dynamic nature of interaction," which originates from the perturbed structures at the fully optimized ones. The behavior of interactions at fully optimized structures corresponds to the static nature, whereas that for the perturbed structures represents the dynamic nature.

QTAIM dual functional analysis will be confirmed as an excellent method to elucidate the nature of weak to strong interactions if the calculated results are demonstrated to be equal to those obtained experimentally. It should be necessary to realize the approximate expression of some QTAIM functions, together with the definition, which connect calculated and experimentally observed values. $G(\boldsymbol{r})$ is defined by eq (2-3), where Ψ is an antisymmetric many-electron

wavefunction with N of the number of electrons.[22] The approximate expression of $G(\boldsymbol{r})$ was proposed in the DFT framework,[23] which is shown by eq (2-4). Consequently, $G_b(\boldsymbol{r}_c)$ is derived from eq (2-4) by applying $\nabla\rho(\boldsymbol{r}) = 0$. Eq (2-5) shows the relation. $V_b(\boldsymbol{r}_c)$ and $H_b(\boldsymbol{r}_c)$ are then given by eqs (2-6) and (2-7), respectively, which are derived from eqs (2-1), (2-2), and (2-5). By applying eqs (2-5)–(2-7), the calculated results are demonstrated to be very close to those of the experimentally determined high-resolution charge densities, exemplified by the N–S–N 3c–4e (three center-four electron interactions) in 2-(2-Pyridylimino)-2*H*-1,2,4-thiadiazolo[2,3-*a*]pyridine.[24]

$$G(\boldsymbol{r}) = (\hbar^2/2m)N\int d\tau' \nabla\Psi \bullet \nabla\Psi \tag{2-3}$$

$$G(\boldsymbol{r}) = (3\hbar^2/10m)(3p^2)^{2/3}\rho(\boldsymbol{r})^{5/3} + (\hbar^2/72m)[\nabla\rho(\boldsymbol{r})]^2/\rho(\boldsymbol{r}) + (\hbar^2/6m)\nabla^2\rho(\boldsymbol{r}) \tag{2-4}$$

$$G_b(\boldsymbol{r}_c) = (3\hbar^2/10m)(3\pi^2)^{2/3}\rho_b(\boldsymbol{r}_c)^{5/3} + (\hbar^2/6m)\nabla^2\rho_b(\boldsymbol{r}_c) \tag{2-5}$$

$$V_b(\boldsymbol{r}_c) = -(3\hbar^2/5m)(3\pi^2)^{2/3}\rho_b(\boldsymbol{r}_c)^{5/3} - (\hbar^2/12m)\nabla^2\rho_b(\boldsymbol{r}_c) \tag{2-6}$$

$$H_b(\boldsymbol{r}_c) = -(3\hbar^2/10m)(3\pi^2)^{2/3}\rho_b(\boldsymbol{r}_c)^{5/3} + (\hbar^2/12m)\nabla^2\rho_b(\boldsymbol{r}_c) \tag{2-7}$$

How can the perturbed structures be generated, necessary to evaluate the dynamic behavior of interactions? They can be obtained by the partial optimization method with an interaction in question being fixed suitably. This primitive method is called POM.[18,19,21] His research group proposed another method recently, exemplified by CT (charge transfer) interactions. The method employs normal coordinates of internal vibrations. His research group calls this method NIV.[21] A motion in NIV corresponds to the zero-point motion of the internal vibration although the magnitude for the displacement of an inter-atomic distance in question is amplified to $\Delta r = wa_o$ (w = ±0.05 and ±0.1). Therefore, the motion in NIV is closely related to the quantified adiabatic process. On the other hand, a perturbed structure by POM must exist on the potential energy surface, therefore, POM must be closely related to the thermal process. The applicability of NIV is examined to a wide range of simple interactions with physical meanings, in relation to the case of

POM, as a first step to develop the method. Here, he demonstrates that NIV is an excellent method to generate the perturbed structures for a wide range of interactions in a unified form. It is another purpose of this chapter to introduce the QTAIM dual functional analysis for experimental chemists for the better understanding weak to strong interactions.

Survey of QTAIM Dual Functional Analysis

$H_b(\boldsymbol{r}_c)$ are plotted versus $H_b(\boldsymbol{r}_c) - V_b(\boldsymbol{r}_c)/2$ in the QTAIM dual functional analysis. Data of a fully optimized structure and those of perturbed structures around the fully optimized one are employed for the plot of an interaction. Figure 2-1 explains the method. The plots for weak to strong interactions show spiral stream, as a whole (see Figure 2-3). Data of the fully optimized structures form an averaged stream, while those for perturbed structures do local streams.

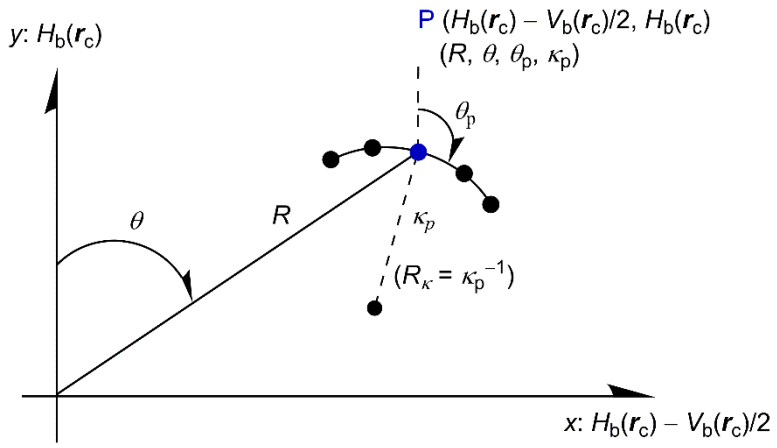

Figure 2-1. Polar (R, θ) coordinate representation of $H_b(\boldsymbol{r}_c)$ versus $H_b(\boldsymbol{r}_c) - V_b(\boldsymbol{r}_c)/2$. A regression curve is also shown, which connect the data at BCPs for perturbed and fully optimized structures.

$$R = (x^2 + y^2)^{1/2} \tag{2-8}$$

$$\theta = 90^o - \tan^{-1}(y/x) \tag{2-9}$$

$$\theta_p = 90^o - \tan^{-1}(dy/dx) \tag{2-10}$$

$$\kappa_p = |d^2y/dx^2| / [1 + (dy/dx)^2]^{3/2} \tag{2-11}$$

$$k_b(\boldsymbol{r}_c) = V_b(\boldsymbol{r}_c)/G_b(\boldsymbol{r}_c) \tag{2-12}$$

$$y/x = (G_b(\boldsymbol{r}_c) + V_b(\boldsymbol{r}_c))/(G_b(\boldsymbol{r}_c) + V_b(\boldsymbol{r}_c)/2) = 2(k + 1)/(k + 2) = 2 - 2/(k + 2) \quad (2\text{-}13)$$

where $(x, y) = (H_b(\boldsymbol{r}_c) - V_b(\boldsymbol{r}_c)/2, H_b(\boldsymbol{r}_c))$

How can the plots of $H_b(\boldsymbol{r}_c)$ versus $H_b(\boldsymbol{r}_c) - V_b(\boldsymbol{r}_c)/2$ be analyzed with physical meanings, which show the spiral stream? While the plots of $H_b(\boldsymbol{r}_c)$ versus $H_b(\boldsymbol{r}_c) - V_b(\boldsymbol{r}_c)/2$ for the data of fully optimized structures are analyzed employing the polar coordinate (R, θ) representation, those for perturbed structures with a fully optimized one are by the (θ_p, κ_p) parameters as shown in Figure 2-1.[18,19,21] R in (R, θ) is defined by eq (2-8). R is given in the energy unit, since distances on the (x, y) = ($H_b(\boldsymbol{r}_c) - V_b(\boldsymbol{r}_c)/2$, $H_b(\boldsymbol{r}_c)$) plane can be expressed in the energy unit. R corresponds to the energy for an interaction at BCP relative to that without any interaction at the origin, since $H_b(\boldsymbol{r}_c) = H_b(\boldsymbol{r}_c) - V_b(\boldsymbol{r}_c)/2 = 0$ at the origin.[18,19,21,25] θ defined by eq (2-9) controls the spiral stream of the plot, which is measured from the y-axis. The acceptable range of θ is limited to $45.0^o < \theta < 206.6^o$.[18,19] The range is further divided into $45.0^o < \theta < 90.0°$ for *pure* CS ($H_b(r_c) > 0$; $H_b(r_c) - V_b(r_c)/2 > 0$), $90.0^o < \theta < 180.0°$ for *regular* CS ($H_b(r_c) < 0$; $H_b(r_c) - V_b(r_c)/2 > 0$) and $180.0° < \theta < 206.6^o$ for SS interactions ($H_b(r_c) < 0$; $H_b(r_c) - V_b(r_c)/2 < 0$). This is the reason for the interactions classified only by θ, which are usually done by $H_b(\boldsymbol{r}_c)$ and $\nabla^2\rho_b(\boldsymbol{r}_c)$, as shown in Scheme 2-1.[18]

Each plot for an interaction shows a specific curve, as shown in Figure 2-1, which must provide important information about the interaction. The curve is expressed by (θ_p, κ_p): θ_p defined by eq (2-10) corresponds to the tangent line measured from the y-direction and κ_p is the curvature of the plot at BCP of the fully optimized structure, which is given by eq (2-11). Eq (2-12) defines k, which is equal to $V_b(\boldsymbol{r}_c)/G_b(\boldsymbol{r}_c)$, serve as a nice parameter to analyze the plots. θ is related to k through y/x as shown in eq (2-13), for example. While (R, θ) correspond to the static nature of interactions, (θ_p, κ_p) represent the dynamic nature of interactions.

Methodological Details in Calculations

A molecule or an adduct was optimized with an interaction in question (r) being fixed to satisfy

eq (2-14) in POM, where r_o shows the distance in the fully optimized structure with a_o of Bohr radius (0.52918 Å). Therefore, r in the perturbed structures must be fixed longer and shorter than r_o by $0.05a_o$ and $0.1a_o$ with other structural parameters being at the minimum values. On the other hand, eq (2-15) explains the method to generate perturbed structures with NIV. The k-th perturbed structures in question ($\mathbf{S}_{kw}$) were obtained by adding the normal coordinates of the k-th internal vibration ($\mathbf{N}_k$) printed out after the frequency analysis to the standard orientation of a fully optimized structure ($\mathbf{S}_o$) in the matrix representation.[26] The coefficient f_{kw} in eq (2-15) controls the difference in structures between $\mathbf{S}_{kw}$ and $\mathbf{S}_o$: f_{kw} will be determined to satisfy eq (2-14) for r in question in the k-th perturbed structures.[27] Therefore, r in $\mathbf{S}_{kw}$ must be longer and shorter than r_o in $\mathbf{S}_o$ by $0.05a_o$ and $0.1a_o$. $\mathbf{N}_k$ of five digits were used to predict $\mathbf{S}_{kw}$, although only two digits are usually printed out.[28]

$$r = r_o + wa_o \ (w = (0), \pm 0.05, \text{ and } \pm 0.1;\ a_o = 0.52918 \text{ Å}) \tag{2-14}$$

$$\mathbf{S}_{kw} = \mathbf{S}_o + f_{kw} \bullet \mathbf{N}_k \tag{2-15}$$

Molecules and adducts were optimized with the 6-311++G(3df,3pd) basis sets of the Gaussian 03 program, unless otherwise noted.[29] The Møller-Plesset second order energy correlation (MP2) level was applied to the calculations.[30] The optimized structures were confirmed by the frequency analysis. QTAIM functions were calculated with the Gaussian 03 program[29] and analyzed by the AIM2000 program.[31] Each plot of $H_b(\boldsymbol{r}_c)$ versus $H_b(\boldsymbol{r}_c) - V_b(\boldsymbol{r}_c)/2$ for an interaction with the data of five points (w = 0, ±0.05, and ±0.1) gave a curve. The curve was analyzed using an auxiliary regression curve assuming a cubic function[32] as shown in eq (2-16). The R_c^2 values (square of correlation coefficients) were usually very good (> 0.99999). Eqs (2-17) and (2-18), necessary to evaluate eqs (2-10) and (2-11), are obtained as the derivatives of eq (2-16), where $(x, y) = (H_b(\boldsymbol{r}_c) - V_b(\boldsymbol{r}_c)/2, H_b(\boldsymbol{r}_c))$.[19]

$$y = c_o + c_1x + c_2x^2 + c_3x^3 \quad (R_c^2\text{: square of correlation coefficient}) \tag{2-16}$$

$$y' = c_1 + 2c_2x + 3c_3x^2 \tag{2-17}$$

$$y'' = 2c_2 + 6c_3x \tag{2-18}$$

While X–Y denotes a bond or an interaction of usual between X and Y, X---Y does for the very weak interaction such as the van der Waals (vdW) interaction, in this chapter. Similarly, X-∗-Y shows an atomic interaction line[1,17] with a BCP between X and Y for the *regular* CS or SS interaction, whereas A--∗--B does for the *pure* CS interaction, for convenience of discussion. NIV is explained exemplified by N=N---H–F, which is optimized to be $C_{\infty v}$. Seven internal vibrations belong to N=N---H–F. They are three starching vibrations of ν_3 (ν_{SG}: 130.6 cm^{-1}), ν_6 (ν_{SG}: 2203.5 cm^{-1}), and ν_7 (ν_{SG}: 4091.2 cm^{-1}) and four degenerated angular deformations of ν_1 and ν_2 (ν_{PI}: 99.5 cm^{-1}) and ν_4 and ν_5 (ν_{PI}: 505.7 cm^{-1}). Angular deformations were reported to affect a little on the dynamic behavior of interactions.[21] Therefore, $\mathbf{N}_3$ (corresponding to ν_3), $\mathbf{N}_6$ (ν_6), and $\mathbf{N}_7$ (ν_7) were employed for NIV. When $\mathbf{N}_3$ was chosen, f_3 = –0.053730 (eq (2-15)) satisfied w = 0.1 in eq (2-14), which resulted in wa_o = 0.052918 Å for H---N, $w'a_o$ = 0.000204 Å for N=N, and $w'a_o$ = –0.000043 Å for H–F, where $r = r_o + wa_o$ for major and $r' = r'_o + w'a_o$ for minor. Consequently, the w'/w values for H---N, N=N, and H–F were evaluated to be 1.000, 0.004, and –0.001, respectively. The displacement in H---N is largest when $\mathbf{N}_3$ (ν_3) is employed for NIV. The H---N interaction is called major and others minor in $\mathbf{N}_3$. NIV with $\mathbf{N}_6$ and $\mathbf{N}_7$ are similarly performed.

Figure 2-2 shows the plots of $H_b(\boldsymbol{r}_c)$ versus $H_b(\boldsymbol{r}_c) - V_b(\boldsymbol{r}_c)/2$ at the *pure* CS region of N-∗-N--∗--H-∗-F for the data obtained employing NIV with $\mathbf{N}_3$, $\mathbf{N}_6$, and $\mathbf{N}_7$, which correspond to major, minor, and minor interactions for N--∗--H, respectively. The process to evaluate the QTAIM parameters of (θ_p, κ_p) for N--∗--H of major is explained, next. Eq (2-19) were obtained by applying eq (2-16) to the plot for the major N--∗--H interaction shown in Figure 2-2, where $(x, y) = (H_b(\boldsymbol{r}_c) - V_b(\boldsymbol{r}_c)/2, H_b(\boldsymbol{r}_c))$. The ($\theta_p$, κ_p) values are calculated according to eqs (2-10) and (2-11) by way of the differential forms of eq (2-19) (cf: eqs (2-17) and (2-18)). Table 2-1 collects the results for

N-*-N--*--H-*-F evaluated with NIV, together with POM, which also contains the w'/w values with $\mathbf{N}_3$, $\mathbf{N}_6$, and $\mathbf{N}_7$. The treatment implies the method to choose most suitable $\mathbf{N}_k$ for an interaction. It can be determined by ν_k first, then w'/w must also be useful, especially when some candidates exist in ν_k. The choice with ν_k and w'/w makes it straightforward for an interaction in Tables 2-1 and 2-2. In the case of POM, the fixed bond is major and the optimized ones under the conditions are minor. The nature of major interactions will be discussed mainly in this chapter, although behavior of minor interactions must also supply important information about the interaction.

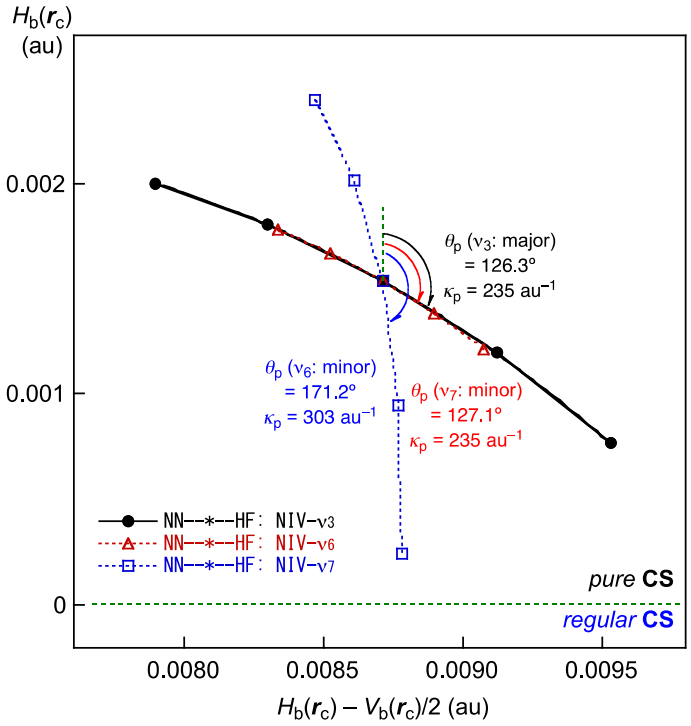

Figure 2-2. Plots of $H_b(\boldsymbol{r}_c)$ versus $H_b(\boldsymbol{r}_c) - V_b(\boldsymbol{r}_c)/2$ for the H--*--F interaction in N=N---H–F. Perturbed structures are generated by NIV with $\mathbf{N}_3$ (●), $\mathbf{N}_6$ (△), and $\mathbf{N}_7$ (□), which correspond to the major, minor, and minor interactions, respectively.

$$y = 0.00849 - 2.884x + 471.49x^2 - 26644x^3 \quad (R_c^2 = 0.99999995) \tag{2-19}$$

Table 2-1. Results of QTAIM dual functional analysis with POM and NIV applied to generate the perturbed structures of N=N---H–F[a,b]

Adduct: Method	BCP[c] (X-*-Y)	ν (cm^{-1})	k_f[d] (mdyne $Å^{-1}$)	w'/w[e]	θ_p[f] (º)	κ_p[g] (au^{-1})	Ch. of ν[h] and *f*[i]
NIV-ν_3	N--*--H	130.6	0.114	1.000	126.3	235.12	ν_{SG}: *r*(N, H)
	N--N*	*130.6*	*0.114*	*0.004*	*193.4*[j]	7.99[j]	ν_{SG}*: r(N, H)*
	H--F*	*130.6*	*0.114*	*–0.001*	*200.6*[j]	*15.35*[j]	ν_{SG}*: r(N, H)*
NIV-ν_6	N-*-N	2203.5	40.057	1.000	197.8	< 0.01	ν_{SG}: *r*(N, N)
	N----H*	*2203.5*	*40.057*	*–0.499*	*127.1*	*302.94*	ν_{SG}*: r(N, N)*
	H--F*	*2203.5*	*40.057*	*–0.003*	*197.3*[j]	*19.4*[j]	ν_{SG}*: r(N, N)*
NIV-ν_7	H-*-F[k]	4091.2	10.438	1.000	204.7	0.02	ν_{SG}: *r*(H, F)
	N----H*	*4091.2*	*10.438*	*–0.950*	*171.2*	*234.86*	ν_{SG}*: r(H, F)*
POM-a	N--*--H			1.000	126.8	239.85	*f*: *r*(N, H)
	H--F*			*–0.011*	*207.3*	*1.95*	*f: r(N, H)*
POM-b	N-*-N[l]			1.000	197.7	< 0.01	f: *r*(N, N)
	N----H*			*0.145*	*124.3*	*458.31*	*f: r(N, N)*
POM-c	H-*-F[m]			1.000	204.7	0.02	*f*: *r*(H, F)
	N----H*			*–1.081*	*168.9*	*259.89*	*f: r(H, F)*

[a] The 6-311++G(3df,3pd) basis sets being employed at the MP2 level. [b] Values are given for the major interactions in plane and the minor ones in italic: See text about the major and minor interactions. [c] Data are given for interaction at BCP, which is shown by * as in N-*-N--*--H-*-F ($C_{\infty v}$). X-*-Y shows the atomic interaction line[1] with a BCP between A and B for the regular CS and SS interactions, whereas A--*--B denotes that for the *pure* CS interactions. [d] Force constant corresponding to the frequency. [e] Ratio of w'/w where w' in $r = r_o + w'a_o$ is for the minor interaction whereas w in $r = r_o + wa_o$ for the major one. [f] See text for the definition. [g] $\kappa_p = |d^2y/dx^2| / [1 + (dy/dx)^2]^{3/2}$. [h] Main character of frequency. [i] Fixed interaction (major) in POM. [j] It may contain some error with small magnitude of w'/w. [k] w'/w (*N-*-N*) < 0.001 (data omitted). [l] w'/w (*H-*-F*) < 0.001 (data omitted). m) w'/w (*N-*-N*) ≤ 0.001 (data omitted).

Results and Discussion

Evaluation of Parameters θ_p and κ_p for Weak to Strong Interactions

The dynamic behavior of various interactions is evaluated with NIV[21] and POM.[17–19] The interactions examined are those in vdW,[33,34] hydrogen bonds (HB),[9,35] molecular complexes through charge transfer (CT-MC),[36] trihalide ions (X_3^-),[36] and trigonal bipyramidal adducts through charge transfer (CT-TBP),[36] together with classical chemical bonds of weak (Cov-w) and strong cases (Cov-s), although CT-MC, X_3^-, and CT-TBP were discussed when the concept was proposed.[21] Table 2-2 collects the results of calculations for θ_p and κ_p of the interactions in question with NIV (denoted by $\theta_{p;NIV}$ and $\kappa_{p;NIV}$, respectively), together with the frequencies (ν) and force constants (k_f). Table 2-2 also collects the θ_p and κ_p values with POM ($\theta_{p;POM}$ and $\kappa_{p;POM}$, respectively), for convenience of comparison. The θ_p and κ_p parameters represent the dynamic behavior of interactions, as mentioned above. Table 2-2 contains $H_b(\boldsymbol{r}_c) - V_b(\boldsymbol{r}_c)/2$, $H_b(\boldsymbol{r}_c)$, $k_b(\boldsymbol{r}_c)$ (= $V_b(\boldsymbol{r}_c)/G_b(\boldsymbol{r}_c)$), and ($R$, θ), which correspond to the static nature of interactions at BCP, together with the fully optimized distances for the interactions (r_o or r_o(X, Y)). Figure 2-3 shows the plots of $H_b(\boldsymbol{r}_c)$ versus $H_b(\boldsymbol{r}_c) - V_b(\boldsymbol{r}_c)/2$ for the various interactions, evaluated with NIV. The separation among the interactions seems very good. As mentioned above, the plots show spiral stream as a whole. The spiral stream is controlled by θ, of which acceptable range is $45.0^o < \theta < 206.6^o$. As shown in Table 2-2, θ_p is evaluated to be larger than θ in the plots, which means that the trend in the spiral stream appears in θ_p first then θ. Namely, the characteristic behavior of interactions appears in θ_p (the dynamic behavior) by taking in advance before it does in θ (the static behavior), when the interactions become stronger.

How are $\theta_{p;NIV}$ and $\theta_{p;POM}$ related to $\kappa_{p;NIV}$ and $\kappa_{p;POM}$, respectively? $\theta_{p;NIV}$ and $\kappa_{p;NIV}$ are compared with $\theta_{p;POM}$ and $\kappa_{p;POM}$, respectively, next, to examine the potency of NIV to generate the perturbed structures necessary to evaluate the dynamic behavior of interactions.

Table 2-2. QTAIM functions and parameters evaluated for weak to strong interactions calculated with NIV and POM methods[a,b]

No	species[c] (X-*-Y)	r_o(X, Y) (Å)	$c\nabla^2\rho_b(\boldsymbol{r}_c)$[d] (au)	$H_b(\boldsymbol{r}_c)$ (au)	$k_b(\boldsymbol{r}_c)$[e]	R (au)	θ (°)	$\theta_{p:POM}$ (°)	$\kappa_{p:POM}$ (au^{-1})
1	He--*--HF[g]	2.2454	0.0022	0.0013	–0.591	0.0025	59.9	57.2	8.50
2	Ne--*--HF[g]	2.1982	0.0050	0.0019	–0.765	0.0054	69.2	84.3	85.37
3	Ar--*--HF[g]	2.5142	0.0043	0.0020	–0.696	0.0048	65.0	76.4	162.97
4	Kr--*--HF[g]	2.6423	0.0040	0.0017	–0.722	0.0043	66.5	80.4	220.94
5	NN--*--HF[g]	2.0293	0.0087	0.0015	–0.903	0.0088	80.0	126.8	236.37
6	HF-*-HF	1.8196	0.0125	–0.0002	–1.007	0.0125	90.8	128.3	108.51
7	HCN-*-HF	1.8238	0.0107	–0.0053	–1.197	0.0120	116.1	168.6	24.21
8	H_2O-*-HOH	1.9427	0.0106	0.0005	–0.976	0.0107	87.3	123.8	156.35
9	Me_2O-*-HOH	1.8636	0.0121	–0.0021	–1.079	0.0123	99.8	148.2	87.70
10	Me_2O-*-Cl_2[g,h]	2.5513	0.0128	0.0007	–0.971	0.0128	86.8	96.4	30.91
11	Me_2O-*-Br_2[h]	2.5913	0.0123	–0.0004	–1.015	0.0123	91.8	106.6	49.64
12	Me_2S-*-Cl_2[h]	2.6331	0.0108	–0.0057	–1.207	0.0122	117.6	163.4	52.73
13	Me_2S-*-Br_2[h]	2.6923	0.0093	–0.0078	–1.296	0.0122	130.0	169.9	40.53
14	Me_2Se-*-Cl_2[h]	2.5700	0.0093	–0.0125	–1.402	0.0156	143.3	181.5	9.13
15	Me_2Se-*-Br_2[h]	2.7286	0.0078	–0.0102	–1.396	0.0128	142.7	180.1	13.49
16	[Cl-*-Cl_2]$^-$	2.2956	0.0133	–0.0220	–1.454	0.0257	149.0	181.6	10.96
17	[Br-*-Br_2]$^-$	2.5474	0.0078	–0.0185	–1.543	0.0201	157.2	183.8	7.38
18	[Cl-*-BrCl]$^-$	2.4022	0.0100	–0.0225	–1.530	0.0246	156.1	182.9	6.21
19	[Br-*-ClBr]$^-$	2.4392	0.0104	–0.0182	–1.465	0.0210	150.1	181.3	11.98
20	Me_2ClS-*-Cl[h]	2.2650	0.0046	–0.0364	–1.798	0.0367	172.8	191.7	5.31
21	Me_2BrS-*-Br[h]	2.4387	0.0048	–0.0258	–1.728	0.0262	169.4	188.5	8.31
22	Me_2ClSe-*-Cl[h]	2.3547	0.0053	–0.0335	–1.759	0.0339	171.0	184.0	0.66
23	Me_2BrSe-*-Br[h]	2.5196	0.0035	–0.0262	–1.787	0.0264	172.3	186.6	1.74
24	Me_2S^+-*-Cl[h]	1.9791	–0.0241	–0.1197	–2.673	0.1221	191.4	198.2	0.03
25	Me_2S^+-*-Br[h]	2.1433	–0.0110	–0.0798	–2.380	0.0806	187.8	193.8	0.32
26	Me_2Se^+-*-Cl[h]	2.1089	–0.0070	–0.0849	–2.197	0.0852	184.7	185.6	1.03
27	Me_2Se^+-*-Br[h]	2.2636	–0.0075	–0.0636	–2.308	0.0640	186.7	190.1	0.37
28	Cl-*-Cl	1.9845	–0.0087	–0.0985	–2.213	0.0988	185.0	194.2	0.62
29	Br-*-Br	2.2690	–0.0040	–0.0586	–2.158	0.0588	183.9	190.4	0.24
30	H_3C-*-Cl	1.7713	–0.0376	–0.1468	–3.052	0.1516	194.4	198.4	0.17
31	H_3C-*-CH_3	1.5236	–0.0718	–0.2097	–4.170	0.2216	198.9	201.1	0.07
32	H_2C-*-CH_2	1.3349	–0.1335	–0.4195	–3.754	0.4402	197.7	199.7	0.002
33	HC-*-CH	1.2107	–0.1529	–0.6048	–3.022	0.6238	194.2	196.1	0.04
34	H_3C-*-H	1.0854	–0.1265	–0.3075	–6.631	0.3325	202.4	202.3	0.12
35	H-*-H	0.7366	–0.1544	–0.3154	–49.261	0.3512	206.1	206.4	0.01

(continued)

No	species (X-*-Y)	Freq (cm^{-1})	k_f (unit[f])	$\theta_{p:NIV}$ (°)	$\kappa_{p:NIV}$ (au^{-1})	comment
1	He--*--HF[g]	69.1	0.013	57.2	8.13	vdW
2	Ne--*--HF[g]	77.6	0.047	84.3	84.79	vdW
3	Ar--*--HF[g]	70.6	0.039	76.4	161.94	vdW
4	Kr--*--HF[g]	64.0	0.029	80.3	219.23	vdW
5	NN--*--HF[g]	130.6	0.114	126.3	235.13	HB
6	HF-*-HF	166.9	0.081	128.5	103.33	HB
7	HCN-*-HF	191.5	0.203	167.7	21.60	HB
8	H_2O-*-HOH	188.1	0.043	116.7	158.13	HB
9	Me_2O-*-HOH	176.6	0.052	146.4	89.37	HB
10	Me_2O-*-Cl_2[g,h]	118.0	0.070	98.6	35.54	CT-MC
11	Me_2O-*-Br_2[h]	100.5	0.037	111.7	59.42	CT-MC
12	Me_2S-*-Cl_2[h]	104.4	0.044	162.8	51.24	CT-MC
13	Me_2S-*-Br_2[h]	114.9	0.059	171.5	33.00	CT-MC
14	Me_2Se-*-Cl_2[h]	123.5	0.058	182.3	14.47	CT-MC
15	Me_2Se-*-Br_2[h]	108.8	0.078	181.0	13.82	CT-MC
16	[Cl-*-Cl_2]$^-$	292.5	1.763	180.2	23.75	X_3^-
17	[Br-*-Br_2]$^-$	198.9	1.840	186.5	6.33	X_3^-
18	[Cl-*-BrCl]$^-$	248.3	1.721	185.2	5.58	X_3^-
19	[Br-*-ClBr]$^-$	271.5	1.689	183.4	10.74	X_3^-
20	Me_2ClS-*-Cl[h]	334.6	0.389	192.8	4.84	CT-TBP
21	Me_2BrS-*-Br[h]	358.5	0.294	188.9	2.89	CT-TBP
22	Me_2ClSe-*-Cl[h]	307.8	0.366	186.3	0.57	CT-TBP
23	Me_2BrSe-*-Br[h]	233.4	0.946	189.0	1.95	CT-TBP
24	Me_2S^+-*-Cl[h]	565.4	2.456	198.2	0.16	Cov-w
25	Me_2S^+-*-Br[h]	450.9	1.450	193.7	0.31	Cov-w
26	Me_2Se^+-*-Cl[h]	465.8	4.625	185.6	1.14	Cov-w
27	Me_2Se^+-*-Br[h]	337.8	2.952	190.0	0.37	Cov-w
28	Cl-*-Cl	577.8	6.878	194.2	0.64	Cov-w
29	Br-*-Br	342.7	5.460	190.9	0.27	Cov-w
30	H_3C-*-Cl	779.0	2.509	198.3	0.19	Cov-s
31	H_3C-*-CH_3	1435.0	1.540	202.6	0.54	Cov-s
32	H_2C-*-CH_2	1680.2	4.708	199.4	0.05	Cov-s
33	HC-*-CH	1968.5	9.214	195.9	0.06	Cov-s
34	H_3C-*-H	3203.6	6.660	202.5	0.12	Cov-s
35	H-*-H	4517.6	12.119	206.4	0.01	Cov-s

[a] Calculated with the 6-311++G(3df,3pd) basis sets at the MP2 level. [b] See also ref. 18. [c] Data are given for interaction at BCP, which is shown by * as in He--*--HF ($C_{\infty v}$). [d] $c = \hbar^2/8m$. [e] $k_b(\boldsymbol{r}_c) = V_b(\boldsymbol{r}_c)/G_b(\boldsymbol{r}_c)$. [f] mDyne $Å^{-1}$. [g] An interaction with a BCP denoted by --*-- stands for the *pure* CS interaction, while -*- for the regular CS or SS interaction. [h] The 6-311+G(3d,2p) basis sets being employed only for C and H in CH_3. See also ref. 21.

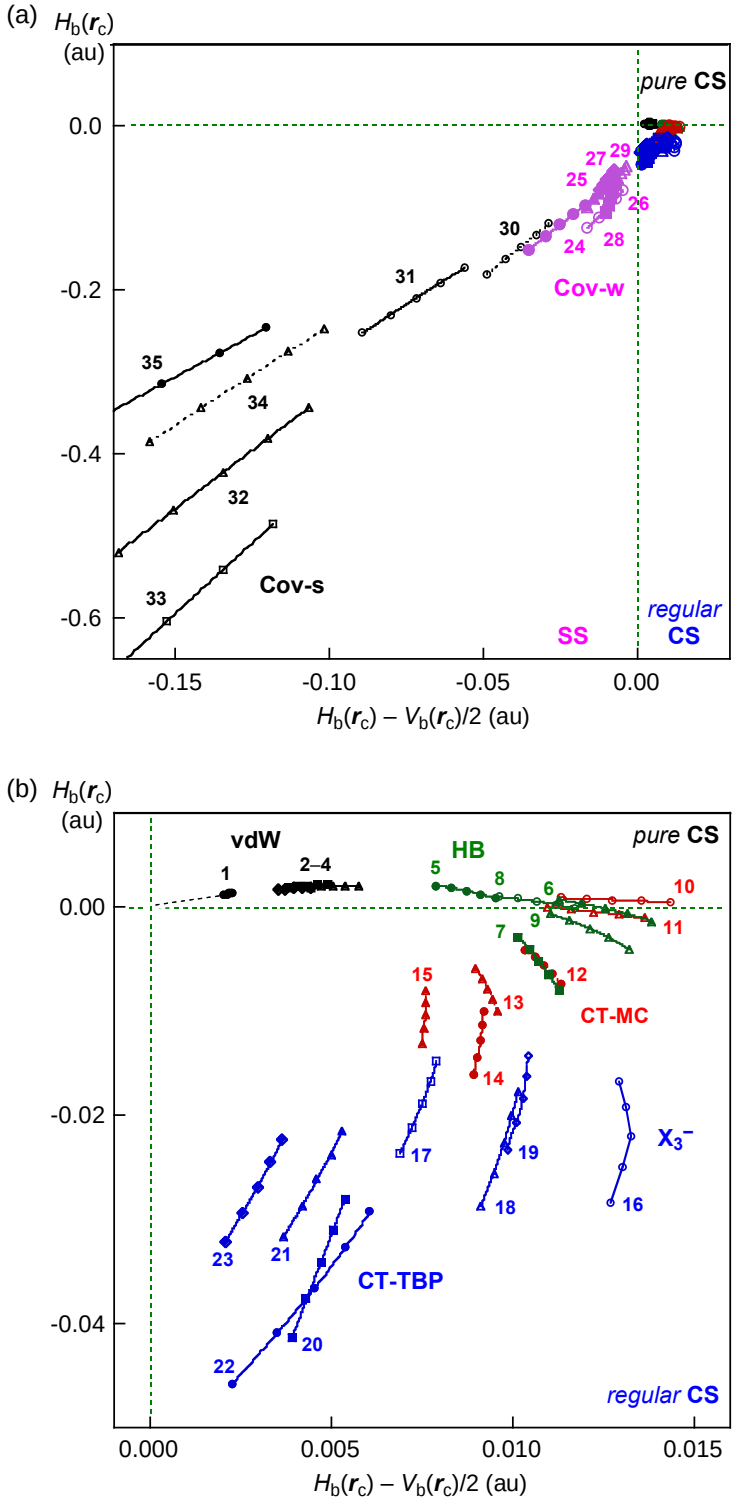

Figure 2-3. Plots of $H_b(\boldsymbol{r}_c)$ versus $H_b(\boldsymbol{r}_c) - V_b(\boldsymbol{r}_c)/2$ for the vdW, HB, and CT-MC, X_3^-, CT-TBP, Cov-w, and Cov-s interactions: (a) Whole picture and (b) magnified one. Numbers for the interactions are the same as those in Table 2-1.

Applicability of NIV to Wide Range of Interactions.

Figures 2-4 and 2-5 show the plots of $\theta_{p;NIV}$ versus $\theta_{p;POM}$ and $\kappa_{p;NIV}$ versus $\kappa_{p;POM}$, respectively. Correlations for the plots are very good, although a few data deviate slightly from the correlations. Eqs (2-20) and (2-21) show the correlations, respectively, analyzed assuming the linear correlation of $y = ax + b$ (a and b are the correlation constant and y-intercept, respectively) with R_c^2 of the square of correlation coefficient. The a values of the correlations are very close to 1.00, as demonstrated by eqs (2-20) and (2-21), which means that $\theta_{p;NIV}$ and $\kappa_{p;NIV}$ are inherently the same as the corresponding $\theta_{p;POM}$ and $\kappa_{p;POM}$, respectively, for the usual interactions in Table 2-2.

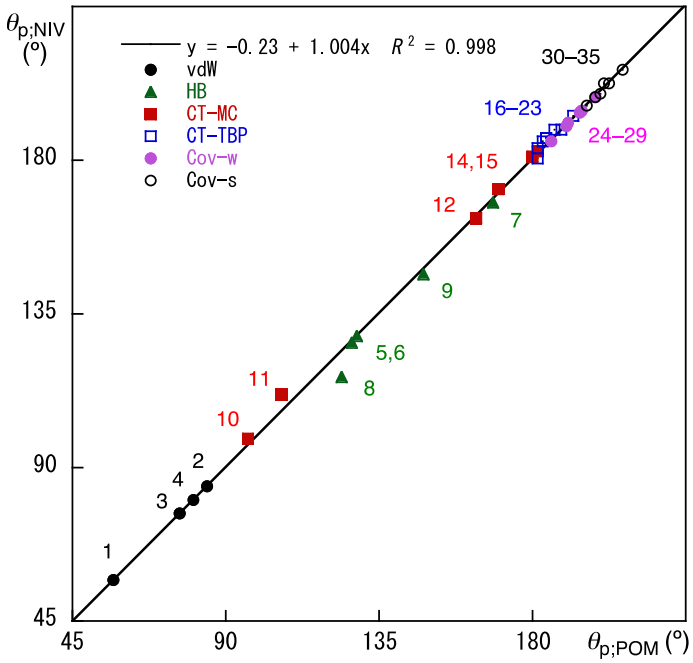

Figure 2-4. Plot of $\theta_{p;NIV}$ versus $\theta_{p;POM}$ for various interactions: Numbers for the data are the same as those in Table 2-1.

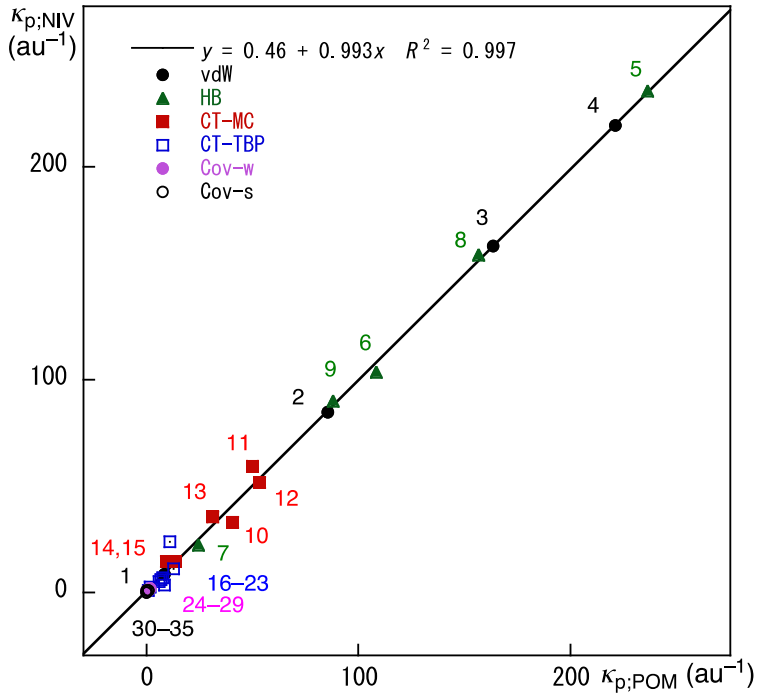

Figure 2-5. Plot of $\kappa_{p;NIV}$ versus $\kappa_{p;POM}$ for various interactions: Numbers for the data are the same as those in Table 2-1.

$$\theta_{p;NIV} = 1.004\,\theta_{p;POM} - 0.23 \qquad (R_c^2 = 0.998) \qquad (2\text{-}20)$$

$$\kappa_{p;NIV} = 0.993\,\kappa_{p;POM} + 0.46 \qquad (R_c^2 = 0.997) \qquad (2\text{-}21)$$

As mentioned above, NIV is closely related to the quantified adiabatic process, whereas POM must be closely related to the thermal process. Consequently, the deviation would occur due to the differences in the unique situation between the perturbed structures. He must be careful when the deviations are examined, since the parameters evaluated with NIV and POM have own intrinsic meanings under given conditions, even if some deviations are observed between those evaluated with NIV and POM.

What differences are observed in θ_p and κ_p when evaluated with NIV and POM? The differences in θ_p ($\Delta\theta_p = \theta_{p;NIV} - \theta_{p;POM}$) are –1.8 to 2.7º, except for H_2O-*-HOH of –7.1º and Me_2O-*-Br_2 (MC) of 5.1º. However, the deviation is not particular for HB, since the differences are small for NN--*--HF ($\Delta\theta_p$ = –0.5º), HF-*-HF ($\Delta\theta_p$ = 0.2º), HCN-*-HF ($\Delta\theta_p$ = –0.9º), Me_2O-*-HOH

($\Delta\theta_p = -1.8^o$). An internal motion in H_2O-∗-HOH seems to mix easily with other motions in the H_2O dimer, which may arise the deviation. In the case of the MC adducts, the $\Delta\theta_p$ values are small for Me_2O-∗-Cl_2 (MC: $\Delta\theta_p = 2.2^o$), Me_2S-∗-Cl_2 (MC: -0.6^o), Me_2S-∗-Br_2 (MC: 1.6^o), Me_2Se-∗-Cl_2 (MC: 0.8^o), and Me_2Se-∗-Br_2 (MC: 0.9^o). The magnitudes of $\Delta\theta_p$ must be small if the internal vibration is well located on the interaction in question. The internal frequency employed to evaluate $\theta_{p;NIV}$ in Me_2O-∗-Br_2 (MC) (ν_3 (A') = 100.5 cm^{-1}) would not be enough located on O-∗-Br, although it must be best among the NIVs.

The $\kappa_{p;NIV}$ values are also very close to $\kappa_{p;POM}$. The differences ($\Delta\kappa_p = \kappa_{p;NIV} - \kappa_{p;POM}$) are within ±2 au^{-1} for the interactions. The $\Delta\kappa_p$ values beyond the limit are predicted for Ar--∗--HF ($\Delta\kappa_p$ = 15.4 au^{-1}), HF-∗-HF ($\Delta\kappa_p = -5.2$ au^{-1}), HCN-∗-HF ($\Delta\kappa_p = -2.6$ au^{-1}), Me_2O-∗-Cl_2 (MC: $\Delta\kappa_p$ = 4.6 au^{-1}), Me_2O-∗-Br_2 (MC: 9.8 au^{-1}), Me_2S-∗-Br_2 (MC: -7.5 au^{-1}), Me_2Se-∗-Cl_2 (MC: 5.3 au^{-1}), and Me_2BrS-∗-Br (TBP: -5.4 au^{-1}), although those for Me_2Se-∗-Br_2 (MC: 0.3 au^{-1}) and Me_2BrSe-∗-Br (TBP: 0.2 au^{-1}) are very small. Large deviations in κ_p usually occur for the adducts of which $\kappa_{p;NIV}$ are large, as shown by Ar--∗--HF ($\Delta\kappa_p$ = 15.4 au^{-1} with $\kappa_{p;NIV}$ = 178.4 au^{-1}), Me_2O-∗-Br_2 (MC: $\Delta\kappa_p$ = 9.8 au^{-1} with $\kappa_{p;NIV}$ = 59.4 au^{-1}) and Me_2S-∗-Br_2 (MC: $\Delta\kappa_p = -7.5$ au^{-1} with $\kappa_{p;NIV}$ = 33.0 au^{-1}). The results show that κ_p are affected more easily by the change in the perturbed structures, relative to the case of θ_p, and magnitudes of $\Delta\kappa_p$ seem large for large κ_p.

After confirmation of the very good applicability of NIV to generate the perturbed structures to evaluate the dynamic behaviors of interactions, next extension is to clarify the characteristic feature in the plots of $H_b(\boldsymbol{r}_c)$ versus $H_b(\boldsymbol{r}_c) - V_b(\boldsymbol{r}_c)/2$ in relation to the treatment.

Characteristic Feature in the plots of $H_b(\boldsymbol{r}_c)$ versus $H_b(\boldsymbol{r}_c) - V_b(\boldsymbol{r}_c)/2$

Plots of $H_b(\boldsymbol{r}_c)$ versus $H_b(\boldsymbol{r}_c) - V_b(\boldsymbol{r}_c)/2$ start substantially from the origin at $(x, y) = (H_b(\boldsymbol{r}_c) - V_b(\boldsymbol{r}_c)/2, H_b(\boldsymbol{r}_c)) = (0, 0)$, where no interactions must be detected with very long interaction distances. The plots go upwards due to the increase of $H_b(\boldsymbol{r}_c) - V_b(\boldsymbol{r}_c)/2$ and $H_b(\boldsymbol{r}_c)$ by the shortening of the interaction distances, where $\theta_p \geq \theta \geq 45^o$. They become maximum at the maximum $H_b(\boldsymbol{r}_c)$, where θ_p

= 90º > θ. The plots bend at θ_p = 90º as $H_b(\boldsymbol{r}_c)$ decrease while $H_b(\boldsymbol{r}_c) - V_b(\boldsymbol{r}_c)/2$ increase further. His research group calls this characteristic point the first bending point (BP-1). A border area between the typical vdW and HB interactions seems to exist around BP-1 (*cf*: Figure 2-3). The plots go across the *x*-intercepts ($H_b(\boldsymbol{r}_c)$ = 0; θ = 90º) and reach the second bending point (BP-2), where $H_b(\boldsymbol{r}_c) - V_b(\boldsymbol{r}_c)/2$ are maxima with θ_p = 180º. Plots go downwards drawing the spiral stream to the right after BP-2 as $H_b(\boldsymbol{r}_c)$ and $H_b(\boldsymbol{r}_c) - V_b(\boldsymbol{r}_c)/2$ decrease. Both $H_b(\boldsymbol{r}_c)$ and $H_b(\boldsymbol{r}_c) - V_b(\boldsymbol{r}_c)/2$ become negative after the *y*-intercept where $H_b(\boldsymbol{r}_c) - V_b(\boldsymbol{r}_c)/2$ = 0 (θ = 180º).

As mentioned above, data of vdW interactions appear in the area of 45º < θ_p < 90º in the first quadrant (see Figure 2-3). The θ value is estimated to be about 70º for θ_p = 90º for the data in Table 2-2. Data for typical HB and CT-MC appear next region of 90º < θ_p < 180º in the first and forth quadrants, although 90º < θ for typical CT-MC. While θ_p is estimated to be around 125º when θ = 90º, θ seems around 150º when θ_p = 180º for the data in Table 2-2. Namely, data for typical HB appear in rough ranges of 70º < θ < 150º and 90º < θ_p < 180º, whereas those for typical CT-MC drop in rough ranges of 90º < θ < 150º and 125º < θ_p < 180º. Similarly, CT-TBP, containing X_3^-, appear in the range of 150º < θ < 180º (forth quadrant), where the range for θ_p is roughly corresponds to 180º < θ_p < 190º. The classical chemical bonds of SS appear in the final range of 180º < θ < 206.6º (third quadrant), where 190º < θ_p < 206.0º, in usual. Indeed, θ must be less than 206.6º, but θ_p would be accidentally larger than 206.6º for the minor interactions. θ_p of 207.3º is predicted for the minor H-∗-F interaction of N=N---H–F when POM is applied to N--∗--H as the major interaction. It is worthwhile to comment that a parameter *k* (= $V_b(\boldsymbol{r}_c)/G_b(\boldsymbol{r}_c)$: eq (2-7)) is also serve as a good measure to classify the interactions. While *k* = 0, –1, –2, and –∞ correspond to θ = 45º, 90º, 180º, and 206.6º, respectively, the *k* values are roughly estimated to be around –0.9 and –1.4 for θ_p = 90º and 180º, respectively. Scheme 2-3 is the same as Scheme 1-2 that summarizes the classification of interactions with θ and θ_p. The role of *k* is also drawn in Scheme 2-3.

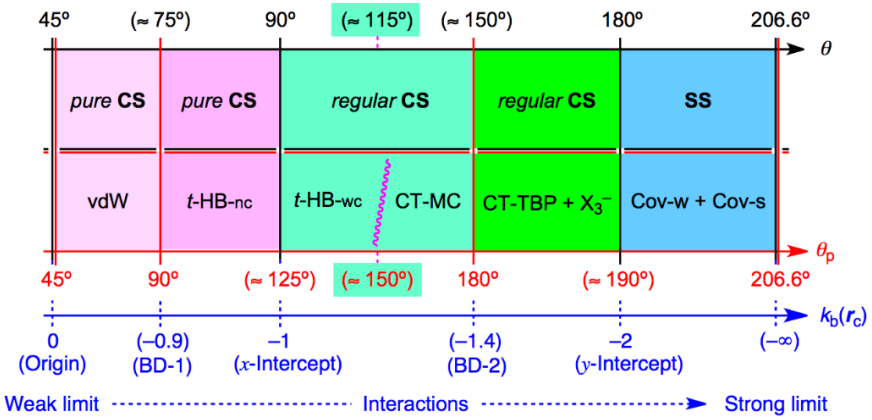

Scheme 2-3. Rough classification of interactions by θ and θ_p, together with $k_b(\boldsymbol{r}_c)$ (= $V_b(\boldsymbol{r}_c)/G_b(\boldsymbol{r}_c)$). The border area between Cov-w and Cov-s seems R of around 0.15 au.

Influence from Minor Interactions

How do the minor interactions affect on the major ones? The ratio of w'/w must be a measure for the magnitudes of the mutual influence between the two interactions. The influence is examined employing Br_3^-, H_2SeBr_2 (TBP), and Me_2ZX_2 (TBP) where X = Cl and Br and Z = S and Se. Table 2-3 summarizes the $\theta_{p;NIV}$ values evaluated under the symmetric and anti-symmetric modes ($\theta_{p;NIV}$ (ν_s) and $\theta_{p;NIV}$ (ν_{as}), respectively) and $\theta_{p;POM}$, together with the corresponding w'/w values. The w'/w values must be 1.000 and –1.000 for ν_s and ν_{as}, respectively, with NIV, as shown in Table 2-3. On the other hand, the values of w'/w will be determined differently with POM. Figure 2-6 shows the plots of θ_p (major) versus w'/w, shown in Table 2-3. The correlations are given in entries 1–6 in Table 2-4.[37]

Table 2-3. Evaluated $\theta_{p:POM}$, $\theta_{p:NIV}$ (ν_s), and $\theta_{p:NIV}$ (ν_{as}) values for Br_3^-, H_2SeBr_2 (TBP), and Me_2ZX_2 (TBP: X = Cl and Br; Z = S and Se), together with the corresponding w'/w values

Species (Sym)	$\theta_{p:POM}$	(w'/w)	$\theta_{p:NIV}$ (ν_s)	(w'/w)	$\theta_{p:NIV}$ (ν_{as})	(w'/w)
[Br-*-Br-*-Br]$^-$ ($C_{\infty v}$)	184.2	(–0.357)	180.1	(1.000)	186.1	(–1.000)
Br-*-(H_2)Se-*-Br (C_{2v})	187.7	(–0.181)	185.9	(1.000)	188.9	(–1.000)
Cl-*-(Me_2)S-*-Cl (C_{2v})	191.7	(–0.340)	190.0	(1.000)	192.8	(–1.000)
Br-*-(Me_2)S-*-Br (C_{2v})	188.5	(–0.272)	188.3	(1.000)	188.9	(–1.000)
Cl-*-(Me_2)Se-*-Cl (C_{2v})	184.0	(–0.306)	180.2	(1.000)	186.3	(–1.000)
Br-*-(Me_2)Se-*-Br (C_{2v})	186.6	(–0.280)	183.7	(1.000)	189.0	(–1.000)

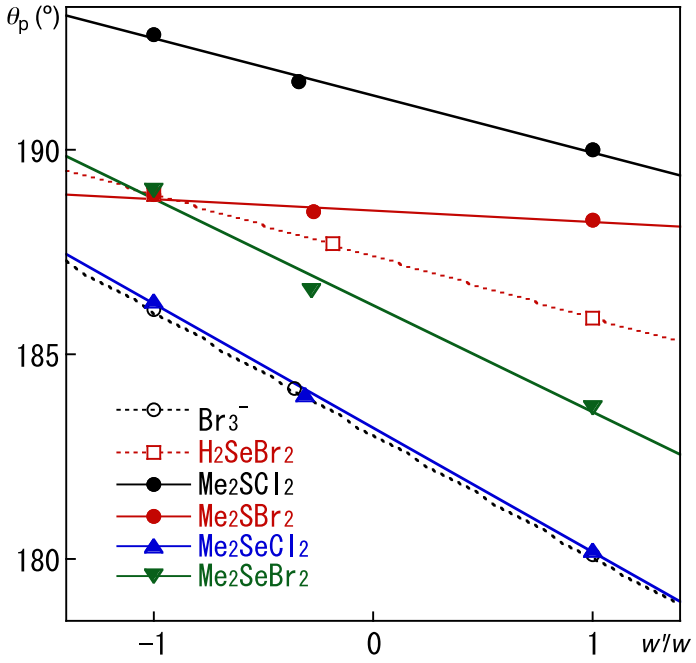

Figure 2-6. Plots of θ_p versus w'/w for Br_3^- and some CT-TBPs.

Table 2-4. Correlations for θ_p versus w'/w for Br_3^- and some CT-TBPs[a]

Entry	a	b	R_c^2	n	Correlation for
1	–3.003	183.1	1.0000	3	Br_3^-
2	–1.502	187.4	0.9999	3	H_2SeBr_2 (TBP)
3	–1.381	191.3	0.995	3	Me_2SCl_2 (TBP)
4	–0.284	188.5	0.885	3	Me_2SBr_2 (TBP)
5	–3.032	183.2	0.999	3	Me_2SeCl_2 (TBP)
6	–2.605	186.2	0.989	3	Me_2SeBr_2 (TBP)

[a] The constants (a, b, R_c^2) are the correlation constant, the y-intercept, and the square of correlation coefficient, respectively, in $y = ax + b$.

The correlations are excellent for Br_3^- and H_2SeBr_2 (TBP) ($R_c^2 > 0.9999$: entries 1 and 2 in Table 2-4). The results demonstrate that θ_p (major) are exactly and almost exactly proportional to w'/w ($-1 < w'/w < 1$) for Br_3^- and H_2SeBr_2 (TBP). In the case of Me_2ZX_2, the correlations are also very good for Me_2SCl_2 (TBP) and Me_2SeCl_2 (TBP) ($R_c^2 > 0.995$: entries 3 and 5 in Table 2-3) and they become (slightly) worse for Me_2SeBr_2 (TBP) ($R_c^2 = 0.989$: entry 6 in Table 2-2) and Me_2SBr_2

(TBP) (R_c^2 = 0.885: entry 4 in Table 2-2). The results may show that two methyl groups in Me_2ZX_2 also affect on θ_p (major), relative to the case of H_2SeBr_2 (TBP). It is noteworthy that the correlations for Me_2ZCl_2 (TBP: Z = S and Se) are better than those for Me_2ZBr_2 (TBP: Z = S and Se), where the Cl–Z–Cl 3c–4e bonds of the former must be stronger than the Br–Z–Br 3c–4e in the latter. The small correlation constant of a (= –0.284) for Me_2SBr_2 (TBP) must also be responsible for the smaller R_c^2 value of 0.885. Minor interactions are demonstrated to influence on the major ones depending on w'/w. The results show that differences in w'/w between NIV and POM must be responsible for the deviations between the two cases. However, a larger deviation would occur when the internal vibration is not well located on the interaction in question. Nevertheless, magnitudes of the differences are usually less than 2º. Therefore, $\theta_{p;NIV}$ are essentially recognized as the same as the corresponding $\theta_{p;POM}$, and so are $\kappa_{p;NIV}$ as $\kappa_{p;POM}$. Therefore, NIV can be applied for usual interactions in wide range of molecules and adducts. The deviation would be the sign from the unique situation of the interaction. He recommends that the set of ($\theta_{p;NIV}$, $\kappa_{p;NIV}$) from ν_{as} should be selected when two sets of ($\theta_{p;NIV}$, $\kappa_{p;NIV}$) are obtained for X–Z–C 3c–4e of the C_{2v} symmetry depending on ν_s and ν_{as}, since the set from ν_{as} must be closer to those with POM.

It is well demonstrated that NIV is applicable to wide range of usual interactions in weak to strong interactions, as well as POM. However, POM may contain some difficulties to generate the perturbed structures necessary to evaluate the dynamic behavior of interactions in some cases. They would be the mutual influence system surrounded by lots of interactions in polycyclic compounds, multi hydrogen-bonded systems, or extended hypervalent bonds. The perturbed structures around TS (transition states) with POM must be substantially different from those predicted by IRC[38] (intrinsic reaction coordinates). NIV will be superior to POM in such cases.

Summary

The dynamic behavior of interactions must be very important, as well as the static one, for the better understanding of interactions in molecules and adducts. Perturbed structures around a fully

optimized structure are necessary to evaluate the dynamic nature. Normal coordinates of internal vibrations (NIV) are proposed to generate the perturbed structures in wide range of weak to strong interactions. POM (partial optimization method) are also applied if the perturbed structures are well obtained. Plots of $H_b(\boldsymbol{r}_c)$ versus $H_b(\boldsymbol{r}_c) - V_b(\boldsymbol{r}_c)/2$ at BCPs must be very useful, since the method incorporates the classification of interactions by signs of $\nabla^2\rho_b(\boldsymbol{r}_c)$ and $H_b(\boldsymbol{r}_c)$ where $H_b(\boldsymbol{r}_c) - V_b(\boldsymbol{r}_c)/2 = (\hbar^2/8m)\nabla^2\rho_b(\boldsymbol{r}_c)$. The plots are analyzed using the polar (R, θ) representation. Only θ in (R, θ) is enough for the classification by signs of $\nabla^2\rho_b(\boldsymbol{r}_c)$ and $H_b(\boldsymbol{r}_c)$. QTAIM parameters of (θ_p, κ_p) are introduced to evaluate the dynamic behavior of interactions: θ_p corresponds to the tangent line measured from the y-direction and κ_p is the curvature of the plot at BCP of the full-optimized structure. NIV is demonstrated to be applicable to usual interactions, as well as POM. The $\theta_{p;NIV}$ and $\kappa_{p;NIV}$ values are substantially equal to $\theta_{p;POM}$ and $\kappa_{p;POM}$, respectively. The differences in $\theta_{p;NIV}$ and $\theta_{p;POM}$ are within around ±2° and those in $\kappa_{p;NIV}$ and $\kappa_{p;POM}$ are within around ±2 au^{-1}, respectively, for usual interactions. Relatively large deviations would occur when the internal vibration is not well located on the interaction in question and/or the perturbation from the minor interaction to the major one becomes larger, which is estimated by the w'/w ratios. The method will help to analyze, evaluate, and classify the nature of chemical bonds and interactions. More complex interaction systems will be analyzed by the QTAIM dual functional analysis with NIV, on the basis established in this work.

References

1 a) *Atoms in Molecules. A Quantum Theory*, ed. by R. F. W. Bader, Oxford University Press, Oxford, UK, **1990**; b) *An Introduction to the Quantum Theory of Atoms in Molecules In The Quantum Theory of Atoms in Molecules: From Solid State to DNA and Drug Design*, ed. by C. F. Matta, R. J. Boyd, WILEY-VCH, Weinheim, Germany, **2007**.

2 a) R. F. W. Bader, T. S. Slee. D. Cremer, E. Kraka, *J. Am. Chem. Soc.* **1983**, *105*, 5061–5068; b) R. F. W. Bader, *Chem. Res.* **1991**, *91*, 893–926; c) R. F. W. Bader, *J. Phys. Chem. A* **1998**, *102*, 7314–7323; d) F. Biegler-König, R. F. W. Bader, T. H. Tang, *J. Comput. Chem.* **1982**, *3*, 317–328; e) R. F. W. Bader, *Acc. Chem. Res.* **1985**, *18*, 9–15; f) T. H. Tang, R. F. W. Bader, P. MacDougall, *Inorg. Chem.* **1985**, *24*, 2047–2053; g) F. Biegler-König, J. Schönbohm, D. Bayles, *J. Comput. Chem*. **2001**, *22*, 545–559; h) F. Biegler-König, J. Schönbohm, *J. Comput. Chem.* **2002**, *23*, 1489–1494.

3 J. Molina, J. A. Dobado, *Theor. Chem. Acc.* **2001**, *105*, 328–337.

4 J. A. Dobado, H. Martinez-Garcia, J. Molina, M. R. Sundberg, *J. Am. Chem. Soc.* **2000**, *122*, 1144–1149.

5 S. K. Ignatov, N. H. Rees, B. R. Tyrrell, S. R. Dubberley, A. G. Razuvaev, P. Mountford, G. I. Nikonov, *Chem. Eur. J.* **2004**, *10*, 4991–4999.

6 S. K. Tripathi, U. Patel, D. Roy, R. B. Sunoj, H. B. Singh, G. Wolmershäuser, R. J. Butcher, *J. Org. Chem.* **2005**, *70*, 9237–9247.

7 R. J. Boyd, S. C. Choi, *Chem. Phys. Lett.* **1986**, *129*, 62–65.

8 M. T. Carroll, R. F. W. Bader, *Mol. Phys.* **1988**, *65*, 695–722.

9 E. Espinosa, E. Molins, C. Lecomte, *Chem. Phys. Lett.* **1998**, *285*, 170–173.

10 S. J. Grabowski, *J. Phys. Chem. A* **2001**, *105*, 10739–10746.

11 a) E. Espinosa, I. Alkorta, J. Elguero, E. Molins, *J. Chem. Phys.* **2002**, *117*, 5529–5542; b) I. Rozas, I. Alkorta, J. Elguero, *J. Am. Chem. Soc.* **2000**, *122*, 11154–11161.

12 M. Domagała, S. Grabowski, K. Urbaniak, G. Mloston, *J. Phys. Chem. A* **2003**, *107*, 2730–2736.

13 S. Grabowski, W. A. Sokalski, J. Leszczynski, *J. Phys. Chem. A* **2005**, *109*, 4331–4341.

14 M. Domagala, S. Grabowski, *J. Phys. Chem. A* **2005**, *109*, 5683–5688.

15 The bond order (BO), which corresponds to the strength of a chemical bond, is correlated to $\rho_b(\boldsymbol{r}_c)$ by the form shown below, where A and B are constants which depend on the nature of the bonded atoms.[1b] BO = $\exp[A\rho_b(\boldsymbol{r}_c) - B]$.

16 W. Nakanishi, T. Nakamoto, S. Hayashi, T. Sasamori, N. Tokitoh, *Chem. Eur. J.* **2007**, *13*, 255–268.

17 W. Nakanishi, S. Hayashi, K. Narahara, *J. Phys. Chem. A* **2008**, *112*, 13593–13599.

18 W. Nakanishi, S. Hayashi, K. Narahara, *J. Phys. Chem. A* **2009**, *113*, 10050–10057.

19 W. Nakanishi, S. Hayashi, *Curr. Org. Chem.* **2010**, *14*, 181–197.

20 K. T. Potts, J. Kane, *J. Org. Chem.* **1974**, *39*, 3783–3785.

21 W. Nakanishi, S. Hayashi, *J. Phys. Chem. A* **2010**, *114*, 7423–7430.

22 C. F. Matta, R. J. Boyd, *An Introduction to the Quantum Theory of Atoms in Molecules In The Quantum Theory of Atoms in Molecules: From Solid State to DNA and Drug Design*, ed. by C. F. Matta, R. J. Boyd, WILEY-VCH, Weinheim, Germany, **2007**, Chap. 1, p. 13.

23 V. G. Tsirelson, "Interpretation of Experimental Electron Densities by Combination of the QTAMC and DFT" In *The Quantum Theory of Atoms in Molecules: From Solid State to DNA and Drug Design*, ed. by C. F. Matta, R. J. Boyd, Wiley-VCH: Weinheim, Germany, **2007**, Chap. 10, p. 263. See also, J. P. Perdew, S. Kurth, "Density Functionals for Non-relativistic Coulomb Systems in the New Century" In *A Primer in Density Functional Theory (Lecture Notes in Physics*; Fiolhais, C.; Nogueira, F.; Marques, M., Eds.; Springer, Berlin, Heidelberg, **2003**, *620*, 1–55; D. A. Kirzhnitz, *Sov, Phys*. *JETP* **1957**, *5*, 64–72.

24 W. Nakanishi, S. Hayashi, M. B. Pitak, M. B. Hursthouse, S. J. Coles, *J. Phys. Chem. A* **2011**, *115*, 11775−11787.

25 The origin of the plot corresponds to those without any interactions at BCPs, where $V_b(\boldsymbol{r}_c) = G_b(\boldsymbol{r}_c) = 0$.

26 For the $m \times n$ matrix representation, m corresponds to the number of atoms and n (= 3) to the x, y, and z components of the space.

27 The values of w = (0), ±0.1, and ±0.2 in $r = r_o + wa_o$ were employed for the perturbed structures in POM in refs. 18, 19, since the bond orders becomes 2/3 and 3/2 times larger at w = +0.2 and –0.2 relative to the original values at w = 0, respectively. However, it seems better to employ the perturbed structures as close as possible to the fully optimized ones in NIV. The perturbed structures closer to the fully optimized one will reduce the errors in the QTAIM functions with the perturbed structures generated by NIV and/or POM. Therefore, w = (0), ±0.05, and ±0.1 for $r = r_o + wa_o$ are employed for the analysis in this chapter. Similarly, it is recommended that w = (0), ±0.025, and ±0.05 for $\theta_s = \theta_{so} + wb_o$ are applied to the perturbed structures when the effect from the angular deformations are discussed, since $\pm 0.1 b_o$ ($\approx \pm 5.73^o$ with $b_o = 180^o/\pi \approx 57.30^o$) would be too large as the perturbations of angles.

28 It is achieved by changing the corresponding parameters in Gaussian 03 from the default values to print out the normal coordinates of five digits for the purpose.

29 *Gaussian 03 (Revision D.05)*, M. J. Frisch, G. W. Trucks, H. B. Schlegel, G. E. Scuseria, M. A. Robb, J. R. Cheeseman, J. A. Montgomery, Jr., T. Vreven, K. N. Kudin, J. C. Burant, J. M. Millam, S. S. Iyengar, J. Tomasi, V. Barone, B. Mennucci, M. Cossi, G. Scalmani, N. Rega, G. A. Petersson, H. Nakatsuji, M. Hada, M. Ehara, K. Toyota, R. Fukuda, J. Hasegawa, M. Ishida, T. Nakajima, Y. Honda, O. Kitao, H. Nakai, M. Klene, X. Li, J. E. Knox, H. P. Hratchian, J. B. Cross, V. Bakken, C. Adamo, J. Jaramillo, R. Gomperts, R. E. Stratmann, O. Yazyev, A. J. Austin, R. Cammi, C. Pomelli, J. W. Ochterski, P. Y. Ayala, K. Morokuma, G. A. Voth, P. Salvador, J. J. Dannenberg, V. G. Zakrzewski, S. Dapprich, A. D. Daniels, M. C. Strain, O. Farkas, D. K. Malick, A. D. Rabuck, K. Raghavachari, J. B. Foresman, J. V. Ortiz, Q. Cui, A. G. Baboul, S. Clifford, J. Cioslowski, B. B. Stefanov, G. Liu, A. Liashenko, P. Piskorz, I.

Komaromi, R. L. Martin, D. J. Fox, T. Keith, M. A. Al-Laham, C. Y. Peng, A. Nanayakkara, M. Challacombe, P. M. W. Gill, B. Johnson, W. Chen, M. W. Wong, C. Gonzalez and J. A. Pople, Gaussian, Inc., Pittsburgh PA, 2004.

30 C. Møller, M. S. Plesset, *Phys. Rev.* **1934**, *46*, 618–622; J. Gauss, *J. Chem. Phys.* **1993**, *99*, 3629–3643; J. Gauss, *Ber. Bunsenges, Phys. Chem.* **1995**, *99*, 1001–1008.

31 The AIM2000 program (Version 2.0) is employed to analyze and visualize atoms-in-molecules: F. Biegler-König, *J. Comput. Chem.* **2000**, *21*, 1040–1048; see also ref. 2g.

32 Indeed, fourth functions can be applied to the five points in a plot, but fourth functions may show an irregular behavior with five points in some cases. Therefore, a regression curve of cubic functions would be more suitable as applied in the text, since the calculation errors in the data will be processed suitably.

33 *Molecular Interactions. From van der Waals to Strongly Bound Complexes*, ed. by S. Scheiner, Wiley, New York, **1997**. For example, A. van der Avoird, P. E. S. Wormer, R. Moszynski, *Theory and Computation of Vibration, Rotation and Tunneling Motions of Van der Waals Complexes and their Spectra*, in Chapter 4; J. E. Del Bene, L. Shavitt, *The Quest for Reliability in Calculated Properties of Hydrogen-bonded Complexes,* in Chapter 5; and T. A. Ford, *Ab Initio Predictions of the Vibrational Spectra of Some Molecular Complexes: Comparison with Experiment,* in Chapter 6. See also other chapters.

34 For van der Waals interactions, see C. E. H. Dessent, K. Müller-Dethlefs, *Chem. Rev.* **2000**, *100*, 3999–4021; P. E. S. Wormer, A. van der Avoird, *Chem. Rev.* **2000**, *100*, 4109–4143.

35 a) *Hydrogen Bonding – A Theoretical Perspective*, ed. by S. Scheiner, Oxford University. Press, New York, **1997**; b) *The Weak Hydrogen Bond in Structural Chemistry and Biology; International Union of Crystallography Monographs on Crystallography*, ed. by G. R. Desiraju, T. Steiner, Oxford University Press, New York, **1999**; c) M. Nishio, *Cryst. Eng. Commun.* **2004**, *6*, 130–158; d) E. Espinosa, M. Souhassou, H. Lachekar, C. Lecomte. *Acta Crystallogr. B*, **1999**, *55*, 563–572; e) E. Espinosa, C. Lecomte, E. Molins. *Chem. Phys. Lett.*

1999, *300*, 745–748; f) E. Espinosa, I. Alkorta, I. Rozas, J. Elguero, E. Molins, *Chem. Phys. Lett.* **2001**, *336*, 457–461; g) C. Gatti, L. Bertini, *Acta Crystallogr A* **2004**, *60*, 438–449.

36 a) *Chemistry of Hypervalent Compounds*, ed. by K.-y. Akiba, Wiley-VCH, New York, **1999**; b) W. Nakanishi, *Hypervalent Chalcogen Compounds In Handbook of Chalcogen Chemistry: New Perspectives in Sulfur, Selenium and Tellurium*, ed. by F. A. Devillanova, Royal Society of Chemistry, Cambridge, **2006**, Chap. 10.3, pp. 644–668.

37 The θ_p values of the major interactions are substantially controlled by the characters of the interactions in question: The influence from the behavior of the minor bonds would not be so severe in usual cases. The κ_p values for the major interactions would show similar behavior.

38 C. Gonzalez and H. B. Schlegel, *J. Chem. Phys.* **1989**, *90*, 2154–2161; C. Gonzalez and H. B. Schlegel, *J. Phys. Chem.* **1990**, *94*, 5523–5527.

Chapter 3

Intramolecular π–π Interactions in Diethanodihydronaphthalene and Derivatives: Dynamic and Static Behavior of the Interactions Elucidated by QTAIM Dual Functional Analysis

Abstract

Dynamic and static behavior of the intramolecular π–π interactions between ethylene moieties in diethanodihydronaphthalene (**3-1a**) and the derivatives (**3-2a**–**3-12a**) are elucidated by employing QTAIM-DFA, which his research group proposed recently. Total electron energy densities $H_b(\boldsymbol{r}_c)$ are plotted versus $H_b(\boldsymbol{r}_c) - V_b(\boldsymbol{r}_c)/2$ at BCPs for the interactions in question in QTAIM-DFA, where $V_b(\boldsymbol{r}_c)$ are potential energy densities at BCPs. After analysis of the plots, the π–π interactions in **3-1a**–**3-12a** are all classified by the *pure* closed shell interactions and characterized to have the vdW nature with MP2/6-311G(d), except for those in **3-10a**–**3-12a**, where the ethylene moieties in **3-1a** are replaced by benzene moieties. The character in **3-10a**–**3-12a** is predicted to have the *typical*-HB (hydrogen bond) nature without covalency, although that in **3-10a** and **3-11a** seems very close to the border area between the two. Indeed, the twisted structures (TS) were predicted for **3-1a**–**3-4a** with MP2/6-311G(d), but the observed non-twisted structures of **3-1a**–**3-3a** were better reproduced with MP2/6-311G(3d). The *typical*-HB nature without covalency was additionally predicted for the interactions between ethylene and benzene moieties in **3-9a** with MP2/6-311G(3d), maybe due to somewhat shorter C---C distances predicted for the interactions in question. The interaction in TS is also discussed exemplified by **3-10a** (C_{2v}).

Introduction

The π–π interactions are extremely important, due to the indispensable role in physical, chemical, and biological sciences. Various types of the π–π interactions have been investigated structurally and energetically, so far.[1–13] He has been much interested in the π–π interactions as a factor to control the fine details of structures and to create delicate properties in materials. Acetylene, diacetylene, and the derivatives are often utilized as the nice building blocks and/or spacers to synthesize materials of high functionalities.[14] Interactions between acetylenes and other molecules are also of very interest. Cyclic compounds containing acetylene and the derivatives often include molecules, due to the effective interactions with the molecules, for instance, if the size of the cavity of the cyclic compounds is suitable to include the molecules. The cylindrical π-orbitals around acetylene and the derivatives would play an important role in the effective interactions.

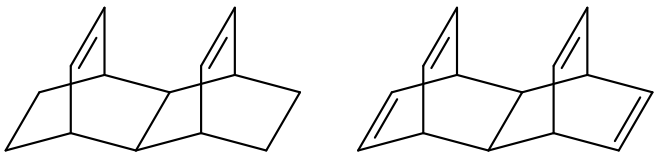

3-1a **4-1b**

Chart 3-1. Structures illustrated for **3-1a** and **4-1b**, excellent candidates for intramolecular π–π interactions

Similar attention has been paid to the interactions containing the ethylene π-orbitals. Intramolecular π–π interactions in diethanodihydronaphthalene (**3-1a**)[8] and diethenodihydro-naphthalene (**4-1b**) must provide a fundamentally important starting point for the intramolecular π–π interactions between ethylene moieties. Chart 3-1 illustrates the structures of **3-1a** and **4-1b**, of which intramolecular π–π interactions are to be clarified. The intramolecular π–π interactions in the derivatives of **3-1a** and **4-1b** must also be the typical candidates to be elucidated. The intramolecular π–π interactions in **3-1a**, **4-1b,** and the derivatives are substantially controlled by the intramolecular π–π distances in the species, which must be determined by the structures. The

distances would be shorter or longer, especially for those in the rigid structures, than those expected for the minima in the intrinsic energy surfaces of the intermolecular π–π interactions.

It must be desirable to employ such basis set system (BSS) that reproduces well the observed distances in question, since the predicted interaction distances will affect (much) on the behavior of the π–π interactions. Namely, it is inevitable to examine the predicted distances, in relation to the observed ones, if the theoretically predicted behavior of the interactions is discussed in relation to the observed distances. In this case, it is necessary for the target molecule of which structure being suitably determined. The structure of **3-1a** has been reported, determined by the X-ray crystallographic analysis,[8] together with some derivatives,[6,8] whereas that of **4-1b** seems not yet, to the best of his research group knowledge. **3-1a** is chosen as the first candidate to clarify the intramolecular π–π interaction, together with the derivatives, therefore. Chart 3-1 illustrates the structures of **3-1a** and the derivatives (**3-2a**–**3-12a**), together with the molecular graphs for **3-1a**–**3-12a** evaluated with MP2/6-311+G(d). Numbers are given for some carbon atoms to specify the interactions.

The quantum theory of atoms-in-molecules (QTAIM) approach, introduced by Bader,[15–17] enables us to analyze the nature of chemical bonds and interactions.[18–23] Recently, his research group proposed QTAIM dual functional analysis (QTAIM-DFA),[24–26] for experimental chemists to analyze their own results, concerning chemical bonds and interactions, by their own image. QTAIM-DFA provides an excellent possibility for evaluating, understanding, and classifying weak to strong interactions in a unified form.[24–27] $H_b(\boldsymbol{r}_c)$ are plotted versus $H_b(\boldsymbol{r}_c) - V_b(\boldsymbol{r}_c)/2$ in QTAIM-DFA, where $H_b(\boldsymbol{r}_c)$ and $V_b(\boldsymbol{r}_c)$ are the total electron energy densities and potential energy densities, respectively, at bond critical points (BCPs). In his research group treatment, data for perturbed structures around fully optimized ones are employed for the plots, in addition to those of the fully optimized structures.[24–28]

His research group also proposed the concept of "the dynamic nature of interactions" originated from the data containing the perturbed structures.[24a,25–27] Data from the fully optimized structures

correspond to the static nature of interactions. QTAIM-DFA is applied to typical chemical bonds and interactions, and rough criteria have been established, which can distinguish the chemical bonds and interactions in question from others. QTAIM-DFA and the criteria are explained in Chapter 2, employing Schemes 2-1–2-3, Figure 2-1 and eqs (2-8)–(2-12). The basic concept of the QTAIM approach is also surveyed in Chapter 2.

QTAIM-DFA is now applied to elucidate the dynamic and static behavior of the intramolecular π–π interactions in **3-1a**–**3-12a**, for the better understanding of the chemistry derived from the π–π interactions. Herein, he presents the results of the investigations on the nature of the intramolecular π–π interactions in question, as the first step to clarify the various types π–π interactions. The interactions are classified and characterized by employing the criteria, as a reference.

Methodological Details in Calculations

The structures were optimized employing the Gaussian 09 programs.[29] Several types of basis sets were examined to search the suitable methods for the purpose. The Møller-Plesset second order energy correlation (MP2) level is applied to the calculations.[30] The DFT level of M06-2X[31] is also employed to examine the methods. The optimized structures were confirmed by the frequency analysis. QTAIM functions were calculated using the Gaussian 09 program package[29] with the same method of the optimizations and the data were analyzed with the AIM2000 program.[32]

Normal coordinates of internal vibrations (NIV) obtained by the frequency analysis were employed to generate the perturbed structures.[33] The method is explained in Chapter 2.

Results and Discussion

Optimizations of 3-1a and Derivatives

How can the intramolecular π---π interactions in **3-1a**–**3-12a** be suitably evaluated? Table 3-1 shows the structural parameters for **3-1a** optimized with the 6-311G(d), 6-311G(3d), and 6-311+G(3d) basis sets at the MP2 level,[34] together with the observed values. The structural

parameters are defined in Scheme 3-1. The averaged values are shown in Table 3-1 as the observed ones, since **3-1a** is optimized retaining the C_{2v} symmetry, whereas the observed structure has the C_1 symmetry.

The magnitudes in the differences between predicted and observed (averaged) values in R_1 are less than 0.01 Å if evaluated with MP2/6-311+G(3d), MP2/6-311G(3d), and MP2/6-311G(d). Therefore, MP2/6-311G(d) is mainly employed for the structural optimizations of **3-1a**–**3-12a** and the whole picture of the intramolecular π–π interactions between ethylene moieties is drawn with the method. (See Table 3-A3 of the Appendix and the footnote for the C---C distances.)

The substantial distortions between ethylene moieties are predicted for **3-2a**–**3-4a**, if optimized with MP2/6-311G(d), although the distortions are negligible in the observed structures of **3-1a**–**3-3a**. Such distortions are not predicted for **3-1a**–**3-4a** with MP2/6-311G(3d) (see Table 3-A5 of the Appendix). Therefore, MP2/6-311G(3d) is also employed to evaluate the interactions, in addition to MP2/6-311G(d), although the species are limited to **3-1a**–**3-7a**, and **3-9a**–**3-11a**. The frequency analysis is not applied to **3-4a**, due to too large number of primitive gaussians. Indeed, the magnitudes of the differences between predicted and observed values in r_1 and θ_3 amount to 0.03 Å and 1°, respectively, if calculated at the MP2 level, but they would not affect so severely on the behavior of the π---π interactions.

Table 3-1. Structural parameters evaluated for **3-1a**,[a] with the observed values[b]

Level/Basis set	R_1 (Å)	R_2 (Å)	r_1 (Å)	r_2 (Å)	θ_1 (°)	θ_2 (°)	θ_3 (°)	θ_4 (°)	ϕ_1 (°)
MP2/6-311+G(3d)	3.0394	2.6283	1.3450	1.4995	97.9	114.1	123.4	96.1	0.0
MP2/6-311G(3d)	3.0396	2.6279	1.3439	1.4997	97.9	114.1	123.4	96.3	0.0
MP2/6-311G(d)	3.0419	2.6335	1.3471	1.5026	97.8	114.1	123.5	96.5	0.0
Observed (average)	3.032	2.620	1.315	1.500	97.9	114.5	124.4	96.8	-0.5

[a] The structural parameters being defined in Scheme 3-1. [b] Ref. 8.

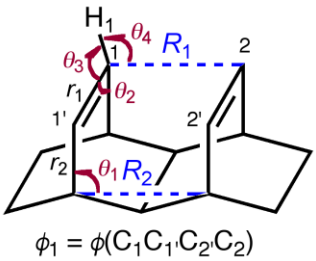

Scheme 3-1. Structural parameters of **3-1a**

The structural parameters of **3-1a** are collected in Table 3-A1 of the Appendix, evaluated with the 6-311G(3d), 6-311+G(3d), 6-311G(3d,p), 6-311+G(3d,p), and 6-311+G(3df,p) basis sets at the M06-2X level. The *R* values are predicted to be longer than the observed value by 0.042–0.045 Å at the M06-2X level, which correspond to $0.079a_o$–$0.085a_o$, where a_o is Bohr radius (0.52918 Å). The magnitudes of the differences seem larger than those expected, although acceptable. The behavior of the interactions in **3-1a**–**3-12a**, evaluated at the M06-2X level, is given in Table 3-A2 of the Appendix.

Molecular graphs and contour plots are examined, before detailed discussion of the interactions with QTAIM-DFA.

Molecular Graphs and Contour Plots for 3-1a–3-12a Evaluated with MP2/6-311G(d)

Figure 3-1 shows the molecular graphs drawn on the optimized structures of **3-1a**–**3-12a**, evaluated with MP2/6-311G(d). BCPs expected for the species are well detected, containing those between the ethylene moieties, together with ring critical points (RCPs) and cage critical points (CCPs). The molecular graphs for **3-1a**–**3-12a** with M06-2X/6-311G(3d) are illustrated in Figure 3-A1 of the Appendix. Figure 3-2 illustrates the contour plots drawn on the planes containing four C atoms of ethylene moieties for **3-1a** (C_{2v}), **3-5a** (C_{2v}), and **3-9a** (C_s), together with **3-3a** (C_2), **3-7a** (C_2), and **3-10a** (C_2) and those on the planes containing two C atoms of an ethylene moiety with a BCP in question. Figure 3-2 clarifies that BCPs appear at the three dimensional saddle point of $\rho(\boldsymbol{r})$.

The negative Laplacian and trajectory plots are shown in Figures 3-A2 and 3-A3 of the Appendix, respectively.

The intramolecular π–π interactions are unambiguously defined by BPs between ethylene moieties. Only one side of interaction will be discussed, if equivalent interactions are detected. The intramolecular π–π interaction between ethylene moieties in **3-1a** (C_{2v}) is characterized by BP, which connects BCP on ^{1}C=$^{1'}$C (shown by $B_{1,1'}$) and $B_{2,2'}$ on ^{2}C=$^{2'}$C (see Figures 3-1 and/or 3-2). BP with BCP in **3-1a** (C_{2v}) is denoted by $B_{1,1'}$-∗-$B_{2,2'}$.[35] Similar $B_{1,1'}$-∗-$B_{2,2'}$ interaction is observed in **3-5a** (C_{2v}). The π–π interaction in **3-2a** (C_2) is characterized by BP of the ^{1}C-∗-$^{2'}$C type. The twisted **3-2a** (C_2) structure optimized with MP2/6-311G(d) would be the reflection of the larger steric repulsion between the ethylene moieties, relative to that in **3-1a** (C_{2v}). The interactions of the ^{k}C-∗-$^{k+1'}$C type are detected in **3-3a** (C_2), **3-4a** (C_2), **3-7a** (C_2), and **3-8a** (C_2), by the further increase of the steric factor between the ethylene moieties. The interactions of the ^{1}C-∗-^{2}C type are detected in **3-9a** (C_s) and **3-11a** (C_2) and **3-6a** (C_2), together with that of the ^{4}C-∗-^{5}C type between the four membered moieties in the backside of the species for each. The similar interactions are detected in **3-10a** (C_2) and **3-12a** (C_2), accompanied by those between the *4,6'*-carbons of the benzene rings (see Figure 3-2).

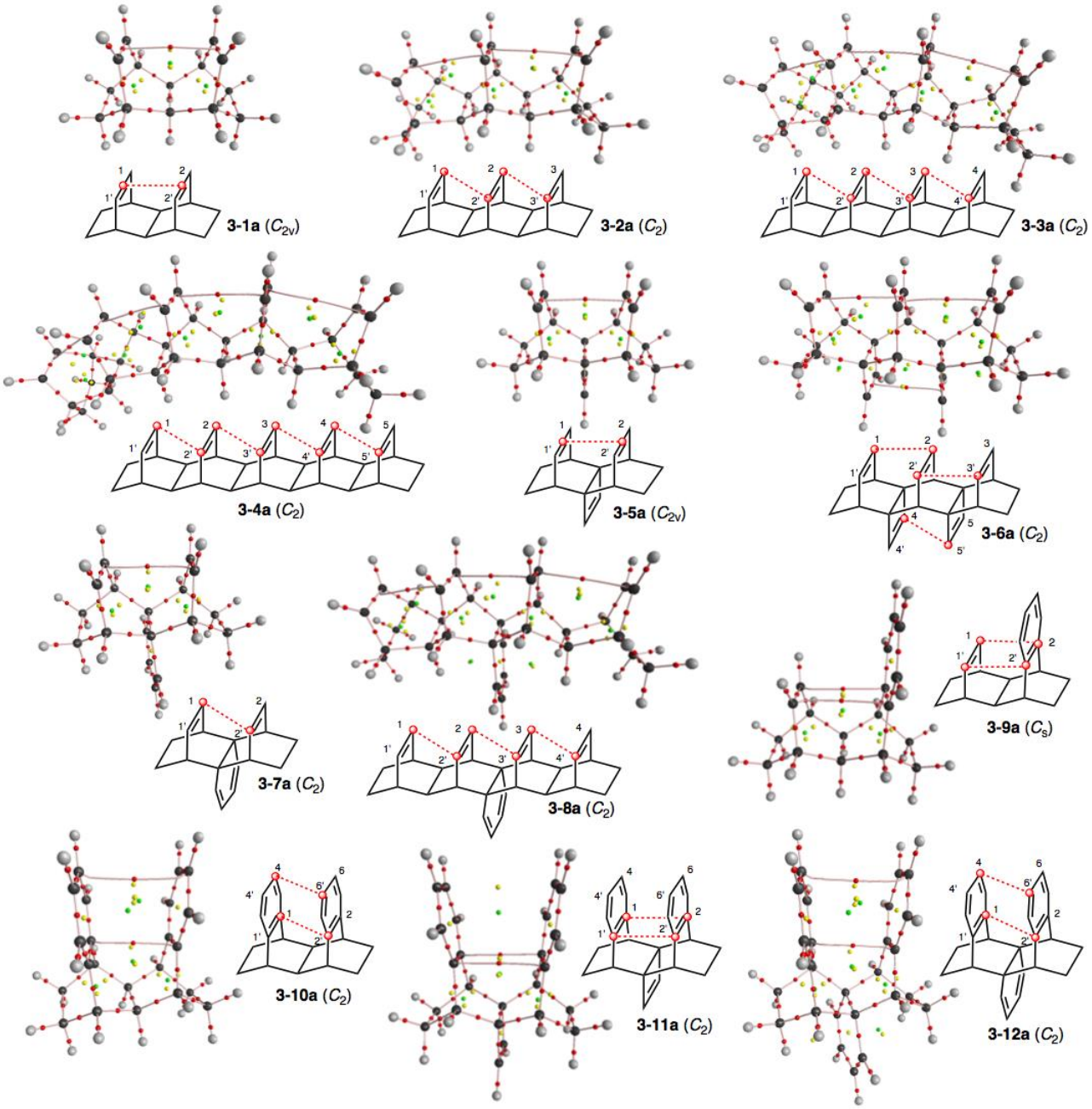

Figure 3-1. Molecular graphs for **3-1a**–**3-12a**, evaluated with MP2/6-311G(d). BCPs are shown by red dots (●), RCPs by yellow dots (●), and CCPs by green dots (●), together with BPs by pink lines (-●-). Carbon atoms are drawn in black (●) and hydrogen atoms in gray (●).

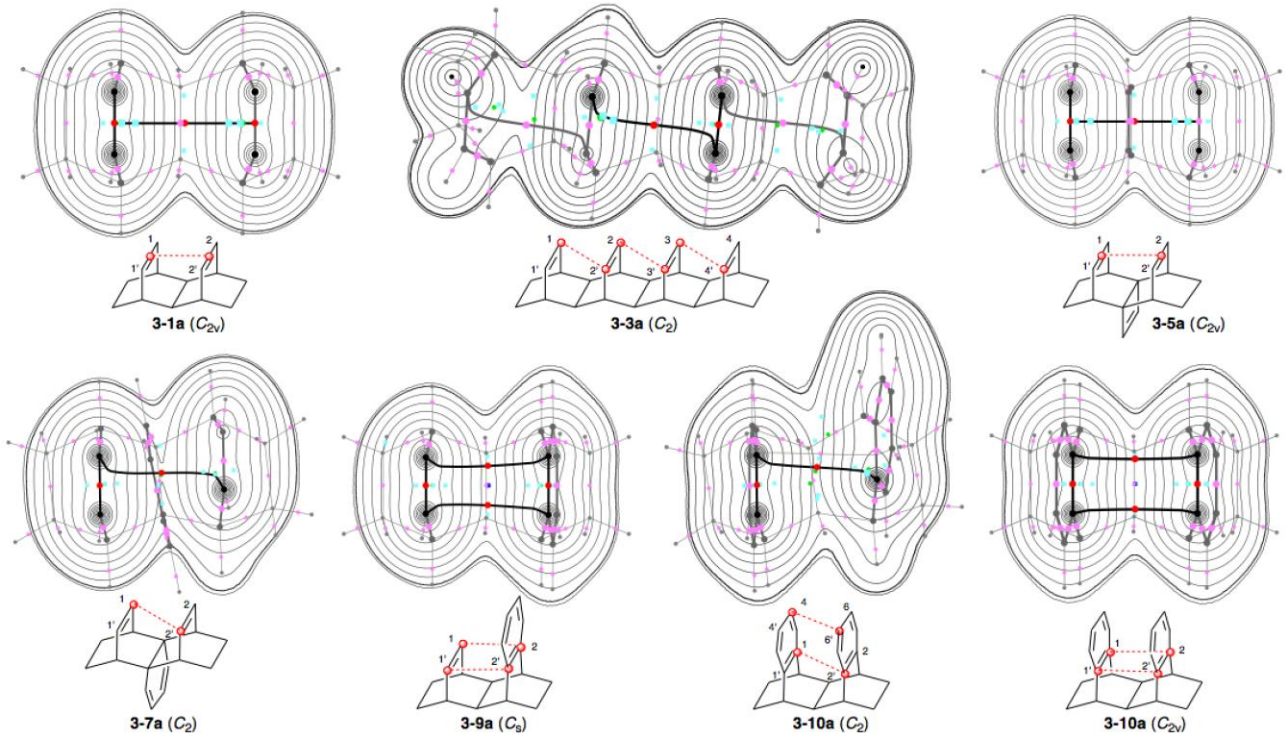

Figure 3-2. Contour plots for **3-1a** (C_{2v}), **3-5a** (C_{2v}), **3-9a** (C_s), and **3-10a** (C_{2v}), together with **3-3a** (C_2), **3-7a** (C_2), and **3-10a** (C_2), drawn on the planes containing four C atoms of ethylene moieties or two C atoms of an ethylene moiety with a BCP in question, evaluated with MP2/6-311G(d). BCPs on the plane are denoted by red dots (●), those outside of the plane in pink dots (●), ring critical points (RCPs) by light blue squares (■), cage critical points (CCPs) by green dots (●), and BPs on the plane by black lines and those outside of the plane by gray lines. Atoms on and outside the plane are in black (●) and gray (●), respectively. The contours (ea_0^{-3}) are at 2^l (l = ±8, ±7, ..., 0) and 0.0047 (heavy line).

Survey of the Intramolecular π–π Interactions in 3-1a–3-12a

The lengths of BPs (r_{BP}) and the straight-line distances (R_{SL}) for **3-1a**–**3-12a** are collected in Table 3-A3 of the Appendix, together with the differences between them ($\Delta r_{BP} = r_{BP} - R_{SL}$). The r_{BP} values are substantially longer than the corresponding R_{SL} for most cases, since BPs curve. Figure 3-3 shows the plot of r_{BP} *versus* R_{SL} for **3-1a**–**3-12a**, evaluated with MP2/6-311G(d). The plot is analyzed separately by several groups, of which correlations are given in the figure. It is demonstrated that r_{BP} are very close to R_{SL} ($0.003 \le r_{BP} - R_{SL} \le 0.018$ Å) for **3-1a** (C_{2v}), **3-5a** (C_{2v}), and **3-10a** (C_{2v}), which are substantially on the dotted line of $y = x$ in Figure 3-3, drawn as a reference. The Δr_{BP} values are 0.367–0.460 Å for **3-2a** (C_2)–**3-4a** (C_2), where the plot of r_{BP} *versus* R_{SL} shows excellent correlation. The twisting in **3-2a** (C_2)–**3-4a** (C_2) seems to affect on the linearly

on Δr_{BP}, although not so much on the linear relationship of the correlation in the plot.

The Δr_{BP} values are 0.784 and 0.718 Å for ^{1}C-∗-$^{2'}$C and ^{4}C-∗-$^{5'}$C, respectively, in **3-6a** (C_2). BPs in **3-6a** (C_2) in question seem to connect two BPs of the C=C bonds at first glance, but they connect two C atoms of the C=C bonds, resulting in the large Δr_{BP} values for **3-6a** (C_2). The plot of r_{BP} *versus* R_{SL} in **3-7a** (C_2) and **3-8a** (C_2) (0.219 Å ≤ Δr_{BP} ≤ 0.300 Å) gives good correlation, where the central C–C bond in the backside of **3-7a** (C_2) and **3-8a** (C_2) are bridged by the 1,3-butadienyl group for each. The Δr_{BP} values are rather small for the ^{1}C-∗-$^{2'}$C and/or ^{1}C-∗-^{2}C interactions in **3-9a** (C_2)– **3-12a** (C_2) (less than 0.1 Å), although the values amount to 0.125 ≤ Δr_{BP} ≤ 0.134 Å for the ^{4}C-∗-$^{6'}$C interactions in **3-10a** (C_2) and **3-12a** (C_2). They also gave a good correlation. The R_{SL}, r_{BP}, and Δr_{BP} values evaluated with MP2/6-311G(3d) are also summarized in Table 3-A3 of the Appendix.

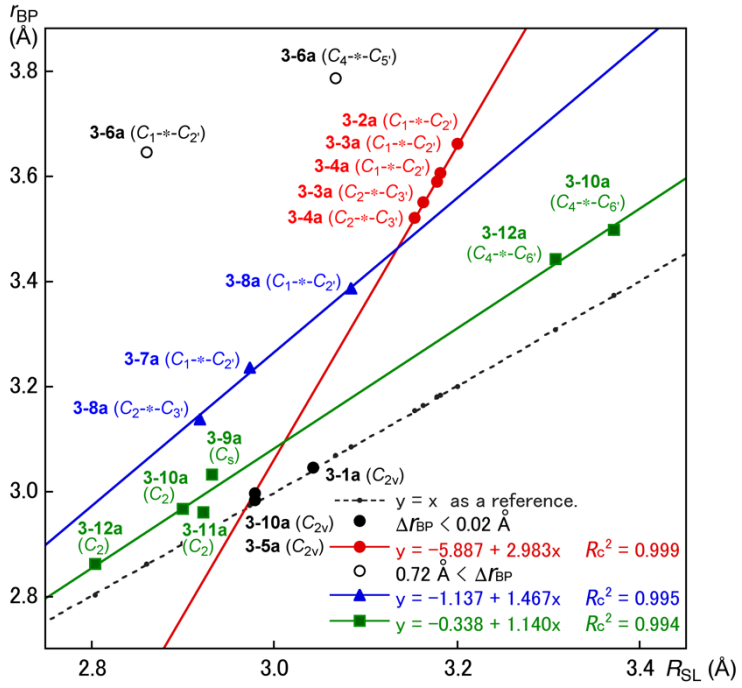

Figure 3-3. Plots of r_{BP} versus R_{SL} for the interactions in **3-1a**–**3-12a**. Interactions in **3-2a**–**3-4a**, **3-7a**–**3-8a**, and **3-9a**–**3-12a** give very good correlations, which are shown in the figure. The r_{BP} values of around 3.0 Å in **3-9a** (C_s)–**3-12a** (C_2) correspond to the ^{1}C-∗-$^{2'}$C and/or ^{1}C-∗-^{2}C interactions of the species.

QTAIM functions are evaluated with MP2/6-311(d) for the intramolecular π–π interactions between ethylene moieties in **3-1a**–**3-12a**. Table 3-2 collects the values. Figure 3-4 shows the plots of $H_b(\boldsymbol{r}_c)$ versus $H_b(\boldsymbol{r}_c) - V_b(\boldsymbol{r}_c)/2$ for the π–π interactions at BCPs of **3-1a**–**3-12a**, containing those for **3-6a**-*4,5'*, **3-10a**-*4,6'*, and **3-12a**-*4,6'*, evaluated with MP2/6-311(d). All data in Figure 3-4 appear in the area of $H_b(\boldsymbol{r}_c) - V_b(\boldsymbol{r}_c)/2 > 0$ and $H_b(\boldsymbol{r}_c) > 0$, therefore, the interactions should be classified by the *pure* closed shell (CS) interactions.

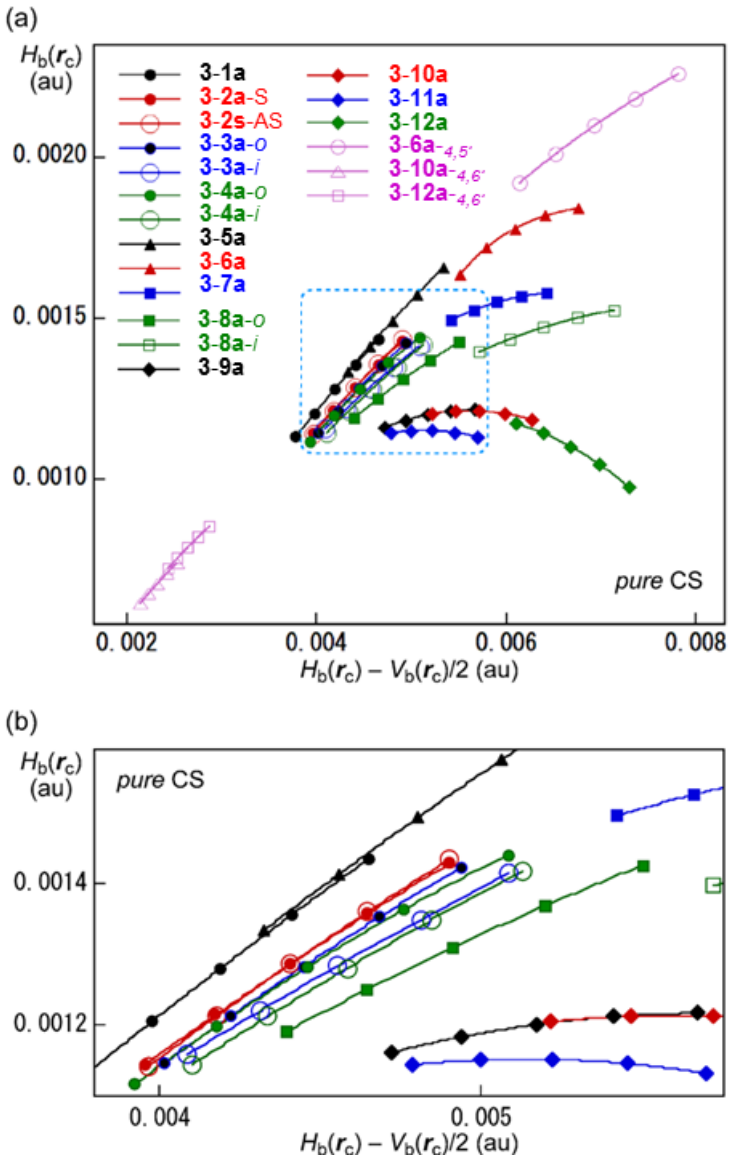

Figure 3-4. Plots of $H_b(\boldsymbol{r}_c)$ versus $H_b(\boldsymbol{r}_c) - V_b(\boldsymbol{r}_c)/2$ for **3-1a**–**3-12a**. Marks and colors are shown in the figure. **3-2a**-S and **3-2a**-AS show the perturbed structures being generated using NIVs of the symmetric and anti-symmetric vibrations, respectively. See Figure 3-1 for the interactions in **3-6a**-4,5', **3-10a**-4,6', and **3-12a**-4,6'.

After clarification of the basic trends in the intramolecular π–π interactions in **3-1a**–**3-12a**, next extension is to elucidate the behavior of the interactions by applying QTAIM-DFA.

Application of QTAIM-DFA to Intramolecular π–π Interactions in 3-1a–3-12a with MP2/6-311G(d)

QTAIM-DFA parameters of (R, θ) and (θ_p, κ_p) are calculated for the intramolecular π–π interactions between ethylene moieties in **3-1a**–**3-12a**, according to eqs (2-8)–(2-12) in Chapter 2. Table 3-2 collects the parameters, the frequencies correlated to NIV employed to generate the perturbed structures and the force constants, k_f, in addition to the QTAIM functions, necessary to discuss the interactions in question.

Table 3-2. Intramolecular π–π interactions between ethylene moieties in **3-1a**–**3-12a**, evaluated with MP2/6-311G(d), together with the symmetries[a]

Species (symmetry)	BP/BCP X-∗-Y	$\rho_b(\boldsymbol{r}_c)$ (au)	$c\nabla^2\rho_b(\boldsymbol{r}_c)$[b] (au)	$H_b(\boldsymbol{r}_c)$ (au)	$k_b(\boldsymbol{r}_c)$[c]	R (au)	θ (°)	Freq (cm^{-1})	k_f[d]	θ_p (°)	κ_p (au^{-1})
3-1a (C_{2v})	$B_{1,1'}$-∗-$B_{2,2'}$	0.0119	0.0042	0.0013	-0.820	0.0044	73.0	185.4	0.068	70.8	37.1
3-2a (C_2)	$^{1'}$C-∗-^{2}C	0.0124	0.0044	0.0013	-0.829	0.0046	73.7	113.3[e]	0.030	73.1	47.9
3-2a (C_2)	$^{1'}$C-∗-^{2}C	0.0124	0.0044	0.0013	-0.829	0.0046	73.7	226.6[f]	0.103	72.5	52.0
3-3a (C_2)	^{1}C-∗-$^{2'}$C	0.0125	0.0044	0.0013	-0.831	0.0046	73.9	167.9	0.066	73.1	57.1
3-3a (C_2)	^{2}C-∗-$^{3'}$C	0.0129	0.0046	0.0013	-0.836	0.0047	74.3	321.4	0.183	75.5	42.3
3-4a (C_2)	^{1}C-∗-$^{2'}$C	0.0126	0.0045	0.0013	-0.832	0.0046	74.0	248.7	0.115	74.0	81.1
3-4a (C_2)	^{2}C-∗-$^{3'}$C	0.0129	0.0046	0.0013	-0.838	0.0048	74.4	299.7	0.148	74.9	53.3
3-5a (C_{2v})	$B_{1,1'}$-∗-$B_{2,2'}$	0.0130	0.0048	0.0015	-0.816	0.0050	72.7	211.2	0.093	72.2	42.1
3-6a (C_2)	$^{1'}$C-∗-$^{2'}$C	0.0157	0.0061	0.0018	-0.829	0.0063	73.7	400.5	0.235	81.1	242
3-7a (C_2)	$^{1'}$C-∗-^{2}C	0.0158	0.0059	0.0016	-0.849	0.0061	75.3	213.0	0.088	85.2	118
3-8a (C_2)	^{1}C-∗-$^{2'}$C	0.0137	0.0049	0.0013	-0.846	0.0051	75.1	279.0	0.134	77.9	55.5
3-8a (C_2)	^{2}C-∗-$^{3'}$C	0.0171	0.0064	0.0015	-0.870	0.0066	77.0	334.1	0.174	84.7	56.1
3-9a (C_s)	^{1}C-∗-^{2}C	0.0130	0.0052	0.0012	-0.869	0.0053	76.9	204.9	0.086	86.5	115
3-10a (C_2)	$^{1'}$C-∗-^{2}C	0.0149	0.0057	0.0012	-0.881	0.0058	78.0	199.3	0.066	90.9	122
3-10a (C_{2v})[g]	$B_{1,1'}$-∗-$B_{2,2'}$	0.0115	0.0047	0.0011	-0.866	0.0048	76.7	202.4	0.089	88.8	119
3-11a (C_2)	^{1}C-∗-^{2}C	0.0128	0.0052	0.0012	-0.876	0.0053	77.5	224.1	0.120	90.6	129
3-12a (C_2)	$^{1'}$C-∗-^{2}C	0.0175	0.0067	0.0011	-0.910	0.0068	80.6	230.9	0.127	99.2	130
3-6a (C_2)[h]	^{4}C-∗-$^{5'}$C	*0.0172*	*0.0069*	*0.0021*	*-0.821*	*0.0072*	*73.1*	*258.9*	*0.168*	*78.4*	*51.2*
3-10a (C_2)[i]	^{4}C-∗-$^{6'}$C	*0.0071*	*0.0023*	*0.0007*	*-0.829*	*0.0024*	*73.7*	*100.8*	*0.030*	*72.0*	*80.5*
3-12a (C_2)[i]	^{4}C-∗-$^{6'}$C	*0.0078*	*0.0026*	*0.0008*	*-0.824*	*0.0028*	*73.4*	*112.0*	*0.037*	*73.3*	*107*

[a] Only one side interaction being shown if equivalent interactions are detected. [b] $c\nabla^2\rho_b(\boldsymbol{r}_c) = H_b(\boldsymbol{r}_c) - V_b(\boldsymbol{r}_c)/2$, where $c = \hbar^2/8m$. [c] $k_b(\boldsymbol{r}_c) = V_b(\boldsymbol{r}_c)/G_b(\boldsymbol{r}_c)$. [d] In mdyn $Å^{-1}$. [e] Symmetric internal vibration. [f] Anti-symmetric internal vibration. [g] For the direction of BP between the ethylene moieties in **3-10a** (C_{2v}), which should be assigned to TS. [h] For the ethylene moieties in the backside of the molecule in ***3-6a*** (C_2). [i] For the benzene rings in ***3-10a*** (C_2) and ***3-12a*** (C_2).

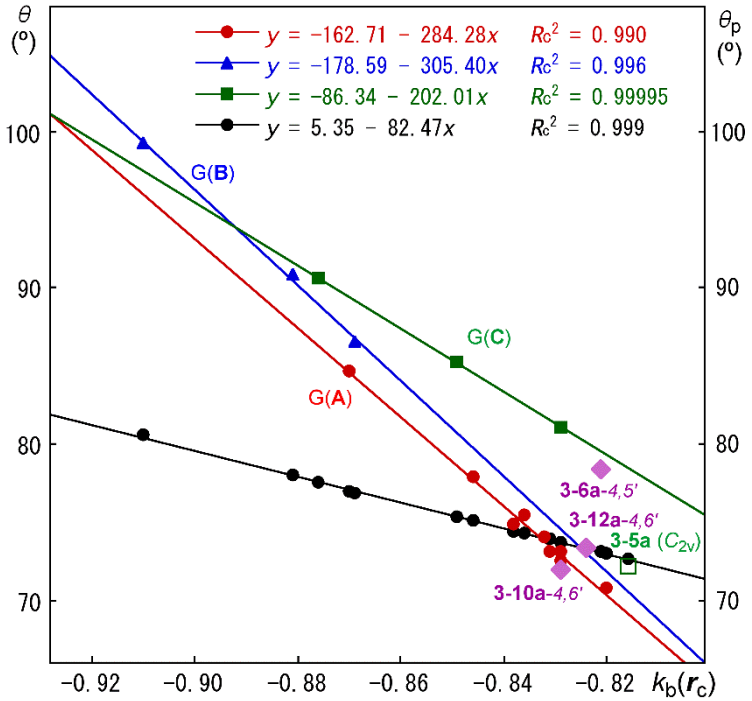

Figure 3-5. Plots of θ and θ_p versus $k_b(\boldsymbol{r}_c)$. While data of θ shown by ●, those of θ_p for G(**A**), G(**B**), and G(**C**) are by ●, ▲, and □, respectively, with those for **3-6a**-*4,5'*, **3-10a**-*4,6'*, and **3-12a**-*4,6'* (G(**D**)) are with ◆. Data for **3-5a** (□) being deviated from the correlation for G(**C**).

How is the trend in the θ□and θ_p values in relation to the structures of **3-1a**–**3-12a**? The θ and θ_p values are plotted versus $k_b(\boldsymbol{r}_c)$ (= $V_b(\boldsymbol{r}_c)/G_b(\boldsymbol{r}_c)$). Figure 3-5 shows the plots. While an excellent correlation is observed in the plot of θ□versus $k_b(\boldsymbol{r}_c)$, the plot of θ_p versus $k_b(\boldsymbol{r}_c)$ is analyzed separated by four groups. Interactions in **3-1a**–**3-4a**, and **3-8a** belong to group **A** (G(**A**)), those in **3-9a**, **3-10a**, and **3-12a** form group **B** (G(**B**)) and those in **3-5a**–**3-7a** and **3-11a** make group **C** (G(**C**)). Each group gives excellent correlation. They are given in the figure. However, a reasonable correlation is not found for the interactions in **3-6a**-*4,5'*, **3-10a**-*4,6'*, and **3-12a**-*4,6'*, which will be called group **D** (G(**D**)).

The results suggest that the static behavior of the interactions, expressed by θ, correlates to $k_b(\boldsymbol{r}_c)$ very well in the interaction region of **3-1a**–**3-12a**. Namely, $k_b(\boldsymbol{r}_c)$ shows the high applicability in the examination of static behavior of interactions. On the other hand, the plot of θ_p versus $k_b(\boldsymbol{r}_c)$ is analyzed by four groups, G(**A**)–G(**D**). The results suggest that the dynamic behavior of the interactions, expressed by θ_p, correlates well with $k_b(\boldsymbol{r}_c)$, if the interactions are segmented into

suitable groups. The 1,3-butadienobridge at the central bond of **3-3a**, as in **3-8a**, seems not change so much the interaction type, since **3-8a** also belongs to G(**A**). The benzobridge at the C=C bond and bis-benzobridges at both C=C in **3-1a** and the bridgehead C–C bond in **3-10a**, as in **3-9a**, **3-10a**, and **3-12a**, seem to affect on the dynamic behavior of the interactions, which form G(**B**). However, ethenobridge in **3-1a** and **3-10a**, bis-ethenobridges in **3-2a**, and 1,3-butadienobridge in **3-1a**, as in **3-5a**, **3-11a**, **3-6a**, and **3-7a**, respectively, seem to change the interaction types, which make G(**C**). A good correlation is not found in G(**D**), since the interaction type is different from others.

The effect of the 1,3-butadienobridge at the central bond of long chained species seems very small, as in **3-8a**. The effect of the benzobridge at the C=C bond and both C=C bonds in **3-1a** seems limiting, since the bridged species belong to G(**B**), except for **3-11a**. The ethenobridge will affect more than the case of the 1,3-butadienobridge on the dynamic behavior of the interactions between the ethylene moieties.

Behavior of Intramolecular π---π Interactions in 3-1a–3-12a, Elucidated by QTAIM-DFA Parameters

The static and dynamic nature of the intramolecular π–π interactions between ethylene moieties in **3-1a**–**3-12a** are classified and characterized based on the θ and θ_p values, respectively,[36] employing those of the standard values as a reference (see Scheme 2-3 in Chapter 2). It must be instructive to survey the criteria, before detail discussion of the nature of the π–π interactions. The criteria tell us that $\theta < 180°$ for the CS interactions ($H_b(\boldsymbol{r}_c) - V_b(\boldsymbol{r}_c)/2 > 0$) and $\theta_p > 180°$ for the shared shell (SS) interactions ($H_b(\boldsymbol{r}_c) - V_b(\boldsymbol{r}_c)/2 < 0$). The CS interactions are sub-divided into *pure* CS interactions of $45° < \theta < 90°$ ($H_b(\boldsymbol{r}_c) > 0$) and *regular* CS interactions of $90° < \theta < 180°$ ($H_b(\boldsymbol{r}_c) < 0$). The θ_p value plays an important role to characterize the interactions. The character in the *pure* CS interactions will be the vdW type for $45° < \theta_p < 90°$ and the *typical*-HB type with no covalency for $90° < \theta_p < 125°$, where $\theta_p = 125°$ is tentatively given corresponding to $\theta = 90°$.

The θ values are less than 90° for all π–π interactions between ethylene moieties in **3-1a**–**3-12a**,

which correspond to *pure* CS region. The θ_p values are also less than 90° for all π–π interactions in **3-1a**–**3-12a**, which predicts the character of the vdW nature, except for those in **3-10a**–**3-12a**. The character of the π–π interactions in **3-10a** (θ_p = 91°), **3-11a** (θ_p = 91°), and **3-12a** (θ_p = 99°) is predicted to have the *typical*-HB (hydrogen bonds) nature[37–40] without covalency, since $\theta_p > 90°$, although θ_p (= 91°) for **3-10a** and **3-11a** are very close to 90°. The character in **3-10a** and **3-11a** seem close to the border area between the vdW nature and the *typical*-HB nature without covalency. The character for **3-9a** with θ_p = 86.5° should be the vdW nature. The *regular* CS interaction ($90° < \theta < 180°$) is not detected for the π–π interactions in **3-1a**–**3-12a**. Similar interactions in G(**D**) seem weaker than the corresponding π–π interactions in the same species. The classification and characterization of the π–π interactions in **3-1a**–**3-12a** based on the θ and θ_p values are summarized in Table 3-3.

Application of QTAIM-DFA to Intramolecular π–π Interactions in 3-1a–3-12a with MP2/6-311G(3d)

Non-distorted structures are predicted for **3-1a**–**3-3a** with MP2/6-311G(3d), which reproduces better the observed structures. The predicted distances between ethylene moieties in **3-1a**–**3-3a** seem somewhat shorter than the observed values. The structure of **3-4a** is also optimized as a non-distorted one, although the frequency analysis is not performed on it. **3-8a** and **3-12a** are not optimized. Figure 3-6 shows the molecular graphs and the contour plots drawn on the optimized structure **3-3a** (C_2) with MP2/6-311G(3d), which is very close to **3-3a** (C_{2v}).

QTAIM functions are evaluated for the intramolecular π–π interactions between ethylene moieties in some of **3-1a**–**3-12a** with MP2/6-311G(3d). QTAIM-DFA parameters of (R, θ) and (θ_p, κ_p) are calculated for the interactions in question, according to eqs (2-3)–(2-6) in Chapter 2. The functions and parameters are collected in Table 3-A4 of the Appendix, together with the frequencies correlated to NIV employed to generate the perturbed structures and the force constant, k_f.

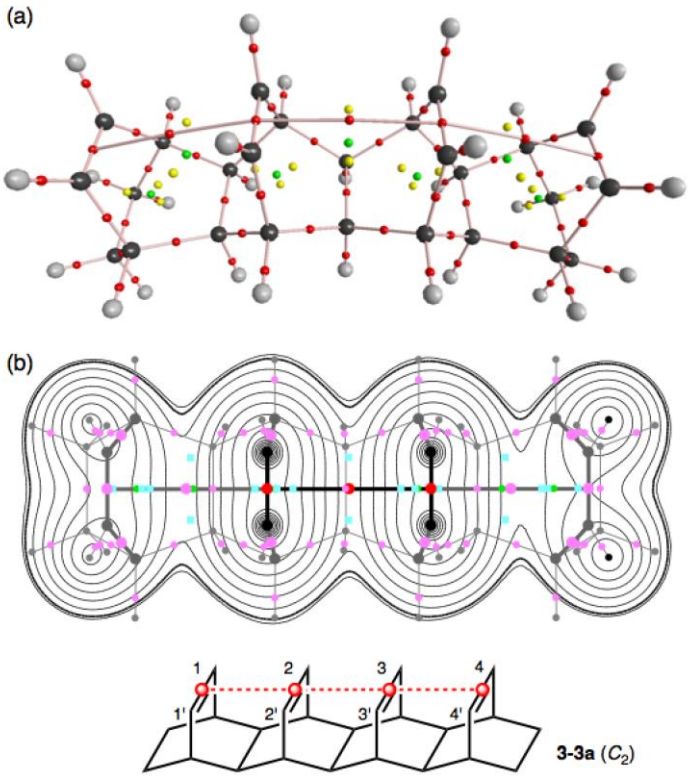

Figure 3-6. Molecular graph (a) and contour plot (b) for **3-3a** (C_2), evaluated with MP2/6-311G(3d).

The plot of R evaluated with MP2/6-311G(3d) (R_{3d}) versus those with MP2/6-311G(d) (R_d) gave a very good correlation ($R_{3d} = 1.003R_d + 0.0001$; $R_c^2 = 0.994$). The plot of θ_{3d} values θ_d also gave a good correlation although data for **3-6a** (C_2) were neglected from the correlation ($\theta_{3d} = 2.12\theta_d + 85.35$; $R_c^2 = 0.977$). The θ_p values evaluated with MP2/6-311G(3d) ($\theta_{p:3d}$) are somewhat larger than those with MP2/6-311G(d) ($\theta_{p:d}$). The $\theta_{p:3d}$ values are plotted versus $\theta_{p:d}$. Figure 3-7 shows the plot. The plot gives a very good correlation as shown in the figure, although data for **3-2a** and **3-3a** are omitted from the correlation. The deviations mainly arise from the different symmetries in the optimized structures with the two basis sets: They are optimized retaining the C_2 symmetry with MP2/6-311G(d), whereas the symmetries are C_{2v} and C_2 (substantially C_{2v}), respectively, with MP2/6-311G(3d) for **3-2a** and **3-3a**. The difference in the symmetries of the optimized structures reflects to BPs drawn in molecular graphs, resulting in the different behavior in the interactions. The θ_p value of 90.8° is predicted for the π–π interaction in **3-9a** (C_s) with MP2/6-311G(3d). It is, therefore, recognized additionally as the *typical*-HB nature without covalency.

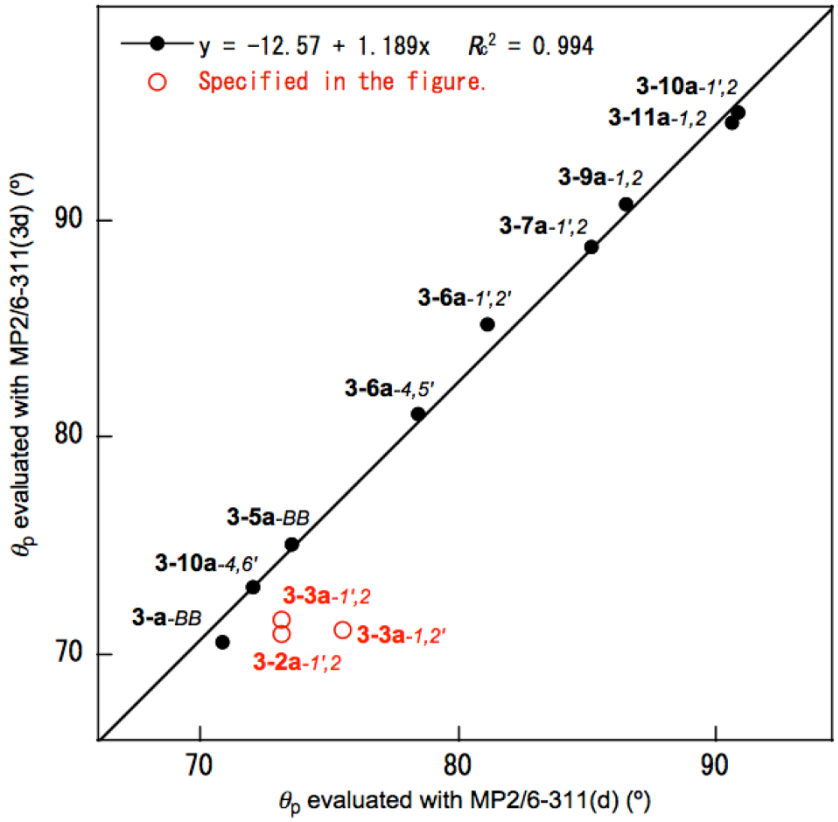

Figure 3-7. Plot of θ_p evaluated with MP2/6-311G(3d) versus θ_p evaluated with MP2/6-311G(d). The plot gave a very good correlation for the interactions as black points, with some deviations as red circles, as shown in the figure.

Table 3-3 contains the classifications and characterizations of the interactions in question evaluated with MP2/6-311G(3d). The structure of **3-1a** optimized with MP2/6-311+G(3d) is very close to that with MP2/6-311G(3d), of which behavior is shown in Table 3-A4 of the Appendix.

Table 3-3. The nature of intramolecular π–π interactions between ethylene moieties in **3-1a**–**3-12a**, classified and characterized by θ and θ_p, respectively, evaluated with the 6-311G(d) basis set at the MP2 level[a]

Species (Symmetry)	BP/BCP X-∗-Y	θ (°)	θ_p (°)	Classified by	Characterized as
MP2/6-311G(d)					
3-1a (C_{2v})	$B_{1,1'}$-∗-$B_{2,2'}$	73.0	70.8	*pure* CS	vdW nature
3-2a (C_2)[b]	^{1}C-∗-$^{2'}$C	73.7	73.1	*pure* CS	vdW nature
3-2a (C_2)[c]	^{1}C-∗-$^{2'}$C	73.7	72.5	*pure* CS	vdW nature
3-3a (C_2)	^{1}C-∗-$^{2'}$C	73.9	73.1	*pure* CS	vdW nature
3-3a (C_2)	^{2}C-∗-$^{3'}$C	74.3	75.5	*pure* CS	vdW nature
3-4a (C_2)	^{1}C-∗-$^{2'}$C	74.0	74.0	*pure* CS	vdW nature
3-4a (C_2)	^{2}C-∗-$^{3'}$C	74.4	74.9	*pure* CS	vdW nature
3-5a (C_{2v})	$B_{1,1'}$-∗-$B_{2,2'}$	72.7	72.2	*pure* CS	vdW nature
3-6a (C_2)	^{1}C-∗-^{2}C	73.7	81.1	*pure* CS	vdW nature
3-6a (C_2)	^{1}C-∗-$^{2'}$C	73.7	85.2	*pure* CS	vdW nature
3-7a (C_2)	^{1}C-∗-$^{2'}$C	75.3	85.2	*pure* CS	vdW nature
3-8a (C_2)	^{1}C-∗-$^{2'}$C	75.1	77.9	*pure* CS	vdW nature
3-8a (C_2)	^{2}C-∗-$^{3'}$C	77.0	84.7	*pure* CS	vdW nature
3-9a (C_s)	^{1}C-∗-^{2}C	76.9	86.5	*pure* CS	vdW nature
3-10a (C_2)	^{1}C-∗-$^{2'}$C	78.0	90.9	*pure* CS	*t*-HB nature[d]
3-11a (C_2)	^{1}C-∗-^{2}C	77.5	90.6	*pure* CS	*t*-HB nature[d]
3-12a (C_2)	^{1}C-∗-$^{2'}$C	80.6	99.2	*pure* CS	*t*-HB nature[d]
3-6a (C_2)[e]	^{4}C-∗-$^{5'}$C	73.1	78.4	*pure* CS	vdW nature
3-10a (C_2)[f]	$^{4'}$C-∗-$^{6'}$C	73.7	72.0	*pure* CS	vdW nature
3-12a (C_2)[f]	^{4}C-∗-$^{6'}$C	73.4	73.3	*pure* CS	vdW nature
MP2/6-311G(3d)					
3-1a (C_{2v})	$B_{1,1'}$-∗-$B_{2,2'}$	69.9	70.5	*pure* CS	vdW nature
3-2a (C_{2v})[b]	$B_{1,1'}$-∗-$B_{2,2'}$	70.4	70.9	*pure* CS	vdW nature
3-3a (C_2)	$B_{2,2'}$-∗-$B_{3,3'}$	70.8	71.6	*pure* CS	vdW nature
3-3a (C_2)	$B_{1,1'}$-∗-$C_{2'}$	70.4	71.1	*pure* CS	vdW nature
3-5a (C_{2v})	^{1}C-∗-^{2}C	69.9	75.0	*pure* CS	vdW nature
3-7a (C_2)	^{1}C-∗-^{2}C	73.8	88.8	*pure* CS	vdW nature
3-9a (C_s)	^{1}C-∗-^{2}C	78.2	90.8	*pure* CS	*t*-HB nature[d]
3-10a (C_2)	^{1}C-∗-$^{2'}$C	80.2	95.0	*pure* CS	*t*-HB nature[d]
3-11a (C_2)	^{1}C-∗-^{2}C	79.4	94.5	*pure* CS	*t*-HB nature[d]
3-6a (C_2)	^{4}C-∗-$^{5'}$C	73.0	81.1	*pure* CS	vdW nature
3-10a (C_2)	^{3}C-∗-$^{4'}$C	71.6	73.1	*pure* CS	vdW nature

[a] Only one side interaction being shown if equivalent interactions are detected. [b] Based on the symmetric internal vibration. [c] Based on the anti-symmetric internal vibration. [d] *Typical*-HB nature without covalency. [e] For the ethylene moieties in the backside of the molecule in ***3-6a*** (C_2). See Figure 3-2 for the interactions. [f] For the benzene rings in ***3-10a*** (C_2) and ***3-12a*** (C_2). See Figure 3-2 for the interactions.

Effect of Distortion on Behavior of the Interactions

The torsional angles must be the measure for the twisting between the ethylene moieties in **3-1a**–**3-12a**. The values are summarized in Table 3-A5 of the Appendix, evaluated with MP2/6-311G(d) and MP2/6-311G(3d) level. The torsional angles of $\phi(^{1}C^{1'}C^{2'}C^{2}C)$ (= ϕ_1) are 0.0° if the species have the C_{2v} or C_s symmetry. Magnitudes of ϕ_1 become larger as the steric factor around the ethylene moieties increases in the C_2 symmetry. The ϕ_1 values are very larger for **3-7a** (C_2) and **3-8a** (C_2) (11.1–11.4°) than **3-2a** (C_2)–**3-6a** (C_2) and **3-11a** (C_2) and largest for **3-10a** (C_2) and **3-12a** (C_2) (17.6°).

There must exist a process connecting two topologically equivalent minima of the C_2 symmetry via a transition state (TS), which should have the C_{2v} symmetry or that very close to it. It must be of very interest to analyze the site exchange process with QTAIM-DFA. The process was tried to follow, exemplified by **3-10a** (C_2). However, the trial was unsuccessful, since the molecular graphs seem to change around **3-10a** (C_{2v}) of TS. The ^{1}C and $^{2'}$C (or $^{1'}$C and ^{2}C) atoms are connected by BP in **3-10a** (C_2) of minima, however, the carbon atoms are not connected by BP in **3-10a** (C_{2v}), instead, the C atoms are connected just in front of them (^{1}C and $^{1'}$C; $^{2'}$C and ^{2}C) through BPs in **3-10a** (C_{2v}) of TS. The fact must prevent to analyze the interactions through QTAIM-DFA. IRC was similarly tried to apply the process but the trial was unsuccessful, either.

Instead, the interaction between the carbon atoms of the ethylene moieties in **3-10a** (C_{2v}) is analyzed with QTAIM-DFA, which is the direction of the BP at TS. Such NIV is employed to generate the perturbed structures that have the motion to the direction of the BP. The direction is almost perpendicular to that of the imaginary frequency. The results are collected in Table 3-2. The interactions in the direction of the BPs in **3-10a** (C_{2v}) of TS are classified by the *pure* CS interactions and characterized to have the HB nature without covalency. Indeed, the π–π interaction in **3-10a** (C_{2v}) is predicted to be weaker than the corresponding interaction in **3-10a** (C_2), but they seem rather close with each other, showing the close stability of **3-10a** (C_{2v}: TS), relative to **3-10a** (C_2).

The behavior of the intramolecular π–π interactions between ethylene moieties in **4-1b** and the derivatives are in Chapter 4. The influence on the behavior by the small steric effect around the interactions will be clarified.

Summary

The nature of intramolecular π–π interactions between the ethylene moieties in **3-1a**–**3-12a** is elucidated with QTAIM-DFA, employing MP2/6-311G(d) and MP2/6-311G(3d). The π–π interaction in **3-1a** (C_{2v}) is characterized by BP, which connects BCP on ^{1}C=$^{1'}$C and $B_{2,2'}$ on ^{2}C=$^{2'}$C in **3-1a** (C_{2v}) (denoted by $B_{1,1'}$-∗-$B_{2,2'}$), so is the interaction in **3-5a** (C_{2v}). The π–π interaction in **3-2a** (C_2) is characterized by BP (^{1}C-∗-$^{2'}$C), where the two ethylene moieties are twisted, maybe due to larger steric repulsion between the ethylene moieties, if evaluated with MP2/6-311G(d). BPs (^{k}C-∗-$^{k+1'}$C) are also detected in **3-3a** (C_2), **3-4a** (C_2), **3-7a** (C_2), and **3-8a** (C_2), by the further increase of the steric repulsion between ethylene moieties, so are those for **3-10a** (C_2) and **3-12a** (C_2), accompanied by BPs (^{4}C-∗-$^{6'}$C) between the benzene rings. BPs (^{1}C-∗-^{2}C) are detected for **3-9a** (C_s) and **3-11a** (C_2), together with **3-6a** (C_2), accompanied by BPs (^{4}C-∗-^{5}C) between the four membered moieties in the backside of the species.

The π–π interactions in **3-1a**–**3-12a** are classified and characterized employing QTAIM-DFA parameters of (R, θ) and (θ_p, κ_p). The θ values are less than 90° for all π–π interactions in **3-1a**–**3-12a**, which correspond to *pure* CS region. The θ_p values are also less than 90° for all π–π interactions in **3-1a**–**3-12a**, which predicts the character of the vdW nature, except for those in **3-10a**–**3-12a**. The character of the π–π interactions in **3-10a** (θ_p = 91°), **3-11a** (θ_p = 91°), and **3-12a** (θ_p = 99°) is predicted to have the *typical*-HB nature without covalency, although the character in **3-10a** and **3-11a** seems very close to the border area between the two, if evaluated with MP2/6-311G(d). There must exist a cite exchange process connecting two topologically equivalent minima of the C_2 symmetry via a transition state (TS). The process was tried to follow, exemplified by **3-10a** (C_2). The attempt was not successful, instead, the nature of the π–π interaction appeared in

TS was clarified, which was perpendicular to the exchange process.

The observed non-twisted structures of **3-2a** and **3-3a** were better reproduced with MP2/6-311G(3d). Therefore, QTAIM-DFA is similarly applied **3-1a**–**3-11a**, except for **3-4a** and **3-8a**, with MP2/6-311G(3d). The nature evaluated with MP2/6-311G(3d) is well correlated to that with MP2/6-311G(d), if the symmetries of the structures optimized with the two methods are close with each other. Data for for **3-2a** and **3-3a** deviated from the correlation, since the symmetries in the optimized structures are substantially different by the two methods. The intramolecular π–π interaction in **3-9a** (C_s) is additionally predicted to have the *typical*-HB nature without covalency, if evaluated with MP2/6-311G(3d).

Appendix

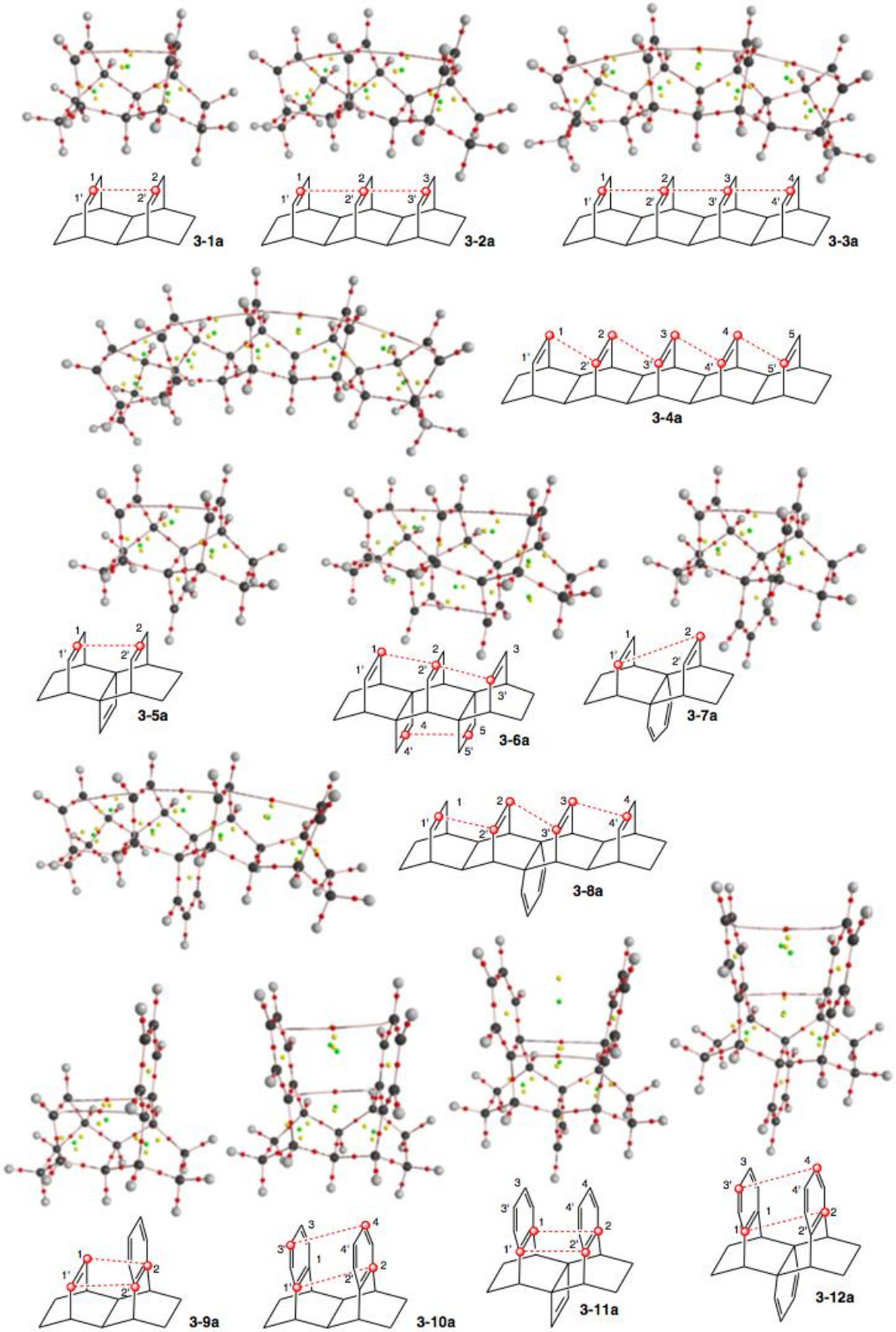

Figure 3-A1. Molecular graphs for **3-1a**–**3-12a**, evaluated with M06-2X/6-311G(3d). BCPs are shown by red dots (●), RCPs by yellow dots (●) and CCPs by green dots (●), together with BPs by pink lines (-●-). Carbon atoms are drawn in black (●) and hydrogen atoms in gray (●).

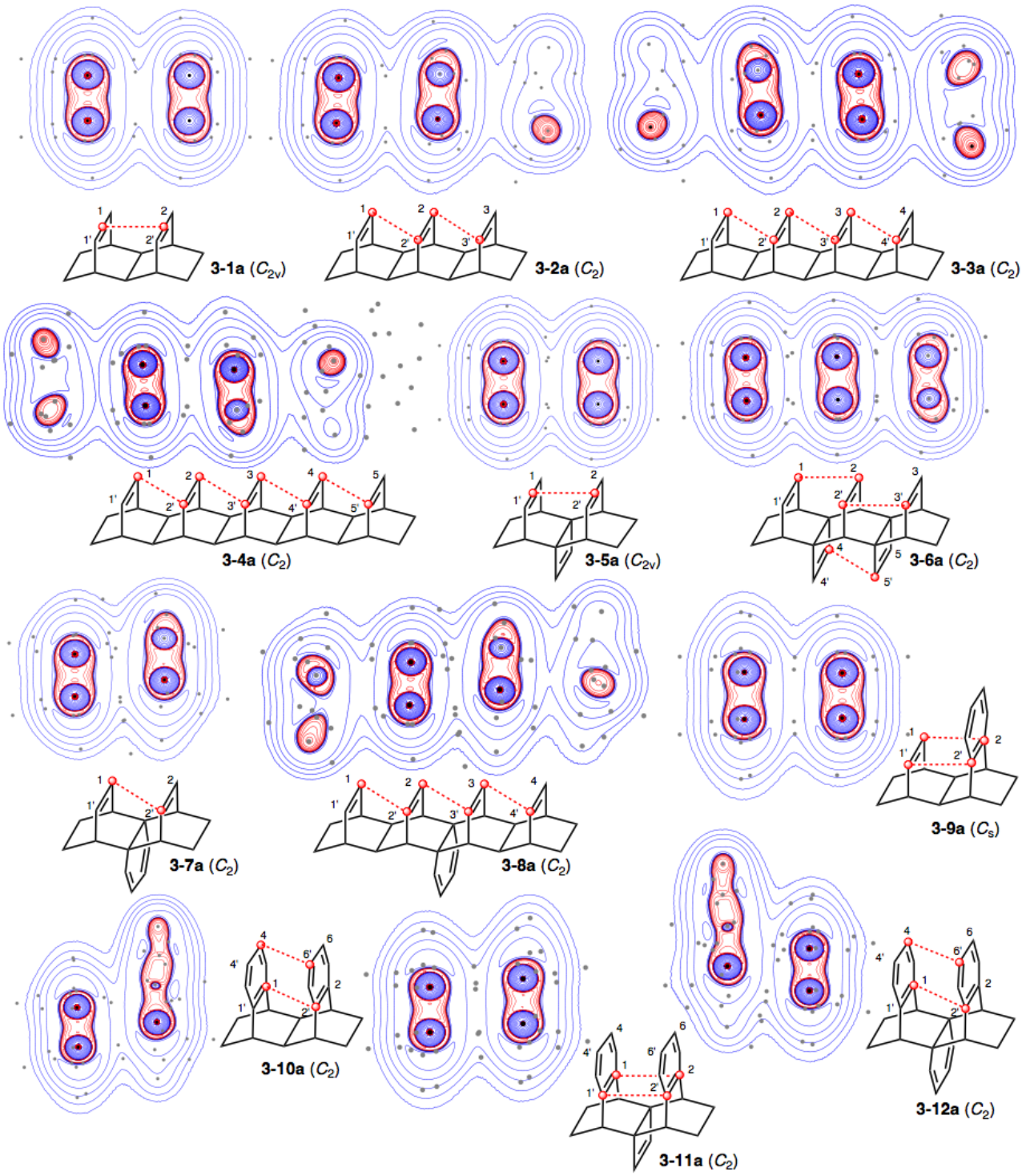

Figure 3-A2. Negative Laplacians for **3-1a**–**3-12a** drawn with MP2/6-311G(d), similarly to the case of Figure 3-2 in the text. Blue and red lines correspond to the positive and negative values, respectively.

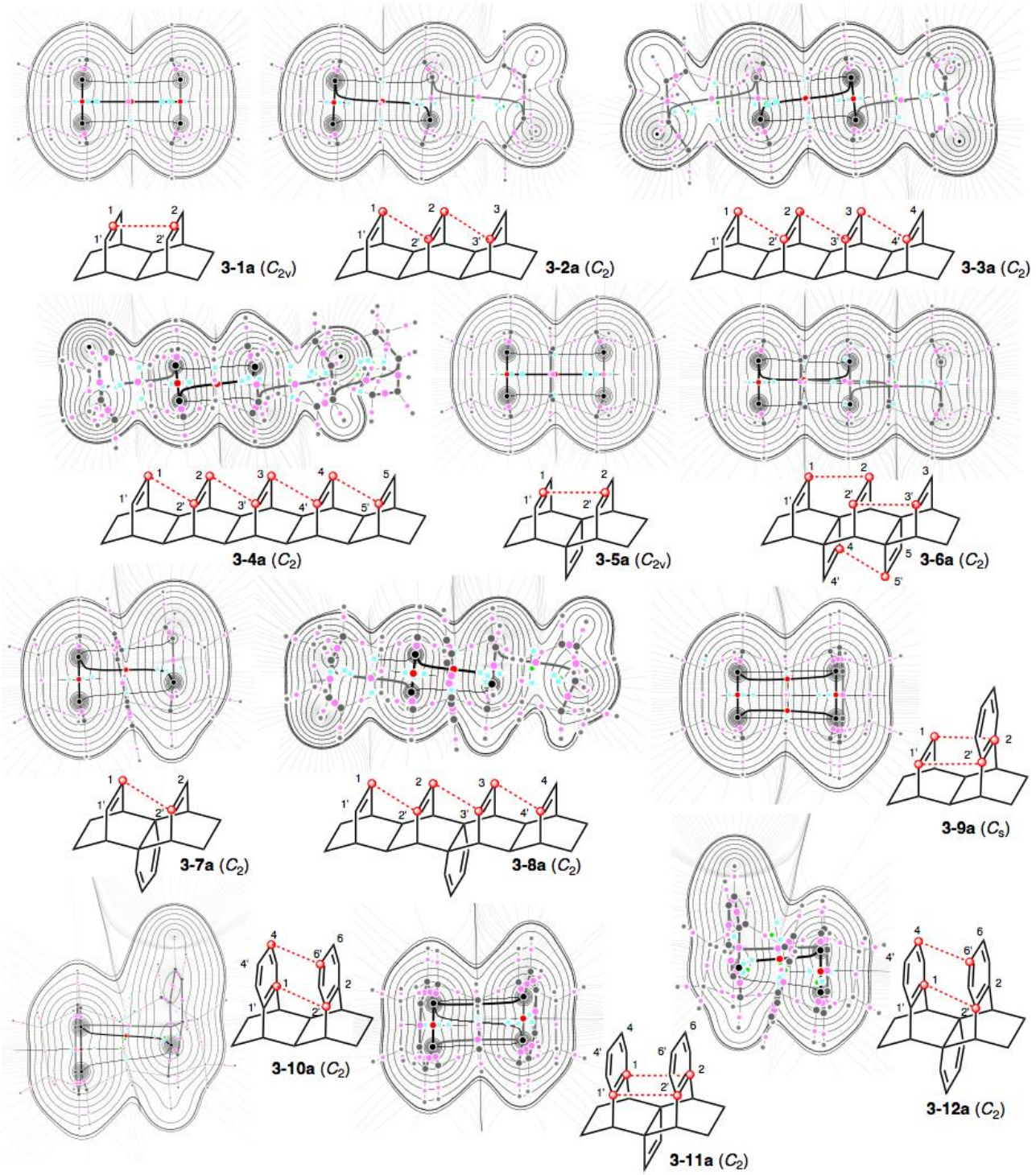

Figure 3-A3. Trajectory plots for **3-1a**–**3-12a** drawn with MP2/6-311G(d), similarly to the case of Figure 3-2 in the text. Colors and marks are the same as those in Figure 3-2.

Table 3-A1. Structural parameters for **3-1a**, evaluated with various method and the observed values[a,b]

Basis set	R (Å)	R' (Å)	r_1 (Å)	r_2 (Å)	θ_1 (º)	θ_2 (º)	θ_3 (º)	θ_4 (º)	ϕ_1 (º)
3-1a/MP2									
6-311+G(3d)	3.0394	2.6283	1.3450	1.4995	97.9	114.1	123.4	96.1	0.0
6-311G(3d)	3.0396	2.6279	1.3439	1.4997	97.9	114.1	123.4	96.3	0.0
6-311G(d)	3.0419	2.6335	1.3471	1.5026	97.8	114.1	123.5	96.5	0.0
3-1a/M06-2X									
6-311+G(3df,p)	3.0745	2.6390	1.3272	1.5041	98.3	114.4	123.7	96.7	0.0
6-311+G(3d,p)	3.0769	2.6411	1.3290	1.5058	98.3	114.3	123.7	96.7	0.0
6-311G(3d,p)	3.0763	2.6406	1.3282	1.5059	98.3	114.3	123.7	96.9	0.0
6-311+G(3d)	3.0744	2.6409	1.3287	1.5057	98.3	114.4	123.7	96.5	0.0
6-311G(3d)	3.0748	2.6403	1.3280	1.5058	98.3	114.4	123.7	96.7	0.0
3-1a/Observed[c]									
	3.036(3)	2.617	1.314	1.499	97.6	114.8	125.0	94.2	-0.5
	3.028(3)	2.623	1.316	1.501	98.2	114.2	123.7	98.4	-0.5
average	3.032	2.620	1.315	1.500	97.9	114.5	124.4	96.8	-0.5

[a] Structural parameters are defined below. [b] The structural parameters being defined in Scheme 3-1. [c] Ref. 8.

Table 3-A2. QTAIM functions and QTAIM-DFA parameters for the intramolecular π–π interactions between ethylene moieties in **3-1a**–**3-12a**, evaluated with M06-2X/6-311G(3d)[a]

Species (symmetry)	Interaction (X-*-Y)	$c\nabla^2\rho_b(\boldsymbol{r}_c)$[b] au	$H_b(\boldsymbol{r}_c)$ au	R au	θ (º)	θ_p (º)	κ_p (au^{-1})
3-1a (C_{2v})	$B_{1,1'}$-*-$B_{2,2'}$	0.00418	0.00172	0.0045	67.56	66.28	55.7
3-2a (C_{2v})	$B_{1,1'}$-*-$B_{2,2'}$	0.00426	0.00173	0.0046	67.83	66.27	61.3
3-3a (C_2)	$B_{1,1'}$-*-$B_{2,2'}$	0.00432	0.00176	0.0047	67.82	67.03	56.2
3-3a (C_2)	$B_{2,2'}$-*-$B_{3,3'}$	0.00451	0.00182	0.0049	68.01	67.59	76.3
3-4a (C_2)	^{1}C-*-$^{2'}$C	0.00437	0.00177	0.0047	67.92	67.17	52.9
3-4a (C_2)	^{2}C-*-$^{3'}$C	0.00449	0.00180	0.0048	68.13	67.52	98.4
3-5a (C_{2v})	$B_{1,1'}$-*-$B_{2,2'}$	0.00482	0.00201	0.0052	67.37	68.59	70.8
3-6a (C_2)	^{1}C-*-$B_{2,2'}$	0.00616	0.00238	0.0066	68.84	74.07	47.3
3-6a (C_2)	$B_{4,4'}$-*-$B_{5,5'}$	0.00721	0.00271	0.0077	69.42	74.97	52.4
3-7a (C_2)	$^{1'}$C-*-^{2}C	0.00565	0.00219	0.0061	68.77	77.79	104.0
3-8a (C_2)	$B_{1,1'}$-*-$^{2'}$C	0.00467	0.00187	0.0050	68.14	68.41	69.1
3-8a (C_2)	^{2}C-*-$^{3'}$C	0.00619	0.00240	0.0066	68.77	74.38	48.4
3-9a (C_s)	^{1}C-*-^{2}C	0.00458	0.00144	0.0048	72.55	77.40	120.7
3-10a (C_2)	$^{1'}$C-*-^{2}C	0.00438	0.00145	0.0046	71.64	77.15	78.6
3-11a (C_2)	^{1}C-*-^{2}C	0.00458	0.00134	0.0048	73.72	89.95	130.0
3-12a (C_2)	$^{1'}$C-*-^{2}C	0.00531	0.00166	0.0056	72.69	80.35	84.9

[a] Only one side interaction being shown if equivalent interactions are detected. [b] $c\nabla^2\rho_b(\boldsymbol{r}_c) = H_b(\boldsymbol{r}_c) - V_b(\boldsymbol{r}_c)/2$, where $c = \hbar^2/8m$.

Table 3-A3. The R_{SL} and r_{BP} values for the intramolecular π–π interactions between ethylene moieties in **3-1a**–**3-12a**, evaluated with MP2/6-311G(d) and MP2/6-311G(3d), together with the Δr_{BP} values and symmetries[a,b]

Species (Symmetry)[c]	BP/BCP[c] X-∗-Y	r_{BP}[c] (Å)	R_{SL}[c] (Å)	Δr_{BP}[c,d] (Å)
3-1a (C_{2v}/C_{2v})	($B_{1,1'}$-∗-$B_{2,2'}$)/($B_{1,1'}$-∗-$B_{2,2'}$)			
		3.0450/3.0413	3.0419/3.0389 (3.032)[e,f]	0.0031/0.0024
3-2a (C_2/C_{2v})	(^{1}C-∗-$^{2'}$C)/($B_{1,1'}$-∗-$B_{2,2'}$)	3.6593/3.0300	3.1995/3.0279 (3.054)[e,f]	0.4598/0.0021
3-3a (C_2/C_2[g])	(^{1}C-∗-$^{2'}$C)/($B_{2,2'}$-∗-$B_{3,3'}$)	3.6041/3.0228	3.1823/3.0180 (3.076)[e,f]	0.4218/0.0048
3-3a (C_2/C_2[g])	(^{2}C-∗-$^{3'}$C)/($B_{1,1'}$-∗-$^{2'}$C)	3.5500/3.6952	3.1632/3.0999 (3.038)[f,h]	0.3868/0.5954
3-4a (C_2/i)	(^{1}C-∗-$^{2'}$C)/*i*	3.5890/*i*	3.1774/*i*	0.4116/*i*
3-4a (C_2/i)	(^{2}C-∗-$^{3'}$C)/*i*	3.5197/*i*	3.1531/*i*	0.3666/*i*
3-5a (C_{2v}/C_{2v})	($B_{1,1'}$-∗-$B_{2,2'}$)/(^{1}C-∗-^{2}C)	2.9812/3.9842	2.9795/2.9747	0.0017/1.0095
3-6a (C_2/C_2)	(^{1}C-∗-^{2}C)/(^{1}C-∗-^{2}C)	3.6443/3.2535	2.8604/2.8505	0.7839/0.4030
3-6a *(C_2/C_2)*	*(^{4}C-∗-$^{5'}$C)/(^{4}C-∗-$^{5'}$C)*	*3.7858/3.5820*	*3.0677/3.0265*	*0.7181/0.5555*
3-7a (C_2/C_2)	(^{1}C-∗-$^{2'}$C)/(^{1}C-∗-$^{2'}$C)	3.2346/3.2271	2.9736/2.9717	0.2610/0.2554
3-8a (C_2/i)	(^{1}C-∗-$^{2'}$C)/*i*	3.3847/*i*	3.0845/*i*	0.3002/*i*
3-8a (C_2/i)	(^{2}C-∗-$^{3'}$C)/*i*	3.1374/*i*	2.9181/*i*	0.2193/*i*
3-9a (C_s/C_s)	(^{1}C-∗-^{2}C)/(^{1}C-∗-^{2}C)	3.0322/3.0194	2.9324/2.9259	0.0998/0.0936
3-10a (C_2/C_2)	(1C-∗-$^{2'}$C)/(^{1}C-∗-$^{2'}$C)	2.9657/2.9880	2.9007/2.9111 (3.048)[e,j]	0.0650/0.0769
3-10a *(C_2/C_2)*	*(^{4}C-∗-$^{6'}$C)/(^{3}C-∗-$^{6'}$C)*	*3.4965/3.4621*	*3.3720/3.3675* (3.860)[j,k]	*0.1245/0.0947*
3-10a (C_{2v}/C_{2v})	(^{1}C-∗-^{2}C)/(^{1}C-∗-^{2}C)	2.9967/2.9857	2.9790/2.9650	0.0177/0.0207
3-11a (C_2/C_1)	(^{1}C-∗-^{2}C)/(^{1}C-∗-^{2}C)	2.9584/2.9688	2.9222/2.9052	0.0362/0.0635
3-12a (C_2/i)	(^{1}C-∗-$^{2'}$C)/*i*	2.8622/*i*	2.8035/*i*	0.0587/*i*
3-12a *(C_2/i)*	*(^{4}C-∗-$^{6'}$C)/i*	*3.4416/i*	*3.3076/i*	*0.1340/i*

[a] Only one side interaction being shown if equivalent interactions are detected. [b] R_{SL} corresponds to the C---C distance of a π–π interaction in **3-1a**–**3-12a**, if BP connects the two C atoms. [c] Values and symmetries evaluated with MP2/6-311G(d) are shown in front of slash (/) and those with MP2/6-311G(3d) are after it. [d] $\Delta r_{BP} = r_{BP} - R_{SL}$. [e] Observed value of R_{SL}(^{1}C-^{2}C). [f] Ref. 8. [g] Very close to C_{2v}. [h] Observed value of R_{SL}(^{2}C-^{3}C). [i] Not optimized. [j] Ref. 6. [k] Observed value of R_{SL}(^{4}C-^{6}C).

Table 3-A4. QTAIM functions and QTAIM-DFA parameters for the π–π interactions in **3-1a**–**3-3a**, **3-5a**–**3-7a**, and **3-9a**–**3-11a** evaluated with MP2/6-311G(3d) and those for **3-1a** with MP2/6-311+G(3d)[a]

Species (symmetry)	BP/BCP X-∗-Y	$\rho_b(\boldsymbol{r}_c)$ (ea_o^{-3})	$c\nabla^2\rho_b(\boldsymbol{r}_c)$[b] (au)	$H_b(\boldsymbol{r}_c)$ (au)	$k_b(\boldsymbol{r}_c)$[c]	R (au)	θ (°)	Freq (cm^{-1})	k_f (unit[d])	θ_p (°)	κ_p (au^{-1})
MP2/6-311G(3d)											
3-1a (C_{2v})	$B_{1,1'}$-∗-$B_{2,2'}$	0.0114	0.0043	0.0016	-0.776	0.0046	69.9	183.1	0.065	70.5	63.4
3-2a (C_2)	$B_{1,1'}$-∗-$B_{2,2'}$	0.0118	0.0044	0.0016	-0.783	0.0047	70.4	113.0[e]	0.029	71.5	63.8
3-2a (C_{2v})	$B_{1,1'}$-∗-$B_{2,2'}$	0.0118	0.0044	0.0016	-0.783	0.0047	70.4	222.5[f]	0.099	70.9	67.0
3-3a (C_2)	$B_{2,2'}$-∗-$B_{3,3'}$	0.0121	0.0045	0.0016	-0.789	0.0048	70.8	250.5	0.119	71.6	63.6
3-3a (C_2)	$B_{1,1'}$-∗-$^{2'}$C	0.0118	0.0044	0.0016	-0.783	0.0047	70.4	163.9	0.062	71.1	62.8
3-5a (C_{2v})[g]	^{1}C-∗-^{2}C	0.0126	0.0049	0.0180	-0.776	0.0052	69.9	209.0	0.090	75.0	103.2
3-6a (C_2)	$^{1'}$C-∗-$^{2'}$C	0.0155	0.0062	0.0018	-0.829	0.0065	73.7	387.7	0.193	85.2	143.1
3-6a (C_2)[h]	$^{4'}$C-∗-^{5}C	0.0174	0.0071	0.0022	-0.820	0.0074	73.0	394.9	0.223	81.1	76.5
3-7a (C_2)	$^{1'}$C-∗-^{2}C	0.0156	0.0059	0.0017	-0.830	0.0062	73.8	213.9	0.090	88.8	143.5
3-9a (C_s)	$^{1'}$C-∗-$^{2'}$C	0.0133	0.0052	0.0011	-0.883	0.0053	78.2	203.2	0.084	90.8	129.4
3-10a (C_2)	$^{3'}$C-∗-^{4}C	0.0068	0.0023	0.0008	-0.800	0.0025	71.6	105.1	0.032	73.1	116.3
3-10a (C_2)[i]	$^{1'}$C-∗-^{2}C	0.0151	0.0056	0.0010	-0.905	0.0057	80.2	105.1	0.032	95.0	90.3
3-11a (C_1)	^{1}C-∗-^{2}C	0.0136	0.0054	0.0010	-0.896	0.0055	79.4	224.5	0.117	94.5	136.2
3-11a (C_1)[i]	$^{1'}$C-∗-$^{2'}$C	0.0136	0.0054	0.0010	-0.896	0.0055	79.4	224.5	0.117	94.5	136.2
MP2/6-311+G(3d)											
3-1a (C_{2v})	$B_{1,1'}$-∗-$B_{2,2'}$	0.0115	0.0043	0.0015	-0.790	0.0045	70.8	181.6	0.064	71.9	62.3

[a] Only one side interaction being shown if equivalent interactions are detected. [b] $c\nabla^2\rho_b(\boldsymbol{r}_c) = H_b(\boldsymbol{r}_c) - V_b(\boldsymbol{r}_c)/2$, where $c = \hbar^2/8m$. [c] $k_b(\boldsymbol{r}_c) = V_b(\boldsymbol{r}_c)/G_b(\boldsymbol{r}_c)$. [d] mdyn Å^{-1}. [e] Based on the symmetric internal vibration. [f] Based on the anti-symmetric internal vibration. [g] Analyzed by employing the perturbed structures generated with w = –0.01, –0.005, 0.005, 0.01, instead of w = –0.1, –0.05, 0.05, 0.1 to maintain the topological equivalency for the molecular graphs of the perturbed structures. [h] For the ethylene moieties in the backside of the molecule in **3-3-6a** (C_2). See Figure 3-1 of the text for the interactions. [i] For the phenyl rings in **3-10a** (C_2) and **3-12a** (C_2). See Figure 3-1 of the text for the interactions.

Table 3-A5. Torsional angles for **3-1a**–**3-12a**, evaluated with MP2/6-311G(d) and/or MP2/6-311G(3d)[a]

Species (sym)	ϕ_1 (°)[b]	ϕ_2 (°)[b]	ϕ_3 (°)[b]	Min[c]/TS
3-1a (C_{2v}/C_{2v})	0.0/0.0			Min
3-2a (C_2/C_{2v})	6.6/0.0			Min
3-3a (C_2/C_2[d])	–7.5/0.0	–8.3/0.0		Min
3-4a (C_2/e)	–7.8/*e*	–8.9/*e*		Min
3-5a (C_{2v}/C_{2v})	0.0/0.0			Min
3-6a (C_2/C_2)	–1.0/–1.9		–1.3[f]/–2.5[f]	Min
3-7a (C_2/C_2)	11.1/11.0			Min
3-8a (C_2/e)	–11.4/*e*	–12.8/*e*		Min
3-9a (C_s/C_s)	0.0/0.0			Min
3-10a (C_2/C_2)	17.6/16.9		19.1[g]/18.3[g]	Min
3-11a (C_2/C_1)	5.3/7.1		5.8[g]/7.9[g]	Min
3-12a (C_2/C_2[d])	17.6/17.4		19.1[g]/18.9[g]	Min
3-10a (C_{2v}/C_{2v})	0.0/0.0		0.0[g]/0.0[g]	TS

[a] Predicted symmetries and the torsional angles in front of slash (/) are those obtained with MP2/6-311G(d), whereas those after it are with MP2/6-311G(3d). [b] $\phi_1 = \phi(^1C^{1'}C^{2'}C^2C)$, $\phi_2 = \phi(^2C^{2'}C^{3'}C^3C)$, and $\phi_3 = \phi(^4C^{4'}C^{6'}C^6C)$. [c] Energy minimum. [d] Very close to C_{2v}. [e] Not optimized. [f] For the ethylene moieties in the backside of the molecule. [g] For the phenyl rings.

References

1 The various ways to achieve cyclic delocalization by joining chains of conjugated π-systems were studied in 1971 by Hoffmann and Goldstein; M. J. Goldstein, R. Hoffmann, *J. Am. Chem. Soc.* **1971**, *93*, 6193–6204.

2 H.-D. Martin and R. Schwesinger, *Chem. Ber.* **1974**, *107*, 3143–3145.

3 G. Sedelmeier, H. Prinzbach, H.-D. Martin, *Chimia*, **1979**, *33*, 329–332.

4 J. Spanget-Larsen, R. Gleiter, G. Klein, C. W. Doecke, L. A. Paquette, *Chem. Ber.* **1980**, *113*, 2120–2126.

5 K. B. Wiberg, M. G. Matturro, P. J. Okarma, M. E. Jason, *J. Am. Chem. Soc.* **1984**, *106*, 2194–2200.

6 C.-T. Lin, N.-J. Wang, Y.-L. Yeh, T.-C. Chou, Tetrahedron, **1995**, *51*, 2907–2928.

7 H. Lange, W. Schäfer, R. Gleiter, P. Camps, S. Vazquez, *J. Org. Chem.* **1998**, *63*, 3478–2480.

8 W. Grimme, J. Wortmann, D. Frowein, J. Lex, G. Chen, R. Gleiter, *J. Chem. Soc., Perkin Trans. 2* **1998,** 1893–1900.

9 H. Wang, W. Wang, W. J. Jin, *Chem. Rev.* **2016**, *116*, 5072–5104.

10 E. Peresypkina, A. Virovets, M. Scheer, *Cryst. Growth Des.* **2016**, *16*, 2335−2341.

11 B. E. Carson, T. M. Parker, E. G. Hohenstein, G. L. Brizius, W. Komorner, R. A. King, D. M. Collard, C. D. Sherrill, *Chem. Eur. J.* **2015**, *21*, 19168–19175.

12 Z. A. Tehrani, K. S. Kim, *Int. J. Quantum Chem.* **2016**, *116*, 622–633.

13 R. L. Gawade, D. K. Chakravarty, A. Kotmale, E. Sangtani, P. V. Joshi, A. Ahmed, M. V. Mane, S. Das, K. Vanka, P. R. Rajamohanan, V. G. Puranik, R. G. Gonnade, *Cryst. Growth Des.* **2016**, *16*, 2416−2428.

14 *Modern Cyclophane Chemistry*, eds. R. Gleiter, H. Hopf, Wiley-VCH, Weinheim, 2004.

15 *Atoms in Molecules. A Quantum Theory*, (Ed.; R. F. W. Bader), Oxford University Press, Oxford, UK, **1990**.

16 Matta, C. F.; Boyd, R. J. *An Introduction to the Quantum Theory of Atoms in Molecules* In *The Quantum Theory of Atoms in Molecules: From Solid State to DNA and Drug Design* (Eds.: C. F. Matta, R. J. Boyd), WILEY-VCH, Weinheim, Germany, **2007**, Chap. 1.

17 a) F. Biegler-König, J. Schönbohm, *J. Comput. Chem.* **2002**, *23*, 1489–1494; b) F. Biegler-König, J. Schönbohm, D. Bayles, *J. Comput. Chem.* **2001**, *22*, 545–559; c) R. F. W. Bader, *J. Phys. Chem. A* **1998**, *102*, 7314–7323; d) R. F. W. Bader, *Chem. Res.* **1991**, *91*, 893–926; e) R. F. W. Bader, *Acc. Chem. Res.* **1985**, *18*, 9–15; f) T. H. Tang, R. F. W. Bader, P. MacDougall, *Inorg. Chem.* **1985**, *24*, 2047–2053; g) R. F. W. Bader, T. S. Slee, D. Cremer, E. Kraka, *J. Am. Chem. Soc.* **1983**, *105*, 5061–5068; h) F. Biegler-König, R. F. W. Bader, T. H. Tang, *J. Comput. Chem.* **1982**, *3*, 317–328.

18 J. A. Dobado, H. Martînez-Garcîa, J. Molina, M. R. Sundberg, *J. Am. Chem. Soc.* **2000**, *122*, 1144–1149.

19 J. Molina, J. A. Dobado, *Theor. Chem. Acc.* **2001**, *105*, 328–337.

20 S. K. Ignatov, N. H. Rees, B. R. Tyrrell, S. R. Dubberley, A. G. Razuvaev, P. Mountford, G. I. Nikonov, *Chem. Eur. J.* **2004**, *10*, 4991–4999.

21 S. K. Tripathi, U. Patel, D. Roy, R. B. Sunoj, H. B. Singh, G. Wolmershäuser, R. J. Butcher, *J. Org. Chem.* **2005**, *70*, 9237–9247.

22 a) M. Yamashita, Y. Yamamoto, K.-y. Akiba, D. Hashizume, F. Iwasaki, N. Takagi, S. Nagase, *J. Am. Chem. Soc.* **2005**, *127*, 435–4371; b) Y. Yamamoto, K.-y. Akiba, *J. Syn. Org. Chem. Jpn.* **2004**, *62*, 1128–1137.

23 W. Nakanishi, T. Nakamoto, S. Hayashi, T. Sasamori, N. Tokitoh, *Chem. Eur. J.* **2007**, *13*, 255–268.

24 a) W. Nakanishi, S. Hayashi, K. Narahara, *J. Phys. Chem. A* **2009**, *113*, 10050–10057; b) W. Nakanishi, S. Hayashi, K. Narahara, *J. Phys. Chem. A* **2008**, *112*, 13593–13599.

25 W. Nakanishi, S. Hayashi, *Curr. Org. Chem.* **2010**, *14*, 181–197.

26 W. Nakanishi, S. Hayashi, *J. Phys. Chem. A* **2010**, *114*, 7423–7430.

27 W. Nakanishi, S. Hayashi, K. Matsuiwa, M. Kitamoto, *Bull. Chem. Soc. Jpn.* **2012**, *85*, 1293–1305.

28 QTAIM-DFA is successfully applied to analyze weak to strong interactions in gas phase. It could also be applied to the interactions in crystals and to those in larger systems, containing bioactive materials. The methodological improvement is inevitable to generate the perturbed structures suitable for the systems.

29 *Gaussian 09, Revision D.01*, M. J. Frisch, G. W. Trucks, H. B. Schlegel, G. E. Scuseria, M. A. Robb, J. R. Cheeseman, G. Scalmani, V. Barone, B. Mennucci, G. A. Petersson, H. Nakatsuji, M. Caricato, X. Li, H. P. Hratchian, A. F. Izmaylov, J. Bloino, G. Zheng, J. L. Sonnenberg, M. Hada, M. Ehara, K. Toyota, R. Fukuda, J. Hasegawa, M. Ishida, T. Nakajima, Y. Honda, O. Kitao, H. Nakai, T. Vreven, J. A. Montgomery, Jr., J. E. Peralta, F. Ogliaro, M. Bearpark, J. J. Heyd, E. Brothers, K. N. Kudin, V. N. Staroverov, R. Kobayashi, J. Normand, K. Raghavachari, A. Rendell, J. C. Burant, S. S. Iyengar, J. Tomasi, M. Cossi, N. Rega, J. M. Millam, M. Klene, J. E. Knox, J. B. Cross, V. Bakken, C. Adamo, J. Jaramillo, R. Gomperts, R. E. Stratmann, O. Yazyev, A. J. Austin, R. Cammi, C. Pomelli, J. W. Ochterski, R. L. Martin, K. Morokuma, V. G. Zakrzewski, G. A. Voth, P. Salvador, J. J. Dannenberg, S. Dapprich, A. D. Daniels, Ö. Farkas, J. B. Foresman, J. V. Ortiz, J. Cioslowski, D. J. Fox, Gaussian, Inc., Wallingford CT, 2009.

30 a) C. Møller, M. S. Plesset, *Phys. Rev.* **1934**, *46*, 618–622; b) J. Gauss, *J. Chem. Phys.* **1993**, *99*, 3629–3643; c) J. Gauss, *Ber. Bunsen-Ges. Phys. Chem.* **1995**, *99*, 1001–1008.

31 Y. Zhao, D. G. Truhlar, *Theor. Chem. Acc.* **2008**, *120*, 215−241.

32 The AIM2000 program (Version 2.0) is employed to analyze and visualize atoms-in-molecules: F. Biegler-König, *J. Comput. Chem.* **2000**, *21*, 1040–1048. See also ref. 15.

33 The values of $w = 0$, ±0.1, and ±0.2 in $r = r_o + wa_o$ were employed for the perturbed structures in POM (partial optimization method) in refs. 24b and 25, since the bond order (BO)[41]

becomes 2/3 and 3/2 times larger at w = +0.2 and –0.2, relative to the original values at w = 0, respectively. However, it seems better to employ the perturbed structures closer to the full-optimized one, which will reduce the errors in the QTAIM functions at the perturbed structures generated by NIV and/or POM (see refs. 24 and 25). Therefore, w = 0, ±0.05, and ±0.1 for $r = r_o + wa_o$ are employed for the analysis in this chapter.

34 For the 6-311G(3d) basis sets, see: a) R. C, Binning Jr. L. A. Curtiss, *J. Comput. Chem.* **1990**, *11*, 1206−1216; b) L. A. Curtiss, M. P. McGrath, J.-P. Blaudeau, N. E. Davis, R. C. Binning Jr. L. Radom, *J. Chem. Phys.* **1995**, *103*, 6104−6113; c) M. P. McGrath, L. Radom, *J. Chem. Phys.* **1991**, *94*, 511−516; d) For the diffuse functions (+ and + +), see: T. Clark, J. Chandrasekhar, G. W. Spitznagel, P. v. R. Schleyer, *J. Comput. Chem.* **1983**, *4*, 294−301.

35 Dots are usually employed to show BCPs in molecular graphs. Therefore, A-•-B would be more suitable to describe BP with BCP. Nevertheless, A-∗-B is employed to emphasize the existence of BCP on BP, in question, in his research group case.

36 The θ_p and κ_p values for the major bonds/interactions would be affected from the minor bonds/interactions around the major ones, however, the influence from the behavior of the minor ones would not be so severe for usual cases.

37 For HBs, see, a) L. Pauling, *The Nature of the Chemical Bond*; Cornell University Press: Ithaca, NY, **1960**; b) *Hydrogen Bonding − New Insights*, *Vol. 3 of the Series*, *Challenges and Advances in Computational Chemistry and Physics*, (Eds.: S. J. Grabowski, J. Leszczynski), Springer: Dordrecht, The Netherlands, **2006**; c) G. Buemi, *Intramolecular Hydrogen Bonds. Methodologies and Strategies for Their Strength Evaluation.* In *Hydrogen Bonding – New Insights, Vol. 3*, Challenges and Advances in Computational Chemistry and Physics, (Ed.: S. J. Grabowski), Springer: New York, **2006**; Chapter 2; d) K.-L. Han, G.-J. Zhao, *Hydrogen Bonding and Transfer in the Excited State*, John Wiley & Sons Ltd.: London, **2010**; e) M. Nishio, *The CH/π Interaction: Evidence, Nature, and Consequences*, Wiley-VCH: New York, **1998**; f) O. Takahashi, Y. Kohno, M. Nishio, *Chem. Rev.* **2010**, *110*, 6049–6076.

38 S. Hayashi, K. Matsuiwa, M. Kitamoto, W. Nakanishi, *J. Phys. Chem. A* **2013**, *117*, 1804-1816.

39 Y. Sugibayashi, S. Hayashi, W. Nakanishi, *Phys. Chem. Chem. Phys.* **2015**, *17*, 28879–28891.

40 S. Hayashi, Y. Sugibayashi, W. Nakanishi, *Phys. Chem. Chem. Phys.* **2016**, *18*, 9948–9960.

41 The bond order (BO), which corresponds to the strength of a chemical bond, is correlated to $\rho_b(\boldsymbol{r}_c)$ by the form shown below, where A and B are constants which depend on the nature of the bonded atoms.[16] $BO = \exp[A\rho_b(\boldsymbol{r}_c) - B]$.

Chapter 4

Behavior of Intramolecular π–π Interactions with Doubly Degenerated Bond Paths Between Carbon Atoms in Opposite Benzene Rings of Diethenodihydronaphthalene and Derivatives, Elucidated by QTAIM Approach

Abstract

Dynamic and static nature of intramolecular π–π interactions between ethylene moieties in diethenodihydronaphthalene (**4-1b**) and derivatives (**4-2b**–**4-12b**) are elucidated by employing QTAIM-DFA. During the course of the investigations, doubly degenerated bond paths were detected between carbon atoms in opposite benzene rings of dibenzo-derivative of **4-1b** with an etheno-bridge on the backside (**4-11b**). It must be very curious, since one BP should correspond to an interaction between two carbon atoms. Intramolecular π–π interactions in **4-1b**–**4-12b** are all classified by the *pure* CS interactions. The interactions between ethylene groups, with no substituents as in **4-1b**–**4-8b**, are predicted to have the vdW nature. Those for **4-9b**–**4-12b** have the HB nature with no covalency, where the ethylene moieties are included in one or two benzene ring(s), except for **4-10b** if evaluated with MP2/6-311G(3d). The character in **4-10b** is close to the borderline area between the vdW and HB nature with no covalency, although should be the vdW type. The interactions in **4-2b**–**4-12b** evaluated with MP2/6-311G(3d) are predicted to be somewhat stronger than the case with MP2/6-311G(d), as a whole.

Introduction

He paid much attention to the π–π interactions, as a factor to control the fine details of structures and to generate delicate properties in materials. Various types of π–π interactions have been investigated in the structural and energetic point of view, where the π–π interactions play an indispensable role in physical, chemical, and biological sciences.[1–14] It is inevitable to clarify the nature of the π–π interactions, for the better understanding of chemistry arising from the interactions. Recently, his research group reported the behavior of the intramolecular π–π interactions, exemplified by those between the ethylene moieties in diethanodihydronaphthalene (**3-1a**) and the derivatives (**3-2a**–**3-12a**), as the first step to clarify the various types π–π interactions.[15] A systematic trend was observed in the behavior of the intramolecular π–π interactions in **3-1a**–**3-12a**.[15]

What will happen if the ethano-bridges at the both edges in **3-1a** are replaced by the etheno-bridges as in diethenodihydro-naphthalene (**4-1b**)? Such consideration led us to examine the behavior of the intramolecular π–π interactions between ethylene moieties in **4-1b** and the derivatives (**4-2b**–**4-12b**). Scheme 4-1 illustrates the structures of **3-1a** and **4-1b**. The structures of **4-1b**–**4-12b** can be found in Figure 4-1, where the molecular graphs[16] are illustrated for **4-1b**–**4-12b**, drawn on the optimized structures with MP2/6-311G(d). Figure 4-1 also illustrates the interactions between ethylene moieties in **4-1b**–**4-12b**. Numbers are given for some carbon atoms in the structures to specify the interactions, for convenience of discussion.

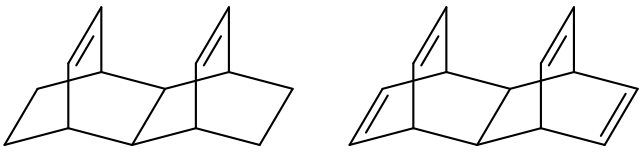

3-1a **4-1b**

Scheme 4-1. Structures illustrated for **3-1a** and **4-1b**, excellent candidates for intramolecular π–π interactions.

QTAIM approach, introduced by Bader,[17–19] enables us to analyze the nature of chemical bonds and interactions.[20–25] The bond critical point (BCP, ∗) is an important concept in QTAIM, which is a point along the bond path (BP) at the interatomic surface at which the charge density $\rho(\boldsymbol{r})$ reaches a minimum. $\rho(\boldsymbol{r})$ at BCP is denoted by $\rho_b(\boldsymbol{r}_c)$, so are other QTAIM functions. His research group searched for such method that enables experimental chemists to analyze their own results, concerning chemical bonds and interactions, by their own image and, recently, proposed QTAIM-DFA.[26–28] In his research group treatment, data from the perturbed structures, of which interaction distances in question are elongated or shortened suitably, relative to those in the fully optimized structures, in addition to those of the fully optimized structures.[26–29] His research group also proposed the concept of dynamic nature of interactions, based on the data from the perturbed structures at the fully optimized structures. QTAIM-DFA is applied to typical chemical bonds and interactions and rough criteria are established. The criteria will distinguish the chemical bonds and interactions, under consideration, from others. QTAIM-DFA will provide an excellent possibility to evaluate, classify, and understand weak to strong interactions in a unified form.[26–29] QTAIM-DFA and the criteria are explained in Chapter 2, employing Schemes 2-1–2-3, Figure 2-1, and eqs (2-8)–(2-12). The basic concept of the QTAIM approach is also surveyed.[26–29]

He consider QTAIM-DFA to be well-suited to elucidate the dynamic and static behavior of the intramolecular π–π interactions in **4-1b**–**4-12b**. Herein, He present the results of the investigations on the nature of the interactions in **4-1b**–**4-12b**. The interactions are classified and characterized by employing the criteria, as a reference. Doubly degenerated bond paths were detected between carbon atoms in opposite benzene rings of **4-11b**, a dibenzo-derivative of **4-1b** with an etheno-bridge on the backside. The detection must be very curious, since one BP should correspond to an interaction between two carbon atoms.

Methodological Details in Calculations

Structures were optimized employing the Gaussian 03[30] and/or Gaussian 09 programs[31] with the

6-311G(d), 6-311G(3d), and/or 6-311+G(3d) basis sets[32] at the Møller-Plesset second order energy correlation (MP2) level,[33] according to the examination in Chapter 3.[15] The methods were denoted by MP2/6-311G(d), MP2/6-311G(3d), MP2/6-311+G(3d), respectively. QTAIM functions were calculated using the Gaussian 09 program package[31] with the same method of the optimizations and the data were analyzed with the AIM2000 program.[34] The optimized structures were confirmed by the frequency analysis. The results of calculations for **4-1b**–**4-12b** with M06-2X/6-311G(3d) are collected in Table 4-A1 of the Appendix.

Normal coordinates of internal vibrations (NIV) obtained by the frequency analysis were employed to generate the perturbed structures. The method is explained in Chapter 2.

Results and Discussion

Optimizations of 4-1b–4-12b

The structures of **4-1b**–**4-12b** were optimized with MP2/6-311G(d), MP2/6-311G(3d), and/or MP2/6-311+G(3d). The structural parameters of **4-1b** are collected in Table 4-A2 of the Appendix. The trend in the structural parameters around the ethylene moieties optimized for **4-1b** seems very similar to those of **3-1a**, where the observed intramolecular ^{1}C---^{2}C distance in **3-1a** was well reproduced with MP2/6-311G(d), MP2/6-311G(3d), and MP2/6-311+G(3d). The magnitudes in the differences between the evaluated and observed ^{1}C---^{2}C distances in **3-1a** are less than 0.01 Å with the methods, as discussed in Chapter 3.[15] The results strongly suggest that the MP2/6-311G(d), MP2/6-311G(3d), and MP2/6-311+G(3d) methods are expected to be highly reliable to optimize the structure of **4-1b**, although the structure of **4-1b** seems not yet determined by the X-ray crystallographic analysis, to the best of his research group knowledge. Therefore, MP2/6-311G(d) is employed to clarify the whole picture for the nature of the intramolecular π–π interactions in **4-1b**–**4-12b**, similarly to the case of **3-1a**–**3-12a**. MP2/6-311G(3d) and/or MP2/6-311+G(3d) are employed, to examine the nature in more detail. Table 4-1 collects the torsional angles of ϕ(^{1}C$^{1'}$C$^{2'}$C^{2}C) (= ϕ_1), ϕ(^{2}C$^{2'}$C$^{3'}$C^{3}C) (= ϕ_2), and ϕ(^{4}C$^{4'}$C$^{5'}$C^{5}C) (= ϕ_3) and the symmetries for **4-1b**–

4-12b, evaluated with MP2/6-311G(d) and MP2/6-311G(3d). The optimized structures **4-1b**–**4-12b** are not shown in figures, but they can be found in molecular graphs, drawn on the optimized structures (see Figure 4-1).

Table 4-1 contains the data for **3-1a**–**3-12a**, similarly obtained. Substantial differences are found in the data between **3-*n*a** and **4-*n*b** (***n*** = 1–12). The C_2 symmetry in the optimized structures of **3-1a**–**3-3a** and **3-7a** changes to the C_{2v} symmetry in the optimized structures of **4-1b**–**4-3b** and **4-7b**, if optimized with MP2/6-311G(d). The magnitudes of ϕ_1 (6.6–11.1º) in **3-1a** (C_2)–**3-3a** (C_2) and **3-7a** (C_2) change ϕ_1 = 0.0º in of **4-1b** (C_{2v})–**4-3b** (C_{2v}) and **4-7b** (C_{2v}). Indeed, the symmetries are not change for other species, but the ϕ_1 values become (much) smaller: ϕ_1 = –3.7º in **4-4b** (C_2) versus ϕ_1 = –7.8º in **3-4a** (C_2) (**4-4b** (C_2: ϕ_1 = –3.7º)/ **3-4a** (C_2: ϕ_1 = –7.8º)), **4-8b** (C_2: ϕ_1 = –7.6º)/**3-8a** (C_2: ϕ_1 = –11.4º), **4-10b** (C_2: ϕ_1 = 13.6º)/**3-10a** (C_2: ϕ_1 = 17.6º), **4-12b** (C_2: ϕ_1 = 11.5º)/**3-12a** (C_2: ϕ_1 = 17.6º). The values are not changed for **4-5b** (C_2: ϕ_1 = 0.0º)/**3-5a** (C_{2v}: ϕ_1 = 0.0º) and **4-9b** (C_s: ϕ_1 = 0.0º)/**3-9a** (C_s: ϕ_1 = 0.0º), which should also be specific.

Table 4-1. Predicted torsional angle for **4-2b**–**4-12b** and **3-2a**–**3-12a**.[a]

Species[b,c] (symmetry)	ϕ_1[d] (au)	ϕ_2[e] (ϕ_3[f]) (º)
4-2b (C_{2v}/C_{2v}) [**3-2a** (C_2/C_{2v})]	0.0/0.0 [6.6/0.0]	
4-3b (C_{2v}/C_{2v}) [**3-3a** (C_2/C_2)]	0.0/0.0 [-7.5/0.0[g]]	0.0/0.0 [-8.3/0.0[g]]
4-4b (C_2/C_2) [**3-4a** (C_2/C_2)]	-3.7/0.0 [-7.8/0.0]	-6.0/0.0 [-8.9/0.0]
4-6b (C_2/C_2) [**3-6a** (C_2/C_2)]	-5.8/-5.6 [-1.0/-1.9]	(-7.2/-6.8) [(-1.3/-2.5)]
4-7b (C_{2v}/C_{2v}) [**3-7a** (C_2/C_2)]	0.0/0.0 [11.1/11.0]	
4-8b (C_2/C_2) [**3-8a** (C_2/C_2)]	7.6/6.4 [-11.4/-9.6]	10.7/10.0 [-12.8/-11.9]
4-10b (C_2/C_2) [**3-10a** (C_2/C_2)]	13.6/12.9 [17.6/16.9]	(15.0[h]/14.3[h]) [(19.1[h]/18.3[h])]
4-11b (C_2/C_1) [**3-11a** (C_2/C_1)]	11.7/11.8 [5.3/7.1]	(13.1[h]/13.3[h]) [(5.8[h]/7.9[h])]
4-12b (C_2/C_2) [**3-12a** (C_2/C_2)]	11.5/11.2[17.6/17.4]	(12.8[h]/12.6[h]) [(19.1[h]/18.9[h])]

[a] Symmetries and the torsional angles are predicted with MP2/6-311G(d) and MP2/6-311G(3d). Values with MP2/6-311G(d) are given in front of slash (/), whereas those with MP2/6-311G(3d) are after it. [b] Data for **4-1b**, **3-1a**, **4-5b**, and **3-5a** are not shown, since ϕ_1 = 0º, due to the C_{2v} symmetry, so are those for **4-9b** and **3-9a**, by the C_s symmetry. [c] Data for **4-4b**, **3-4a**, **4-8b**, **3-8a**, **4-12b**, and **3-12a** are given without frequency analysis, if optimized with MP2/6-311G(3d). [d] ϕ_1 = ϕ(^{1}C$^{1'}$C$^{2'}$C^{2}C). [e] ϕ_2 = ϕ(^{2}C$^{2'}$C$^{3'}$C^{3}C). [f] ϕ_3 = ϕ(^{4}C$^{4'}$C$^{5'}$C^{5}C), which is given parenthesis. [g] Very close to C_{2v}. [h] For the phenyl rings.

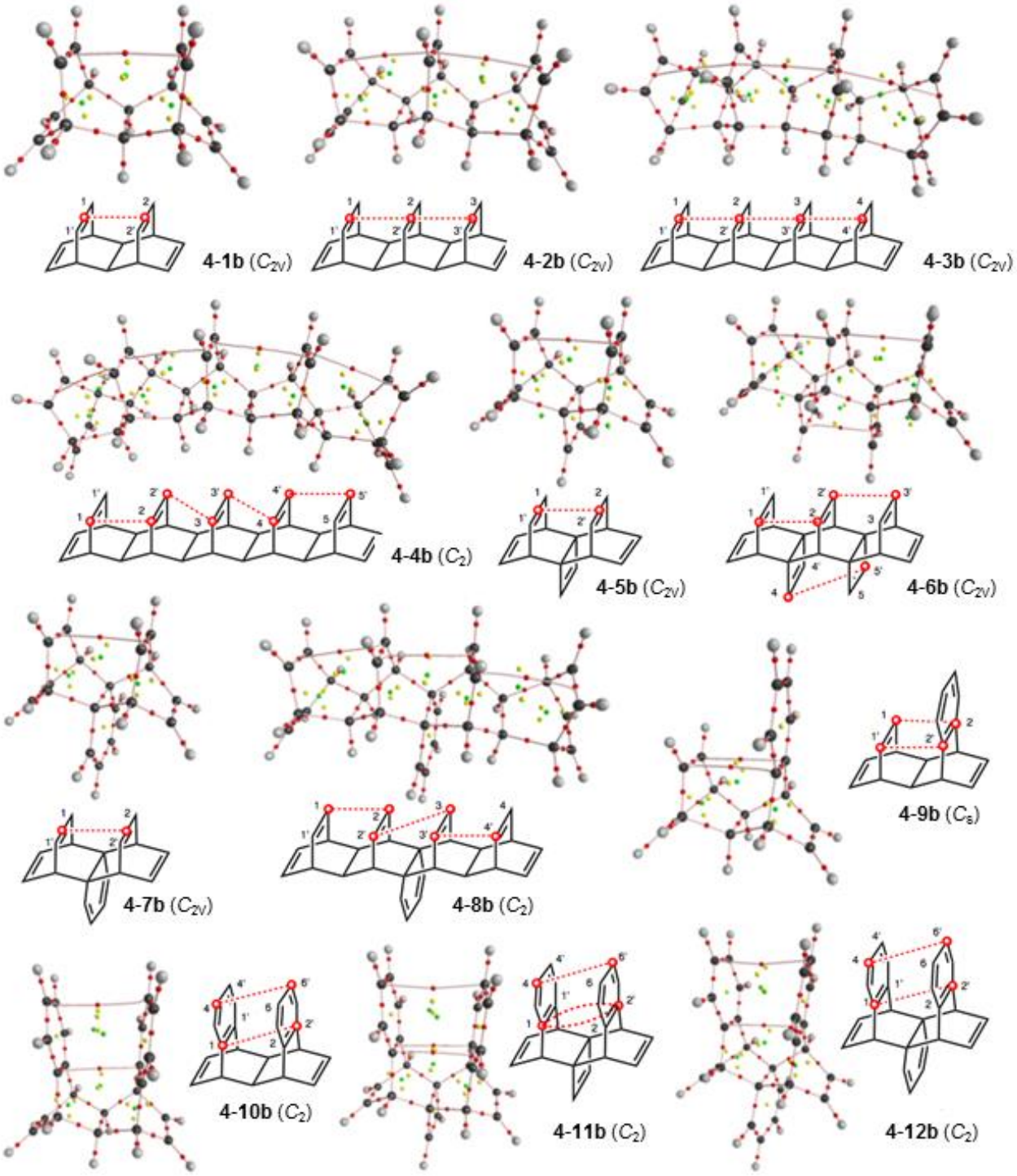

Figure 4-1. Molecular graphs for **4-1b**–**4-12b**, evaluated with the 6-311G(d). BCPs are denoted by red dots (●), RCPs by yellow dots (●) and CCPs by green dots (●), together with BPs by dark pink line (-●-). Carbon atoms are drawn in black (●) and hydrogen atoms in gray (●).

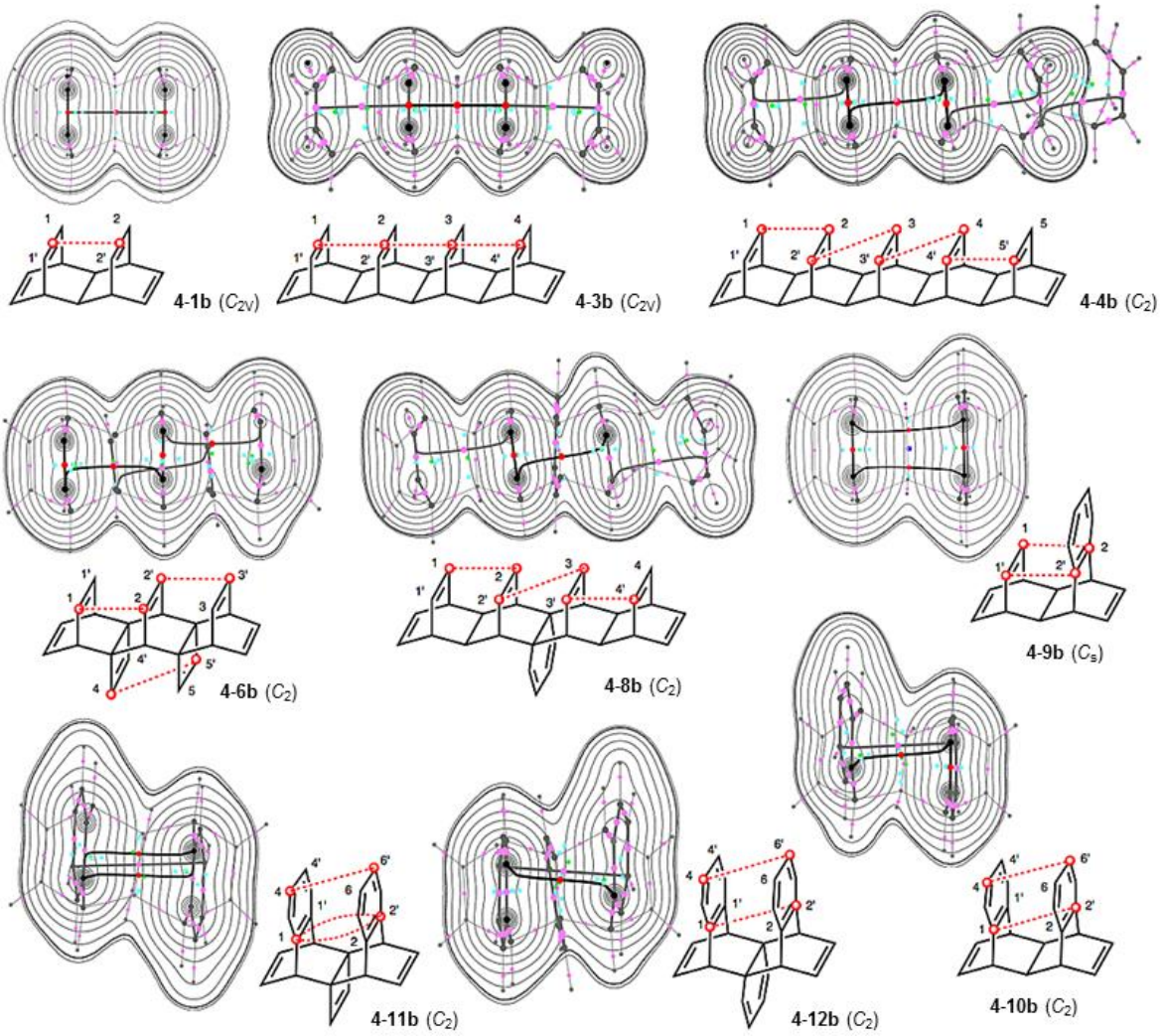

Figure 4-2. Contour plots for **4-1b** (C_{2v}), **4-3b** (C_{2v}), **4-4b** (C_2), **4-6b** (C_2), and **4-8b** (C_2)– **4-12b** (C_2), drawn on the planes containing four C atoms of ethylene moieties or two C atoms of an ethylene moiety with a BCP in question, evaluated with MP2 6-311G(d). BCPs on the plane are denoted by red dots (●), those outside of the plane in dark pink dots (●), ring critical points (RCPs) on and outside the plane by blue squares (■) and light blue ones (■), respectively, cage critical points (CCPs) by green dots (●), and BPs on the plane by black lines and those outside of the plane are by gray lines. Carbon atoms are in black (●) and hydrogen atoms are in gray (●). The contours (ea_0^{-3}) are at 2^l (l = ±8, ±7, ..., 0) with 0.0047 (heavy line).

The magnitudes in ϕ_1 decrease for most of **4-1b**–**4-12b**, relative to the corresponding **3-1a**–**3-12a**, maybe due to the slight decreased of the steric effect around the ethylene moieties in the species. It is of very interest, since the ϕ_1 value for **4-6b** (C_2) becomes larger, relative to **3-6a** (C_2), contrary to the expectation. Similar change was observed for ϕ_1 in **4-11b** (C_2), relative to **3-11a** (C_2).

Peculiar BPs observed in **4-11b** (C_2) will be discussed later, although it seems difficult to explain the reasons for the increase in ϕ_1 in **3-6a** (C_2) and **4-11b** (C_2) based on the observed results.

Before detail discussion on the intramolecular π–π interactions in **4-1b**–**4-12b**, molecular graphs and contour plots are examined, next.

Molecular Graphs and Contour Plots Around Intramolecular π-∗-π Interactions in 4-1b–4-12b

Figure 4-1 shows the molecular graphs drawn on the optimized structures of **4-1b**–**4-12b** with MP2/6-311G(d). Figure 4-2 illustrates the contour plots drawn on the plane containing four C atoms of ethylene moieties with at least one BCP in question or on the plane containing two C atoms of an ethylene moiety with a BCP in question. BCPs are well detected, expected for **4-1b**–**4-12b**, containing those between the ethylene moieties, together with ring critical points (RCPs) and cage critical points (CCPs). BCPs appear at the three-dimensional saddle points of $\rho(\mathbf{r})$ (see, Figures 4-1 and 4-2, respectively). The intramolecular π–π interactions defined by BPs seem to be affected by the slight change in structures of **4-1b**–**4-12b**, relative to the case of **3-1a**–**3-12a**.[15] The change in the predicted symmetries in the optimized structures would be mainly responsible for the differences, together with the interaction distances (see Table 4-1).

The intramolecular π–π interactions between ethylene moieties in **4-1b**–**4-12b** can be unambiguously defined by the bond paths (BPs), where only one side of interaction will be discussed, if equivalent interactions are detected. The π–π interaction between ethylene moieties in **4-1b** (C_{2v}) is characterized by BP, which connects BCPs at the center of $^{1}C=^{1'}C$ (shown by $B_{1,1'}$) and $B_{2,2'}$ at the center of $^{2}C=^{2'}C$. The BP with BCP in **4-1b** (C_{2v}) will be denoted by $B_{1,1'}$-∗-$B_{2,2'}$. Similar interaction of the $B_{1,1'}$-∗-$B_{2,2'}$ type is detected for **4-2b** (C_{2v}), **4-3b** (C_{2v}), **4-5b** (C_{2v}), and **4-7b** (C_{2v}). The π–π interactions in **3-4a** (C_2) are characterized by BPs of the $^{1'}C$-∗-$^{2'}C$ and ^{2}C-∗-$^{3'}C$ types, where the adjacent ethylene moieties are twisted to give the C_2 symmetry. Similar

interactions are observed in **4-6b** (C_2) and **4-8b** (C_2), as a whole, where **4-6b** (C_2) contains BP (^{4}C-∗-$^{5'}$C) between the ethylene moieties at the backside of the species. The ^{1}C-∗-^{2}C and $^{1'}$C-∗-$^{2'}$C type interactions are detected in **4-9b** (Cs).

The ^{1}C-∗-$^{2'}$C type interaction is detected for each of **4-10b** (C_2) and **4-12b** (C_2), accompanied by BP (^{4}C-∗-$^{6'}$C) between adjacent phenyl groups, where the steric repulsion between the phenyl rings would be large. BPs between the phenyl rings in **4-11b** (C_2) are described as BP (^{1}C-∗-$^{2'}$C), BP (^{1}C-∗-$^{2'}$C), and BP (^{4}C-∗-$^{6'}$C). It is noteworthy that BP (^{1}C-∗-$^{2'}$C) and BP (^{1}C-∗-$^{2'}$C) are doubly degenerated between C_1 and $C_{2'}$ in **4-11b** (C_2), which is discussed next, in more detail.

Doubly Degenerated BPs Between Carbon Atoms in 4-11b (C_2)

To confirm the doubly degenerated BPs between ^{1}C and $^{2'}$C in the opposite phenyl rings of **4-11b** (C_2), **4-11b** (C_2) was further optimized with MP2/6-311G(3d). The ϕ(^{1}C$^{1'}$C$^{2'}$C^{2}C) (= ϕ_1) value was 11.8º in the optimized structure of **4-11b** (C_2) with MP2/6-311G(3d), which was very close to ϕ_1 = 11.7º for **4-11b** (C_2) optimized with MP2/6-311G(d). Figure 4-3 shows the molecular graph for **4-11b** (C_2), drawn on the fully structure optimized with MP2/6-311G(3d). BPs between the opposite phenyl groups in **4-11b** (C_2: ϕ_A = 11.8°) are described by BP (^{1}C-∗-$^{2'}$C), BP (^{1}C-∗-$^{2'}$C), and BP (^{4}C-∗-$^{6'}$C). The first two BPs are doubly degenerated between ^{1}C and $^{2'}$C, again, similarly to the case of **4-11b** (C_2: ϕ_A = 11.7°) shown in Figure 4-1. The contour plot of $\rho(\boldsymbol{r})$ for **4-11b** (C_2: ϕ_A = 11.8°) further confirms the doubly degenerated BPs in the species, as illustrated in Figure 4-3. The appearance of the doubly degenerated BPs between the carbon atoms must be very curious, since one BP with a BCP is expected to correspond to an interaction between two carbon atoms.

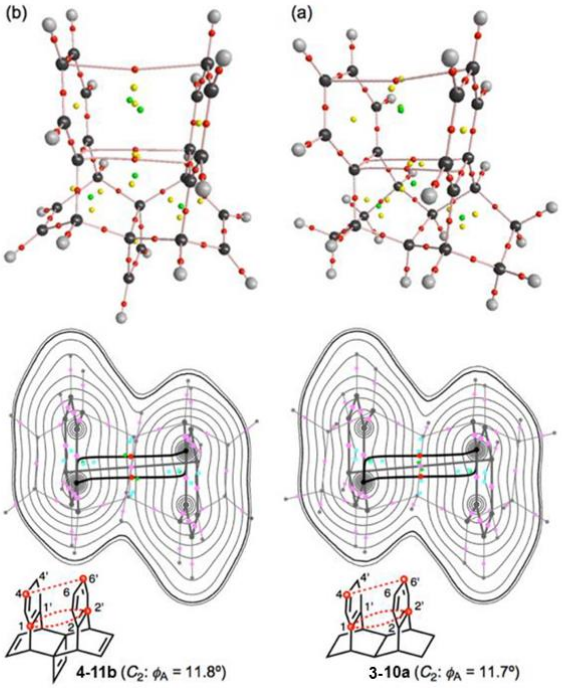

Figure 4-3. Molecular graph and contour plot of **4-11b** (C_2: ϕ_A = 11.8°) evaluated with MP2/6-311(3d) (a) and molecular graph and contour plot of **3-10a** (C_2: ϕ_A = 11.7°) with MP2/6-311(d) (b). See Figures 4-1 and 4-2 for the marks with the meanings.

He searched for such doubly degenerated BPs between carbon atoms and examined the site exchange process between **3-10a** (C_2: ϕ_A = 17.6°) and its topological isomer, **3-10a'** (C_2: ϕ_A = –17.6°). Various perturbed structures are generated between **3-10a** (C_2: ϕ_A = 17.6°) and **3-10a** (C_{2v}: ϕ_A = 0.0°).[15] Molecular graphs are drawn on the perturbed structures, which are shown in Figure 4-A3 of Appendix, along with ϕ_A of 17.6°, 14.6°, 11.7°, 10.2°, 0.0°, and –17.6°. The structures with ϕ_A = 17.6°, 0.0° and –17.6° correspond to **3-10a** (C_2: ϕ_A = 17.6°), **3-10a** (C_{2v}: ϕ_A = 0.0°), and **3-10a'** (C_2: ϕ_A = –17.6°), respectively. Molecular graphs of **3-10a** (C_2: ϕ_A = 14.6°) and **3-10a** (C_2: ϕ_A = 10.2°) are topologically identical to those of **3-10a** (C_2: ϕ_A = 17.6°) and **3-10a** (C_{2v}: ϕ_A = 0.0°), respectively. However, the molecular graph of **3-10a** (C_2: ϕ_A = 11.7°) is (very) different from those of others in **3-10a** (C_2).

Figure 4-3 illustrates the molecular graph of **3-10a** (C_2: ϕ_A = 11.7°). The opposite benzene rings in **3-10a** (C_2: ϕ_A = 11.7°) are connected by three atomic interaction lines (AL),[16] which are AL (^{1}C-*-$^{2'}$C), AL (^{1}C-*-$^{2'}$C), and AL (^{4}C-*-$^{6'}$C). The first two ALs are doubly degenerated between ^{1}C

and $^{2'}$C, similarly to the case of **4-11b** (C_2: ϕ_A = 11.7 and 11.8°). Figure 4-3 also draws the contour plot of $\rho(\boldsymbol{r})$ for **3-10a** (C_2: ϕ_A = 11.7°), which further confirms the doubly degenerated ALs in the species. The doubly degenerated BPs and/or ALs between C atoms are detected under the limited conditions of the fully optimized structure of **4-11b** (C_2: ϕ_A = 11.7 and 11.8°) and perturbed one of **3-10a** (C_2: ϕ_A = 11.7°). The BCPs on the degenerated BPs are located at the three dimensional saddle points of $\rho(\boldsymbol{r})$ for **4-11b** (C_2: ϕ_A = 11.7 and 11.8°) and ALs of the perturbed one of **3-10a** (C_2: ϕ_A = 11.7°), as shown in Figure 4-3, similarly to the case of usual BPs or ALs. The negative Laplacian and trajectory plots for **4-11b** (C_2: ϕ_A= 11.8°) and **3-10a** (C_2: ϕ_A = 11.7°) are drawn in Figure 4-A4 of the Appendix.

The doubly generated BPs in **4-11b** (C_2: ϕ_A = 11.7 and 11.8°) and ALs in **3-10a** (C_2: ϕ_A = 11.7°) are similarly analyzed with QTAIM-DFA, which will be discussed later.

Feature of Intramolecular π-∗-π Interactions in 4-1b–4-12b

Most of BPs in **4-1b**–**4-12b** seem curve, as shown in Figures 4-1 and 4-2. Therefore, the distances in BPs between the ethylene moieties (r_{BP}) will be substantially longer than the corresponding straight-line distances (R_{SL}). The r_{BP} and R_{SL} values for the intramolecular π–π interactions between the ethylene moieties in **4-1b**–**4-12b** are collected in Table 4-A3 of the Appendix, together with the differences between them ($\Delta r_{BP} = r_{BP} - R_{SL}$). Figure 4-4 shows the plot of r_{BP} *versus* R_{SL} for **4-1b**–**4-12b**, evaluated with MP2/6-311G(d). The plot is analyzed by devising the data into four groups (G(**A**)–G(**D**)), although the data for ^{1}C-∗-$^{2'}$C in **4-4b** (C_2) (Δr_{BP} = 0.739 Å) and $^{1'}$C-∗-^{2}C in **4-11b** (C_2) (Δr_{BP} = 0.474 Å) seem to deviate from the correlations. The correlations for G(**A**)–G(**D**) are given in the figure. Data for the B-∗-B type in **4-1b** (C_{2v})–**4-3b** (C_{2v}), **4-5b** (C_{2v}), and **4-7b** (C_{2v}) belong to G(**A**), of which Δr_{BP} values are less than 0.003 Å. The correlation for G(**A**) is excellent. The interactions can be approximated as straight ones. G(**B**) contains data for ^{1}C-∗-^{2}C in **4-9b** (C_2) and ^{1}C-∗-$^{2'}$C in **4-10b** (C_2) and **4-12b** (C_2), of which Δr_{BP} are 0.102–0.134 Å. While **4-10b** (C_2) and **4-12b** (C_2) are much twisted, **4-9b** (C_2) seems not. Nevertheless, BPs of these

species curve similarly with each other. Data for ^{4}C-∗-$^{6'}$C of the phenyl groups in **4-10b** (C_2)–**4-12b** (C_2) make G(**C**) with $0.027 \leq \Delta r_{BP} \leq 0.042$ Å. Data for ^{4}C-∗-$^{5'}$C of the etheno-bridges in the backside of **4-6b** (C_2) (Δr_{BP} = 0.293 Å) and $^{2'}$C-∗-^{3}C in **4-8b** (C_2) (Δr_{BP} = 0.271 Å) drop on the correlation line for G(**C**), therefore, they are added to G(**C**), although tentative. Data for ^{2}C-∗-$^{3'}$C in **4-4b** (C_2) and ^{1}C-∗-^{2}C in **4-6b** (C_2) and **4-8b** (C_2) are tentatively assembled to G(**D**) ($0.500 \leq \Delta r_{BP} \leq$ 0.606 Å), which also give a good correlation.

After clarification of the basic trends in the π–π interactions, next extension is to elucidate the dynamic and static behavior of the intramolecular π–π interactions between ethylene moieties in **4-1b**–**4-12b**, which will be discussed, employing QTAIM-DFA**.**

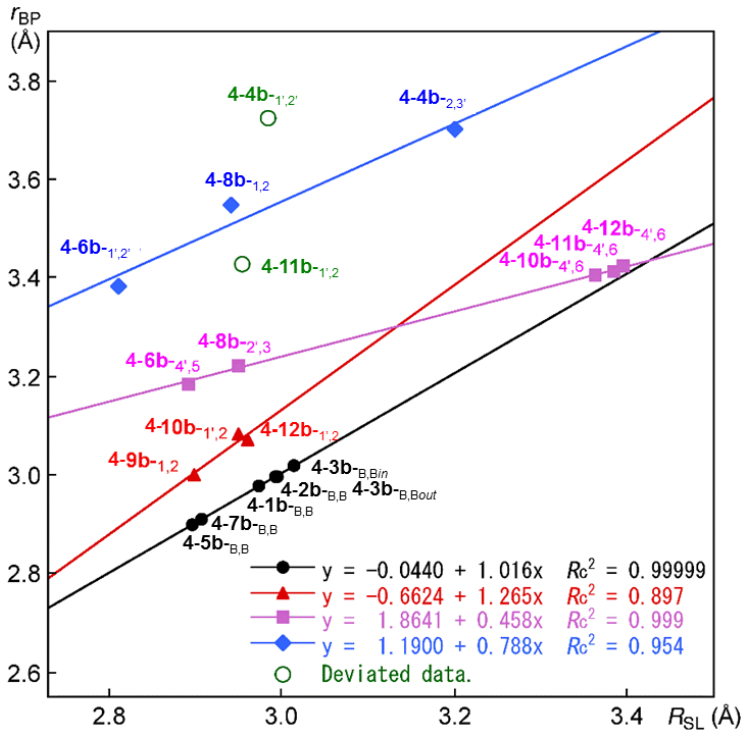

Figure 4-4. Plots of r_{BP} versus R_{SL} for all interactions in **4-1b**–**4-12b**, which are analyzed separated by four groups: Interactions in **4-1b**–**4-3b**, **4-5b,** and **4-7b** belong to G(**A**). While G(**B**) contains those in **4-9b** (C_2), **4-10b** (C_2), and **4-12b** (C_2), data for ^{4}C-∗-$^{6'}$C of phenyl groups in **4-10b**–**4-12b** and etheno-bridges in **4-6b** make G(**C**), together with $^{2'}$C-∗-^{3}C in **4-8b**. Those for **4-4b** (^{2}C-∗-$^{3'}$C), **4-6b**, and **4-8b** forms G(**D**), although tentative. Data for **4-4b** ($^{1'}$C-∗-$^{2'}$C) and **4-11b** ($^{1'}$C-∗-^{2}C) deviated from the correlation.

Evaluation of QTAIM-DFA Parameters for Intramolecular π-*-π Interactions in 4-1b–4-12b with MP2/6-311G(d)

Table 4-2 collects the QTAIM functions for the intramolecular π–π interactions between ethylene moieties in **4-1b**–**4-12b** at BCPs, evaluated with MP2/6-311G(d). Figure 4-5 shows the plots of $H_b(\boldsymbol{r}_c)$ versus $H_b(\boldsymbol{r}_c) - V_b(\boldsymbol{r}_c)/2$ for the interactions in question in **4-1b**–**4-12b**, containing those for **4-6b**-*4,5'*, **4-10b**-*4,6'*, **4-11b**-*4,6'*, and **4-12b**-*4,6'*. All data appear in the *pure* CS region of $H_b(\boldsymbol{r}_c) > 0$ and $H_b(\boldsymbol{r}_c) - V_b(\boldsymbol{r}_c)/2 > 0$. The plots are analyzed according to eqs (2-8)–(2-12) of Chapter 2 by applying QTAIM-DFA. Table 4-2 summarizes the QTAIM-DFA parameters of (R, θ) and (θ_p, κ_p), together with the frequencies corresponding to NIV to generate the perturbed structures and the force constants.

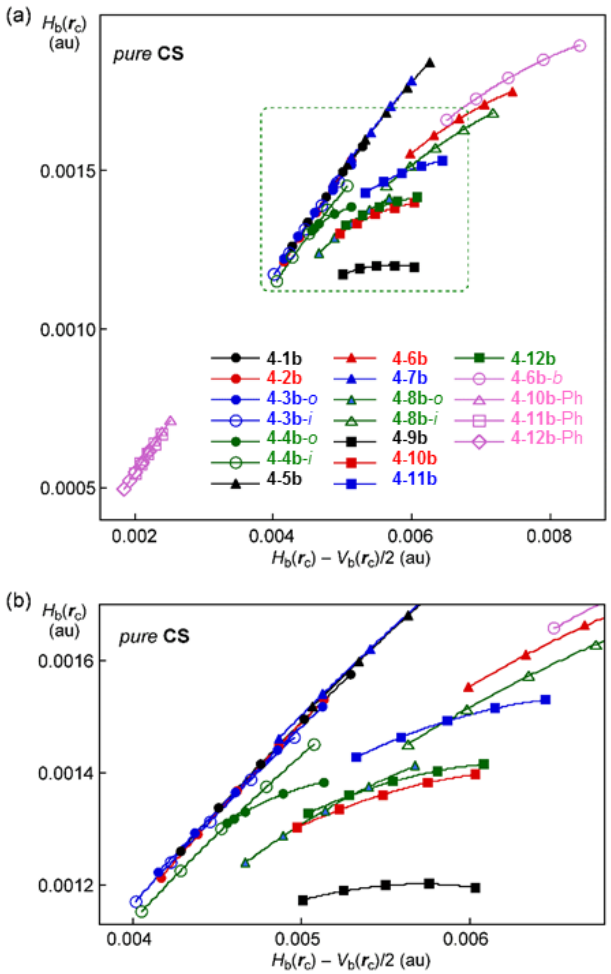

Figure 4-5. Plots of $H_b(\boldsymbol{r}_c)$ versus $H_b(\boldsymbol{r}_c) - V_b(\boldsymbol{r}_c)/2$ for **4-1b**–**4-12b**. Whole picture (a) and the magnified one (b). Marks and colors are shown in the figure. See Figures 4-1 and 4-2 for the interactions of **4-6b**-*4,5'*, **4-10b**-*4,6'*, **4-11b**-*4,6'*, and **4-12b**-*4,6'*.

The dynamic and static nature of the intramolecular π–π interactions between ethylene moieties in **4-1b**–**4-12b** are classified and characterized based on the θ and θ_p values, respectively, employing the standard values in the criteria, as a reference (see Scheme 2-3 of Chapter 2).[26,27] The θ and θ_p values are less than 90º for all π–π interactions between ethylene moieties in **4-1b**–**4-12b**, if evaluated with MP2/6-311G(d), as shown in Table 4-2. Therefore, the interactions in question are classified by the *pure* CS interactions and predicted to have the character of the vdW nature. However, the interaction in **4-9b** seems rather close to the border area between the vdW nature and the *typical*-HB nature with no covalency, since θ_p = 88.6º, which is close to 90º.

Table 4-2. QTAIM functions and QTAIM-DFA parameters for intramolecular π–π interactions between ethylene moieties in **4-1b**–**4-12b,** together with the symmetries, the frequencies closely related to the interactions, and the force constants, evaluated with MP2/6-311(d)[a,b]

Species (symmetry)	BP/BCP X-∗-Y	$\rho_b(\boldsymbol{r}_c)$ (au)	$c\nabla^2\rho_b(\boldsymbol{r}_c)$[c] (au)	$H_b(\boldsymbol{r}_c)$ (au)	$k_b(\boldsymbol{r}_c)$[d]	R (au)	θ (°)	ν (cm^{-1})	k_f[e]	θ_p (°)	κ_p (au^{-1})
4-1b (C_{2v})	$B_{1,1'}$-∗-$B_{2,2'}$	0.0133	0.0048	0.0014	-0.825	0.005	73.4	200.3	0.081	72.7	42.4
4-2b (C_{2v})	$B_{1,1'}$-∗-$B_{2,2'}$	0.0130	0.0046	0.0014	-0.826	0.0048	73.5	225.4	0.102	71.8	42.0
4-3b (C_{2v})	$B_{1,1'}$-∗-$B_{2,2'}$	0.0130	0.0046	0.0014	-0.826	0.0048	73.5	268.1	0.121	73.1	37.8
4-3b (C_{2v})	$B_{2,2'}$-∗-$B_{3,3'}$	0.0126	0.0045	0.0013	-0.827	0.0046	73.6	312.3	0.170	72.7	37.3
4-4b (C_2)	$^{1'}$C-∗-$^{2'}$C	0.0131	0.0047	0.0013	-0.834	0.0049	74.1	252.8	0.126	80.5	249
4-4b (C_2)	^{2}C-∗-$^{3'}$C	0.0128	0.0045	0.0013	-0.833	0.0047	74.0	297.8	0.150	73.6	50.3
4-5b (C_{2v})	$B_{1,1'}$-∗-$B_{2,2'}$	0.0149	0.0056	0.0017	-0.825	0.0059	73.4	234.3	0.112	74.7	46.0
4-6b (C_2)	^{1}C-∗-^{2}C	0.0171	0.0067	0.0017	-0.858	0.0069	76.0	262.7	0.197	82.2	58.4
4-7b (C_{2v})	$B_{1,1'}$-∗-$B_{2,2'}$	0.0146	0.0054	0.0016	-0.824	0.0056	73.3	209.9	0.098	74.3	47.4
4-8b (C_2)	^{1}C-∗-^{2}C	0.0141	0.0051	0.0013	-0.851	0.0053	75.5	277.5	0.131	80.1	98.6
4-8b (C_2)	$^{2'}$C-∗-^{3}C	0.0169	0.0064	0.0016	-0.859	0.0065	76.1	329.6	0.175	81.4	47.7
4-9b (C_s)	^{1}C-∗-^{2}C	0.0139	0.0055	0.0012	-0.878	0.0056	77.7	220.2	0.106	88.6	116
4-10b (C_2)	$^{1'}$C-∗-^{2}C	0.0140	0.0055	0.0014	-0.858	0.0056	76.1	216.3	0.109	84.7	95.3
4-11b (C_2)	^{1}C-∗-^{2}C	0.0145	0.0059	0.0015	-0.854	0.0061	75.7	237.9	0.143	84.7	94.7
4-12b (C_2)	$^{1'}$C-∗-^{2}C	0.0145	0.0057	0.0015	-0.854	0.0059	75.7	226.4	0.109	85.5	104
4-6b (C_2)[f]	$^{4'}$C-∗-$^{5'}$C	0.0189	0.0074	0.0018	-0.862	0.0076	76.4	262.7	0.197	82.8	46.5
4-10b (C_2)[f]	$^{4'}$C-∗-$^{6'}$C	0.0070	0.0023	0.0006	-0.836	0.0024	74.3	110.3	0.038	72.7	63.9
4-11b (C_2[f]	$^{4'}$C-∗-$^{6'}$C	0.0067	0.0022	0.0006	-0.839	0.0023	74.5	113.1	0.037	72.3	43.3
4-12b (C_2)[f]	^{4}C-∗-$^{6'}$C	0.0068	0.0022	0.0006	-0.838	0.0023	74.4	113.3	0.037	72.4	48.9
3-10a *(C_2)*[g]	$^{1'}$C-∗-^{2}C	*0.0140*	*0.0055*	*0.0014*	*-0.858*	*0.0056*	*76.1*	*216.3*	*0.109*	*84.7*	*95.3*
3-10a *(C_2)*[g]	^{4}C-∗-$^{6'}$C	*0.0070*	*0.0023*	*0.0006*	*-0.836*	*0.0024*	*74.3*	*110.3*	*0.038*	*72.7*	*63.9*

[a] Only one side interaction being shown if equivalent interactions are detected. [b] Data are given at BCP for interaction in question, which is shown by -∗-. [c] $c\nabla^2\rho_b(\boldsymbol{r}_c) = H_b(\boldsymbol{r}_c) - V_b(\boldsymbol{r}_c)/2$, where $c = -\hbar^2/8m$. [d] $k_b(\boldsymbol{r}_c) = V_b(\boldsymbol{r}_c)/G_b(\boldsymbol{r}_c)$. [e] Force constant for ν_n. [f] See Figures 4-1 for the interactions. [g] $\phi(^1C^{1'}C^{2'}C^2C) = 11.7^o$.

How is the trend in θ and θ_p for the intramolecular π–π interactions between ethylene moieties in **4-1b**–**4-12b**? The θ and θ_p values are plotted versus $k_b(\boldsymbol{r}_c)$, which is defined by $V_b(\boldsymbol{r}_c)/G_b(\boldsymbol{r}_c)$. Figure 4-6 shows the plots. While the plot of θ versus $k_b(\boldsymbol{r}_c)$ gives an excellent correlation, the plot of θ_p versus $k_b(\boldsymbol{r}_c)$ is analyzed as three correlations. While θ_p for the $B_{1,1'}$-*-$B_{2,2'}$ type in **4-1b** (C_{2v})–**4-3b** (C_{2v}), ^{2}C-*-$^{3'}$C in **4-4b** (C_2), ^{1}C-*-^{2}C in **4-6b** (C_2), **4-8b** (C_2), and **4-9b** (C_2), $^{2'}$C-*-^{3}C in **4-8b** (C_2), and ^{4}C-*-$^{5'}$C in **4-6b** (C_2) make group **A'** (G(**A'**)), those for ^{1}C-*-^{2}C in **4-4b** (C_2), $B_{1,1'}$-*-$B_{2,2'}$ in **4-5b** (C_{2v}) and **4-7b** (C_{2v}), and ^{1}C-*-$^{2'}$C in **4-10b** (C_2)– **4-12b** (C_2) do G(**B'**). The values for ^{4}C-*-$^{6'}$C in **4-10b** (C_2)–**4-12b** (C_2) belong to G(**C'**). The correlations are given in the figure. The static behavior of the intramolecular π–π interactions between ethylene moieties in **4-1b**–**4-12b**, expressed by θ, correlates very well with $k_b(\boldsymbol{r}_c)$. The results show the high applicability of $k_b(\boldsymbol{r}_c)$ in the examination of static behavior of interactions. On the other hand, the dynamic behavior of the interactions, expressed by θ_p, correlates well with $k_b(\boldsymbol{r}_c)$, although it is necessary for the interactions to be segmented into suitable types.

The parameters are similarly obtained with higher BSSs of MP2/6-311G(3d) and/or MP2/6-311+G(3d), although species are somewhat limited. The results are discussed, next.

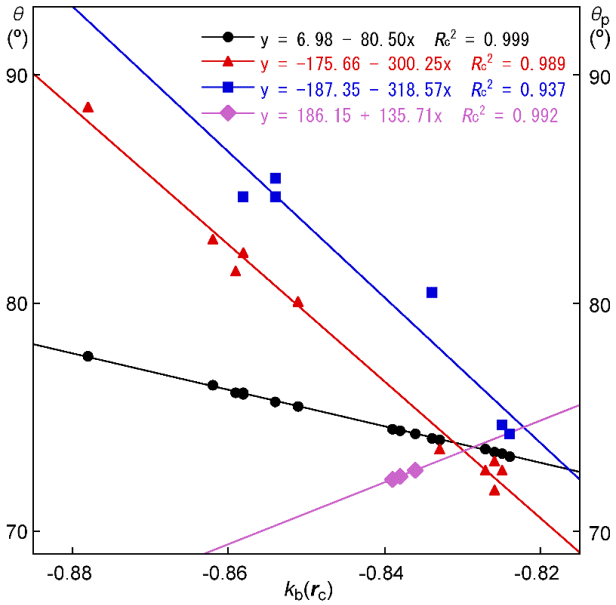

Figure 4-6. Plots of θ and θ_p versus $k_b(\boldsymbol{r}_c)$. While data of θ versus $k_b(\boldsymbol{r}_c)$ shown in ●, θ_p versus $k_b(\boldsymbol{r}_c)$ of G(**A'**) and G(**B'**) are in ▲ and ■, respectively, with those of G(**C'**) for **4-10b**-4,6', **4-11b**-4,6', and **4-12b**-4,6' are in ◆.

Nature of Intramolecular π–π Interactions in 4-1b–4-12b, Predicted with Higher Basis Set Systems

QTAIM-DFA parameters were also evaluated with MP2/6-311G(3d) and/or MP2/6-311+G(3d). The results are collected in Table 4-A3 of the Appendix, together with QTAIM functions necessary to discuss the interactions in question. Table 4-A3 contains the frequencies correlated to NIV employed to generate the perturbed structures and the force constants, k_f. The results should be closely related to those in Table 4-2.

The dynamic and static nature of the intramolecular π–π interactions between ethylene moieties in **4-1b**–**4-3b**, **4-5b**–**4-7b**, and **4-9b**–**4-12b** are examined by employing θ and θ_p evaluated with MP2/6-311G(3d). Table 4-3 summarizes the results. The intramolecular π–π interactions are all classified by the *pure* CS interactions ($\theta < 90^o$). The π–π interactions in **4-1b**–**4-3b** and **4-5b**–**4-7b** are all predicted to have the vdW nature ($\theta_p < 90^o$), except for $^{4'}$C-∗-$^{5'}$C in **4-6b**, which is predicted to have the HB nature with no covalency ($\theta_p = 95.3^o$). On the other hand, the intramolecular π–π interactions in **4-9b**–**4-12b** are all predicted to have the HB nature with no covalency ($\theta_p > 90^o$), except for $^{1'}$C-∗-^{2}C in **4-10b** (C_2). Indeed, $^{1'}$C-∗-^{2}C in **4-10b** (C_2) should be characterized as the vdW nature ($\theta_p = 89.6^o$), but it must exist in the borderline area between the vdW nature and the HB nature with no covalency. The θ_p value of 100.2º for **4-11b** is largest among the data in Table 4-3.

Table 4-3 also collects the nature of the intramolecular π–π interactions in **3-1a**–**3-3a** and **3-5a**–**3-7a** and **3-9a**–**3-12a**, similarly predicted with MP2/6-311G(3d), for convenience of comparison. The intramolecular π–π interactions in **3-1a**–**3-3a** and **3-5a**–**3-7a** are all characterized as the vdW nature ($\theta < 90^o$). Those in **3-9a**–**3-12a** are characterized as the HB nature with no covalency, although the $^{4'}C$-∗-$^{6'}C$ interactions in **3-11a** and **3-12a** are as the vdW nature.

How are the relationships between the QTAIM-DFA parameters in **4-1b**–**4-3b**, **4-5b**–**4-7b**, and **4-9b**–**4-12b** evaluated with MP2/6-311G(3d) and those with MP2/6-311G(d)? The R values in (R, θ) evaluated with MP2/6-311G(3d) correlate well with those with MP2/6-311G(d) (y = 1.036x – 0.0001: R_c^2 = 0.984) (see Figure 4-A1 of the Appendix). The plot of θ evaluated with

MP2/6-311G(3d) versus those with MP2/6-311G(d) is analyzed as two correlations, as shown in Figure 4-A2 of the Appendix. The correlations are y = 2.074x – 78.9 (R_c^2 = 0.984) for **4-3b**, **4-10b**-$_{1',2}$, and **4-11b** and y = 1.959x – 73.2 (R_c^2 = 0.991) for others as shown in Figures 4-A1 and 4-A2 of the Appendix. The θ_p values evaluated with MP2/6-311G(3d) are larger than those with MP2/6-311G(d), except those for **4-3b** (C_{2v}). Figure 4-7 shows the plot of θ_p evaluated with MP2/6-311G(3d) versus those with MP2/6-311G(d). The plot gives a good correlation, which is shown in the figure, although data for **4-6b**-$_{1',2}$, **4-6b**-$_{4,5'}$, and **4-11b**-$_{1,2}$ deviate from the correlation. Indeed, the data for **4-6b**-$_{1',2}$ and **4-6b**-$_{4,5'}$ deviate downside and upside, respectively, from the correlation line in the plot, but the average values of θ_p of 85.0º evaluated with MP2/6-311G(3d) seems close to θ_p of 82.5º with MP2/6-311G(d). The large deviation in **4-11b**-$_{1,2}$ would correspond to the characteristic the doubly degenerated BPs for the species.

2.7. Behavior of Intramolecular π-∗-π Interactions in 4-1b–4-12b versus That in 3-1a–3-12a

The R_{SL} values for **4-1b**–**4-12b** are shorter than the corresponding values in **3-1a**–**3-12a**, respectively, by 0.03–0.21 Å, except for **4-10b** (C_2)/**4-10a** (C_2)–**4-12b** (C_2)/**4-12a** (C_2). The slight change from the ethano-bridge in **3-1a**–**3-12a** to the etheno-bridge in **4-1b**–**4-12b** causes rather large differences in R_{SL}. The intramolecular π–π interactions between ethylene moieties in **4-1b**–**4-12b** are predicted to have the slightly stronger nature, relative to that in corresponding **3-1a**–**3-12a**, respectively, except for **4-6b** (C_2) versus **3-6a** (C_2) (**4-6b** (C_2)/**3-6a** (C_2)), (**4-7b** (C_{2v})/**3-7a** (C_{2v}), and **4-10b** (C_2)/**3-10a** (C_2)), judging from the θ_p values evaluated with MP2/6-311G(3d). However, further investigations seem necessary to clarify the reason for the change in the dynamic nature of the interactions.

Table 4-3. Predicted nature of intramolecular π–π interactions between ethylene moieties in **4-1b**–**4-3b**, **4-5b**–**4-7b**, and **4-9b**–**4-12b**, together with **3-1a**–**3-3a**, **3-5a**–**3-7a**, and **3-9a**–**3-11a**, based on the QTAIM-DFA parameters of θ and θ_p, evaluated with MP2/6-311(3d)[a,b]

Species (symmetry)	BP/BCP X-∗-Y	θ (°)	θ_p (°)	Nature (predicted)	Species (symmetry)	BP/BCP X-∗-Y	θ (°)	θ_p (°)	Nature (predicted)
4-1b (C_{2v})	$B_{1,1'}$-∗-$B_{2,2'}$	70.5	73.6	*p*-CS/vdW	**3-1a** (C_{2v})	$B_{1,1'}$-∗-$B_{2,2'}$	69.9	70.5	*p*-CS/vdW
4-2b (C_{2v})	$B_{1,1'}$-∗-$B_{2,2'}$	70.7	73.2	*p*-CS/vdW	**3-2a** (C_2)	^{1}C-∗-$^{2'}$C	70.4	70.9	*p*-CS/vdW
4-3b (C_{2v})	$B_{1,1'}$-∗-$B_{2,2'}$	73.6	71.5	*p*-CS/vdW	**3-3a** (C_2)	^{1}C-∗-$^{2'}$C	70.8	71.6	*p*-CS/vdW
4-3b (C_{2v})	$B_{2,2'}$-∗-$B_{3,3'}$	73.5	72.0	*p*-CS/vdW	**3-3a** (C_2)	^{2}C-∗-$^{3'}$C	70.4	71.1	*p*-CS/vdW
4-5b (C_{2v})	$B_{1,1'}$-∗-$B_{2,2'}$	70.7	76.1	*p*-CS/vdW	**3-5a** (C_{2v})	$B_{1,1'}$-∗-$B_{2,2'}$	69.9	75.0	*p*-CS/vdW
4-6b (C_2)	^{1}C-∗-^{2}C	75.2	74.6	*p*-CS/vdW	**3-6a** (C_2)	^{1}C-∗-^{2}C	73.7	85.2	*p*-CS/vdW
4-7b (C_{2v})	$B_{1,1'}$-∗-$B_{2,2'}$	70.5	75.8	*p*-CS/vdW	**3-7a** (C_2)	^{1}C-∗-$^{2'}$C	73.5	88.8	*p*-CS/vdW
4-9b (C_s)	^{1}C-∗-^{2}C	79.5	93.7	*p*-CS/*t*-HB[c]	**3-9a** (C_s)	^{1}C-∗-^{2}C	78.2	90.8	*p*-CS/*t*-HB[c]
4-10b (C_2)	$^{1'}$C-∗-^{2}C	78.5	89.6	*p*-CS/vdW	**3-10a** (C_2)	^{1}C-∗-$^{2'}$C	80.2	95.0	*p*-CS/*t*-HB[c]
4-11b (C_2)	$^{1'}$C-∗-^{2}C	78.5	100.2	*p*-CS/*t*-HB[c]	**3-11a** (C_2)	^{1}C-∗-^{2}C	79.4	94.5	*p*-CS/*t*-HB[c]
4-12b (C_2)	$^{1'}$C-∗-^{2}C	78.2	92.3	*p*-CS/*t*-HB[c]					
4-6b (C_2)[d]	$^{4'}$C-∗-$^{5'}$C	*76.1*	*95.3*	*p*-CS/*t*-HB[c]	***3-6a*** (C_2)[e]	$^{4'}$C-∗-$^{5'}$C	*73.0*	*81.1*	*p-CS/vdW*
4-10b (C_2)[d]	$^{4'}$C-∗-$^{6'}$C	*72.1*	*73.7*	*p-CS/vdW*	***3-10a*** (C_2)	$^{4'}$C-∗-$^{6'}$C	*71.6*	*73.1*	*p-CS/vdW*
4-12b (C_2)[d]	$^{4'}$C-∗-$^{6'}$C	*72.1*	*73.1*	*p-CS/vdW*					

[a] See text for BSSs. [b] Data are given at BCP for interaction in question, which is shown by -∗-. [c] *Typical*-HB nature without covalency. [d] Corresponding to the interaction in question. [e] For the ethylene moieties in the backside of the molecule in **3-6a** (C_2). See Figures 4-1 for the interactions and ref 15.

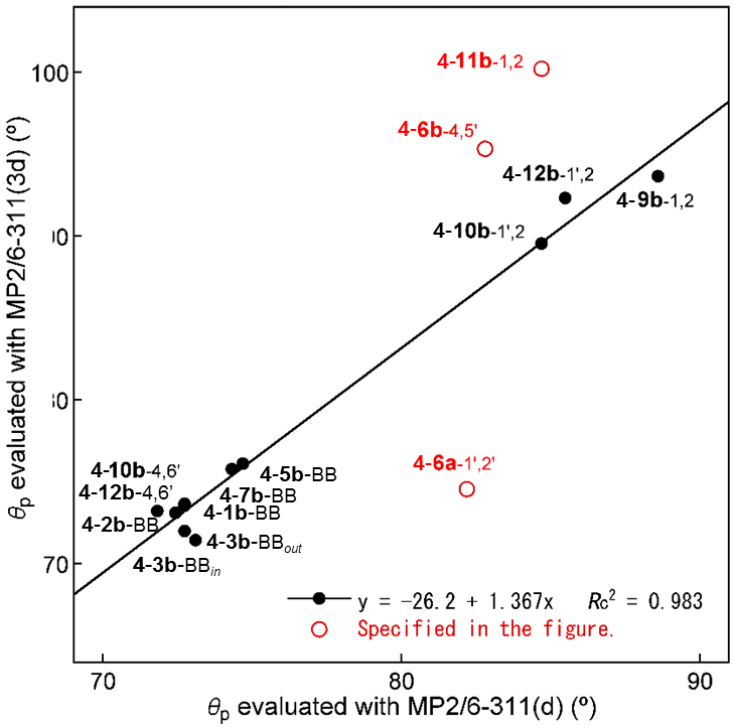

Figure 4-7. Plot of θ_p evaluated with the MP2/6-311G(3d) versus those with the MP2/6-311G(d), which gave a good correlation for most interactions (●) with some deviations (◯), as shown in the figure.

Nature of Doubly Generated BPs and ALs

The QTAIM-DFA parameters for the intramolecular π–π interactions between the opposite phenyl moieties in **3-10a** (C_2: ϕ_A = 11.7°) are calculated similarly to the case of **4-11b** (C_2: ϕ_A = 11.7°) with MP2/6-311G(d). The perturbed structures are generated with NIV, which correspond to the internal vibrations of **3-10a** (C_{2v}: ϕ_A = 0.0°) of which direction is substantially the same as the $^{1'}C$---^{2}C direction. The data for **3-10a** (C_2: ϕ_A = 11.7°) are collected in Table 4-2. The data for **4-11b** (C_2: ϕ_A = 11.8°) evaluated with MP2/6-311G(3d) are shown in Table 4-3, while those for **4-11b** (C_2: ϕ_A = 11.7°) in Table 4-2.

The BPs for the intramolecular π–π interactions in **4-11b** (C_2: ϕ_A = 11.7–11.8°) and ALs in **3-10a** (C_2: ϕ_A = 11.7°) are all classified by the *pure* CS interactions. The interactions between the opposite benzene rings in **4-11b** (C_2: ϕ_A = 11.7°) and **3-10a** (C_2: ϕ_A = 11.7°) are characterized as the vdW nature, based on the θ and θ_p values, if evaluated with MP2/6-311G(d). However, the degenerated BP (^{1}C-∗-$^{2'}$C) and BP (^{1}C-∗-$^{2'}$C) in **4-11b** (C_2: ϕ_A = 11.8°) are predicted to have the HB nature with no covalency, if evaluated with MP2/6-311G(3d).

Summary

The behavior of the intramolecular π–π interactions is elucidated, exemplified by diethenodihydronaphthalene (**4-1b**) and the derivatives (**4-2b**–**4-12b**), employing QTAIM-DFA. The behavior for **4-1b**–**4-12b** is discussed by comparing that for the corresponding diethanodihydronaphthalene (**3-1a**) and the derivatives (**3-2a**–**3-12a**), respectively. The C_2 structures (ϕ_l: 6.6–11.1º) for **3-1a**–**3-3a** and **3-7a** change to the C_{2v} structures (ϕ_l = 0.0º) for **4-1b**–**4-3b** and **4-7b**, respectively, if optimized with MP2/6-311G(d). The ϕ_l value of 7.8º for **3-4a** (C_2) becomes (much) smaller to ϕ_l = (–)3.7º for **4-4b** (C_2), although the C_2 symmetry is maintained under the optimizations, for example. While R_{SL} for **4-1b**–**4-9b** are predicted to be shorter than the corresponding values in **3-1a**–**3-9a**, respectively, R_{SL} for **4-10b**–**4-12b** are longer than the

corresponding values for **3-10a**–**3-12a**, respectively. The change in the symmetries, the ϕ_I values, and the interaction distances must responsible for the differences in the interactions between the two systems.

During the course of the investigations, doubly degenerated BPs are detected between the carbon atoms of the opposite phenyl rings in the minimum structures of **4-11b** (C_2: ϕ_A = 11.7°) optimized with MP2/6-311G(d) and **4-11b** (C_2: ϕ_A = 11.8°) with MP2/6-311G(3d). The doubly degenerated BPs are described by BP (^{1}C-∗-$^{2'}$C) and BP (^{1}C-∗-$^{2'}$C). The appearance of the doubly degenerated BPs must be very curious, since one BP with a BCP is expected to correspond to an interaction between two carbon atoms. Similarly, the doubly degenerated atomic interaction lines (ALs) are detected in the perturbed structure of **3-10a** (C_2: ϕ_A = 11.7°) between the minimum structure of **3-10a** (C_2: ϕ_A = 17.6°) and the transition state for the site exchange process between **3-10a** (C_2: ϕ_A = 17.6°) and its topological isomer, **3-10a'** (C_2: ϕ_A = –17.6°). The doubly degenerated ALs are described by AL (^{1}C-∗-$^{2'}$C) and AL (^{1}C-∗-$^{2'}$C). Indeed, the doubly degenerated BPs and ALs are detected in **4-11b** (C_2: ϕ_A = 11.7° and 11.8°) and **3-10a** (C_2: ϕ_A = 11.7°), respectively, but the requirements for the appearance would be very severe, since ϕ_A are around 11.7–11.8° for both cases.

The intramolecular π–π interactions between ethylene moieties in **4-1b**–**4-12b** are predicted to be somewhat stronger than the corresponding interactions in **3-1a**–**3-12a**, respectively, judging from the θ_p values, except for **4-6b** (C_2) versus **3-6a** (C_2) (**4-6b** (C_2)/**3-6a** (C_2)), **4-7b** (C_{2v})/**3-7a** (C_2), and **4-10b** (C_2)/**3-10a** (C_2), if evaluated with MP2/6-311G(3d), although **4-4b** (C_2)/**3-4a** (C_2), **4-8b** (C_2)/**3-8a** (C_2) and **4-12b** (C_2)/**3-12a** (C_2) are not examined. The nature of the intramolecular π–π interactions between ethylene moieties in **4-1b**–**4-12b** is well elucidated by employing QTAIM-DFA.

Appendix

Table 4-A1. π–π Interaction distance at calculated **4-1b**–**4-12b**, together with symmetries and the appearance or non-appearance of bond critical points (BCP) between them.

Species (X-∗-Y)	Distance (Å)	Symmetry	BCP
MP2/6-311G(3d)			
4-1b (^{1}C-∗-^{2}C)	2.96535	C_{2v}	Yes
4-2b (^{1}C-∗-^{2}C)	2.98579	C_{2v}	Yes
4-3b (^{1}C-∗-^{2}C)	2.99576	C_{2v}	Yes
4-3b (^{2}C-∗-^{3}C)	3.01473	C_{2v}	Yes
4-5b (^{1}C-∗-^{2}C)	2.88828	C_{2v}	Yes
4-7b (^{1}C-∗-^{2}C)	2.89741	C_{2v}	Yes
4-9b (^{1}C-∗-^{2}C)	2.88778	C_{s}	Yes
4-10b (^{1}C-∗-^{2}C)	2.92507	C_{2}	No
4-10b (^{1}C-∗-$^{2'}$C)	2.96480	C_{2}	Yes
4-10b (^{3}C-∗-^{4}C)	3.59253	C_{2}	No
4-10b (^{3}C-∗-$^{4'}$C)	3.36869	C_{2}	Yes
M06-2X/6-311G(3d)			
4-1b (^{1}C-∗-^{2}C)	3.00644	C_{2v}	Yes
4-2b (^{1}C-∗-^{2}C)	3.03018	C_{2v}	Yes
4-3b (^{1}C-∗-^{2}C)	3.02512	C_{2v}	Yes
4-3b (^{2}C-∗-^{3}C)	3.03792	C_{2v}	Yes
4-4b (^{1}C-∗-^{2}C)	3.02318	C_{2}	No
4-4b (BCP-∗-^{2}C)	3.07558	C_{2}	Yes
4-4b (^{2}C-∗-^{3}C)	3.04636	C_{2}	No
4-4b ($^{2'}$C-∗-^{3}C)	3.28151	C_{2}	Yes
4-5b (^{1}C-∗-^{2}C)	2.92077	C_{2v}	Yes
4-6b (^{1}C-∗-^{2}C)	2.83508	C_{2v}	Yes
4-6b (^{3}C-∗-^{4}C)	2.80216	C_{2v}	Yes
4-7b (^{1}C-∗-^{2}C)	2.92619	C_{2v}	Yes
4-8b (^{1}C-∗-^{2}C)	2.99384	C_{2}	Yes
4-8b (^{2}C-∗-^{3}C)	2.87663	C_{2}	Yes
4-9b (^{1}C-∗-^{2}C)	2.96000	C_{s}	Yes
4-10b (^{1}C-∗-^{2}C)	3.03486	C_{2}	Yes
4-10b (^{1}C-∗-$^{2'}$C)	3.17033	C_{2}	No
4-10b (^{3}C-∗-^{4}C)	3.88698	C_{2}	No
4-10b (^{3}C-∗-$^{4'}$C)	3.73929	C_{2}	No
4-11b (^{1}C-∗-^{2}C)	2.97106	C_{1}	Yes
4-11b (^{1}C-∗-$^{2'}$C)	3.14515	C_{1}	No
4-11b (^{3}C-∗-^{4}C)	3.78090	C_{1}	No
4-11b (^{3}C-∗-$^{4'}$C)	3.78424	C_{1}	No
4-12b (^{1}C-∗-^{2}C)	2.97889	C_{1}	Yes
4-12b ($^{1'}$C-∗-^{2}C)	3.13443	C_{1}	No
4-12b (^{3}C-∗-^{4}C)	3.77542	C_{1}	No
4-12b ($^{3'}$C-∗-^{4}C)	3.75831	C_{1}	No

Table 4-A2. Distances of $r(^{1}C\text{-}*\text{-}^{2}C)$ for **4-1b** and **3-1a**, evaluated with various method and the observed values[a]

Method	**4-1b**	**3-1a**
MP2/6-311+G(3d)	2.9623	3.0394
MP2/6-311G(3d)	2.9653	3.0396
MP2/6-311G(d)	2.9654	
M062X/6-311+G(3df,p)		3.0745
M062X/6-311+G(3d,p)		3.0769
M062X/6-311G(3d,p)		3.0763
M062X/6-311+G(3d)	3.0045	3.0744
M062X/6-311G(3d)	3.0064	3.0748
Observed		3.036,3.028[b]

[a] In Å. [b] Ref. 38.

Table 4-A3. Intramolecular π–π interactions between ethylene moieties in **4-1b**–**4-12b**, evaluated with the 6-311(d) basis set at the MP2 level, together with the R_{SL} and r_{BP} values and the symmetry[a]

Species (Symmetry)	BP with BCP X-*-Y	r_{BP} (Å)	R_{SL} (Å)	Δr_{BP}[b] (Å)
4-1b (C_{2v})	$B_{1,1'}$-*-$B_{2,2'}$	2.9762	2.9742	0.0020
4-2b (C_{2v})	$B_{1,1'}$-*-$B_{2,2'}$	2.9956	2.9931	0.0025
4-3b (C_{2v})	$B_{1,1'}$-*-$B_{2,2'}$	2.9975	2.9949	0.0026
4-3b (C_{2v})	$B_{2,2'}$-*-$B_{3,3'}$	3.0186	3.0156	0.0030
4-4b (C_2)	$^{1'}C$-*-$^{2'}C$	3.7249	2.9856	0.7394
4-4b (C_2)	^{2}C-*-$^{3'}C$	3.6999	3.2000	0.4999
4-5b (C_{2v})	$B_{1,1'}$-*-$B_{2,2'}$	2.8982	2.8971	0.0011
4-6b (C_2)	$^{1'}C$-*-$^{2'}C$	3.3809	2.8115	0.5695
4-6b (C_2)	$^{4'}C$-*-^{5}C	3.1853	2.8927	0.2926
4-7b (C_{2v})	$B_{1,1'}$-*-$B_{2,2'}$	2.9087	2.9075	0.0012
4-8b (C_2)	^{1}C-*-^{2}C	3.5488	2.9424	0.6064
4-8b (C_2)	$^{2'}C$-*-^{3}C	3.2212	2.9499	0.2713
4-9b (C_s)	^{1}C-*-^{2}C	3.0019	2.8998	0.1021
4-10b (C_2)	$^{1'}C$-*-^{2}C	3.0697	2.9613	0.1084
4-10b (C_2)	$^{4'}C$-*-^{6}C	3.4056	3.3638	0.0417
4-11b (C_2)	$^{1'}C$-*-^{2}C	3.4295	2.9557	0.4739
4-11b (C_2)	$^{4'}C$-*-^{6}C	3.4228	3.3955	0.0274
4-12b (C_2)	$^{1'}C$-*-^{2}C	3.0841	2.9507	0.1334
4-12b (C_2)	$^{4'}C$-*-^{6}C	3.4120	3.3843	0.0277

[a] Only one side interaction being shown if equivalent interactions are detected. [b] $\Delta r_{BP} = r_{BP} - R_{SL}$.

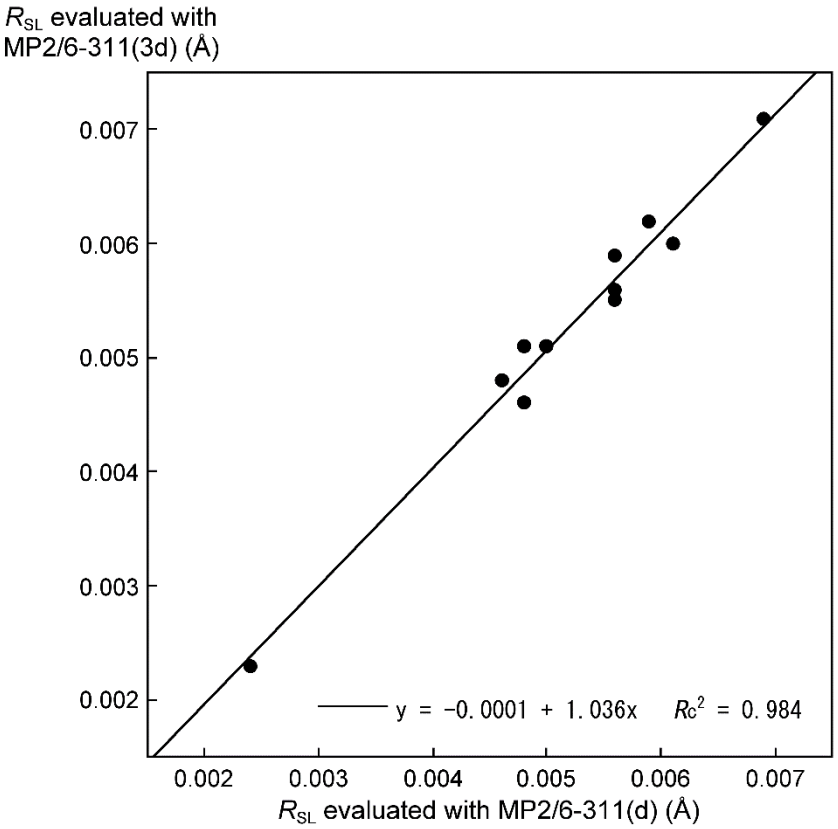

Figure 4-A1. The *R* values evaluated with MP2/6-311G(3d) versus those with MP2/6-311G(d).

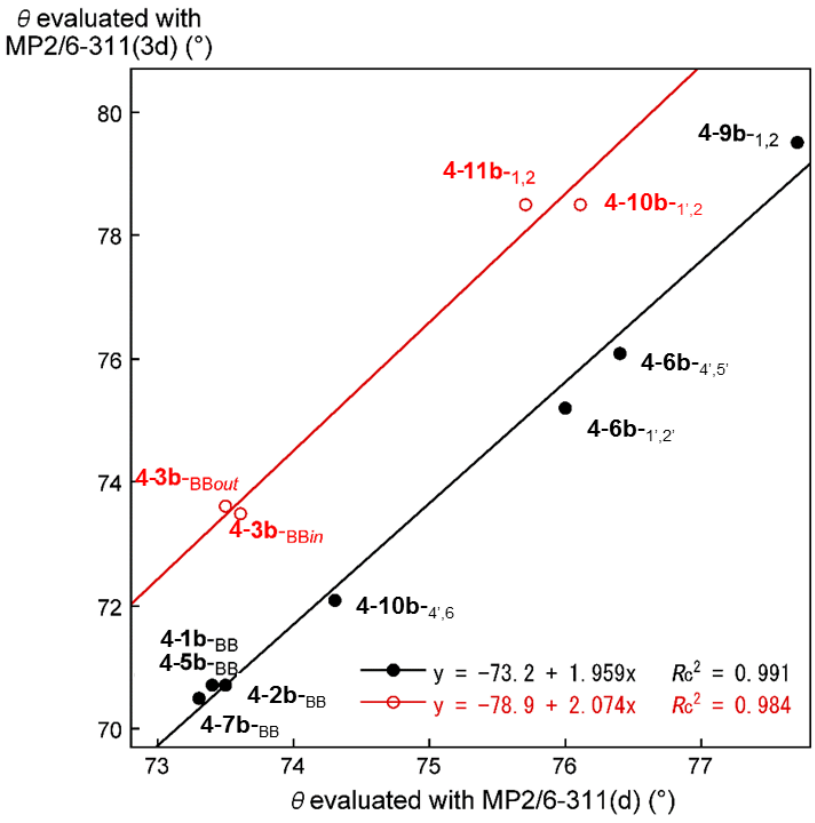

Figure 4-A2. The *θ* values evaluated with MP2/6-311G(3d) versus those with MP2/6-311G(d).

Figure 4-A3 shows the story for the change in molecular graph of **3-10a** in the site exchange between **3-10a** (C_2) via **3-10a** (C_{2v}) of TS. It must be noteworthy that doubly degenerated BPs with BCPs are detected for the ^{1}C-∗-$^{2'}$C interactions between the ethylene moieties in a structure ($\phi_A \approx 11.7°$) appeared in the site exchange process of **3-10a**.

(a) Side View

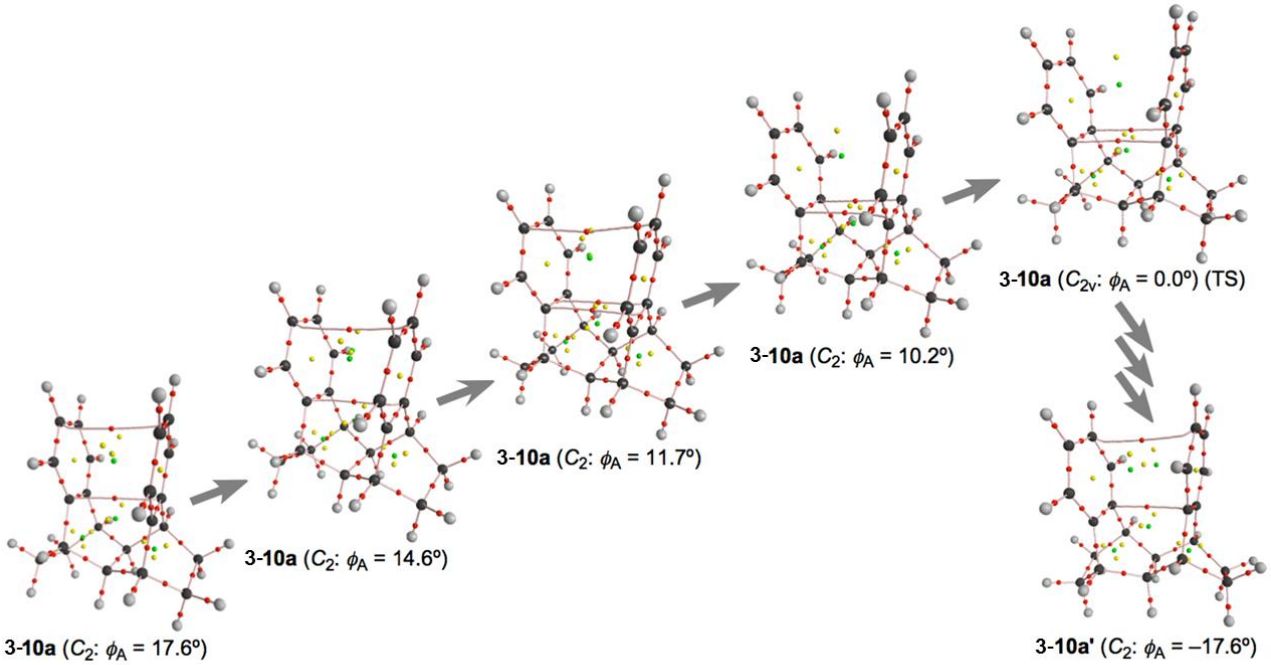

(b) Top View

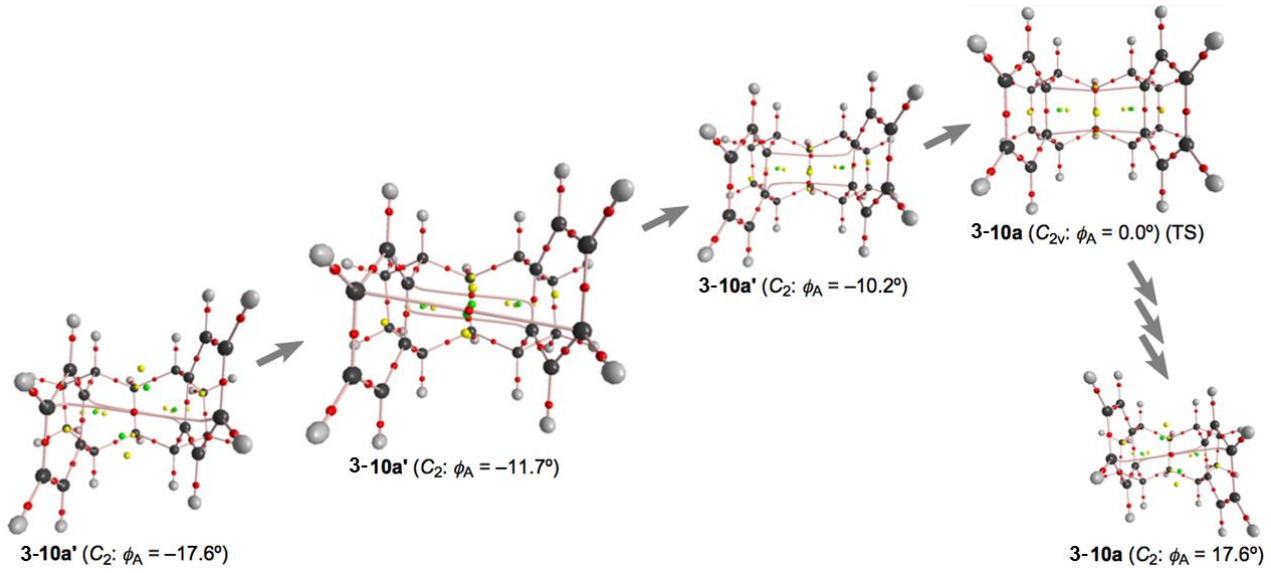

Figure 4-A3. Molecular graphs drawn on the structures appeared in the site exchange process between **3-10a** (C_2: ϕ_A = 17.6°) and the topologically equivalent **3-10a'** (C_2: ϕ_A = –17.6°), containing **3-10a** (C_2: ϕ_A = 0.0°), which would be the transition state between them.

Table 4-A4. QTAIM functions and QTAIM-DFA parameters for intramolecular π–π interactions, together with the frequencies closely related to the interactions and the force constants in **3-10a** (C_{2v}), **4-10b** (C_{2v}), and derivatives[a]

Species (symmetry)	BP/BCP (X-*-Y)	$\rho_b(\boldsymbol{r}_c)$ (ea_o^{-3})	$c\nabla^2\rho_b(\boldsymbol{r}_c)$[b] (au)	$H_b(\boldsymbol{r}_c)$ (au)	$k_b(\boldsymbol{r}_c)$[c]
3-1a (C_{2v}: ϕ_A = 0.0°)	$B_{1,1'}$-*-$B_{2,2'}$	0.0119	0.0042	0.0013	–0.820
3-10a (C_2: ϕ_A = 17.6°)	($^{1'}$C-*-^{2}C)	0.0149	0.0057	0.0012	–0.881
3-10a (C_2: ϕ_A = 17.6°)	($^{4'}$C-*-$^{6'}$C)[d]	0.0071	0.0023	0.0007	–0.829
3-10a (C_{2v}: ϕ_A = 0.0°)	($^{1'}$C-*-^{2}C)	0.0140	0.0055	0.0014	–0.858
3-10a (C_2: ϕ_A = 11.7°)	($^{1'}$C-*-^{2}C)	0.0140	0.0055	0.0014	–0.858
3-10a (C_2: ϕ_A = 11.7°)	($^{4'}$C-*-$^{6'}$C)[d]	0.0070	0.0023	0.0006	–0.836
3-11a (C_2)	(^{1}C-*-^{2}C)	0.0128	0.0052	0.0012	–0.876
4-1b (C_{2v}: ϕ_A = 0.0°)	$B_{1,1'}$-*-$B_{2,2'}$	0.0133	0.0048	0.0014	–0.825
4-11b (C_2: ϕ_A = 11.7°)	(^{1}C-*-^{2}C)	0.0145	0.0059	0.0015	–0.854
4-11b (C_2: ϕ_A = 11.7°)	($^{4'}$C-*-$^{6'}$C)[d]	0.0067	0.0022	0.0006	–0.839

[a]Evaluated with MP2/6-311G(d). [b]$c\nabla^2\rho_b(\boldsymbol{r}_c) = H_b(\boldsymbol{r}_c) - V_b(\boldsymbol{r}_c)/2$, where $c = \hbar^2/8m$. [c]$k_b(\boldsymbol{r}_c) = V_b(\boldsymbol{r}_c)/G_b(\boldsymbol{r}_c)$. [d]See Figure 4-A3 for the interactions.

(continues)

Species (symmetry)	BP/BCP (X-*-Y)	R (au)	θ (°)	Freq[e] (cm^{-1})	k_f[f] (mDyn $Å^{-1}$)	θ_p (°)	κ_p (au^{-1})	classification/ characterization
3-1a (C_{2v}: ϕ_A = 0.0°)	$B_{1,1'}$-*-$B_{2,2'}$	0.0044	73.0	185.4	0.068	70.8	37.1	*p*-CS/vdW
3-10a (C_2: ϕ_A = 17.6°)	($^{1'}$C-*-^{2}C)	0.0058	78.0	199.3	0.066	90.0	122.0	*p*-CS/vdW
3-10a (C_2: ϕ_A = 17.6°)	($^{4'}$C-*-$^{6'}$C)[d]	0.0024	73.7	100.8	0.030	72.0	80.5	*p*-CS/vdW
3-10a (C_{2v}: ϕ_A = 0.0°)	($^{1'}$C-*-^{2}C)	0.0056	76.1	216.3	0.109	84.7	95.3	*p*-CS/vdW
3-10a (C_2: ϕ_A = 11.7°)	($^{1'}$C-*-^{2}C)	0.0056	76.1	216.3	0.109	84.7	95.3	*p*-CS/vdW
3-10a (C_2: ϕ_A = 11.7°)	($^{4'}$C-*-$^{6'}$C)[d]	0.0024	74.3	110.3	0.038	72.7	63.9	*p*-CS/vdW
3-11a (C_2)	(^{1}C-*-^{2}C)	0.0053	77.5	224.1	0.120	90.6	129	*p*-CS/vdW
4-1b (C_{2v}: ϕ_A = 0.0°)	$B_{1,1'}$-*-$B_{2,2'}$	0.0050	73.4	200.3	0.081	72.7	42.4	*p*-CS/vdW
4-11b (C_2: ϕ_A = 11.7°)	(^{1}C-*-^{2}C)	0.0061	75.7	237.9	0.143	84.7	94.7	*p*-CS/vdW
4-11b (C_2: ϕ_A = 11.7°)	($^{4'}$C-*-$^{6'}$C)[d]	0.0023	74.5	113.1	0.037	72.3	43.3	*p*-CS/vdW

[d]See Figure 4-A3 for the interactions. [e] Corresponding to the interaction in question. [f]Force constant for ν_n.

Such molecular graphs containing the degenerated BPs between C atoms are looked for and the very similar molecular graph was found for **4-11b** (C_2), which corresponds to the dibenzo-derivative of **4-1b** with the etheno-bridge between the central carbon atoms.

The fully optimized structure **4-11b** (C_2) is with ϕ_A = 11.7º. It must be of very interest, since ϕ_A = 11.7º in the fully optimized structure of **4-11b** (C_2) is just the ϕ_A range of **3-10a** (C_2), which is

expected to give the molecular graph identical to that shown in Figure 4-1 in the text. The opposite benzene rings in **4-11b** (C_2: ϕ_A = 11.7º) are connected by BP (^{1}C-∗-$^{2'}$C) and BP (^{1}C-∗-$^{2'}$C) with BP (^{4}C-∗-$^{6'}$C), where the first two are degenerated between the ^{1}C and $^{2'}$C atoms.

Figure 4-A4 shows negative Laplacian of $\rho(\boldsymbol{r})$ and the trajectory plot of **4-11b** (C_2), drawn on the plane containing the ^{1}C and $^{2'}$C atoms and the two BCPs in question. The degenerated BPs in **4-11b** (C_2) are clearly described again in the contour plot, where BCPs are located at the three dimensional saddle points of $\rho(\boldsymbol{r})$. The BCPs in question are shown to be located in the positive area of $\nabla^2\rho_b(\boldsymbol{r}_c)$, therefore, the interactions correspond to the BCPs are classified by the *pure* closed shell (CS) interactions. The space around the species seems reasonably divided into atoms in **4-11b** (C_2) as described by the trajectory plot.

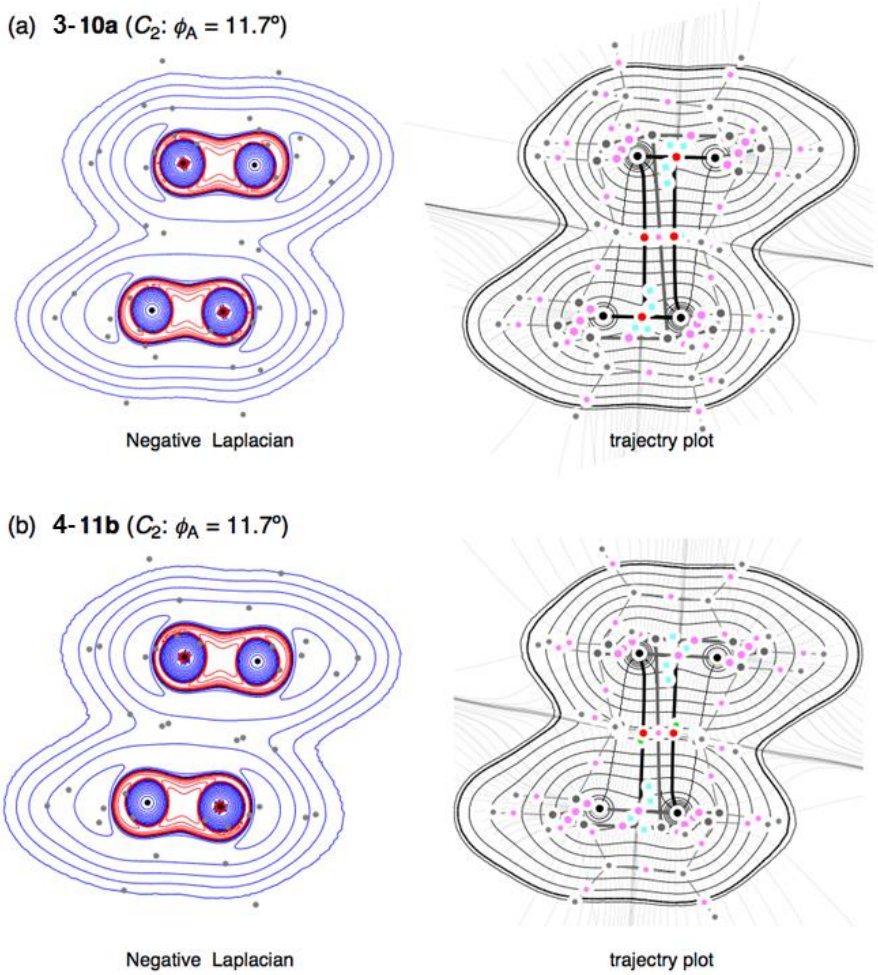

Figure 4-A4. Negative Laplacians and the trajectory plots for **3-10a** (C_2: ϕ_A = 11.7º) (a) and **4-11b** (C_2: ϕ_A = 11.7º) (b) drawn with MP2/6-311G(d), similarly to the case of Figure 4-1 in the text. Blue and red lines correspond to the positive and negative values, respectively.

References

1 The various ways to achieve cyclic delocalization by joining chains of conjugated π-systems were studied in 1971 by Hoffmann and Goldstein; M. J. Goldstein, R. Hoffmann, *J. Am. Chem. Soc.* **1971**, *93*, 6193–6204.

2 H.-D. Martin and R. Schwesinger, *Chem. Ber.* **1974**, *107*, 3143–3145.

3 G. Sedelmeier, H. Prinzbach, H.-D. Martin, *Chimia*, **1979**, *33*, 329–332.

4 J. Spanget-Larsen, R. Gleiter, G. Klein, C. W. Doecke, L. A. Paquette, *Chem. Ber.* **1980**, *113*, 2120–2126.

5 K. B. Wiberg, M. G. Matturro, P. J. Okarma, M. E. Jason, *J. Am. Chem. Soc.* **1984**, *106*, 2194–2200.

6 C.-T. Lin, N.-J. Wang, Y.-L. Yeh, T.-C. Chou, Tetrahedron, **1995**, *51*, 2907–2928.

7 H. Lange, W. Schäfer, R. Gleiter, P. Camps, S. Vazquez, *J. Org. Chem.* **1998**, *63*, 3478–2480.

8 W. Grimme, J. Wortmann, D. Frowein, J. Lex, G. Chen, R. Gleiter, *J. Chem. Soc., Perkin Trans. 2* **1998,** 1893–1900.

9 H. Wang, W. Wang, W. J. Jin, *Chem. Rev.* **2016**, http://dx.doi.org/10.1021/acs.chemrev.5b00527.

10 E. Peresypkina, A. Virovets, M. Scheer, *Cryst. Growth Des.* **2016**, http://dx.doi.org/10.1021/acs.cgd.6b00136.

11 B. E. Carson, T. M. Parker, E. G. Hohenstein, G. L. Brizius, W. Komorner, R. A. King, D. M. Collard, C. D. Sherrill, *Chem. Eur. J.* **2015**, *21*, 19168–19175.

12 Z. A. Tehrani, K. S. Kim, Int. J. Quantum Chem. **2016**, *116*, 622–633.

13 R. L. Gawade, D. K. Chakravarty, A. Kotmale, E. Sangtani, P. V. Joshi, A. Ahmed, M. V. Mane, S. Das, K. Vanka, P. R. Rajamohanan, V. G. Puranik, R. G. Gonnade, *Cryst. Growth Des.* **2016**, DOI: 10.1021/acs.cgd.6b00204.

14 *Modern Cyclophane Chemistry*, eds. R. Gleiter, H. Hopf, Wiley-VCH, Weinheim, 2004.

15 K. Matsuiwa, S. Hayashi, W. Nakanishi, M. Kitamoto, *ChemistrySelect* **2016**, *1*, 2344–2353.

16 A union of closures of BPs or atomic interaction lines (ALs) for a given structure of a species is called a molecular graph. The interactions in a molecular graph of a fully optimized structure are described by BPs, whereas those in a molecular graph of a non-minimum structure are by ALs.

17 (*a*) *Atoms in Molecules. A Quantum Theory* (Ed. R. F. W. Bader), Oxford University Press, Oxford, UK, **1990**.

18 C. F. Matta, R. J. Boyd, *An Introduction to the Quantum Theory of Atoms in Molecules* In *The Quantum Theory of Atoms in Molecules: From Solid State to DNA and Drug Design*, (Eds. C. F. Matta, R. J. Boyd), Wiley-VCH, Weinheim, Germany, **2007**, Chap. 1.

19 a) F. Biegler-König, R. F. W. Bader, T. H. Tang, *J. Comput. Chem.* **1982**, *3*, 317–328; b) R. F. W. Bader, T. S. Slee. D. Cremer, E. Kraka, *J. Am. Chem. Soc.* **1983**, *105*, 5061–5068; c) R. F. W. Bader, *Acc. Chem. Res.* **1985**, *18*, 9–15; d) T. H. Tang, R. F. W. Bader, P. MacDougall, *Inorg. Chem.* **1985**, *24*, 2047–2053; e) R. F. W. Bader, *Chem. Res.* **1991**, *91*, 893–926; f) R. F. W. Bader, *J. Phys. Chem. A* **1998**, *102*, 7314–7323; g) F. Biegler-König, J. Schönbohm, D. Bayles, *J. Comput. Chem.* **2001**, *22*, 545–559; h) F. Biegler-König, J. Schönbohm, *J. Comput. Chem.* **2002**, *23*, 1489–1494.

20 J. A. Dobado, H. Martînez-Garcîa, J. Molina, M. R. Sundberg, *J. Am. Chem. Soc.* **2000**, *122*, 1144–1149.

21 J. Molina, J. A. Dobado, *Theor. Chem. Acc.* **2001**, *105*, 328–337.

22 S. K. Ignatov, N. H. Rees, B. R. Tyrrell, S. R. Dubberley, A. G. Razuvaev, P. Mountford, G. I. Nikonov, *Chem. Eur. J.* **2004**, *10*, 4991–4999.

23 S. K. Tripathi, U. Patel, D. Roy, R. B. Sunoj, H. B. Singh, G. Wolmershäuser, R. J. Butcher, *J. Org. Chem.* **2005**, *70*, 9237–9247.

24 a) M. Yamashita, Y. Yamamoto, K.-y. Akiba, D. Hashizume, F. Iwasaki, N. Takagi, S. Nagase, *J. Am. Chem. Soc.* **2005**, *127*, 435–4371; b) Y. Yamamoto, K.-y. Akiba, *J. Syn. Org. Chem. Jpn.* **2004**, *62*, 1128–1137.

25 W. Nakanishi, T. Nakamoto, S. Hayashi, T. Sasamori, N. Tokitoh, *Chem. Eur. J.* **2007**, *13*, 255–268.

26 a) W. Nakanishi, S. Hayashi, K. Narahara, *J. Phys. Chem. A* **2009**, *113*, 10050–10057; b) W. Nakanishi, S. Hayashi, K. Narahara, *J. Phys. Chem. A* **2008**, *112*, 13593–13599.

27 W. Nakanishi, S. Hayashi, *Curr. Org. Chem.* **2010**, *14*, 181–197.

28 W. Nakanishi, S. Hayashi, *J. Phys. Chem. A* **2010**, *114*, 7423–7430.

29 W. Nakanishi, S. Hayashi, K. Matsuiwa, M. Kitamoto, *Bull. Chem. Soc. Jpn.* **2012**, *85*, 1293–1305.

30 *Gaussian 03 (Revision D.02)*, M. J. Frisch, G. W. Trucks, H. B. Schlegel, G. E. Scuseria, M. A. Robb, J. R. Cheeseman, J. A. Montgomery, Jr., T. Vreven, K. N. Kudin, J. C. Burant, J. M. Millam, S. S. Iyengar, J. Tomasi, V. Barone, B. Mennucci, M. Cossi, G. Scalmani, N. Rega, G. A. Petersson, H. Nakatsuji, M. Hada, M. Ehara, K. Toyota, R. Fukuda, J. Hasegawa, M. Ishida, T. Nakajima, Y. Honda, O. Kitao, H. Nakai, M. Klene, X. Li, J. E. Knox, H. P. Hratchian, J. B. Cross, V. Bakken, C. Adamo, J. Jaramillo, R. Gomperts, R. E. Stratmann, O. Yazyev, A. J. Austin, R. Cammi, C. Pomelli, J. W. Ochterski, P. Y. Ayala, K. Morokuma, G. A. Voth, P. Salvador, J. J. Dannenberg, V. G. Zakrzewski, S. Dapprich, A. D. Daniels, M. C. Strain, O. Farkas, D. K. Malick, A. D. Rabuck, K. Raghavachari, J. B. Foresman, J. V. Ortiz, Q. Cui, A. G. Baboul, S. Clifford, J. Cioslowski, B. B. Stefanov, G. Liu, A. Liashenko, P. Piskorz, I. Komaromi, R. L. Martin, D. J. Fox, T. Keith, M. A. Al-Laham, C. Y. Peng, A. Nanayakkara, M. Challacombe, P. M. W. Gill, B. Johnson, W. Chen, M. W. Wong, C. Gonzalez, J. A. Pople, Gaussian, Inc.; Wallingford CT, **2004**.

31 *Gaussian 09, Revision D.01*, M. J. Frisch, G. W. Trucks, H. B. Schlegel, G. E. Scuseria, M. A. Robb, J. R. Cheeseman, G. Scalmani, V. Barone, B. Mennucci, G. A. Petersson, H. Nakatsuji, M. Caricato, X. Li, H. P. Hratchian, A. F. Izmaylov, J. Bloino, G. Zheng, J. L. Sonnenberg, M. Hada, M. Ehara, K. Toyota, R. Fukuda, J. Hasegawa, M. Ishida, T. Nakajima, Y. Honda, O. Kitao, H. Nakai, T. Vreven, J. A. Montgomery, Jr., J. E. Peralta, F. Ogliaro, M. Bearpark, J. J.

Heyd, E. Brothers, K. N. Kudin, V. N. Staroverov, R. Kobayashi, J. Normand, K. Raghavachari, A. Rendell, J. C. Burant, S. S. Iyengar, J. Tomasi, M. Cossi, N. Rega, J. M. Millam, M. Klene, J. E. Knox, J. B. Cross, V. Bakken, C. Adamo, J. Jaramillo, R. Gomperts, R. E. Stratmann, O. Yazyev, A. J. Austin, R. Cammi, C. Pomelli, J. W. Ochterski, R. L. Martin, K. Morokuma, V. G. Zakrzewski, G. A. Voth, P. Salvador, J. J. Dannenberg, S. Dapprich, A. D. Daniels, Ö. Farkas, J. B. Foresman, J. V. Ortiz, J. Cioslowski, D. J. Fox, Gaussian, Inc., Wallingford CT, 2009.

32 For the 6-311G basis sets, see: a) R. C. Binning Jr., L. A. Curtiss, *J. Comput. Chem.* **1990**, *11*, 1206–1216; b) L. A. Curtiss, M. P. McGrath, J.-P. Blaudeau, N. E. Davis, R. C. Binning Jr., L. Radom, *J. Chem. Phys.* **1995**, *103*, 6104–6113; c) M. P. McGrath, L. Radom, *J. Chem. Phys.* **1991**, *94*, 511–516. For the diffuse functions (+ and ++), see: T. Clark, J. Chandrasekhar, G. W. Spitznagel, P. v. R. Schleyer, *J. Comput. Chem.* **1983**, *4*, 294–301.

33 a) C. Møller, M. S. Plesset, *Phys. Rev.* **1934**, *46*, 618–622; b) J. Gauss, *J. Chem. Phys.* **1993**, *99*, 3629–3643; c) J. Gauss, *Ber. Bunsen-Ges. Phys. Chem.* **1995**, *99*, 1001–1008.

34 The AIM2000 program (*Version* 2.0) is employed to analyze and visualize atoms-in-molecules: F. Biegler-König, *J. Comput. Chem.* **2000**, *21*, 1040−1048. See also ref 19g.

35 For the *m*×*n* matrix representation, m corresponds to the number of atoms and *n* (= 3) to the *x*, *y*, and *z* components of the space.

36 It is achieved by changing the corresponding parameters in Gaussian 03 and Gaussian 09 from the default values to print out the normal coordinates of five digits for the purpose.

37 W. Nakanishi, S. Hayashi, *J. Phys. Chem. A* **2013**, *117*, 1795−1803.

38 W. Grimme, H. T. Kämmerling, J. Lex, R. Gleiter, J. Heinze, M. Dietrich, *Angew*. *Chem*. *Int*. *Ed*. *Engl*. **1991**, 30, 205.

Chapter 5

Behavior of Intramolecular π–π Interactions in [2.2]- and [3.3]Cyclophanes, Elucidated by QTAIM Dual Functional Analysis: Requirements for Appearance of Bond Critical Points Between the Phenyl Moieties

Abstract

Dynamic and static nature of the intramolecular π–π interactions between phenyl moieties is elucidated for cyclophanes, 1,4-$C_6H_4(C_nH_{2n})_2C_6H_4$-1',4' (**5-1** ($n$ = 2) and **5-2** (n = 3)), 1,3,5-$C_6H_3(C_nH_{2n})_3C_6H_3$-1',3',5' (**5-3** ($n$ = 2) and **5-4** (n = 3)), $C_6(C_nH_{2n})_6C_6$ (**5-5** (n = 2) and **5-6** (n = 3)), and 1',4'-$C_6H_4(C_nH_{2n})_2$-1,4-C_6H_2-2,5-$(C_nH_{2n})_2C_6H_4$-2'',5'' (**5-7** (n = 2) and **5-8** (n = 3)). QTAIM-DFA was applied for the elucidations, together with QC calculations. While the BPs are detected for the intramolecular π–π interactions in **5-2**, **5-4**, **5-6**, and **5-8**, they are not detected for those in **5-1**, **5-5**, and **5-7**. In the case of **5-3**, BPs are not detected for those between the bridgehead carbon atoms of (^{1}C, $^{1'}$C), (^{3}C, $^{3'}$C), and (^{5}C, $^{5'}$C), whereas they appear between the non-bridgehead carbon atoms of (^{2}C, $^{2'}$C), (^{4}C, $^{4'}$C), and (^{6}C, $^{6'}$C). The intramolecular π–π interactions in the cyclophanes are all classified by the *pure* closed shell interactions. While the intramolecular π–π interactions in **5-2**, **5-4**, **5-6**, and **5-8** are characterized as the vdW nature, those in **5-3** are predicted to have the *typical* HB nature without covalency. The interaction distances between (^{2}C, $^{2'}$C), (^{4}C, $^{4'}$C), and (^{6}C, $^{6'}$C) in **5-3** are shorter than those connected by BPs, although the distances would not be the key parameters for BPs to appear in cyclophanes.

Introduction

Much attention has been paid to the π–π interactions, due to the indispensable role in physical, chemical, and biological sciences. The π-orbitals in aromatic rings, as well as those in ethylene and acetylene moieties, are particularly pivotal in organic supra-molecules and nanomaterials, together with the stabilization of proteins, enzyme-drug complexes, DNA-protein complexes.[1–15] His research group have been much interested in the π–π interactions as the factor to control the fine details of structures and to create delicate properties in materials, in addition to the structural and energetic point of view. He described the behavior of the intramolecular π–π interactions between the ethylene moieties in Chapter 3 and 4, as the first step to clarify the various types of π–π interactions, exemplified by diethanodihydronaphthalene (**3-1a**), diethenodihydronaphthalene (**4-1b**), and the derivatives.[8] They provided a fundamentally important starting point to understand the π–π interactions between the ethylene moieties.

The intramolecular π–π interactions between phenyl moieties must also be fundamentally important, as well as those between the ethylene moieties. Such π–π interactions between phenyl moieties can be found typically in cyclophanes, although helicenes would also be the nice candidates to investigate the interactions.[16] [2.2]Paracyclophane (**5-1**) was first prepared by Cram and coworkers and the structure was determined by the X-ray crystallographic analysis.[15] The structure is demonstrated to have the D_{2h} symmetry, which is denoted by **5-1** (D_{2h}) in this Chapter. Various types of cyclophanes have also been prepared so far, containing [*m.n*]cyclophanes of the ortho, meta, para, and the mixed types, together with the multi-layered ones.[14] The structures have also been determined for many cases.

How is the nature of the intramolecular π–π interactions between phenyl moieties in cyclophanes? What are the similarities and differences in the intramolecular π–π interactions between the phenyl moieties in cyclophanes and those between the ethylene moieties in **3-1a**, **4-1b**, and the derivatives? The behavior of intramolecular π–π interactions between phenyl moieties in cyclophanes is to be clarified, which will supply another type of fundamentally important information for the

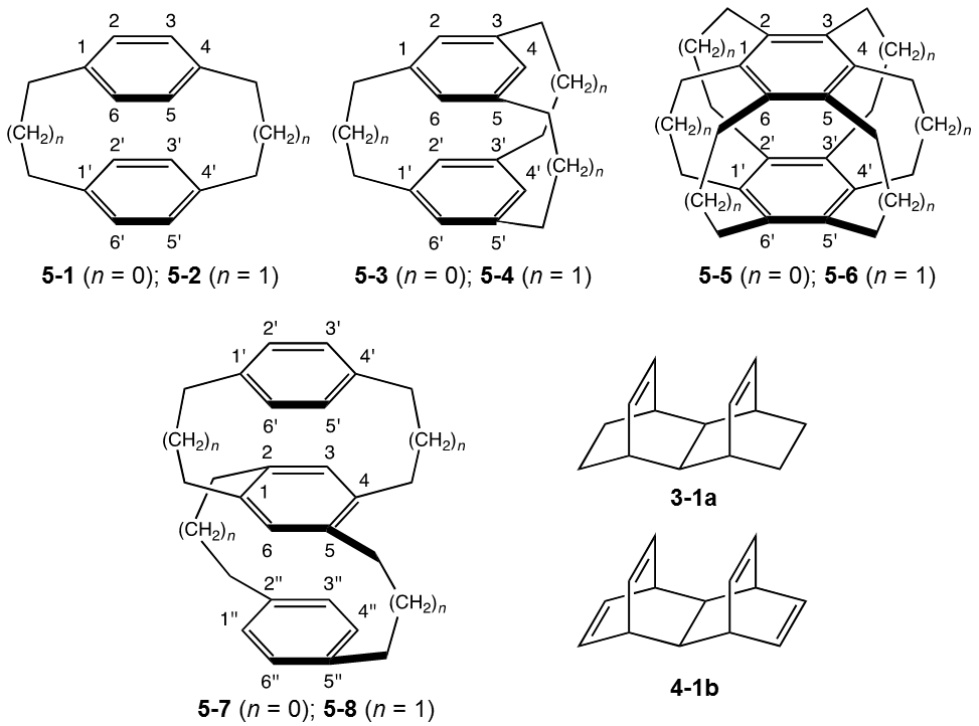

Scheme 5-1. Structures illustrated for **5-1**–**5-8**, together with **3-1a** and **4-1b**.

intermolecular π–π interactions. The nature of the intramolecular π–π interactions is elucidated, exemplified by [2.2]- and [3.3]cyclophanes (**5-1**[17] and **5-2**,[18] respectively), [2.2.2]- and [3.3.3]cyclophanes (**5-3**[19] and **5-4**,[20] respectively) and [2.2.2.2.2.2]- and [3.3.3.3.3.3]cyclophanes (**5-5**[21] and **5-6**,[22] respectively), together with the three-layered cyclophanes (**5-7** and **5-8**[23]). Scheme 5-1 illustrates the structures of **5-1**–**5-8**, together with **3-1a** and **4-1b**.

How can the nature of the intramolecular π–π interactions in cyclophanes be clarified? QTAIM approach, introduced by Bader,[24–26] enables us to analyze the nature of chemical bonds and interactions.[27–31] The bond critical point (BCP, ∗[32]) is an important concept in QTAIM, which is a point along the BP at the interatomic surface at which the charge density $\rho(\boldsymbol{r})$ reaches a minimum. $\rho(\boldsymbol{r})$ at BCP is denoted by $\rho_b(\boldsymbol{r}_c)$, so are other QTAIM functions. Galembeck et al. applied QTAIM approach to the through-bond and through-space interactions in [2.2]cyclophanes.[33]

QTAIM approach becomes much popular in the experimental field of chemical sciences. His research group searched for such method that enables experimental chemists to analyze their own results, concerning chemical bonds and interactions, by their own image and proposed QTAIM dual

functional analysis (QTAIM-DFA).[34–38] $H_b(\boldsymbol{r}_c)$ are plotted versus $H_b(\boldsymbol{r}_c) - V_b(\boldsymbol{r}_c)/2$ in QTAIM-DFA, where $H_b(\boldsymbol{r}_c)$ and $V_b(\boldsymbol{r}_c)$ are the total electron energy densities and potential energy densities, respectively, at BCPs. In his research group treatment, data for perturbed structures around fully-optimized ones are employed for the plots, in addition to the fully-optimized structures.[34–38] His research group proposed the concept of "the dynamic nature of interactions" originated from the data containing the perturbed structures,[34a,35–38] whereas data from the fully-optimized structures correspond to the static nature of interactions. QTAIM-DFA provides an excellent possibility to evaluate, classify and understand weak to strong interactions in a unified form.[39–41] QTAIM-DFA is applied to typical chemical bonds and interactions and rough criteria have been established, which can distinguish the chemical bonds and interactions in question from others. QTAIM-DFA and the criteria are explained in Chapter 2, employing Schemes 2-1 and 2-3, Figure 2-1, Eqs. (2-1)–(2-2) and Eqs. (2-8)–(2-12). The basic concept of the QTAIM approach, introduced by Bader,[24–26] is also surveyed.

QTAIM-DFA is now applied to elucidate the dynamic and static nature of the intramolecular π–π interactions in **5-1**–**5-8**. Herein, He present the results of the investigations on the nature of the π–π interactions in **5-1**–**5-8**. The interactions are classified and characterized by employing the criteria, as a reference.

Methodological Details in Calculations

Molecules are optimized with the 6-311G(3d) basis set (basis set system B: BSS-B) and the 6-311+G(3d) basis set (BSS-C)[42] of the Gaussian 03 program,[43] employing the pre-optimized structures with the 6-31+G(d,p) basis set (BSS-A). The DFT level of M06-2X[44] is applied to the optimizations, together with the Møller-Plesset second order energy correlation (MP2) level.[45] The CAM-B3LYP level is also applied, additionally.[46,47] Optimized structures were confirmed by the frequency analysis. QTAIM functions were calculated using the Gaussian 03 program package[43] with the same method

for the optimizations. QTAIM functions were analyzed with the AIM2000 program.[48] Optimizations with M06-2X/BSS-C reproduced the observed structures most effectively, therefore, the results with M06-2X/BSS-C will be mainly discussed in the text.

Normal coordinates of internal vibrations (NIV) obtained by the frequency analysis were employed to generate the perturbed structures.[34a,35–38] The method is explained in Chapter 2.

Results and Discussion

Structural Feature of Cyclophanes

[2.2]-Paracyclophane (**5-1**) was optimized with BSS-B and/or BSS-C at the MP2 and M06-2X levels, assuming the D_{2h}, D_2, and C_2 symmetries. The results are summarized in Table 5-A1 of the Appendix. While two imaginary frequencies were predicted for **5-1** (D_{2h}), all positive frequencies were for **5-1** (D_2) and **5-1** (C_2) with MP2/BSS-B and MP2/BSS-C. On the other hand, one imaginary frequency was predicted for **5-1** (D_{2h}), while all positive frequencies were for **5-1** (D_2) and **5-1** (C_2) with M06-2X/BSS-B and M06-2X/BSS-C. The optimized structure of **5-1** (D_2) seems very close to that of **5-1** (D_{2h}). While **5-1** (C_2) is predicted as the global minimum at the MP2 level, **5-1** (D_2) is the global one at the M06-2X level. The optimized noncovalent (C, C) distances in **5-1** (D_2) seem best reproduced with M06-2X/BSS-C, as a whole.

He must be careful when the nature of intramolecular π–π interactions in cyclophanes is discussed, since the noncovalent distances will not be determined at the energy minima of the interactions. Instead, they are fixed at the shorter (or longer) distances, relative to the intermolecular cases, since the intramolecular π–π interaction distances are substantially controlled by the framework of the molecules. While the $r(^1C, ^{1'}C)$ and $r(^4C, ^{4'}C)$ values in **5-1** (D_2) are evaluated to be 2.788 Å, $r(^2C, ^{2'}C)$ and $r(^3C, ^{3'}C)$ are 3.092 Å with M06-2X/BSS-C. The predicted $r(^1C, ^{1'}C)$ and $r(^2C, ^{2'}C)$ values are longer and shorter than the observed ones by 0.002 Å and 0.007 Å, respectively. The differences in magnitudes between the predicted and observed values ($\Delta r = r_{calcd} - r_{obsd}$) of 0.013 Å corresponds

to half of the intervals of adjacent data points in the plots of $H_b(\boldsymbol{r}_c)$ versus $H_b(\boldsymbol{r}_c) - V_b(\boldsymbol{r}_c)/2$ ($0.05a_o/2$ = 0.013 Å) (cf: Fig. 5-4). Therefore, the Δr values of less than 0.013 Å should be desirable for QTAIM-DFA, if the predicted nature is discussed in relation to the observed structures. The magnitude of 0.026 Å would be acceptable for QTAIM-DFA, which corresponds to the intervals of adjacent data points in the plots (0.05ao = 0.026 Å). The structure of **5-1** (D_2) is desirable for QTAIM-DFA, if optimized with M06-2X/BSS-C. [3.3]Paracyclophane (**5-2**) was similarly optimized, retaining the C_i symmetry, with MP2/BSS-B, MP2/BSS-C and M06-2X/BSS-C. The results are summarized in Table 5-A2 of the Appendix. The structure of **5-2** (C_i) seems best reproduced with M06-2X/BSS-C, again. The Δr values are 0.001 Å and –0.005 Å for $r(^1\text{C}, ^{1'}\text{C})$ and $r(^2\text{C}, ^{2'}\text{C})$, respectively. The structure of **5-2** (C_i) optimized with M06-2X/BSS-C is also desirable for QTAIM-DFA.

Cyclophanes **5-3**–**5-8** are similarly optimized with MP2/BSS-B, M06-2X/BSS-B, and/or M06-2X/BSS-C. The results are collected in Tables 5-A3–5-A8 of the Appendix. In the case of **5-6**, one imaginary frequency was predicted for each of the optimized structures of **5-6** (C_2) and **5-6** (C_1) with M06-2X/BSS-B and **5-6** (D_2) and **5-6** (C_2) with M06-2X/BSS-C. Then, all positive frequencies were confirmed for **5-6** (D_2) and **5-6** (C_2) by the optimizations with CAM-B3LYP/BSS-C. The optimized structure of **5-6** (C_2) was predicted to be more stable than **5-6** (D_2). The predicted energy surface must be very gentle around the internal vibration in question at the M06-2X level, resulting in the prediction of the imaginary frequency for the internal vibration. His research group sometimes encounter such observations.[41a,c] Two types of structures were optimized for **5-8**, retaining the C_2 symmetry, which are called **5-8a** (C_2) and **5-8b** (C_2). Three phenyl moieties are twisted more in **5-8b** (C_2).

Table 5-1 collects the noncovalent ^{a}C---^{b}C distances between the phenyl moieties ($r(^a\text{C}, ^b\text{C})$) in **5-1**–**5-8**, evaluated with M06-2X/BSS-C, together with the sum of the three angles around ^{a}C and ^{b}C ($\Sigma\theta_a$ and $\Sigma\theta_b$, respectively) , instead of other structural parameters. Table 5-1 contains the sign for the appearance or disappearance of BP between ^{a}C and ^{b}C with BCP on it (BP/BCP), employing Yes or No, respectively.

After clarification of the structural feature of **5-1**–**5-8**, molecular graphs and contour plots are examined, before detail discussion of the intramolecular π–π interactions.

Table 5-1. Noncovalent ^{a}C---^{b}C distances in question and sum of three angles around ^{a}C and ^{b}C of ^{a}C---^{b}C in the optimized structures of **5-1**–**5-8**, together with appearance and disappearance of bond paths with bond critical points (BPs/BCPs) between ^{a}C and ^{b}C.[a]

^{a}C-^{b}C	r(^{a}C, ^{b}C)/Å	$\Sigma\theta_a$/°	$\Sigma\theta_b$/°	BP/BCP
$C_6H_4(CH_2CH_2)_2C_6H_4$ (**5-1**: D_2)				
^{1}C-$^{1'}$C	2.7878	358.48	358.48	No
^{2}C-$^{2'}$C	3.0923	359.23	359.23	No
^{1}C-$^{2'}$C	3.3061	358.48	359.23	No
^{1}C-$^{6'}$C	3.1889	358.48	359.23	No
$C_6H_4(CH_2CH_2CH_2)_2C_6H_4$ (**5-2**: C_i)				
^{1}C-$^{1'}$C	3.1474	359.65	359.94	Yes
^{1}C-$^{2'}$C	3.3028	359.65	359.81	No
^{3}C-$^{3'}$C	3.2959	359.65	359.85	No
$C_6H_3(CH_2CH_2)_3C_6H_3$ (**5-3**: D_3)				
^{1}C-$^{1'}$C	2.7641	356.12	356.18	No
^{2}C-$^{2'}$C	2.8436	358.87	358.87	Yes
$C_6H_3(CH_2CH_2CH_2)_3C_6H_3$ (**5-4**: C_1)				
^{1}C-$^{1'}$C	3.1054	359.51	359.51	Yes
^{2}C-$^{2'}$C	3.1831	359.67	359.67	Yes
^{3}C-$^{3'}$C	3.0953	359.47	359.47	Yes
^{4}C-$^{4'}$C	3.1036	359.70	359.70	Yes
^{5}C-$^{5'}$C	3.0798	359.49	359.49	Yes
^{6}C-$^{6'}$C	3.1356	359.66	359.66	Yes
$C_6(CH_2CH_2)_6C_6$ (**5-5**: D_6)				
^{1}C-$^{1'}$C	2.6551	355.72	355.72	No
$C_6(CH_2CH_2CH_2)_6C_6$ (**5-6**: C_2)				
^{1}C-$^{1'}$C	2.9290	359.88	359.88	Yes
$C_6(CH_2CH_2)_6C_6$ (**5-7**: D_2)				
^{1}C-$^{1'}$C	2.7741	359.55	358.35	No
$C_6(CH_2CH_2CH_2)_6C_6$ (**5-8**: $C_{2\text{-a}}$)				
^{1}C-$^{1'}$C	3.1184	359.99	359.91	Yes
$C_6(CH_2CH_2CH_2)_6C_6$ (**5-8**: $C_{2\text{-b}}$)				
^{1}C-$^{1'}$C	3.1274	359.97	359.80	Yes

[a] with M06-2X/BSS-C.

Molecular Graphs and Contour Plots of $\rho(\mathbf{r})$ Around the Intramolecular π–π Interactions in 5-1–5-8

Figure 5-1 illustrates the molecular graphs for **5-1**–**5-8**, drawn on the structures optimized with M06-2X/BSS-C. In the case of the two-layered cyclophanes, BPs/BCPs are not detected between carbon atoms of the face-to-face phenyl moieties in **5-1** (D_2),[23] **5-5** (D_6) and **5-7** (D_2), ethano-bridged cyclophanes. Indeed, BPs are detected between the non-bridgehead carbon atoms of BP (^{2}C-∗-$^{2'}$C), BP (^{4}C-∗-$^{4'}$C) and BP (^{6}C-∗-$^{6'}$C), but they do not appear between the bridgehead carbon atoms of BP (^{1}C-∗-$^{1'}$C), BP (^{3}C-∗-$^{3'}$C), and BP (^{5}C-∗-$^{5'}$C) in **5-3** (D_3), an ethano-bridged cyclophane. On the other hand, BPs/BCPs are detected for BP (^{1}C-∗-$^{1'}$C) and BP (^{6}C-∗-$^{6'}$C) in **5-2** (C_i) and BP (^{i}C-∗-$^{i'}$C) (i = 1–6) in **5-4** (C_1) and **5-6** (C_2), 1,3-propylidene-bridged cyclophanes. For the three-layered cyclophanes, BPs/BCPs are detected between the two phenyl moieties for BP (^{1}C-∗-$^{1'}$C), BP (^{4}C-∗-$^{4'}$C), BP (^{2}C-∗-$^{2'}$C) and BP (^{5}C-∗-$^{5'}$C) in **5-8a** (C_2) and **5-8b** (C_2), 1,3-propylidene-bridged cyclophanes. Such BPs/BCPs are not observed in **5-7** (D_2), ethano-bridged cyclophanes. Figure 5-2 shows the contour plots of $\rho(\boldsymbol{r})$, drawn on a plane containing the π–π interactions, exemplified by **5-1** (D_2) and **5-2** (C_i). BCPs appear at the three-dimensional saddle points of $\rho(\boldsymbol{r})$.

Figure 5-1 clearly demonstrates that BPs/BCPs appear between the bridgehead carbon atoms of the face-to-face phenyl moieties in the 1,3-propylidene-bridged cyclophanes, **5-2** (C_i) **5-4** (C_1), **5-6** (C_2), **5-8a** (C_2), and **5-8b** (C_2). However, BPs/BCPs are not detected between the bridgehead carbon atoms of the phenyl moieties in the ethano-bridged cyclophanes, **5-1** (D_2), **5-3** (D_3), **5-5** (D_6), and **5-7** (D_2). It is noteworthy that BPs/BCPs are observed between the non-bridgehead carbon atoms in the face-to-face phenyl moieties in **5-3** (D_3) and **5-4** (C_1).

Galembeck *et al*. never detect BP along the intramolecular π–π interactions in **5-1**, whereas BP was detected between the non-bridgehead ortho-carbon atoms of the phenyl moieties of *syn*- and *anti*-[2.2]metacyclophanes.[33] The results in this Chapter for **5-1** (D_2) are in accordance with those by Galembeck et al. The results for **5-3** (D_3) may correspond to those for *syn*- and *anti*-

[2.2]metacyclophanes, although the structures seem very different with each other. However, BPs do not appear between the non-bridgehead atoms of each face-to-face phenyl moieties in **5-7** (D_2). On the other hand, BPs are detected between the bridgehead and/or non-bridgehead atoms of the face-to-face phenyl moieties in the 1,3-propylidene-bridged cyclophanes.

The reason of the disappearance of BPs/BCPs for the intermolecular π–π interactions in **5-1** was not specified by Galembeck *et al*.[33] Highly theoretical treatment must be necessary to clarify the reason for the appearance and disappearance of BPs/BCPs. Pendâs and coworkers discussed BPs as privileged exchange channels, using the interacting quantum atom (IQA) framework.[50] They have investigated how BPs between an atom A and atom B in its environment appear to be determined by competition among the A–B exchange-correlation energies that always contribute to stabilize the A–B interactions. And they have predicted that a BP is found between two atoms by examining a number of archetypal simple systems: (1) there is no other competing atom in its vicinity, so there must be a direct exchange route between them or (2) its $\mathbf{V}_{xc}$ term is the largest among several possibilities, where $\mathbf{V}_{xc}$ stands for a quantum-mechanical correction coming from the exchange correlation second-order density.[50] It has also indicated that interaction energies between both atoms cannot be universally used to predict the existence of a BP between them.[51] Moreover, they are not correlated to distances or to the density values at BCPs. On the contrary, the exchange contribution is shown to be an appropriate descriptor.[51] Similarly, theoretical treatments are applied to various interactions, employing QTAIM-defined an atomic interaction line (AIL: presence or absence), IQA-defined interaction energy and its components, NCI (non-covalent interactions)-defined isosurfaces, and deformation density.[52]

The reason for the appearance and disappearance of BPs/BCPs in the cyclophanes would be rationalized by applying above theory. However, the theoretical treatment seems beyond the scope of this Chapter. Instead, the observed results are summarized, employing the data in Table 5-1. It is confirmed that the interaction distances cannot be the key parameters for the reason. The predicted $r(^1\mathrm{C}, ^{1'}\mathrm{C})$ distance in **5-1** (D_2) (2.788 Å) is shorter than the corresponding value in **5-2** (D_i) (3.147 Å)

and r(^{i}C, $^{i'}$C) in **5-5** (D_6) (2.655 Å) are predicted to be shorter than those of **5-6** (C_2) (2.929 Å). BPs/BCPs are not observed for the interactions of the shorter distances. The $\Sigma\theta$ values around the C atoms in question seem to explain the results, better. The values around ^{1}C and $^{1'}$C are evaluated to be 356.5° for **5-3** (D_3), while the values around ^{2}C and $^{2'}$C are 358.9°. The $\Sigma\theta$ value in **5-5** (D_6) (356.1°) is smaller than that around ^{1}C for **5-3** (D_3) (356.5°) and **5-6** (C_2) (359.9°), therefore, it would be more difficult for BP/BCP to appear in **5-5** (D_6). However, BP is not detected between (^{2}C-∗-$^{2'}$C) in **5-1** (D_2), either, irrespective of $\Sigma\theta$ = 359.38° in which is larger than 358.9° around ^{2}C and $^{2'}$C in **5-3** (D_3). BP/BCP will appear in **5-2** (D_i), **5-4** (C_1), and **5-6** (C_2), if the $\Sigma\theta$ value in question is larger than 359.5°. The results for **5-7** (D_2), **5-8a** (C_2), and **5-8b** (C_2) seem to be explained similarly, based on the $\Sigma\theta$ values (see Table 5-1).

Figure 5-2 makes us imagine that atomic 2p-orbitals (AOs (2p)) at ^{1}C and $^{1'}$C in **5-1** (D_2) extend more outside of the phenyl rings than the cases of **5-2** (D_i). As a result, AOs (2p) at ^{1}C and $^{1'}$C in **5-1** (D_2) would be more difficult to overlap with each other, than the case of **5-2** (D_i). Namely, it is difficult to find a suitable route between ^{1}C and $^{1'}$C in **5-1** (D_2) along the normal lines to the contour plots of $\rho(\boldsymbol{r})$. The expectation is in accordance with the appearance of BP (^{1}C-∗-$^{1'}$C) in **5-2** (D_i) and disappearance of BP (^{1}C-∗-$^{1'}$C) in **5-1** (D_2). The deformation of the benzene rings occurs also in **5-2** (D_i), although not so severe, which results in the substantial curving of BP (^{1}C-∗-$^{1'}$C) in **5-2** (D_i) ($\Delta r_{BP} = r_{BP} - R_{SL}$ = 0.117 Å, see Figure 5-3). The overlap between AOs (2p) at ^{1}C and $^{1'}$C in **5-1** (D_2) would be less effective through the hybridization with AOs (2s) at ^{1}C and $^{1'}$C, due to the lower planarity around ^{1}C and $^{1'}$C, relative to the cases of **5-2** (D_i). The appearance or disappearance of BPs/BCPs in **5-3** (D_3) can be understood, similarly, together with the cases of **5-5** (D_6) versus **5-6** (C_2) and **5-7** (D_2) versus **5-8** (C_2). The explanations will help the instinctive understanding the appearance or disappearance of BPs/BCPs in such system, although they would not be so theoretical.[52]

The nature of the intramolecular π–π interactions in cyclophanes is discussed, next.

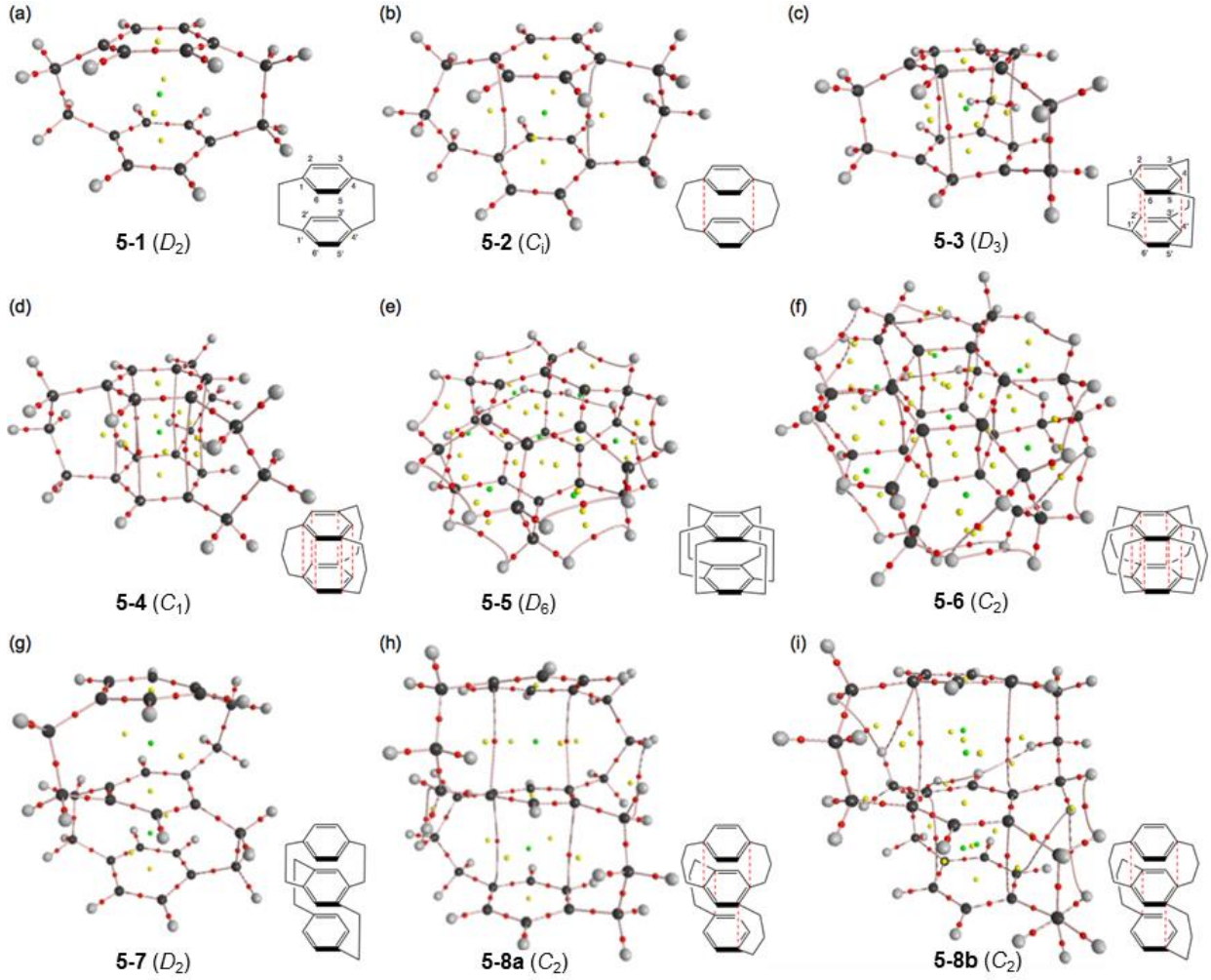

Figure 5-1. Molecular graphs of **5-1–5-8**. The bond critical points (BCPs) are denoted by red dots on the bond paths by pink lines, ring critical points (RCPs) by yellow dots, and the cage critical point (CCP) by a green dots. Carbon atoms are in black and hydrogen atoms in gray.

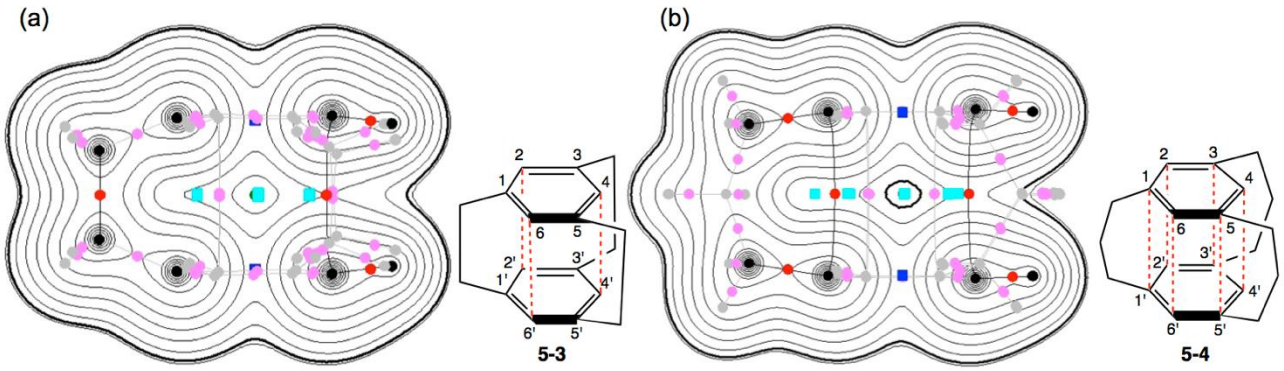

Figure 5-2. Contour plots of $\rho(\boldsymbol{r})$ for **5-1** (D_2) (a) and **5-2** (C_i) (b), drawn on the planes containing the intramolecular π–π interactions, evaluated with theM06-2X/BSS-C. The magnified contour plots of $\rho(\boldsymbol{r})$ around the ^{1}C-∗-$^{1'}$C area are also shown for **5-1** (D_2) (a') and **5-2** (C_i) (b'). BCPs on the plane are denoted by red dots, those outside the plane in dark pink dots, ring critical points (RCPs) on and outside the plane by blue squares and light blue ones, respectively, cage critical points (CCPs) by green dots, and BPs on the plane by black lines and those outside of the plane are by gray lines. Carbon atoms are in black and hydrogen atoms are in gray. The contours (ea_0^{-3}) are at 2^l (l = ±8, ±7, ..., 0) with 0.0047 (heavy line).

Survey of intramolecular π---π interactions in 5-1–5-8

BPs for the intramolecular π–π interactions in cyclophanes seem straight for most cases, as shown in Figure 5-1. The lengths of BPs (r_{BP}) and the corresponding straight-line distances (R_{SL}) for the intramolecular π–π interactions are collected in Table 5-A9 of the Appendix, together with the differences between them ($\Delta r_{BP} = r_{BP} - R_{SL}$). The Δr_{BP} values are all less than about 0.03 Å, except for **5-2** (C_i) (^{1}C–$^{1'}$C: Δr_{BP} = 0.117 Å), **5-8a** (C_2) (^{2}C–$^{2''}$C: 0.086 Å), **5-8b** (C_2) (^{1}C–$^{1''}$C: 0.195 Å) and **5-8b** (C_2) (^{2}C–$^{2''}$C: 0.398 Å). The r_{BP} values are plotted versus R_{SL}. Figure 5-3 shows the plot. The results show that BPs for the intramolecular π–π interactions can be well approximated by the straight line for $\Delta r_{BP} \leq 0.03$ Å ($y = 0.995x + 0.043$ $R_c^2 = 0.995$ for $\Delta r_{BP} \leq 0.03$ Å).

QTAIM functions of $\rho_b(\boldsymbol{r}_c)$, $H_b(\boldsymbol{r}_c) - V_b(\boldsymbol{r}_c)/2$, $H_b(\boldsymbol{r}_c)$, and k ($=V_b(\boldsymbol{r}_c)/G_b(\boldsymbol{r}_c)$) are calculated for the intramolecular π–π interactions in question at BCPs. Table 5-2 collects the QTAIM functions for the intramolecular π–π interactions. Figure 5-4 shows the plot of $H_b(\boldsymbol{r}_c)$ versus $H_b(\boldsymbol{r}_c) - V_b(\boldsymbol{r}_c)/2$ for the selected data of fully-optimized structures in Table 5-2, together with those of the perturbed structures around the fully-optimized ones. The data for the interactions appear in the region of $0 < H_b(\boldsymbol{r}_c)$ and $0 < H_b(\boldsymbol{r}_c) - V_b(\boldsymbol{r}_c)/2$. Therefore, the intramolecular π–π interactions in cyclophanes should be classified by the *pure* CS interactions.

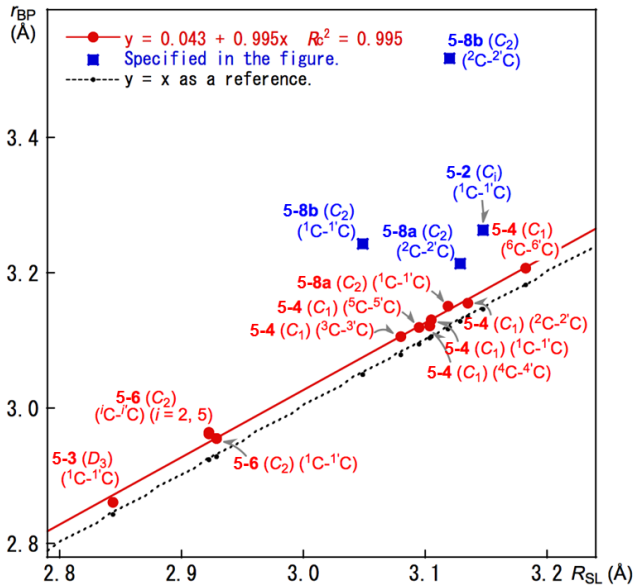

Figure 5-3. Plots of r_{BP} versus R_{SL} for **5-2** (C_i), **5-3** (D_3), **5-4** (C_1), **5-6** (C_2), **5-8a** (C_2), and **5-8b** (C_2). Only one side interaction is shown if equivalent interactions are detected.

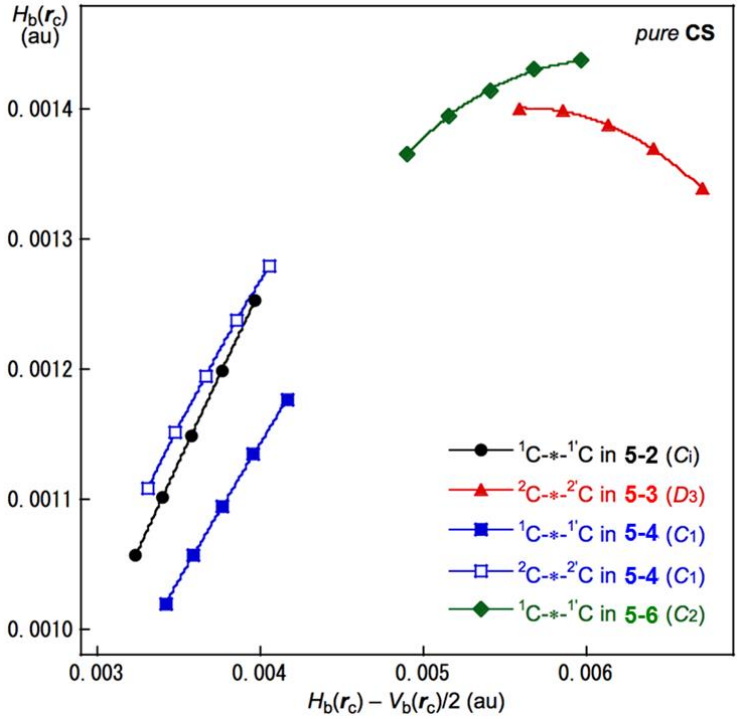

Figure 5-4. Plots of $H_b(\boldsymbol{r}_c)$ versus $H_b(\boldsymbol{r}_c) - V_b(\boldsymbol{r}_c)/2$ for the selected intramolecular π–π interactions at BCPs for **5-2**–**5-4** and **5-6**.

Behaviors of the intramolecular π–π interactions in 5-1–5-8, elucidated by QTAIM-DFA parameters

QTAIM-DFA parameters of (R, θ) and (θ_p, κ_p) are calculated by analyzing the plots for the intramolecular π–π interactions between the phenyl moieties in **5-2** (C_i), **5-3** (D_3), **5-4** (C_1), **5-6** (C_2), **5-8a** (C_2), and **5-8b** (C_2), according to Eqs (2-8)–(2-11) in Chapter 2. Table 5-2 also collects the (R, θ) and (θ_p, κ_p) values for the interactions, together with the frequencies correlated to NIV employed to generate the perturbed structures and the force constants, k_f.

The dynamic and static nature of the intramolecular π–π interactions between the phenyl moieties in **5-2** (C_i), **5-3** (D_3), **5-4** (C_1), **5-6** (C_2), **5-8a** (C_2), and **5-8b** (C_2) are classified and characterized based on the θ and θ_p values, respectively, employing those of the standard values as a reference.

It must be instructive to survey the criteria, before discussion of the nature of the π–π interactions in detail. The criteria tell us that $\theta < 180°$ for the closed shell (CS) interactions ($H_b(\boldsymbol{r}_c) - V_b(\boldsymbol{r}_c)/2 > 0$) and $180° < \theta$ for the shared shell (SS) interactions ($H_b(\boldsymbol{r}_c) - V_b(\boldsymbol{r}_c)/2 < 0$). The CS interactions are sub-

divided into *pure* CS interactions of 45° < θ < 90° ($H_b(\boldsymbol{r}_c) > 0$) and *regular* CS interactions of 90° < θ < 180° ($H_b(\boldsymbol{r}_c) < 0$). The θ_p value plays an important role to characterize the interactions. The character of the *pure* CS interactions will be the vdW type for 45° < θ_p < 90° and the *typical*-HB type without covalency for 90° < θ_p < 125°, where θ_p = 125° is tentatively given corresponding to θ = 90°.

On the other hand, the character of the *regular* CS interactions will be the *typical*-HB type with covalency for 125° < θ_p < 150°, where θ_p = 150° is tentatively given as the border line between the *typical*-HB nature with covalency and the CT-MC nature. The borderline between CT-MC nature and CT-TBP nature is defined by θ_p = 180°. As a result, 150° < θ_p < 180° for CT-MC and 180° < θ_p < 190° for CT-TBP, where θ_p = 190° is tentatively given corresponding to θ = 180°.

As shown in Table 5-2, the θ values for the π–π interactions of **5-2** (C_i), **5-3** (D_3), **5-4** (C_1), **5-6** (C_2), **5-8a** (C_2), and **5-8b** (C_2) are all less than 90°, therefore, the interactions are classified by the pure CS interactions. The θ_p values in Table 5-2 are all also less than 90°, except for ^{2}C-∗-$^{2'}$C, ^{4}C-∗-$^{4'}$C, ^{6}C-∗-$^{6'}$C in **5-3** (D_3). Consequently, the intramolecular π–π interactions between the face-to-face phenyl moieties in **5-2** (C_i), **5-4** (C_1), **5-6** (C_2), **5-8a** (C_2), and **5-8b** (C_2) are characterized to have the vdW nature, although the π–π interactions for ^{2}C-∗-$^{2'}$C in **5-3** (D_3) are predicted to have the *typical* HB nature without covalency. Table 5-2 summarizes the classifications and characterizations of the π–π interactions in the cyclophanes. BPs/BCPs are not detected for the intramolecular π–π interactions in ethano-bridged cyclophanes of **5-1** (D_2), **5-5** (D_6) and **5-7** (D_2), contrary to the case of the 1,3-propylidene-bridged cyclophanes of **5-2** (C_i), **5-4** (C_1), **5-6** (C_2), **5-8a** (C_2), and **5-8b** (C_2). In the case of an ethano-bridged cyclophane **5-3** (D_3), BPs/BCPs are not detected between the bridgehead carbon atoms of BP (^{1}C-∗-$^{1'}$C), BP (^{3}C-∗-$^{3'}$C), and BP (^{5}C-∗-$^{5'}$C), but they are detected between the non bridgehead carbon atoms of BP (^{2}C-∗-$^{2'}$C), BP (^{4}C-∗-$^{4'}$C), and BP (^{6}C-∗-$^{6'}$C). It is noteworthy that BP (^{2}C-∗-$^{2'}$C), BP (^{4}C-∗-$^{4'}$C), and BP (^{6}C-∗-$^{6'}$C) are predicted to be stronger than others, which have the *typical* HB nature without covalency. The interaction distance is shorter than others given in Table 5-1, although the interaction distances cannot be the key parameters for BPs to appear in cyclophanes.

Table 5-2. QTAIM functions and QTAIM-DFA parameters for the intramolecular π-∗-π interactions between phenyl moieties in **5-2**–**5-4**, **5-6**, and **5-8**[a].

Cyclophane[b] Interaction	$\rho_b(\boldsymbol{r}_c)$ (au)	$c\nabla^2\rho_b(\boldsymbol{r}_c)$[c] (au)	$H_b(\boldsymbol{r}_c)$ (au)	$k_b(\boldsymbol{r}_c)$[d]	R (au)	θ (°)	V_n (n)[e] (cm^{-1})	k_f[f]	θ_p (°)	κ_p (au^{-1})	classification/ character
5-2 (C_i: ^{1}C-∗-$^{1'}$C)	0.0089	0.0036	0.0011	-0.809	0.0038	72.2	171.4 (5)	0.102	75.0	15.1	*p*-CS/vdW[g]
5-3 (D_3: ^{2}C-∗-$^{2'}$C)	0.0156	0.0061	0.0014	-0.872	0.0063	77.2	337.1 (8)	0.559	94.5	108.8	*p*-CS/*t*-HB[h]
5-4 (C_1: ^{1}C -∗-$^{1'}$C)	0.0091	0.0038	0.0011	-0.830	0.0039	73.8	226.0 (6)	0.170	78.1	21.0	*p*-CS/vdW[g]
5-4 (C_1: ^{2}C -∗-$^{2'}$C)	0.0092	0.0037	0.0012	-0.805	0.0039	71.9	226.0 (6)	0.170	76.9	66.2	*p*-CS/vdW[g]
5-4 (C_1: ^{3}C -∗-$^{3'}$C)	0.0095	0.0040	0.0011	-0.832	0.0041	73.9	226.0 (6)	0.170	78.6	38.6	*p*-CS/vdW[g]
5-4 (C_1: ^{4}C -∗-$^{4'}$C)	0.0096	0.0039	0.0013	-0.806	0.0041	72.0	226.0 (6)	0.170	77.0	66.3	*p*-CS/vdW[g]
5-4 (C_1: ^{5}C -∗-$^{5'}$C)	0.0092	0.0038	0.0011	-0.831	0.0040	73.8	226.0 (6)	0.170	78.6	29.2	*p*-CS/vdW[g]
5-4 (C_1: ^{6}C -∗-$^{6'}$C)	0.0087	0.0034	0.0011	-0.803	0.0036	71.8	226.0 (6)	0.170	75.8	69.1	*p*-CS/vdW[g]
5-6 (C_2: ^{1}C -∗-$^{1'}$C)[i]	0.0124	0.0054	0.0014	-0.850	0.0056	75.4	301.6 (13)	0.397	86.2	108.1	*p*-CS/vdW[g]
5-6 (C_2: ^{2}C -∗-$^{2'}$C)[i]	0.0127	0.0056	0.0014	-0.852	0.0058	75.5	301.6 (13)	0.397	86.1	85.5	*p*-CS/vdW[g]
5-8a(C_2: ^{1}C -∗-$^{1'}$C)	0.0108	0.0044	0.0015	-0.795	0.0046	71.2	204.0 (11)	0.131	81.2	175.5	*p*-CS/vdW[g]
5-8a(C_2: ^{4}C -∗-$^{4'}$C)	0.0100	0.0039	0.0013	-0.798	0.0042	71.4	204.0 (11)	0.131	73.3	16.8	*p*-CS/vdW[g]
5-8b(C_2: ^{1}C -∗-$^{1'}$C)	0.0089	0.0036	0.0011	-0.818	0.0038	72.9	189.9 (10)	0.088	79.4	13.3	*p*-CS/vdW[g]
5-8b(C_2: ^{4}C -∗-$^{4'}$C)	0.0090	0.0037	0.0012	-0.811	0.0039	72.4	189.9 (10)	0.088	75.8	16.3	*p*-CS/vdW[g]

[a] Evaluated with M06-2X/BS-C (the 6-311+G(3d) basis set at the DFT level of M06-2X). [b] Symmetry is also given. Only one side interaction is shown if equivalent interactions are detected. [c] $H_b(\boldsymbol{r}_c) - V_b(\boldsymbol{r}_c)/2$ where $c = \hbar^2/8m$. [d] $k_b(\boldsymbol{r}_c) = V_b(\boldsymbol{r}_c)/G_b(\boldsymbol{r}_c)$. [e] Corresponding to the motion of the intramolecular π–π interactions in question. [f] Force constant corresponding to ν_n. [g] Van der Waals nature appeared at the *pure*-CS region. [h] *typical*-Hydrogen bond nature without covalency appeared at the *pure*-CS region. [i] With one imaginary frequency corresponding to the motion of the six central CH_2 groups on a plane formed by the six CH_2 groups.

Summary

The nature of the intramolecular π–π interactions is elucidated for those between the face-to-face phenyl moieties in cyclophanes **5-1**–**5-8**, by employing QTAIM-DFA with M06-2X/BSS-C. The differences between predicted and observed noncovalent C---C distances between the phenyl moieties were less than 0.01 Å for **5-1** (D_2) and **5-2** (C_i) with M06-2X/BSS-C. Therefore, the calculated results can be well discussed in relation to the observed structures. Two conformers were optimized as minima for the three-layered cyclophane, **5-8a** (C_2) and **5-8b** (C_2), although one for the two-layered

cyclophanes. While BPs are not detected for the intramolecular π-π interactions between phenyl moieties in **5-1** (D_2), **5-5** (D_6) and **5-7** (D_2), BPs are detected for those in **5-2** (C_i), **5-4** (C_1), **5-6** (C_2), **5-8a** (C_2), **5-8b** (C_2), and **5-3** (D_3). In the case of **5-3** (D_3), BPs are detected between the non-bridgehead carbons of (^{2}C-∗-$^{2'}$C), (^{4}C-∗-$^{4'}$C) and (^{6}C-∗-$^{6'}$C), but disappeared between the bridgehead carbons of (^{1}C-∗-$^{1'}$C), (^{3}C-∗-$^{3'}$C) and (^{5}C-∗-$^{5'}$C).

QTAIM-DFA parameters of (R, θ) and (θ_p, κ_p) are obtained for the intramolecular π–π interactions in **5-2** (C_i), **5-4** (C_1), **5-6** (C_2), **5-8a** (C_2), **5-8b** (C_2), and **5-3** (D_3), by analyzing the plots of $H_b(\boldsymbol{r}_c)$ versus $H_b(\boldsymbol{r}_c) - V_b(\boldsymbol{r}_c)/2$ for the interactions. The intramolecular π–π interactions in **5-2** (C_i), **5-4** (C_1), **5-6** (C_2), **5-8a** (C_2), **5-8b** (C_2), and **5-3** (D_3) are all classified by the pure closed shell (CS) interactions. While the intramolecular π–π interactions between the phenyl moieties in **5-2** (C_i), **5-4** (C_1), **5-6** (C_2), **5-8a** (C_2), and **5-8b** (C_2) are characterized as the vdW nature, BP (^{2}C-∗-$^{2'}$C), BP (^{4}C-∗-$^{4'}$C), and BP (^{6}C-∗-$^{6'}$C) in **5-3** (D_3) are predicted to have the *typical* HB nature without covalency. It is noteworthy that BP (^{2}C-∗-$^{2'}$C), BP (^{4}C-∗-$^{4'}$C), and BP (^{6}C-∗-$^{6'}$C) in **5-3** (D_3) are predicted to be stronger than others. Indeed, the interaction distance is shorter than others detected by BPs, but they cannot be the key parameters for BPs to appear in cyclophanes. The planarity around C in the phenyl rings seems better parameter for the appearance or disappearance of BPs, although the reason must be very complex. The interactions in cyclophanes are well analyzed with QTAIM-DFA. The predicted results will be well discussed in relation to the observed structures, since the optimized structures reproduce well the observed ones.

Appendix

Table 5-A1. Optimized distances between carbon atoms in different benzene rings in cyclophane, $C_6H_4(CH_2CH_2)_2C_6H_4$ (**5-1**), together with the observed values.

Compd	$r(C_1, C_{1'})$ (Å)	$r(C_2, C_{2'})^a$ (Å)	$r(C_3, C_{3'})^b$ (Å)	$r(C_4, C_{4'})$ (Å)	ν_1 (cm^{-1})	ν_2 (cm^{-1})	ΔE (kJ mol^{-1})
MP2/BSS-B (6-311G(3d))							
5-1 (D_{2h})	2.7374_1	3.0223_7	3.0223_7	2.7374_1	–61.7 (AU)	–34.7 (B3G)	0.00
5-1 (D_2)[c]	2.7480_0	3.0415_7	3.0415_7	2.7480_0	50.3 (B3)	76.1 (A)	–1.65
5-1 (C_2)	2.7478_8	3.0416_0	3.0416_1	2.7478_9	51.9 (A)	78.7 (A)	–2.64
MP2/BSS-C (6-311+G(3d))							
5-1 (D_{2h})	2.7368_1	3.0225_1	3.0225_1	2.7368_0	–61.2 (AU)	–33.7 (B3G)	0.00
5-1 (D_2)	2.7484_1	3.0427_3	3.0427_3	2.7484_1	46.9 (B3)	75.4 (A)	–1.67
5-1 (C_2)	2.7482_5	3.0428_8	3.0428_8	2.7482_7	49.4 (A)	77.8 (A)	–2.88
M06-2X/BSS-B (6-311G(3d))							
5-1 (D_{2h})	2.7803_1	3.0796_9	3.0796_9	2.7803_1	–47.0 (AU)	48.8 (B3G)	0.00
5-1 (D_2)[c]	2.7874_0	3.0925_1	3.0925_1	2.7874_0	72.1 (A)	73.0 (B3)	–1.23
5-1 (C_2)	2.7872_0	3.0962_3	3.0939_3	2.7916_4	55.9 (A)	75.0 (A)	–0.67
M06-2X/BSS-C (6-311+G(3d))							
5-1 (D_{2h})	2.7806_2	3.0792_9	3.0792_9	2.7806_2	–48.9 (AU)	50.1 (B3G)	0.00
5-1 (D_2)[c]	2.7878_1	3.0923_1	3.0923_1	2.7878_1	71.5 (A)	73.4 (B3)	–1.25
5-1 (C_2)	2.7876_7	3.0937_8	3.0961_3	2.7921_8	57.6 (A)	74.4 (A)	–0.70
Observed (X-ray)[d]							
5-1 (D_{2h})	2.786	3.099	3.099	2.786			

[a] The same as $r(C_6, C_{6'})$. [b] The same as $r(C_5, C_{5'})$. [c] Could be recognized as D_2. [d] Ref 16 in the text.

Table 5-A2. Optimized distances between carbon atoms in different benzene rings in cyclophane, $C_6H_4(CH_2CH_2CH_2)_2C_6H_4$ (**5-2**), together with the observed values

Compd	$r(^1C, ^{1'}C)$ (Å)	$r(^2C, ^{2'}C)^a$ (Å)	$r(^3C, ^{3'}C)^b$ (Å)	$r(^1C, ^{2'}C)$ (Å)	$r(^1C, ^{6'}C)$ (Å)	ν_1 (cm^{-1})	ν_2 (cm^{-1})	Method
5-2 (C_i)	3.0924	3.2400	3.2540	3.1529	3.6485	57.1 (AG)	71.1 (AU)	MP2/A
5-2 (C_i)	3.0575	3.1854	3.1970	3.0543	3.6383	70.0 (AU)	70.1 (AG)	MP2/B
5-2 (C_i)	3.0573	3.1877	3.1989	3.0535	3.6404	68.4 (AU)	68.6 (AG)	MP2/C
5-2 (C_i)	3.1474	3.3028	3.2936	3.3482	3.7475	53.3 (AG)	73.9 (AU)	M06-2X/C
5-2	3.137	3.299	3.310	3.316	3.622			obsd (X-ray)[c]

[a] The same as $r(^6C, ^{6'}C)$. [b] The same as $r(^5C, ^{5'}C)$. [c] Ref 17 in the text.

Table 5-A3. Optimized distances between carbon atoms in different benzene rings in cyclophane, $C_6H_3(CH_2CH_2)_3C_6H_3$ (**5-3**), together with the observed values

Compd	$r(^1C, ^{1'}C)$ (Å)	$r(^2C, ^{2'}C)$ (Å)	$r(^1C, ^{2'}C)$ (Å)	$r(^1C, ^6C)$ (Å)	ν_1 (cm^{-1})	ν_2 (cm^{-1})	Method
5-3 (D_3)	2.7222	2.7750	3.0726	3.0976	17.9 (A1)	117.1 (E)	MP2/B
5-3 (D_3)	2.7641	2.8436	3.1014	3.1593	82.1 (A1)	136.8 (E)	M06-2X/C
5-3 (C_2)	2.7631	2.8424	2.7625[a]	2.8427[b]	40.7 (A)	124.9 (B)	M06-2X/C
5-3	2.749	2.831	3.113	3.113			obsd (X-ray)[c]

[a] $r(^3C, ^{3'}C)$. [b] $r(^4C, ^{4'}C)$. [c] Ref 18 in the text.

Table 5-A4. Optimized distances between carbon atoms in different benzene rings in cyclophane, $C_6H_3(CH_2CH_2CH_2)_3C_6H_3$ (**5-4**), together with the observed values.

Compd	$r(^1C, ^{1'}C)$ (Å)	$r(^2C, ^{2'}C)$ (Å)	$r(^3C, ^{3'}C)$ (Å)	$r(^4C, ^{4'}C)$ (Å)	$r(^5C, ^{5'}C)$ (Å)	$r(^6C, ^{6'}C)$ (Å)	$\nu_{1:A}$ (cm^{-1})	$\nu_{2:A}$ (cm^{-1})	Method
5-4 (C_1)	3.0153	3.0281	3.0341	3.1259	3.0485	3.0724	7.5	71.5	MP2/B
5-4 (C_1)	3.0791	3.1024	3.0945	3.1346	3.1046	3.1816	42.6	95.5	M06-2X/B
5-4 (C_1)	3.1054	3.1831	3.0923	3.1054	3.0798	3.1356	40.6	94.5	M06-2X/C
5-4	3.082	3.127	3.089	3.125	3.093	3.138			obsd (X-ray)[a]

[a] Ref 19 in the text.

Table 5-A5. Optimized distances between carbon atoms in different benzene rings in cyclophane, $C_6(CH_2CH_2)_6C_6$ (**5-5**), together with the observed values.

Compd	$r(^1C, ^{1'}C)$ (Å)	$r(^2C, ^{2'}C)$ (Å)	$r(^3C, ^{3'}C)$[b] (Å)	$r(^1C, ^{2'}C)$ (Å)	$r(^1C, ^{6'}C)$ (Å)	$\nu_{1:A1}$ (cm^{-1})	$\nu_{2:E1}$ (cm^{-1})	Method
5-5 (D_6)	2.6053	2.6053	2.6053	2.9147	3.0106	161.9	180.5	MP2/B
5-5 (D_6)	2.6556	2.6556	2.6556	2.9550	3.0509	164.8	202.1	M06-2X/B
5-5 (D_6)	2.6551	2.6551	2.6551	2.9544	3.0511	164.3	201.5	M06-2X/C
5-5	2.620	2.623	2.630	2.980	2.982			obsd (X-ray)[a]

[a] Ref 20 in the text.

Table 5-A6. Optimized distances between carbon atoms in different benzene rings in cyclophane, $C_6(CH_2CH_2CH_2)_6C_6$ (**5-6**), together with the observed values.

Compd	$r(^1C, ^{1'}C)$ (Å)	$r(^2C, ^{2'}C)$ (Å)	$r(^4C, ^{4'}C)$ (Å)	$r(^5C, ^{5'}C)$ (Å)	$r(^1C, ^{2'}C)$ (Å)	$r(^1C, ^{6'}C)$ (Å)	ν_1 (cm^{-1})	ν_2 (cm^{-1})	Method
5-6 (C_2)	2.9290	2.9228_1	2.9290	2.9228_3	3.2001	3.2826	–24.1	67.0	M06-2X/B
5-6 (C_1)	2.9290	2.9228_2	2.9290	2.9228_6	3.2000	3.2825	–24.1	67.0	M06-2X/B
5-6 (D_2)	2.9290	2.9229_9	2.9290	2.9229_9	3.2006	3.2831	–24.6	66.7	M06-2X/C
5-6 (C_2)	2.9290	2.9229_8	2.9290	2.9229_5	3.2003	3.2828	–24.2	67.0	M06-2X/C
5-6 (D_2)	2.9335	2.9294_8	2.9335	2.9294_8	3.2185	3.2770	60.1	65.3	CAM-B3LYP/C
5-6 (C_2)	2.9336	2.9294_5	2.9336	2.9294_6	3.2185	3.2770	60.3	65.6	CAM-B3LYP/C
5-6 (C_1)	2.924	2.930	2.924	2.930	3.244	3.249			obsd (X-ray)[a]

[a] Ref 21 in the text.

Table 5-A7. Optimized and observed distances between benzene rings in cyclophane, $C_{18}H_{10}C_8H_{16}$ (**5-7**).

Compd	$r(^1C, ^{1'}C)$ $r(^1C, ^{1''}C)$ (Å)	$r(^2C, ^{2'}C)$ $r(^2C, ^{2''}C)$ (Å)	$r(^3C, ^{3'}C)$ $r(^3C, ^{3''}C)$ (Å)	$r(^4C, ^{4'}C)$ $r(^4C, ^{4''}C)$ (Å)	$r(^1C, ^{2'}C)$ $r(^1C, ^{2''}C)$ (Å)	$r(^1C, ^{6'}C)$ $r(^1C, ^{6''}C)$ (Å)	ν_1 ν_2 (cm^{-1})	Method
5-7 (D_2)	2.7213	3.1270	3.0094	2.7213	3.2483	3.1078	*a*	MP2/B
	3.1270	2.7213	3.0094	3.1270	3.2194	3.5230	*a*	
5-7 (D_2)	2.7741	3.2160	3.0787	2.7741	3.2959	3.2986	17.8 (B1)	M06-2X/C
	3.2160	2.7741	3.0787	3.2160	3.2931	3.5843	40.5 (A)	
5-7 (C_2)	2.7741	3.1260	3.0788	2.7741	3.2959	3.1659	17.8 (B)	M06-2X/C
	3.1260	2.7741	3.0788	3.1260	3.2931	3.5844	40.0 (A)	

[a] Not calculated.

Table 5-A8. Optimized and observed distances between benzene rings in cyclophane, $C_{18}H_{10}C_{12}H_{24}$ (**5-8**).

Compd	$r(^1C, ^{1'}C)$ $r(^1C, ^{1''}C)$ (Å)	$r(^2C, ^{2'}C)$ $r(^2C, ^{2''}C)$ (Å)	$r(^3C, ^{3'}C)$ $r(^3C, ^{3''}C)$ (Å)	$r(^4C, ^{4'}C)$ $r(^4C, ^{4''}C)$ (Å)	$r(^5C, ^{5'}C)$ $r(^5C, ^{5''}C)$ (Å)	$r(^6C, ^{6'}C)$ $r(^6C, ^{6''}C)$ (Å)	$r(^1C, ^{2'}C)$ $r(^1C, ^{2''}C)$	ν_2 ν_1 (cm^{-1})	Method
5-8a (C_2)	3.1172	3.4124	3.3372	3.1275	3.2895	3.2006	3.2526	28.1 (A)	M06-2X/B
	3.2895	3.1275	3.3372	3.4124	3.1172	3.2006	3.4883	37.5 (B)	
5-8a (C_2)	3.1184	3.4114	3.3362	3.1285	3.2930	3.2042	3.6062	27.5 (A)	M06-2X/C
	3.2930	3.1285	3.3362	3.4114	3.1184	3.2042	3.7258	37.0 (B)	
5-8b (C_2)	3.1191	3.2980	3.2309	3.1259	3.3914	3.3050	3.8165	42.1 (A)	M06-2X/B
	3.3914	3.1259	3.2309	3.2980	3.1191	3.3050	3.2980	67.6 (A)	
5-8b (C_2)	3.1206	3.2994	3.2319	3.1274	3.3943	3.3073	3.8187	42.1 (A)	M06-2X/C
	3.3943	3.1274	3.2319	3.2994	3.1206	3.3073	3.3943	67.6 (A)	
5-8 (C_1-A)	3.113	3.186	3.276	3.132	3.355	3.453	3.458		obsd (X-ray)[a]
	3.285	3.192	3.122	3.452	3.358	3.129	3.506		
5-8 (C_1-B)	3.103	3.429	3.351	3.136	3.285	3.188	3.660		obsd (X-ray)[a]
	3.289	3.139	3.352	3.447	3.112	3.170	3.548		
5-8 (C_1)	3.113	3.248	3.330	3.117	3.273	3.345	3.400		obsd (X-ray)[b]
	3.289	3.231	3.140	3.425	3.343	3.129	3.538		

[a] Ref 22a in the text. [b] Ref 22b in the text.

Table 5-A9. Lengths of bond paths (r_{BP}) with components (r_{BP1} and r_{BP2}) and the corresponding straight-line distances (R_{SL}) for noncovalent [a]C---[b]C interactions between phenyl moieties of cyclophanes[a]

Compound (X–Y)	r_{BP1} (Å)	r_{BP2} (Å)	r_{BP}[b] (Å)	R_{SL} (Å)	Δr_{BP}[c] (Å)
$C_6H_4(CH_2CH_2CH_2)_2C_6H_4$ (**5-2**: C_i)					
^{1}C-$^{1'}$C	1.6873	1.5768	3.2641	3.1474	0.1167
$C_6H_3(CH_2CH_2)_3C_6H_3$ (**5-3**: D_3)					
^{2}C-$^{2'}$C	1.4310	1.4310	2.8621	2.8436	0.0185
$C_6H_3(CH_2CH_2CH_2)_3C_6H_3$ (**5-4**: C_1)					
^{1}C-$^{1'}$C	1.5658	1.5658	3.1316	3.1054	0.0262
^{2}C-$^{2'}$C	1.6041	1.6041	3.2083	3.1831	0.0252
^{3}C-$^{3'}$C	1.5603	1.5603	3.1206	3.0923	0.0283
^{4}C-$^{4'}$C	1.5613	1.5613	3.1226	3.1054	0.0172
^{5}C-$^{5'}$C	1.5528	1.5528	3.1056	3.0798	0.0258
^{6}C-$^{6'}$C	1.5782	1.5782	3.1564	3.1356	0.0208
$C_6(CH_2CH_2CH_2)_6C_6$ (**5-6**: C_2)					
^{1}C-$^{1'}$C	1.4776	1.4777	2.9554	2.9290	0.0264
^{2}C-$^{2'}$C	1.5040	1.4592	2.9632	2.9230	0.0402
$C_6(CH_2CH_2CH_2)_6C_6$ (**5-8a**: C_2)					
^{1}C-$^{1'}$C	1.5798	1.5708	3.1506	3.1184	0.0322
^{6}C-$^{6'}$C	1.5629	1.6511	3.2140	3.2042	0.0098
$C_6(CH_2CH_2CH_2)_6C_6$ (**5-8b**: C_2)					
^{1}C-$^{1'}$C	1.5397	1.7038	3.2435	3.1206	0.1945
^{6}C-$^{6'}$C	1.5547	1.9639	3.5186	3.3073	0.2113

[a] Optimized with M06-2X/BSS-C. [b] $r_{BP} = r_{BP1} + r_{BP2}$. [c] $\Delta r_{BP} = \Delta r_{BP} - R_{SL}$.

Table 5-A10. C–C distances and bond orders in various cyclophanes, together with the appearance or nonappearance of bond critical points between two carbon atoms

^{a}C-^{b}C	r(^{a}C, ^{b}C)/Å	$\Sigma\theta_a$/$^{\circ a}$	$\Sigma\theta_b$/$^{\circ a}$	WBI^{b}	BCP	Method
$C_6H_4(CH_2CH_2)_2C_6H_4$ (**5-1**: D_2)						
^{1}C-$^{1'}$C	2.78781	358.46	358.46	0.0056	No	M06-2X
^{1}C-$^{2'}$C	3.16171	358.46	359.26	0.0023	No	M06-2X
^{1}C-$^{6'}$C	3.33246	358.46	359.40	0.0015	No	M06-2X
^{2}C-$^{2'}$C	3.09231	359.40	359.26	0.0022	No	M06-2X
$C_6H_4(CH_2CH_2CH_2)_2C_6H_4$ (**5-2**: C_i)						
^{1}C-$^{1'}$C	3.14742	359.65	359.94	0.0027	Yes	M06-2X
^{2}C-$^{2'}$C	3.30279	359.82	359.81	0.0005	No	M06-2X
^{3}C-$^{3'}$C	3.29359	359.82	359.85	0.0015	No	M06-2X
^{4}C-$^{4'}$C	3.14742	359.82	359.94	0.0034	Yes	M06-2X
^{1}C-$^{2'}$C	3.34817	359.65	359.81	0.0019	No	M06-2X
^{1}C-$^{6'}$C	3.74752	359.65	359.85	0.0014	No	M06-2X
$C_6H_3(CH_2CH_2)_3C_6H_3$ (**5-3**: D_3)						
^{1}C-$^{1'}$C	2.76413	356.48	356.18	0.0091	No	M06-2X
^{2}C-$^{2'}$C	2.84358	358.93	358.90	0.0136	Yes	M06-2X
$C_6H_3(CH_2CH_2CH_2)_3C_6H_3$ (**5-4**: C_1)						
^{1}C-$^{1'}$C	3.10535	359.51	359.51	0.0029	Yes	M06-2X
^{2}C-$^{2'}$C	3.18305	359.67	359.67	0.0018	Yes	M06-2X
$C_6(CH_2CH_2)_6C_6$ (**5-5**: D_6)						
^{1}C-$^{1'}$C	2.65513	356.07	356.07	0.0171	No	M06-2X
$C_6(CH_2CH_2CH_2)_6C_6$ (**5-6**: C_2)						
^{1}C-$^{1'}$C	2.92898	359.88	359.88	0.0065	Yes	M06-2X
$C_6(CH_2CH_2)_6C_6$ (**5-7**: D_2)						
^{1}C-$^{1'}$C	2.77406	356.07	356.07	0.0171	No	M06-2X
$C_6(CH_2CH_2CH_2)_6C_6$ (**5-8a**: C_2)						
^{1}C-$^{1'}$C	3.11841	359.88	359.88	0.0065	Yes	M06-2X

^{a} Sum of three angles around ^{a}C and ^{b}C ($\Sigma\theta_a$ and $\Sigma\theta_b$, respectively). ^{b} Wiberg bond index matrix in the NAO basis.

Table 5-A11. AIM functions and parameters for the intramolecular π-∗-π interactions in **5-2**–**5-4**, **5-6**, and **5-8**, calculated with NIV at the DFT (M06-2X) level[a]

Compound[b] Interaction	$\rho_b(\boldsymbol{r}_c)$ (au)	$c\nabla^2\rho_b(\boldsymbol{r}_c)$[c] (au)	$H_b(\boldsymbol{r}_c)$ (au)	k[d]	R (au)	θ (°)	ν_n (n)[e] (cm^{-1})	k_f[f] (unit[g])	$\theta_{p:NIV}$ (°)	$\kappa_{p:NIV}$ (au^{-1})	Character
Cyclophane											
5-2 (C_i: ^{1}C-∗-$^{2'}$C)	0.0089	0.0036	0.0011	-0.809	0.0038	72.2	171.4 (5)	0.102	75.0	16.9	*p*-CS/vdW
5-3 (D_3:[h] ^{2}C-∗-$^{2'}$C)	0.0156	0.0061	0.0014	-0.872	0.0063	77.2	337.1 (8)	0.559	94.5	131.2	*p*-CS/HB
5-4 (C_1: ^{1}C-∗-$^{1'}$C)	0.0091	0.0038	0.0011	-0.830	0.0039	73.8	226.0 (6)	0.170	78.1	19.6	*p*-CS/vdW
5-4 (C_1: ^{2}C-∗-$^{2'}$C)	0.0092	0.0037	0.0012	-0.805	0.0039	71.9	226.0 (6)	0.170	76.9	66.3	*p*-CS/vdW
5-4 (C_1: ^{3}C-∗-$^{3'}$C)	0.0095	0.0040	0.0011	-0.832	0.0041	73.9	226.0 (6)	0.170	78.6	38.6	*p*-CS/vdW
5-4 (C_1: ^{4}C-∗-$^{4'}$C)	0.0096	0.0039	0.0013	-0.806	0.0041	72.0	226.0 (6)	0.170	77.0	66.3	*p*-CS/vdW
5-4 (C_1: ^{5}C-∗-$^{5'}$C)	0.0092	0.0038	0.0011	-0.831	0.0040	73.8	226.0 (6)	0.170	78.6	29.2	*p*-CS/vdW
5-4 (C_1: ^{6}C-∗-$^{6'}$C)	0.0087	0.0034	0.0011	-0.803	0.0036	71.8	226.0 (6)	0.170	75.8	69.1	*p*-CS/vdW
5-6 (C_2: ^{1}C-∗-$^{1'}$C)	0.0124	0.0054	0.0014	-0.850	0.0056	75.4	301.6 (13)	0.397	86.2	108.1	*p*-CS/vdW
5-6 (C_2: ^{2}C-∗-$^{2'}$C)	0.0127	0.0056	0.0014	-0.852	0.0058	75.5	301.6 (13)	0.397	86.1	85.5	*p*-CS/vdW
5-8a (C_2: ^{1}C-∗-$^{1''}$C)	0.0089	0.0036	0.0011	-0.818	0.0038	72.9	189.9 (10)	0.088	79.4	13.3	*p*-CS/vdW
5-8a (C_2: ^{2}C-∗-$^{2''}$C)	0.0090	0.0037	0.0012	-0.811	0.0039	72.4	189.9 (10)	0.088	75.8	16.3	*p*-CS/vdW
5-8b (C_2: ^{1}C-∗-$^{1''}$C)	0.0108	0.0044	0.0015	-0.795	0.0046	71.2	204.0 (11)	0.131	81.2	175.5	*p*-CS/vdW
5-8b (C_2: ^{2}C-∗-$^{2''}$C)	0.0100	0.0039	0.0013	-0.798	0.0042	71.4	204.0 (11)	0.131	73.3	16.8	*p*-CS/vdW
Standard interaction											
He-∗-HF[i]	0.0022	0.0099	0.0007	-0.625	0.0014	61.4	44.6 (1)	0.005	57.2	69.9	*p*-CS/vdW
Ne-∗-HF[j]	0.0066	0.0353	0.0020	-0.712	0.0048	65.9	68.2 (1)	0.037	78.6	86.9	*p*-CS/vdW
Ar-∗-HF[k]	0.0089	0.0045	0.0022	-0.696	0.0050	64.0	47.7 (1)	0.018	75.3	125.5	*p*-CS/vdW
Kr-∗-HF[l]	0.0101	0.0045	0.0019	-0.722	0.0049	66.7	99.1 (1)	0.070	82.1	180.6	*p*-CS/vdW
NN-∗-HF[m]	0.0173	0.0085	0.0025	-0.903	0.0089	73.4	121.4 (3)	0.099	105.1	215.2	*p*-CS/HB
H_2O-∗-HOH[n]	0.0244	0.0932	0.0016	-0.924	0.0118	82.0	197.7 (1)	0.074	111.3	184.1	*p*-CS/HB
HF--∗--HF[o]	0.0259	0.0140	0.0012	-1.007	0.0141	84.9	182.4 (1)	0.087	110.8	90.2	*p*-CS/HB
Me_2O-∗-HOH[p]	0.0275	0.1028	0.0008	-0.968	0.0129	86.4	190.2 (1)	0.060	121.4	176.6	*p*-CS/HB

[a] With the 6-311+G(3d) basis set at the DFT level of M06-2X. [b] Symmetry is also given. [c] $= H_b(\boldsymbol{r}_c) - V_b(\boldsymbol{r}_c)/2$ with $c = \hbar^2/8m$. [d] $k = V_b(\boldsymbol{r}_c)/G_b(\boldsymbol{r}_c)$. [e] Corresponding to the motion of the intramolecular π-π interactions in question. [f] Force constant corresponding to ν_n. [g] mdyn $Å^{-1}$. [h] Evaluated for the structure optimized at the DFT level of CAM-B3LYP. [i] r(He--H_F) = 2.4377 Å. [j] r(Ne, H_F) = 2.2446 Å. [k] r(Ar--H_F) = 2.4926 Å. [l] r(Kr--H_F) = 2.5800 Å. [m] r(N--H_F) = 2.0613 Å. [n] r(O--H) = 1.9366 Å. [o] r(O--H) = 1.9110 Å. [p] r(F--H_F) = 1.8011 Å.

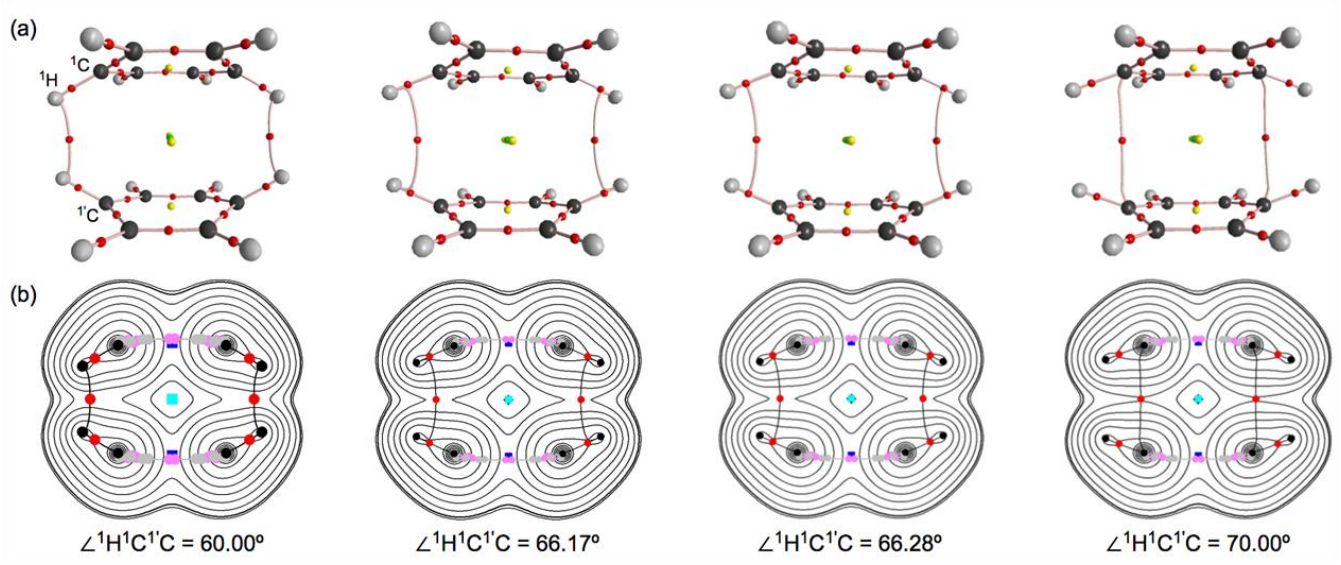

Figure 5-A1. Molecular graphs (a) and contour plots of $\rho(\boldsymbol{r})$ (b) for benzene dimer (**5-9**) (D_2), a mode derived from **5-1** (D_2), at ∠^{1}H^{1}C$^{1'}$C of 60.0°, 66.17°, 66.28° and 70.0°.

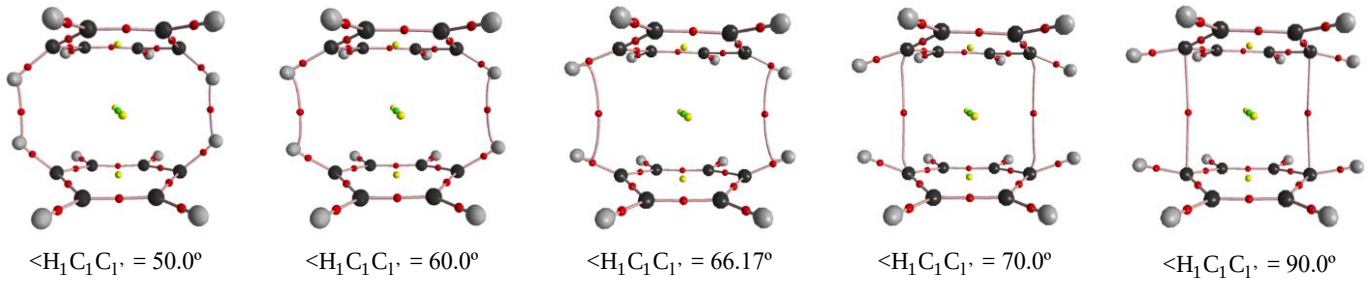

Figure 5-A2. Molecular graphs for **5-9** (D_2) with various ∠^{1}H^{1}C$^{1'}$C values.

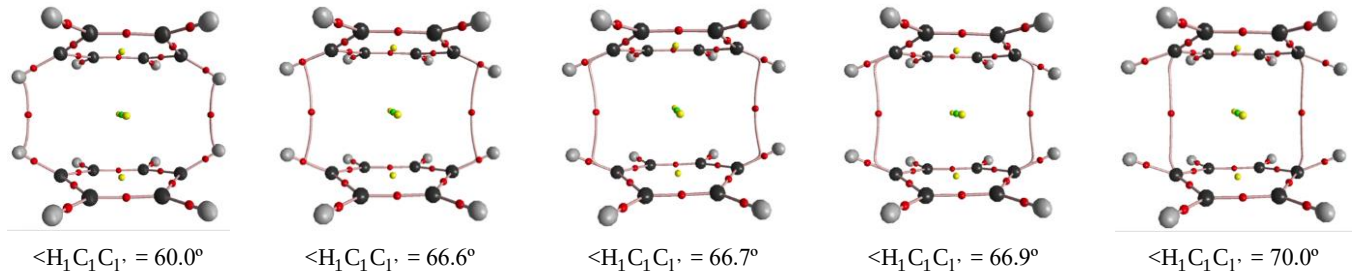

Figure 5-A3. Molecular graphs for **5-9** (D_2) with various ∠^{1}H^{1}C$^{1'}$C values.

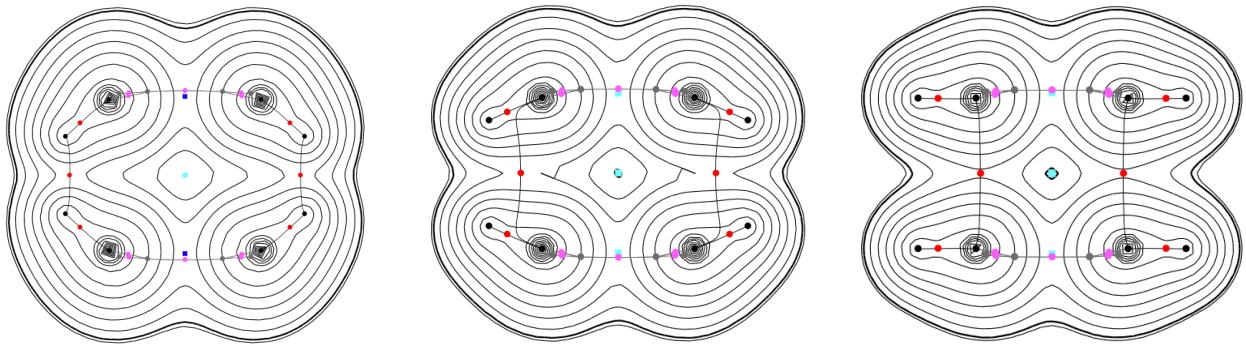

Figure 5-A4. Contour plots of $\rho(\boldsymbol{r})$ of **5-9** (D_{2h}), a mode derived from **5-1** (D_2), at $\angle^1H^1C^{1'}C = 50.0^o$, 66.9º and 90.0º, drawn on the σ_h plane.

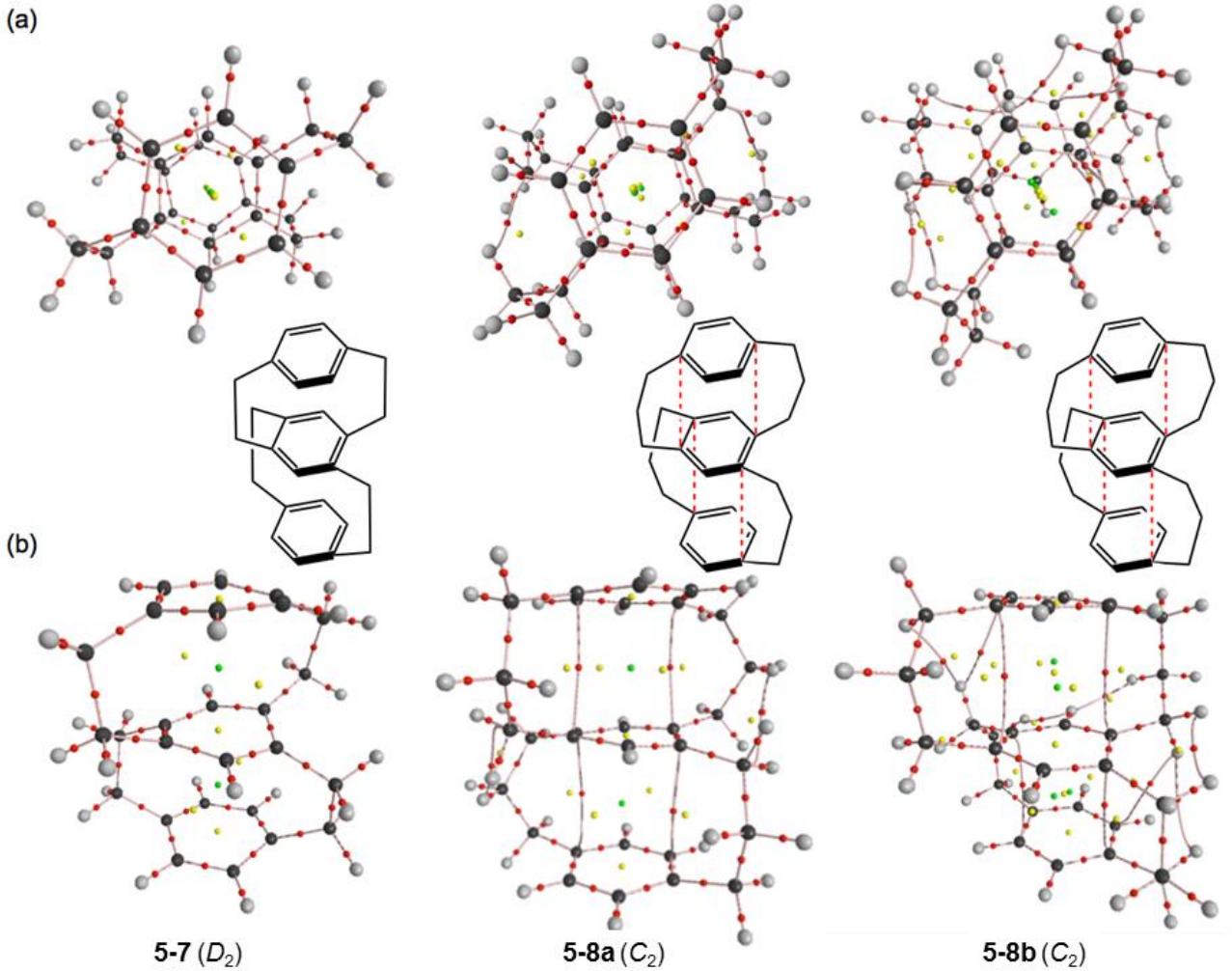

Figure 5-A5. Molecular graphs of **5-7** and **5-8**: each consists of top view (a) and side view (b). The bond critical points (BCPs) are denoted by red dots, ring critical points (RCPs) by yellow dots, and the cage critical point (CCP) by a green dots. Carbon atoms are in black and hydrogen atoms in gray.

References

1 The various ways to achieve cyclic delocalization by joining chains of conjugated π-systems were studied in 1971 by Hoffmann and Goldstein; M. J. Goldstein, R. Hoffmann, *J. Am. Chem. Soc.*, **1971**, *93*, 6193–6204.

2 H.-D. Martin and R. Schwesinger, *Chem. Ber.*, **1974**, *107*, 3143–3145.

3 G. Sedelmeier, H. Prinzbach and H.-D. Martin, *Chimia.*, **1979**, *33*, 329–332.

4 J. Spanget-Larsen, R. Gleiter, G. Klein, C. W. Doecke and L. A. Paquette, *Chem. Ber.*, **1980**, *113*, 2120–2126.

5 K. B. Wiberg, M. G. Matturro, P. J. Okarma and M. E. Jason, *J. Am. Chem. Soc.*, **1984**, *106*, 2194–2200.

6 C.-T. Lin, N.-J. Wang, Y.-L. Yeh and T.-C. Chou, *Tetrahedron*, **1995**, *51*, 2907–2928.

7 H. Lange, W. Schäfer, R. Gleiter, P. Camps and S. Vazquez, *J. Org. Chem.*, **1998**, *63*, 3478–2480.

8 W. Grimme, J. Wortmann, D. Frowein, J. Lex, G. Chen and R. Gleiter, *J. Chem. Soc., Perkin Trans. 2*, **1998**, 1893–1900.

9 H. Wang, W. Wang and W. J. Jin, *Chem. Rev.*, **2016**, *116*, 5072–5104.

10 E. Peresypkina, A. Virovets and M. Scheer, *Cryst. Growth Des.*, **2016**, *16*, 2335−2341.

11 B. E. Carson, T. M. Parker, E. G. Hohenstein, G. L. Brizius, W. Komorner, R. A. King, D. M. Collard and C. D. Sherrill, *Chem. Eur. J.*, **2015**, *21*, 19168–19175.

12 Z. A. Tehrani and K. S. Kim, *Int. J. Quantum Chem.*, **2016**, *116*, 622–633.

13 R. L. Gawade, D. K. Chakravarty, A. Kotmale, E. Sangtani, P. V. Joshi, A. Ahmed, M. V. Mane, S. Das, K. Vanka, P. R. Rajamohanan, V. G. Puranik and R. G. Gonnade, *Cryst. Growth Des.*, **2016**, *16*, 2416−2428.

14 *Modern Cyclophane Chemistry*, eds. R. Gleiter and H. Hopf, Wiley-VCH, Weinheim, 2004.

15 D. J. Cram and J. M. Cram, *J. Am. Chem. Soc.*, **1951**, *73*, 5691–5704. See also D. J. Cram and J. M. Cram, *Acc. Chem. Res.*, **1971**, *4*, 204–213.

16 (a) K. Lonsdale, H. J. Milledge and K. V. Krishna Rao, *Proc. R. Soc. London, Ser. A*, **1960**, *255*, 82 (DXYLEN and DXYLEN01); (b) H. Hope, J. Bernstein and K. N. Trueblood, *Acta Crystallogr., Sect. B: Struct. Crystallogr. Cryst. Chem.*, **1972**, *28*, 1733 (DXYLEN12); (c) K. A. Lyssenko, M. Yu. Antipin and D. Yu. Antonov, *Chem. Phys. Chem.*, **2003**, *4*, 817 (DXYLEN13); (d) H. Wolf, D. Leusser, M. R. V. Jrgensen, R. Herbst-Irmer, Y.-S. Chen, E.-W. Scheidt, W. Scherer, Bo B. Iversen and D. Stalke, *Chem.-Eur. J.*, **2014**, *20*, 7048−7053 (DXYLEN14–DXYLEN23).

17 P. K. Gantzel and K. N. Trueblood, *Acta Crystallogr.*, **1965**, *18*, 958 (PCYCPH).

18 A. W. Hanson, *Cryst. Struct. Commun.*, **1980**, *9*, 1243 (CYLPHN).

19 M. Yasutake, T. Koga, Y. Sakamoto, S. Komatsu, M. Zhou, K. Sako, H. Tatemitsu, S. Onaka, Y. Aso, S. Inoue and T. Shinmyozu, *J. Am. Chem. Soc.*, **2002**, *124*, 10136 (CALXET).

20 A. W. Hanson and T. S. Cameron, *J. Chem. Res.*, **1980**, *336*, 4201 (CLOPNA).

21 M. Yasutake, Y. Sakamoto, S. Onaka, K. Sako, H. Tatemitsu and T. Shinmyozu, *Tetrahedron Lett.*, **2000**, *41*,7933 (QAQZIR).

22 (a) M. Shibahara, M. Watanabe, T. Iwanaga, T. Matsumoto, K. Ideta and T. Shinmyozu, *J. Org. Chem.*, **2008**, *73*, 4433 (NODLIC); (b) A. Muranaka, M. Shibahara, M. Watanabe, T. Matsumoto, T. Shinmyozu and N. Kobayashi, *J. Org. Chem.*, **2008**, *73*, 9125 (XOHJOU).

23 *Atoms in Molecules. A Quantum Theory*, ed. R. F. W. Bader, Oxford University Press, Oxford, UK, **1990**.

24 C. F. Matta and R. J. Boyd, *An Introduction to the Quantum Theory of Atoms in Molecules* In *The Quantum Theory of Atoms in Molecules: From Solid State to DNA and Drug Design*, eds. C. F. Matta and R. J. Boyd, WILEY-VCH, Weinheim, Germany, **2007**, chap. 1.

25 (a) F. Biegler-König and J. Schönbohm, *J. Comput. Chem.*, **2002**, *23*, 1489–1494; (b) F. Biegler-König, J. Schönbohm and D. Bayles, *J. Comput. Chem.*, **2001**, *22*, 545–559; (c) R. F. W. Bader, *J. Phys. Chem. A*, **1998**, *102*, 7314–7323; (d) T. H. Tang, R. F. W. Bader, P. MacDougall, *Inorg. Chem.* **1985**, *24*, 2047–2053; (e) R. F. W. Bader, *Chem. Res.*, **1991**, *91*, 893–926; (f) R. F. W.

Bader, *J. Phys. Chem. A* **1998**, *102*, 7314–7323; g) F. Biegler-König, J. Schönbohm, D. Bayles, *J. Comput. Chem*. **2001**, *22*, 545–559; h) F. Biegler-König, J. Schönbohm, *J. Comput. Chem*. **2002**, *23*, 1489–1494.

26 J. A. Dobado, H. Martînez-Garcîa, J. Molina and M. R. Sundberg, *J. Am. Chem. Soc*., **2000**, *122*, 1144–1149.

27 J. Molina and J. A. Dobado, *Theor. Chem. Acc*., **2001**, *105*, 328–337.

28 S. K. Ignatov, N. H. Rees, B. R. Tyrrell, S. R. Dubberley, A. G. Razuvaev, P. Mountford and G. I. Nikonov, *Chem. Eur. J*., **2004**, *10*, 4991–4999.

29 S. K. Tripathi, U. Patel, D. Roy, R. B. Sunoj, H. B. Singh, G. Wolmershäuser and R. J. Butcher, *J. Org. Chem*., **2005**, *70*, 9237–9247.

30 W. Nakanishi, T. Nakamoto, S. Hayashi, T. Sasamori and N. Tokitoh, *Chem. Eur. J*., **2007**, *13*, 255–268.

31 G. F. Caramori, S. E. Galembeck and K. K. Laali, J. Org. Chem., 2005, 70, 3242–3250.

32 Dots are usually employed to show BCPs in molecular graphs. Therefore, A-•-B would be more suitable to describe BP with BCP. Nevertheless, A-∗-B is employed to emphasize the existence of BCP on BP, in question, in his research group case.

33 G. F. Caramori, S. E. Galembeck, *J. Phys. Chem. A* **2007**, *111*, 1705–1712. See also G. F. Caramori, S. E. Galembeck, K. K. Laali, *J. Org. Chem*. **2005**, *70*, 3242–3250.

34 (a) W. Nakanishi, S. Hayashi and K. Narahara, *J. Phys. Chem. A*., **2009**, *113*, 10050–10057; (b) W. Nakanishi, S. Hayashi and K. Narahara, *J. Phys. Chem. A*., **2008**, *112*, 13593–13599.

35 W. Nakanishi and S. Hayashi, *Curr. Org. Chem*., **2010**, *14*, 181–197.

36 W. Nakanishi and S. Hayashi, *J. Phys. Chem. A*, **2010**, *114*, 7423–7430.

37 W. Nakanishi, S. Hayashi, K. Matsuiwa and M. Kitamoto, *Bull. Chem. Soc. Jpn*., **2012**, *85*, 1293–1305.

38 W. Nakanishi and S. Hayashi, *J. Phys. Chem. A*, **2013**, *117*, 1795−1803.

39 W. Nakanishi, S. Hayashi, M. B. Pitak, M. B. Hursthouse and S. J. Coles, *J. Phys. Chem. A*, **2011**, *115*, 11775–11787.

40 S. Hayashi, K. Matsuiwa, M. Kitamoto and W. Nakanishi, *J. Phys. Chem. A*, **2013**, *117*, 1804–1816.

41 Recent applications of QTAIM-DFA, see, (a) Y. Sugibayashi, S. Hayashi and W. Nakanishi, *Phys. Chem. Chem. Phys*., **2015**, *17*, 28879–28891; (b) Y. Sugibayashi, S. Hayashi and W. Nakanishi, *Chem. Phys. Chem*., **2016**, 2579–2589; (c) S. Hayashi, Y. Sugibayashi and W. Nakanishi, *Phys. Chem. Chem. Phys*., **2016**, *18*, 9948–9960; (d) S. Hayashi, K. Matsuiwa, N. Nishizawa and W. Nakanishi, *J. Org. Chem*., **2015**, *80*, 11963–11976; (e) W. Nakanishi, Y. Tsubomoto and S. Hayashi, *RSC Adv*., **2016**, *6*, 93195–93204.

42 For the 6-311G basis sets, see: (a) R. C. Binning Jr. and L. A. Curtiss, *J. Comput. Chem*., **1990**, *11*, 1206–1216; (b) L. A. Curtiss, M. P. McGrath, J.-P. Blaudeau, N. E. Davis, R. C. Binning Jr. and L. Radom, *J. Chem. Phys*., **1995**, *103*, 6104–6113; c) M. P. McGrath and L. Radom, *J. Chem. Phys*., **1991**, *94*, 511–516. For the diffuse functions (+ and ++), see: T. Clark, J. Chandrasekhar, G. W. Spitznagel and P. v. R. Schleyer, *J. Comput. Chem*., **1983**, *4*, 294–301.

43 *Gaussian 03 (Revision D.02)*, M. J. Frisch, G. W. Trucks, H. B. Schlegel, G. E. Scuseria, M. A. Robb, J. R. Cheeseman, J. A. Montgomery, Jr., T. Vreven, K. N. Kudin, J. C. Burant, J. M. Millam, S. S. Iyengar, J. Tomasi, V. Barone, B. Mennucci, M. Cossi, G. Scalmani, N. Rega, G. A. Petersson, H. Nakatsuji, M. Hada, M. Ehara, K. Toyota, R. Fukuda, J. Hasegawa, M. Ishida, T. Nakajima, Y. Honda, O. Kitao, H. Nakai, M. Klene, X. Li, J. E. Knox, H. P. Hratchian, J. B. Cross, V. Bakken, C. Adamo, J. Jaramillo, R. Gomperts, R. E. Stratmann, O. Yazyev, A. J. Austin, R. Cammi, C. Pomelli, J. W. Ochterski, P. Y. Ayala, K. Morokuma, G. A. Voth, P. Salvador, J. J. Dannenberg, V. G. Zakrzewski, S. Dapprich, A. D. Daniels, M. C. Strain, O. Farkas, D. K. Malick, A. D. Rabuck, K. Raghavachari, J. B. Foresman, J. V. Ortiz, Q. Cui, A. G. Baboul, S. Clifford, J. Cioslowski, B. B. Stefanov, G. Liu, A. Liashenko, P. Piskorz, I. Komaromi, R. L. Martin, D. J. Fox, T. Keith, M. A. Al-Laham, C. Y. Peng, A. Nanayakkara, M.

Challacombe, P. M. W. Gill, B. Johnson, W. Chen, M. W. Wong, C. Gonzalez, J. A. Pople, Gaussian, Inc.; Wallingford CT, **2004**.

44 Y. Zhao and D. G. Truhlar, *Theor. Chem. Acc*., **2008**, *120*, 215−241.

45 T. Yanai, D. P. Tew and N. C. Handy, *Chem. Phys. Lett*., **2004**, *393*, 51−57.

46 (a) C. Møller and M. S. Plesset, Phys. Rev., 1934, 46, 618–622; (b) J. Gauss, *J. Chem. Phys*., **1993**, *99*, 3629–3643; (c) J. Gauss, Ber. Bunsen-Ges. *Phys. Chem*., **1995**, *99*, 1001–1008.

47 The AIM2000 program (Version 2.0) is employed to analyze and visualize atoms-in-molecules: F. Biegler-König, *J. Comput. Chem*., **2000**, *21*, 1040–1048. See also ref 26g.

48 For the *m*×*n* matrix representation, m corresponds to the number of atoms and *n* (= 3) to the *x*, *y* and *z* components of the space.

49 A. M. Pendâs, E. Francisco, M. A. Blanco, C. Gatti, *Chem. Eur. J*. **2007**, *13*, 9362 – 9371.

50 V. Tognetti, L. Joubert, *J. Chem. Phys*. **2013**, *138*, 024102-1–024102-8.

51 I. Cukrowski, J. H. de Lange, A. S. Adeyinka, P. Mangondo, Comput. *Theo. Chem*. **2015**, *1053*, 60–76.

52 The contribution of the deformation around ^{1}C and $^{1'}$C to the appearance and disappearance of BPs/BCPs is examined, employing benzene dimer, a mode derived from **5-1** (D_2). The results are discussed in the Appendix (see, Figure 5-A1 in the Appendix).

Chapter 6

Dynamic and Static Behavior of E–E' Bonds in Neutral and Charged Forms of HEE'H, MeEE'Me, and *cyclo*-1,2-EE'$(CH_2)_3$ (E, E' = O, S, Se, and Te) Elucidated by QTAIM Dual Functional Analysis

Abstract

The nature of the E-∗-E' bonds in neutral, mono-anionic, mono-cationic, and di-cationic forms of HEE'H (**6-1**), MeEE'Me (**6-2**), and cyclo-1,2-EE'$(CH_2)_3$ (**6-3**) (E, E' = O, S, Se, Te) is investigated by applying QTAIM-DFA. $H_b(\boldsymbol{r}_c)$ are plotted versus $H_b(\boldsymbol{r}_c) - V_b(\boldsymbol{r}_c)/2$ for the data of E-∗-E' at BCPs of fully-optimized structures and perturbed structures around the fully-optimized ones. Plots for the fully-optimized structures are analyzed by the polar coordinate (R, θ) representation. The (θ_p, κ_p) parameters are derived from those of the perturbed structures: θ_p corresponds to the tangent line of each plot and κ_p is the curvature. While (R, θ) correspond to the static nature, (θ_p, κ_p) represent the dynamic nature of interactions. The nature of E-∗-E' in the neutral and charged species is classified using θ and θ_p of the standard values as a reference. Data for E-∗-E' in the neutral forms of **6-1**–**6-3** appear in the SS region ($180^o < \theta$), except for MeS-∗-TeMe (**6-2c**), which does in the *regular* CS region ($\theta < 180^o$). The E–E' bonds in the mono-anionic forms of **6-1**–**6-3** become much longer and weakened. Therefore, data of the mono-anionic forms appear in the *regular* CS region. On the other hand, the strengths of E-∗-E' in the mono- and di-cationic forms are almost equal to those in the neutral forms of **6-1**–**6-3** by the QTAIM dual functional analysis, irrespective of the shorter E-∗-E' lengths in the cationic forms, relative to the neutral forms.

Introduction

Much attention has been paid to the chalcogen-chalcogen bonds/interactions (E–E': E, E' = S, Se, and Te,[1] together with O), due to the indispensable role in physical, chemical, and biological sciences.[2–5] The S–S bond plays a crucial role to maintain the three dimensional structures of peptides and in biological activities such as detoxification of hydroperoxides in the glutathione peroxidase process, together with the S–Se and Se–Se bonds.[6,7] The E–E' bonds show typical behaviors in the redox process. They are easily oxidized and reduced. The easy oxidation and reduction of the E–E' bonds enriche the chalcogen chemistry.

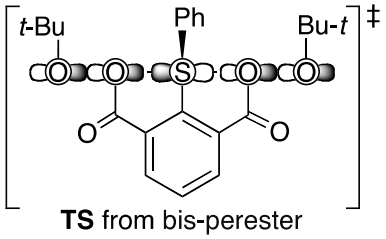

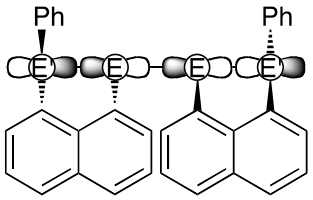

(E, E') = (Se, Se), (S, S), (Se, S), and (S, Se)

Scheme 6-1. Nonbonding interaction models of TS from bis-perester 2-PhSC$_6$H$_3$(COOOBu-*t*)$_2$-1,3 and the n(E')---σ*(E–E)---n(E') type extended hypervalent 4c–6e for 1-(8-PhE'C$_{10}$H$_6$)EE(C$_{10}$H$_6$E'Ph-8')-1'

The E–E' bonds are encounterd on a routine basis in dichalcogenides, REE'R'. The E–E' bonds must be much better acceptors, relative to the E–C or E'–C bonds, since the energies of σ*(E–E') must be much lower than those of σ*(E–C) or σ*(E'–C), although E and E' act as good donors with their lone pair orbitals. The high accepting ability of σ*(E–E') is typically demonstrated. Martin and coworkers observed the facile O–O bond cleavage in *t*-butyl *o*-(methylthio)perbenzoates,[8] where the effective donor-acceptor interactions of the n(S)---σ*(O–O) type lower the energy of the transition

state. They also reported the linear interaction of five atoms through σ-bonds of the σ*(O–O)---n_p(S)---σ*(O–O) type in the transition state (**TS**‡) to give a sulfurane in the extremely facile thermal decomposition of bis-perester 2-PhSC_6H_3(COOOBu-*t*)$_2$-1,3 (Scheme 6-1).[8] The high accepting ability of σ*(S–S) and σ*(Se–Se) is clearly demonstrated by the preparation and identification of 1-(8-PhE'$C_{10}H_6$)EE($C_{10}H_6$E'Ph-8')-1', where (E, E') = (Se, Se), (S, S), (Se, S) and (S, Se).[9] The structures are determined by the X-ray crystallographic analysis. The four $E_2E'_2$ atoms in 1-(8-PhE'$C_{10}H_6$)EE($C_{10}H_6$E'Ph-8')-1' align linearly (Scheme 6-1). Nakanishi and coworkers called the linear alignment of the four $E_2E'_2$ atoms of the n(E')---σ*(E–E)---n(E') type extended hypervalent 4c–6e (four center-six electron interactions). The energy lowering effect by the formation of $E_2E'_2$ 4c–6e must be responsible for the linear alignment.[9]

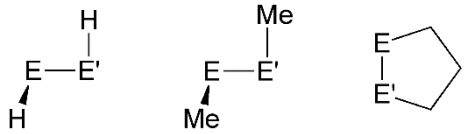

6-1 **6-2** **6-3**

(E, E') = **a**: (S, S), **b**: (S, Se), **c**: (S, Te)
d: (Se, Se), **e**: (Se, Te), **f**: (Te, Te)
g: (O, O), **h**: (O, S), **i**: (O, Se), **j**: (O, Te)

Chart 6-1. Compounds **6-1**–**6-3**

The behavior of the E–E' bonds seems well described at first glance, however, it is still of highly importance to clarify the causality in the phenomena of the bonds, with physical necessity. Therefore, behaviors of the E–E' bonds of neutral, anionic, monocationic and dicationic forms of REE'R are investigated employing the QTAIM dual functional analysis, exemplified by HEE'H (**6-1**: **a** (E, E') = (S, S), **b** (S, Se), **c** (S, Te), **d** (Se, Se), **e** (Se, Te), **f** (Te, Te), **g** (O, O), **h** (O, S) , **i** (O, Se) , **j** (O, Te)), MeEE'Me (**6-2a**–**6-2j**), and *cyclo*-1,2-EE'$(CH_2)_3$ (**6-3a**–**6-3j**) (E, E' = O, S, Se, and Te) (Chart 6-1). E and E' are chosen so as to the electronegativity of E (χ_E) is less than or equal to that of E' ($\chi_{E'}$).[10] Cyclic dichalcogenides **6-3** are the example of *cis*-dichalcogenides. Another aim of the analysis is to construct the firm basis to clarify the E---E' *trans*-annular interactions in *cyclo*-E$(CH_2CH_2CH_2)_2$E' (**6-**

4), their dications (**6-4**$^{2+}$) and the dimers ((**6-4**)$_2^{2+}$) reported by research groups of Furukawa[11] and Glass.[12] The cyclic dichalcogenides **6-3** are the candidates for the purpose.

The quantum theory of atoms-in-molecules (QTAIM) approach, introduced by Bader,[13–15] enables us to analyze the nature of chemical bonds and interactions.[16–21] QTAIM-DFA provides an excellent possibility for evaluating, understanding, and classifying weak to strong interactions in a unified form.[22–25] $H_b(\boldsymbol{r}_c)$ are plotted versus $H_b(\boldsymbol{r}_c) - V_b(\boldsymbol{r}_c)/2$ in QTAIM-DFA, where $H_b(\boldsymbol{r}_c)$ and $V_b(\boldsymbol{r}_c)$ are the total electron energy densities and potential energy densities, respectively, at bond critical points (BCPs). In his research group treatment, data for perturbed structures around fully optimized ones are employed for the plots, in addition to those of the fully optimized structures.[22–26]

His research group also proposed the concept of "the dynamic nature of interactions" originated from the data containing the perturbed structures.[22a,23–25] Data from the fully optimized structures correspond to the static nature of interactions. QTAIM-DFA is applied to typical chemical bonds and interactions, and rough criteria have been established, which can distinguish the chemical bonds and interactions in question from others. QTAIM-DFA and the criteria are explained in Chapter 2, employing Schemes 2-1–2-3, Figure 2-1 and eqs (2-8)–(2-12). The basic concept of the QTAIM approach is also surveyed in Chapter 2.

He considers this method to be well-suited to clarify the dynamic and static nature of the E–E' bonds/interactions (E, E' = O, S, Se, and Te) in **6-1**–**6-3**. The E–E' bonds/interactions in neutral, cationic, and anionic forms of **6-1**–**6-3** have been chosen for the investigations. Normal coordinates of internal vibrations (NIV) will be employed to generate the perturbed structures necessary to clarify the dynamic behaviors. Results of the calculations on **6-1**–**6-3** with E, E' = S, Se, and Te (**a**–**f**) will be discussed in the text and those with (E, E') = (O, O), (O, S), (O, Se), (O, Te) (**g**–**j**) are given in the Appendix.

The nature of E–E' in the neutral and charged species of **6-1**–**6-3** will be discussed on the basis of the θ and θ_p values, using Scheme 2-3 of Chapter 2 as a reference.

Methodological Details in Calculations

Neutral, anionic, mono-cationic, and di-cationic forms of **6-1**–**6-3** were optimized using the Gaussian 03 program package.[27] Calculations are performed at the Møller-Plesset second order energy correlation (MP2) level[28] employing the 6-311++G(3d,p)[29] basis set for H, C, O, S, and Se and that of the (7433111/743111/7411/2 + 1s1p1d1f) type[30] for Te for **6-1** and **6-2**, and the 6-311+G(3d) basis set for O, S, and Se and that of the (7433111/743111/7411/2 + 1s1p1d1f) type for Te with the 6-311++G(d) basis set for C and H for **6-3**. Unrestricted UMP2 method is applied to the odd electron systems. The structures were confirmed by the frequency analysis performed on the optimized structures with the same basis sets at the same level of the optimizations. QTAIM functions were calculated using the Gaussian 03 program package[27] with the same basis sets at the same level of the optimizations and they were analyzed by the AIM2000 program.[31]

Normal coordinates of internal vibrations (NIV) obtained by the frequency analysis were employed to generate the perturbed structures. The method is explained in Chapter 2.

Results and Discussion

Structural Feature in Neutral and Charged Forms of Dichalcogenides

Neutral, mono-anionic, mono-cationic, and di-cationic forms of **6-1** (**6-1a**–**6-1f**), **6-2** (**6-2a**–**6-2f**), and **6-3** (**6-3a**–**6-3f**) are optimized and the frequency analysis was performed on the optimized structures to confirm the structures. Table 6-1 collects the optimized E–E', E–H, and E'–H distances (r_o(E, E'), r_o(E, H), r_o(E', H), respectively), together with the angles and torsional angles around the E–E' bonds (∠E'EH, ∠EE'H, and ϕ(HEE'H), respectively) for **6-1**. Tables 6-2 and 6-3 collect the corresponding values of r_o(E, E'), r_o(E, C), r_o(E', C), ∠E'EC, ∠EE'C, and ϕ(CEE'C) in **6-2** and **6-3**, respectively.

Structures of mono-anionic forms of **6-1** (**6-1**$^-$) (92.1º ≤ ϕ(HEE'H) ≤ 94.1º) are similar to those of the corresponding neutral species in **6-1** (C_2: 90.4º ≤ ϕ(HEE'H) ≤ 91.1º), although the E–E' distances (r(E, E')) elongate much (0.57–0.70 Å) in **6-1**$^-$. Both **6-1** and **6-1**$^-$ have the non-planar structures,

which are C_2 for E = E' but C_1 if E ≠ E'.[32] The structures are abbreviated as $C_{2:np}$ and $C_{1:np}$, respectively. However, they will be called $C_{2:np}$–type, as a whole, if necessary. In the case of **6-2**$^-$, the *trans*-forms with ϕ(CEE'C) ≈ 180.0º are optimized, in addition to the $C_{2:np}$–type structures (84.0º ≤ ϕ(CEE'C) ≤ 88.1º). Both *cis*- (ϕ(HEE'H) ≈ 0.0º or ϕ(CEE'C) ≈ 0.0º) and *trans*-forms (ϕ(HEE'H) ≈ 180.0º or ϕ(CEE'C) ≈ 180.0º) are optimized for mono-cationic forms of **6-1** and **6-2**, (**6-1**$^+$ and **6-2**$^+$, respectively), so are the di-cationic forms (**6-1**$^{2+}$ and **6-2**$^{2+}$, respectively). On the other hand, only *cis*-forms are detected in **6-3**. The ϕ(CEE'C) values decrease in the order of neutral (**6-3**: 0º ≤ ϕ(CEE'C) ≤ 47º) > mono-anionic (**6-3**$^-$: 0º ≤ ϕ(CEE'C) ≤ 12º) > mono-cationic (**6-3**$^+$: 0º ≤ ϕ(CEE'C) ≤ 4º) ≥ di-cationic (**6-3**$^{2+}$: 0º ≤ ϕ(CEE'C) ≤ 1º) forms.

The E–E' bonds shorten in the formation of the mono-cationic forms and they do further when the mono-cationic forms change to di-cationic forms, as expected. However, the magnitudes of the shortening of E–E' in the formation of mono-cationic forms are much smaller than those of the elongation in the formation of the mono-anionic forms. The ratios of the magnitudes are 4–8% for the homo-nuclear E–E and 10–12% for the hetero-nuclear E–E' (E ≠ E') in the formation of the mono-cationic forms, relative to the case of the mono-cationic forms, in **6-1** and **6-2**. On the other hand, the rations for the homo-nuclear E–E in the formation of the di-cationic forms, relative to the formation of the mono-cationic forms, are 110–140% and 161–185% in **6-1** and **6-2**, respectively. The rations for the hetero-nuclear E–E' (E ≠ E') are 110–118% and 103–128% in **6-1** and **6-2**, respectively. In the case of **6-3**, the values are 130–175% for the homo-nuclear E–E and 109–128% for the hetero-nuclear E–E' (E ≠ E'). An electron will be accepted in LUMO of σ*(E–E') in the formation of a mono-anionic form, whereas it will be removed from HOMO of a lone pair orbital of E' (when E ≠ E') or E (if E = E') in the formation of mono-cationic forms. Therefore, the ratios of the magnitudes in the formation of mono-cationic forms are very small, relative to the case of mono-anionic forms. The structures of mono-cationic forms must be planar of *cis*- and *trans*-forms. An electron will be further removed from the singly occupied π*(S–Se) in the formation of di-cationic forms. The E–H and/or E'–H distances change in the inverse directions of the E–E' distances in the formation of the charged species

in **6-1**, so do E–C and/or E'–C distances in **6-2**. The behavior in **6-3** is similar to that of **6-2** but it must be more complex.

Figure 6-1 shows the optimized structures of **6-1b** ($C_{1:np}$) and **6-1b**$^{-}$ ($C_{1:np}$), together with ψ_{20}–ψ_{27} and the characters. Figure 6-2 depicts the structures of **6-1b**$^{+}$ ($C_{s:cis}$), **6-1b**$^{+}$ ($C_{s:trans}$), **6-1b**$^{2+}$ ($C_{s:cis}$), and **6-1b**$^{2+}$ ($C_{s:trans}$), together with ψ_{22}–ψ_{26} and the characters. The characters of ψ_{20} and ψ_{21} are commonly $A1_{oSe} + A1_{oS}$ and $A1_{oSe} - A1_{oS}$, respectively, as seen in Figure 6-1. Table 6-4 summarizes the characters of ψ_{22}–ψ_{27} for the species.

Table 6-1. Distances, angles, and torsional angles for neutral and charged forms of HEE'H (**6-1**), together with relative energies, optimized at the MP2 level[a]

Compd	r_o(E, E') (Å)	Δr_o(E, E') (Å)	ϕ(CEE'C) (º)	r_o(E, H) (Å)	∠E'EH (º)	r_o(E', H) (Å)	∠EE'H (º)	ΔE^b (eV)	Sym-metry
Neutral form: $C_{2:np}$-type									
6-1a	2.0813	0.0000	91.1	1.3366	97.9	1.3366	97.9	0.00	$C_{2:np}$
6-1b	2.2229	0.0000	90.9	1.3365	97.3	1.4635	96.5	0.00	$C_{1:np}$
6-1c	2.3907	0.0000	90.5	1.3364	96.8	1.6625	95.8	0.00	$C_{1:np}$
6-1d	2.3537	0.0000	90.6	1.4634	96.1	1.4634	96.1	0.00	$C_{2:np}$
6-1e	2.5147	0.0000	90.4	1.4568	95.8	1.6620	95.6	0.00	$C_{1:np}$
6-1f	2.6896	0.0000	90.5	1.6619	95.7	1.6619	95.7	0.00	$C_{2:np}$
Mono-anionic form: $C_{2:np}$-type									
6-1a$^-$	2.7826	0.7013	94.1	1.3348	86.7	1.3348	86.7	–0.74	$C_{2:np}$
6-1b$^-$	2.8708	0.6479	93.0	1.3357	88.2	1.4610	87.4	–0.88	$C_{1:np}$
6-1c$^-$	2.9759	0.5852	93.3	1.3357	88.5	1.6592	85.9	–0.98	$C_{1:np}$
6-1d$^-$	2.9791	0.6254	92.1	1.4620	88.5	1.4620	88.5	–1.01	$C_{2:np}$
6-1e$^-$	3.0879	0.5732	92.6	1.4554	88.8	1.6596	86.6	–1.08	$C_{1:np}$
6-1f$^-$	3.2739	0.5843	93.6	1.6598	87.1	1.6598	87.1	–1.17	C_{2np}
Mono-cationic: *cis*-type									
6-1a$^+$	2.0237	–0.0576	0.0	1.3450	97.9	1.3450	97.9	8.89	C_{2v}
6-1b$^+$	2.1528	–0.0701	0.0	1.3450	97.6	1.4687	95.7	8.68	C_s
6-1c$^+$	2.3302	–0.0605	0.0	1.3432	95.1	1.6642	94.9	8.44	C_s
6-1d$^+$	2.3087	–0.0450	0.0	1.4692	95.1	1.4692	95.1	8.46	C_{2v}
6-1e$^+$	2.4524	–0.0623	0.0	1.4623	93.8	1.6630	93.9	8.31	C_s
6-1f$^+$	2.6651	–0.0245	0.0	1.6632	92.3	1.6632	92.3	8.06	C_{2v}
Mono-cationic: *trans*-type									
6-1a$^+$	2.0149	–0.0664	180.0	1.3468	93.5	1.3468	93.5	8.75	C_s
6-1b$^+$	2.1454	–0.0775	180.0	1.3469	93.8	1.4702	91.5	8.57	C_s
6-1c$^+$	2.3228	–0.0679	180.0	1.3450	93.0	1.6646	90.3	8.35	C_s
6-1d$^+$	2.2989	–0.0548	180.0	1.4709	91.4	1.4709	91.4	8.36	C_{2h}
6-1e$^+$	2.4443	–0.0704	180.0	1.4642	91.4	1.6642	90.0	8.22	C_s
6-1f$^+$	2.6545	–0.0351	180.0	1.6649	89.7	1.6649	89.7	7.98	C_{2h}
Di-cationic: *cis*-type									
6-1a^{2+}	1.9835	–0.0978	0.0	1.3744	99.5	1.3744	99.5	25.32	C_{2v}
6-1b^{2+}	2.1429	–0.0800	0.0	1.3705	98.6	1.4953	96.6	24.51	C_s
6-1c^{2+}	2.3120	–0.0787	0.0	1.3655	97.0	1.6837	94.5	23.52	C_s
6-1d^{2+}	2.2948	–0.0589	0.0	1.4926	96.0	1.4926	96.0	23.77	C_{2v}
6-1e^{2+}	2.4582	–0.0565	0.0	1.4836	94.7	1.6809	93.6	22.94	C_s
6-1f^{2+}	2.6588	–0.0308	0.0	1.6790	92.4	1.6790	92.4	22.12	C_{2v}
Di-cationic: *trans*-type									
6-1a^{2+}	1.9742	–0.1071	180.0	1.3768	94.4	1.3768	94.4	21.31	C_{2h}
6-1b^{2+}	2.1326	–0.0903	180.0	1.3728	94.4	1.4976	91.6	20.65	C_s
6-1c^{2+}	2.3039	–0.0868	180.0	1.3675	94.5	1.6848	89.2	19.84	C_s
6-1d^{2+}	2.2830	–0.0707	180.0	1.4946	91.8	1.4946	91.8	20.05	C_{2h}
6-1e^{2+}	2.4478	–0.0669	180.0	1.4857	92.1	1.6826	89.1	19.36	C_s
6-1f^{2+}	2.6466	–0.0430	180.0	1.6809	89.4	1.6809	89.4	18.67	C_{2h}

[a] The 6-311++G(3d,p) basis set for H, S, and Se and that of the (7433111/743111/7411/2 + 1s1p1d1f) type for Te. [b] E(**6-1a**) = –796.54518 au, E(**6-1b**) = –2798.79682 au, E(**6-1c**) = –7010.73697 au, E(**6-1d**) = –4801.04822 au, E(**6-1e**) = –9013.14578 au, and E(**6-1f**) = –13224.92744 au.

Table 6-2. Distances, angles, and torsional angles for neutral and charged forms of MeEE'Me (**6-2**), together with relative energies, optimized at the MP2 level[a]

Compd	r_o(E, E') (Å)	Δr_o(E, E') (Å)	ϕ(CEE'C) (º)	r_o(E, C) (Å)	∠E'EC (º)	r_o(E', C) (Å)	∠EE'C (º)	ΔE (eV)	Sym-metry
Neutral forms: $C_{2:np}$-type									
6-2a	2.0581	0.0000	85.8	1.8115	102.3	1.8115	102.3	0.00	$C_{2:np}$
6-2b	2.1980	0.0000	85.7	1.8139	102.3	1.9497	99.4	0.00	$C_{1:np}$
6-2c	2.3714	0.0000	86.0	1.8212	102.9	2.1402	97.3	0.00	$C_{1:np}$
6-2d	2.3240	0.0000	86.0	1.9525	99.6	1.9525	99.6	0.00	$C_{2:np}$
6-2e	2.4951	0.0000	86.6	1.9592	100.2	2.1424	97.5	0.00	$C_{1:np}$
6-2f	2.6697	0.0000	88.0	2.1481	98.0	2.1481	98.0	0.00	$C_{2:np}$
Mono-anionic forms: $C_{2:np}$-type									
6-2a$^-$	2.7556	0.6975	87.3	1.8171	57.2	1.8171	57.2	–0.15	$C_{2:np}$
6-2b$^-$	2.8394	0.6414	86.0	1.8189	90.8	1.9597	86.1	–0.34	$C_{1:np}$
6-2c$^-$	2.9215	0.5501	85.1	1.8215	93.5	2.1578	81.6	–0.50	$C_{1:np}$
6-2d$^-$	2.9377	0.6137	84.6	1.9617	87.5	1.9617	87.5	–0.50	$C_{2:np}$
6-2e$^-$	3.0357	0.5406	84.0	1.9643	90.0	2.1593	82.8	–0.61	$C_{1:np}$
6-2f$^-$	3.2052	0.5355	88.1	2.1613	84.2	2.1613	84.2	–0.73	$C_{2:np}$
Mono-anionic forms: *trans*-type									
6-2a$^-$	2.7404	0.6823	180.0	1.8144	58.4	1.8144	58.4	–0.14	C_{2h}
6-2b$^-$	2.8231	0.6251	180.0	1.8159	89.1	1.9558	83.7	–0.33	C_s
6-2c$^-$	2.8944	0.5230	180.0	1.8173	92.1	2.1536	78.5	–0.51	C_s
6-2d$^-$	2.9212	0.5972	180.0	1.9579	85.3	1.9579	85.3	–0.48	C_{2h}
6-2e$^-$	3.0087	0.5136	180.0	1.9594	88.2	2.15509	79.8	–0.61	C_s
6-2f$^-$	3.1676	0.4979	180.0	2.1566	61.2	2.1566	61.2	–0.74	C_{2h}
Mono-cationic forms: *cis*-type									
6-2a$^+$	2.0175	–0.0406	0.0	1.8028	107.7	1.8028	107.7	7.99	C_2
6-2b$^+$	2.1479	–0.0501	0.0	1.8056	107.8	1.9401	104.0	7.87	C_1
6-2c$^+$	2.3213	–0.0501	0.0	1.8207	106.8	2.1219	101.1	7.72	C_1
6-2d$^+$	2.2914	–0.0326	0.0	1.9437	104.0	1.9437	104.0	7.73	C_2
6-2e$^+$	2.4446	–0.0505	0.0	1.9552	103.8	2.1266	100.8	7.62	C_1
6-2f$^+$	2.6551	–0.0146	0.0	2.1365	100.0	2.1365	100.0	7.44	C_{2v}
Mono-cationic: *trans*-type									
6-2a$^+$	2.0060	–0.0521	180.0	1.8092	100.5	1.8092	100.5	7.81	C_2
6-2b$^+$	2.1335	–0.0645	180.0	1.8125	101.8	1.9464	97.1	7.73	C_1
6-2c$^+$	2.3115	–0.0599	180.0	1.8274	102.7	2.1233	93.9	7.60	C_1
6-2d$^+$	2.2797	–0.0443	180.0	1.9498	97.8	1.9498	97.8	7.60	C_2
6-2e$^+$	2.4331	–0.0620	180.0	1.9578	103.2	2.1170	98.0	7.51	C_1
6-2f$^+$	2.6438	–0.0259	180.0	2.1399	95.4	2.1399	95.4	7.34	C_2
Di-cationic: *cis*-type									
6-2a^{2+}	1.9701	–0.0880	0.1	1.7829	112.0	1.7829	112.0	22.45	C_2
6-2b^{2+}	2.1250	–0.0730	0.0	1.7813	112.9	1.93300	108.0	22.00	C_s
6-2c^{2+}	2.3036	–0.0678	0.0	1.8040	112.9	2.1103	104.2	21.31	C_s
6-2d^{2+}	2.2632	–0.0608	0.2	1.9367	107.2	1.9367	107.2	21.59	C_2
6-2e^{2+}	2.4409	–0.0542	0.0	1.9491	108.8	2.1161	104.3	20.93	C_1
6-2f^{2+}	2.6334	–0.0363	0.4	2.1296	103.0	2.1296	103.0	20.35	C_2
Di-cationic: *trans*-type									
6-2a^{2+}	1.9618	–0.0963	180.0	1.7854	105.3	1.7854	105.3	22.22	C_2
6-2b^{2+}	2.1152	–0.0828	180.0	1.7896	106.7	1.9356	100.4	21.81	C_1
6-2c^{2+}	2.2962	–0.0752	180.0	1.8118	107.7	2.1111	96.8	21.15	C_1
6-2d^{2+}	2.2525	–0.0715	180.0	1.9404	102.0	1.9404	102.0	21.41	C_2
6-2e^{2+}	2.4313	–0.0638	180.0	1.9578	103.2	2.1170	98.0	20.79	C_1
6-2f^{2+}	2.6229	–0.0468	180.0	2.1314	99.2	2.1314	99.2	20.23	C_2

[a] The 6-311++G(3d,p) basis set for H, C, S, and Se and that of the (7433111/743111/7411/2 + 1s1p1d1f) type for Te. [b] E(**6-2a**) = –874.93462 au, E(**6-2b**) = –2877.34364 au, E(**6-2c**) = –7089.13373 au, E(**6-2d**) = –4879.75366 au, E(**6-2e**) = –9091.54524 au, and E(**6-2f**) = –13303.33454 au.

Table 6-3. Distances, angles, and torsional angles for neutral and charged forms of *cyclo*-1,2-EE'$(CH_2)_3$ (**6-3**), together with relative energies, optimized at the MP2 level[a]

Compd	r_o(E, E') (Å)	Δr_o(E, E') (Å)	ϕ(CEE'C) (º)	r_o(E, C) (Å)	∠E'EC (º)	r_o(E', C) (Å)	∠EE'C (º)	ΔE (eV)	Sym-metry
Neutral: *cis*-type									
6-3a	2.0823	0.0000	–47.0	1.8169	90.4	1.8169	90.4	0.00	C_1
6-3b	2.2418	0.0000	–23.6	1.8123	91.9	1.9792	92.4	0.00	C_1
6-3c	2.4129	0.0000	–22.1	1.8218	92.1	2.1696	87.7	0.00	C_1
6-3d	2.3671	0.0000	–6.6	1.9695	92.4	1.9588	90.7	0.00	C_1
6-3e	2.5407	0.0000	–17.7	1.9635	89.1	2.1707	88.3	0.00	C_1
6-3f	2.7298	0.0000	0.0	2.1654	87.4	2.1654	87.4	0.00	C_1
Mono-anionic: *cis*-type									
6-3a$^-$	2.8240	0.7417	0.0	1.8148	85.3	1.8148	85.3	–0.49	C_1
6-3b$^-$	2.8982	0.6564	–0.9	1.8162	86.9	1.9620	82.0	–0.61	C_1
6-3c$^-$	2.9659	0.5530	–11.9	1.8167	87.3	2.1710	79.5	–0.73	C_1
6-3d$^-$	2.9880	0.6209	0.0	1.9635	83.4	1.9635	83.4	–0.74	C_1
6-3e$^-$	3.0780	0.5373	–11.0	1.9634	83.5	2.1713	80.7	–0.82	C_1
6-3f$^-$	3.2451	0.5153	–9.4	2.1718	82.8	2.1659	78.1	–0.94	C_1
Mono-cationic: *cis*-type									
6-3a$^+$	2.0121	–0.0702	0.0	1.8288	97.2	1.8288	97.2	7.49	C_1
6-3b$^+$	2.1389	–0.1029	–0.6	1.8314	97.7	1.9669	92.9	7.42	C_1
6-3c$^+$	2.3119	–0.1010	–3.6	1.8452	97.2	2.1488	88.6	7.32	C_1
6-3d$^+$	2.2798	–0.0873	0.0	1.9712	93.3	1.9712	93.3	7.28	C_1
6-3e$^+$	2.4318	–0.1089	–2.1	1.9850	93.6	2.1547	89.0	7.20	C_1
6-3f$^+$	2.6380	–0.0918	0.0	2.1670	88.7	2.1670	88.7	7.00	C_s
Di-cationic: *cis*-type									
6-3a^{2+}	1.9593	–0.1230	0.0	1.8192	98.5	1.8192	98.5	21.87	C_1
6-3b^{2+}	2.1098	–0.1320	0.6	1.8229	98.8	1.9707	93.3	21.47	C_1
6-3c^{2+}	2.2884	–0.1245	–0.1	1.8465	98.8	2.1474	88.4	20.84	C_1
6-3d^{2+}	2.2441	–0.1230	0.0	1.9773	94.0	1.9773	94.0	21.04	C_1
6-3e^{2+}	2.4215	–0.1192	–0.6	1.9974	94.2	2.1550	89.1	20.43	C_1
6-3f^{2+}	2.6103	–0.1195	0.0	2.1721	89.3	2.1721	89.3	19.94	C_s

[a] The 6-311+G(3d) basis set for S and Se and that of the (7433111/743111/7411/2 + 1s1p1d1f) type for Te with the 6-311++G(d) basis set for C and H. [b] E(**6-3a**) = –912.93985 au, E(**6-3b**) = –2915.35107 au, E(**6-3c**) = –7127.14075 au, E(**6-3d**) = –4917.76156 au, E(**6-3e**) = –9129.55222 au, and E(**6-3f**) = –13341.33888 au.

MO's of ψ_{26} and ψ_{27} are HOMO and LUMO, respectively, and ψ_{20}–ψ_{26} correspond to the occupied valence orbitals in **6-1b**. An electron will be accepted in ψ_{27} (LUMO), resulting in the formation of **6-1b**$^-$. On the other hand, an electron will be removed from ψ_{26} (HOMO) of **6-1b**, resulting in the formation of **6-1b**$^+$. **6-1b**$^-$ and **6-1b**$^+$ correspond to radical anion and radical cation, respectively. The number of α-spin electrons is assumed to be larger than that of β-spin electrons by one, therefore, an orbital energy occupied by an α-spin electron must be more stable than that by a

β-spin electron, if those of the orbitals of the same number are compared. MOs of **6-1b**$^{-}$ and **6-1b**$^{+}$ occupied by α-spin electrons are depicted in Figures 6-1 and 6-2.

Table 6-4. Main characters of ψ_{22}–ψ_{27} for various structures in HSSeH (**6-1b**), **6-1b**$^{-}$, **6-1b**$^{+}$, and **6-1b**$^{2+}$[a]

Compounds	ψ_{22}	ψ_{23}	ψ_{24}	ψ_{25}	ψ_{26}	ψ_{27}
6-1b ($C_{1:np}$)	$B2_{Se} + B2_{S}$	$B2_{Se} - B2_{S}$	$A1_{Se} + A1_{S}$	$B1_{S}$	$B1_{Se}$[b]	σ*(Se–S)[c]
6-1b^{-} ($C_{1:np}$: α)	$B2_{S}$	$B2_{Se}$	$A1_{Se} + A1_{S}$	$B1_{S}$	$B1_{Se}$	σ*(Se–S)[d]
6-1b^{-} ($C_{1:np}$: β)	σ_p(S–H)	σ_p(Se–H)	$B1_{S}$	$B1_{Se}$	σ(Se–S)	σ*(Se–S)[c]
6-1b^{+} ($C_{s:cis}$: α)	$B2_{Se} + B2_{S}$	$B2_{Se} - B2_{S}$	$B1_{Se} + B1_{S}$	$B2_{Se} + A1_{S}$	$B1_{Se} - B1_{S}$[d]	σ*(Se–S)
6-1b^{+} ($C_{s:cis}$: β)	$B2_{Se} + B2_{S}$	$B2_{Se} - B2_{S}$	$A1_{Se} + A1_{S}$	$B1_{Se} + B1_{S}$	$B1_{Se} - B1_{S}$[c]	σ*(Se–S)
6-1b^{+} ($C_{s:trans}$: α)	$B2_{Se} + B2_{S}$	$B2_{Se} - B2_{S}$	$B1_{Se} + B1_{S}$	$A1_{Se} + A1_{S}$	$B1_{Se} - B1_{S}$[d]	σ*(Se–S)
6-1b^{+} ($C_{s:trans}$: β)	$B2_{Se} + B2_{S}$	$B2_{Se} - B2_{S}$	$A1_{Se} + A1_{S}$	$B1_{Se} + B1_{S}$	$B1_{Se} - B1_{S}$[c]	σ*(Se–S)
6-1b^{2+} ($C_{s:cis}$)	$B2_{Se} + B2_{S}$	$B2_{Se} + A1_{S}$	$A1_{Se} + B2_{S}$	$B1_{Se} + B1_{S}$[b]	$B1_{Se} - B1_{S}$[c]	σ*(Se–S)
6-1b^{2+} ($C_{s:trans}$)	$B2_{Se} + B2_{S}$	$B2_{Se} - B2_{S}$	$A1_{Se} + A1_{S}$	$B1_{Se} + B1_{S}$[b]	$B1_{Se} - B1_{S}$[c]	σ*(Se–S)

[a] Characters of ψ_{20} and ψ_{21} are commonly $A1_{oSe} + A1_{oS}$ and $A1_{oSe} - A1_{oS}$, respectively (see Figure 6-1). [b] HOMO. [c] LUMO. [d] SOMO.

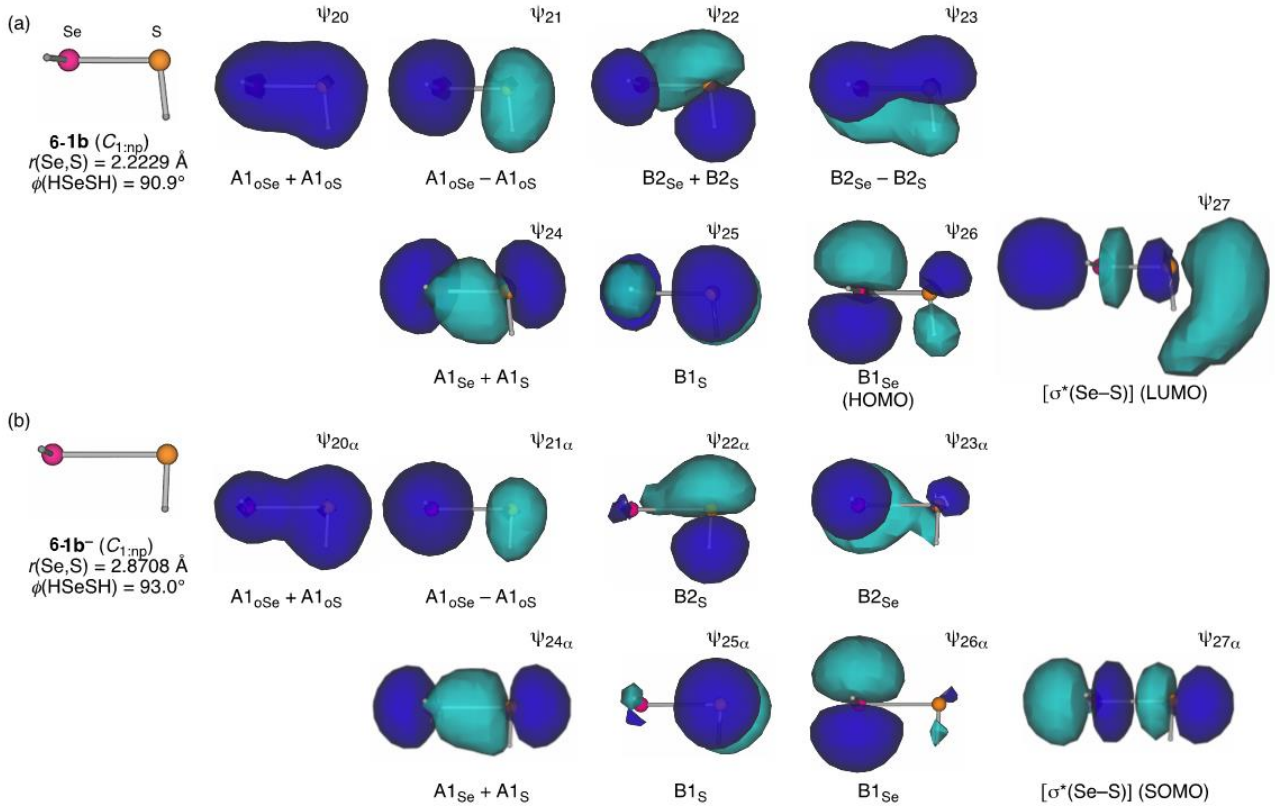

Figure 6-1. Structures and ψ_{20}–ψ_{27}, together with the characters, for (a) HSSeH (**6-1b** ($C_{1:np}$)) and (b) **6-1b**$^{-}$ ($C_{1:np}$).

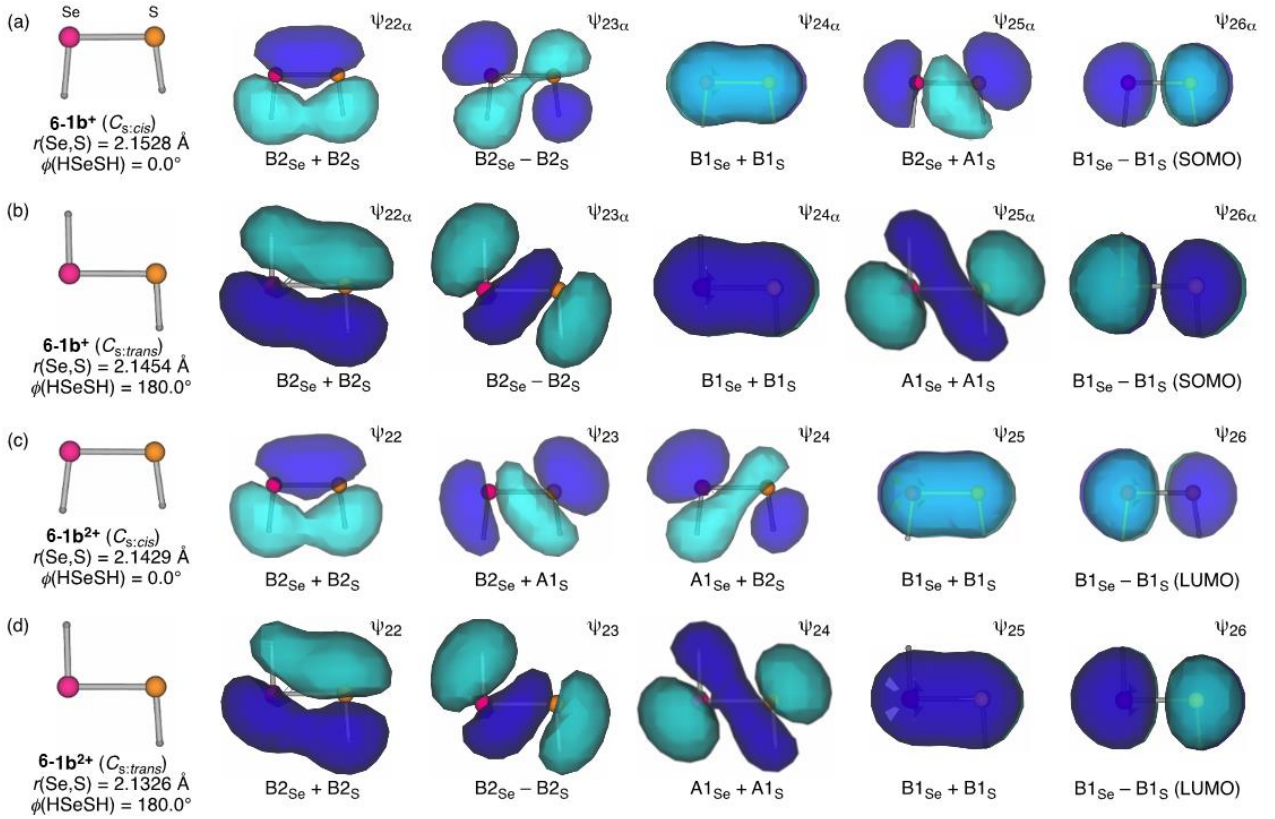

Figure 6-2. Structures and ψ_{22}–ψ_{26}, together with the main characters, for (a) **6-1b**$^{+}$ ($C_{s:cis}$), (b) **6-1b**$^{+}$ ($C_{s:trans}$), (c) **6-1b**$^{2+}$ ($C_{s:cis}$), and (d) **6-1b**$^{2+}$ ($C_{s:trans}$).

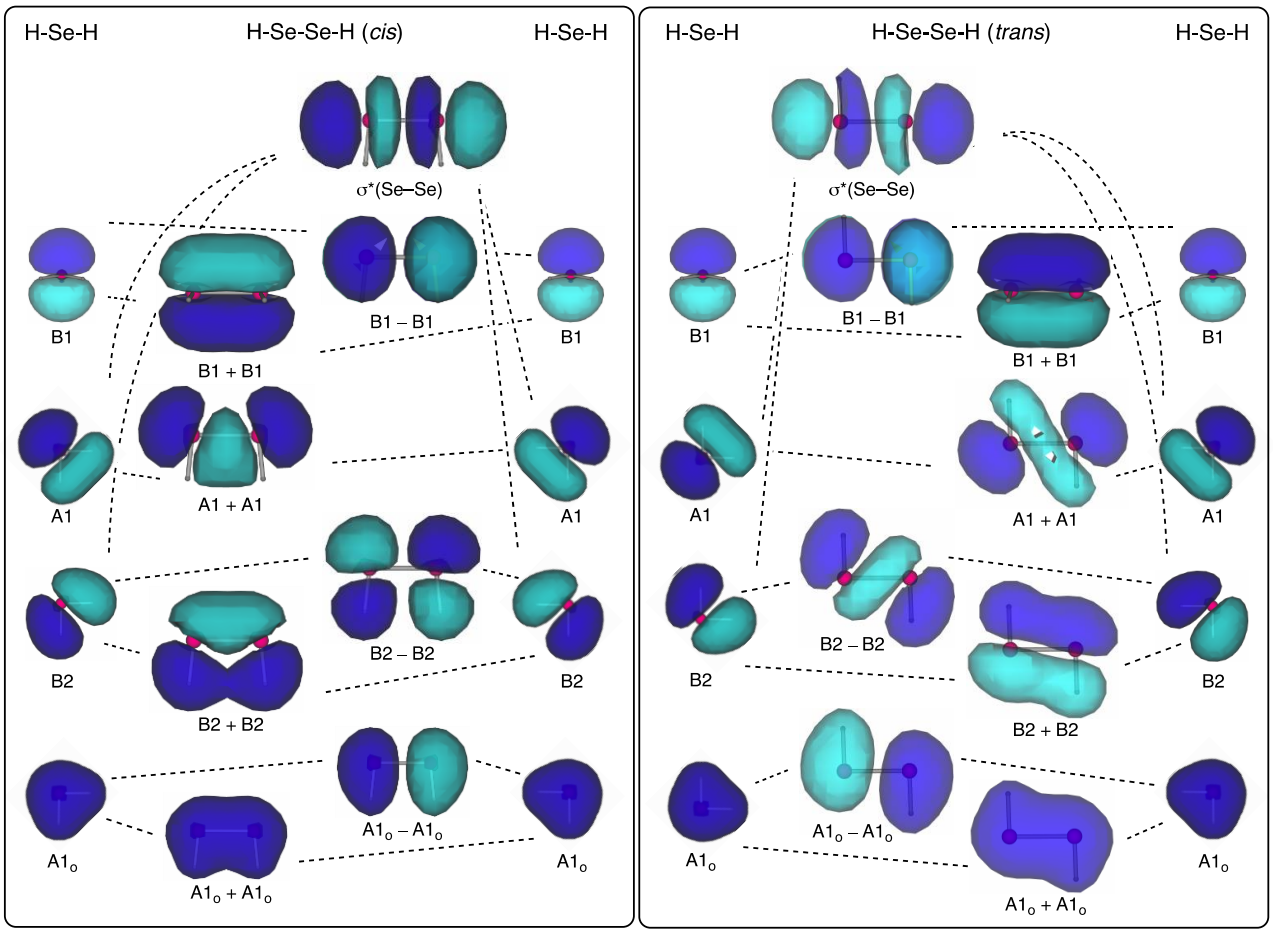

Figure 6-3. Approximate orbital interactions between $2SeH_2$ to produce HSeSeH (**6-1d**).

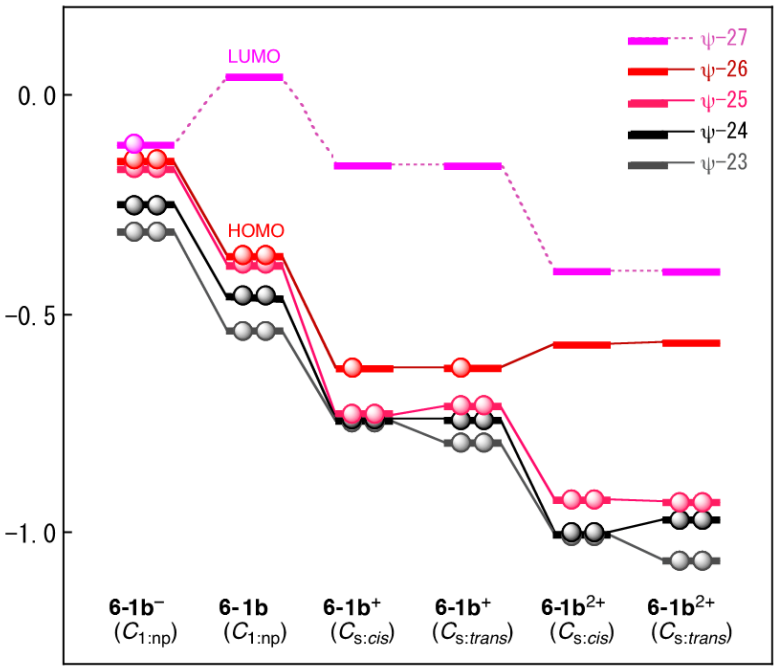

Figure 6-4. Approximate energy diagram for **6-1b**, **6-1b**$^-$, **6-1b**$^+$, and **6-1b**$^{2+}$. MOs of ψ_{23}–ψ_{27} are described. Energies of α-spin orbitals are employed for **6-1b**$^-$ and **6-1b**$^+$ for the description and β-spin electrons are added to the corresponding α-spin levels for clarity.

Most of MOs in **6-1b**$^-$ ($C_{1:np}$) such as $\psi_{22}\alpha$ (ψ_{22} occupied by an α–spin electron), $\psi_{25}\alpha$, $\psi_{26}\alpha$, and $\psi_{22}\beta$–$\psi_{25}\beta$ appear almost without the S---Se interaction. The interaction in **6-1b**$^-$ ($C_{1:np}$) must be much smaller than those of other cases at the very longer S---Se distance of 2.87 Å. Figure 6-3 explains the construction of MOs of HEE'H from the components, employing approximate orbital interactions in planar HSeSeH (**6-1d**) of *cis*- and *trans*-forms from $2H_2Se$, which can be essentially applied to the case of HSSeH (**6-1b**). Figure 6-4 shows the approximate energy diagram for ψ_{23}–ψ_{27} in **6-1b**, **6-1b**$^-$, **6-1b**$^+$, and **6-1b**$^{2+}$. Energies of α-spin orbitals are employed for **6-1b**$^-$ and **6-1b**$^+$ in the Figure. β-Spin electrons are added to the corresponding α-spin MOs in Figure 6-4, for clarity. Energies of the β-spin electrons are less than that of the corresponding α-spin electrons, although they are somewhat complex than simply expected, as shown in Table 6-4.

The mechanisms of the redox processes will be explained exemplified by **6-1b**. As shown in Figure 6-1, the p-type lone pair orbitals on Se and/or S (n_p(Se) and n_p(S), respectively: $B1_{Se}$ and $B1_S$, respectively) construct HOMO or HOMO-1, respectively, whereas LUMO localizes on the S–Se bond forming σ^*(S–Se) in **6-1b** ($C_{1:np}$). The $C_{1:np}$ structure of neutral HSSeH originates mainly from the repulsive interactions between n_p(Se) and n_p(S), since they are filled with electrons. The S–Se bond in **6-1b** ($C_{1:np}$) is expected to be described as the usual chemical bonds of σ(2c–2e) (two center-two electron bonds) as a whole, although the σ(2c–2e) character seems diverse to some MOs in Figure 6-1.

If an electron is added to **6-1b** ($C_{1:np}$), it will be accepted in σ^*(S–Se). Therefore, two electrons are in σ(S–Se) with one in σ^*(S–Se). As a result, SSe σ(2c–3e) is formed in this process, resulting in a large elongation of the S–Se bond in the anionic form of the non-planar C_1 symmetry, **6-1b**$^-$ ($C_{1:np}$). The expectation is in accordance with the calculated results for **6-1b**$^-$ ($C_{1:np}$) shown in Table 6-1. The structure of **6-1b**$^-$ ($C_{1:np}$) is essentially the same as that of **6-1b** ($C_{1:np}$), although the S–Se bond is much elongated. On the other hand, an electron will be removed from n_p(Se) (HOMO) in the one-electron reduction, which lower the repulsive energy between n_p(Se) and n_p(S). SSe π(2c–3e) will form in **6-1b**$^+$ in place of n_p(Se) and n_p(S) in **6-1b** ($C_{1:np}$), since the predicted structures of **6-1b**$^+$ are

planar of the *cis*- or *trans*-forms. The *cis*- and *trans*-forms are well explained based on the energy lowering effect of SSe π(2c–3e) as shown in Table 6-1. SSe π(2c–3e) in **6-1b**$^{+}$ change to SSe π(2c–2e) in **6-1b**$^{2+}$, if one more electron is removed from **6-1b**$^{+}$. The structures of **6-1b**$^{2+}$ are close to those of **6-1b**$^{+}$. The S–Se bond in **6-1b**$^{2+}$ becomes shorter than that of **6-1b**$^{+}$.

The redox processes observed in **6-1b** are commonly predicted for **6-1**. The mechanisms in **6-2** can also be understood based on those of **6-1**, although the *trans*-forms appear in **6-2**$^{-}$, in addition the $C_{2:np}$-type. The *trans*-forms would be stabilized by the hyperconjugative interactions between EE' σ(2c–3e) and the two p-type orbitals of the Me groups if the four C, E, E', and C atoms are on a co-plane. The σ∗(E–E') orbital should be on the plane. Such effective hyperconjugative interactions are lacking in **6-1**. The reduced repulsive interactions between the lone pair orbitals, due to the elongated E–E' distances, must also be important in **6-2**$^{-}$, although the *cis*-forms are not detected in **6-2**$^{-}$. The attractive hyperconjugative interactions seem not so effective relative to the steric repulsion between the Me groups in **6-2**.

An electron will be removed from n_p(E') or n_p(E) in the one-electron oxidation, which lower the repulsive energy between n_p(E') and n_p(E) in REE'R. EE' π(2c–3e) will form in place of n_p(E') and n_p(E), if the four atoms around the EE' bond appear in a plane, which stabilize the planar structures of REE'R. The formation of the *cis*- and *trans*-forms of mono-cationic forms in **6-1** and **6-2** (**6-1**$^{+}$ and **6-2**$^{+}$, respectively) are well predicted based on the energy lowering effect of EE' π(2c–3e). EE' π(2c–3e) in **6-1**$^{+}$ and **6-2**$^{+}$ go to **6-1**$^{2+}$ and **6-2**$^{2+}$, if one more electron is removed from each of the mono-cationic forms. The structures of **6-1**$^{2+}$ and **6-2**$^{2+}$ are predicted to be close to those of **6-1**$^{+}$ and **6-2**$^{+}$, respectively, although the E–E' become shorter in **6-2**$^{2+}$, relative to the case of **6-2**$^{+}$. The behavior of **6-3** in the redox processes can be understood as that of **6-2** of the *cis*-form.

Contour Plots, Negative Laplacians, and Trajectory Plots Around the E-∗-E' Bonds

Contour Plots of $\rho_b(\boldsymbol{r}_c)$, negative Laplacians, and trajectory plots around the E-∗-E' bonds are drawn for **6-1**–**6-3**. Figures 6-5 and 6-6 show the maps, negative Laplacians, and trajectory plots,

exemplified by **6-3b** and **6-3b**$^{2+}$, respectively. While four S, Se, C, and C atoms are on a plain in **6-3b**, four C S, Se, and C atoms are in **6-3b**$^{2+}$. The behavior of the S–Se–C–C interaction in **6-3b** and the C–S–Se–C interaction in **6-3b**$^{2+}$ is well described in the Figures. Figure 6-7 depicts the S–Se stretching in **6-3b**, **6-3b**$^{-}$, **6-3b**$^{+}$, and **6-3b**$^{2+}$, necessary to evaluate the dynamic nature of the bond, for an example.

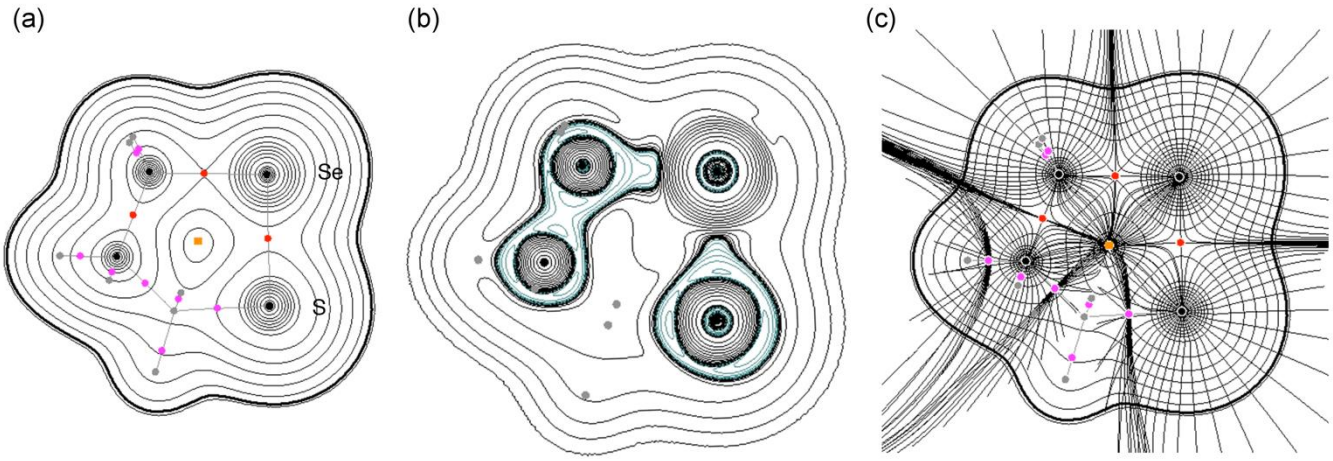

Figure 6-5. Contour plots of $\rho_b(\boldsymbol{r}_c)$ (a), negative Laplacian with the negative areas in blue and positive ones in black (b), and trajectory plot (c) are drawn on the CSeS plane of **6-3b**.

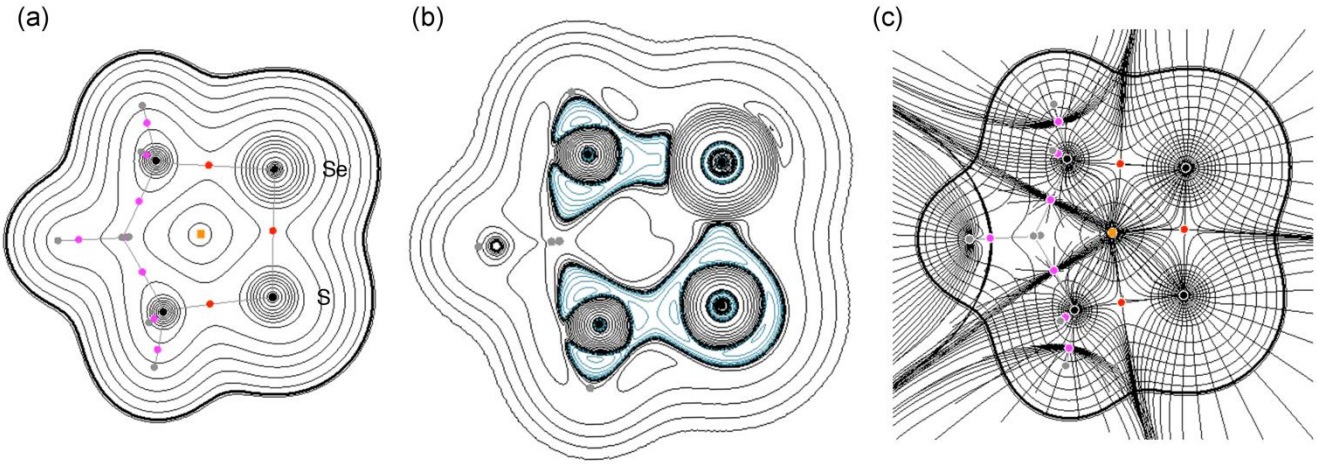

Figure 6-6. Contour plots of $\rho_b(\boldsymbol{r}_c)$ (a), negative Laplacian with the negative areas in blue and positive ones in black (b), and trajectory plot (c) are drawn on the CSeS plane of **6-3b**$^{2+}$.

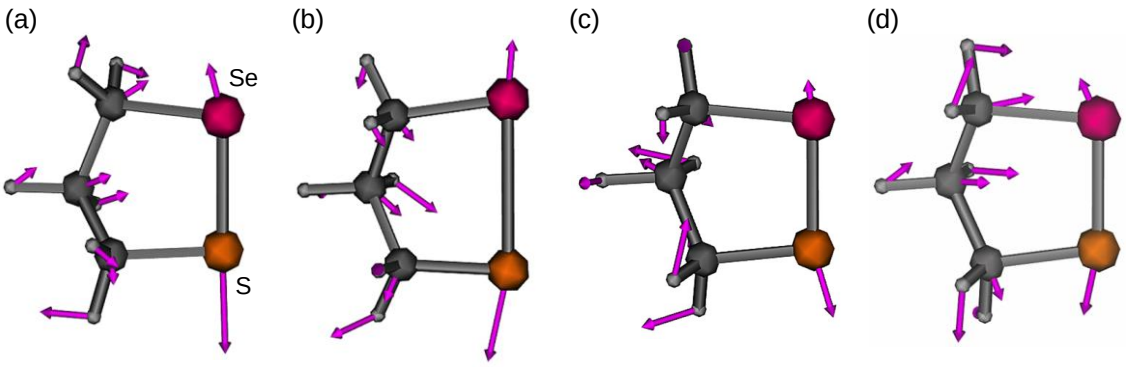

Figure 6-7. The S–Se stretching mode of (a) **6-3b** (ν_4), (b) **6-3b**$^-$ (ν_2), (c) **6-3b**$^+$ (ν_5), and (d) **6-3b**$^{2+}$ (ν_4).

QTAIM Parameters of (R, θ) and (θ_p, κ_p) for E-∗-E' of 6-1–6-3, Evaluated with QTAIM Dual Functional Analysis

Tables 6-5–6-7 collect the QTAIM functions of $\rho_b(\boldsymbol{r}_c)$, $H_b(\boldsymbol{r}_c) - V_b(\boldsymbol{r}_c)/2$, $H_b(\boldsymbol{r}_c)$, and $k_b(\boldsymbol{r}_c)$ (= $V_b(\boldsymbol{r}_c)/G_b(\boldsymbol{r}_c)$) at BCP of E-∗-E' in the neutral, anionic, mono-cationic, and di-cationic forms of **6-1**–**6-3**, respectively. $H_b(\boldsymbol{r}_c) - V_b(\boldsymbol{r}_c)/2$ are plotted versus $H_b(\boldsymbol{r}_c)$ for the fully-optimized data in Tables 6-5–6-7, together with those of the perturbed structures around the fully-optimized ones. Each plot for the neutral, anionic, mono-cationic, or di-cationic form in **6-1**–**6-3** is essentially the same if the same interaction of the same form is compared. Figures 6-8–6-10 show the plots for **6-1**–**6-3**.

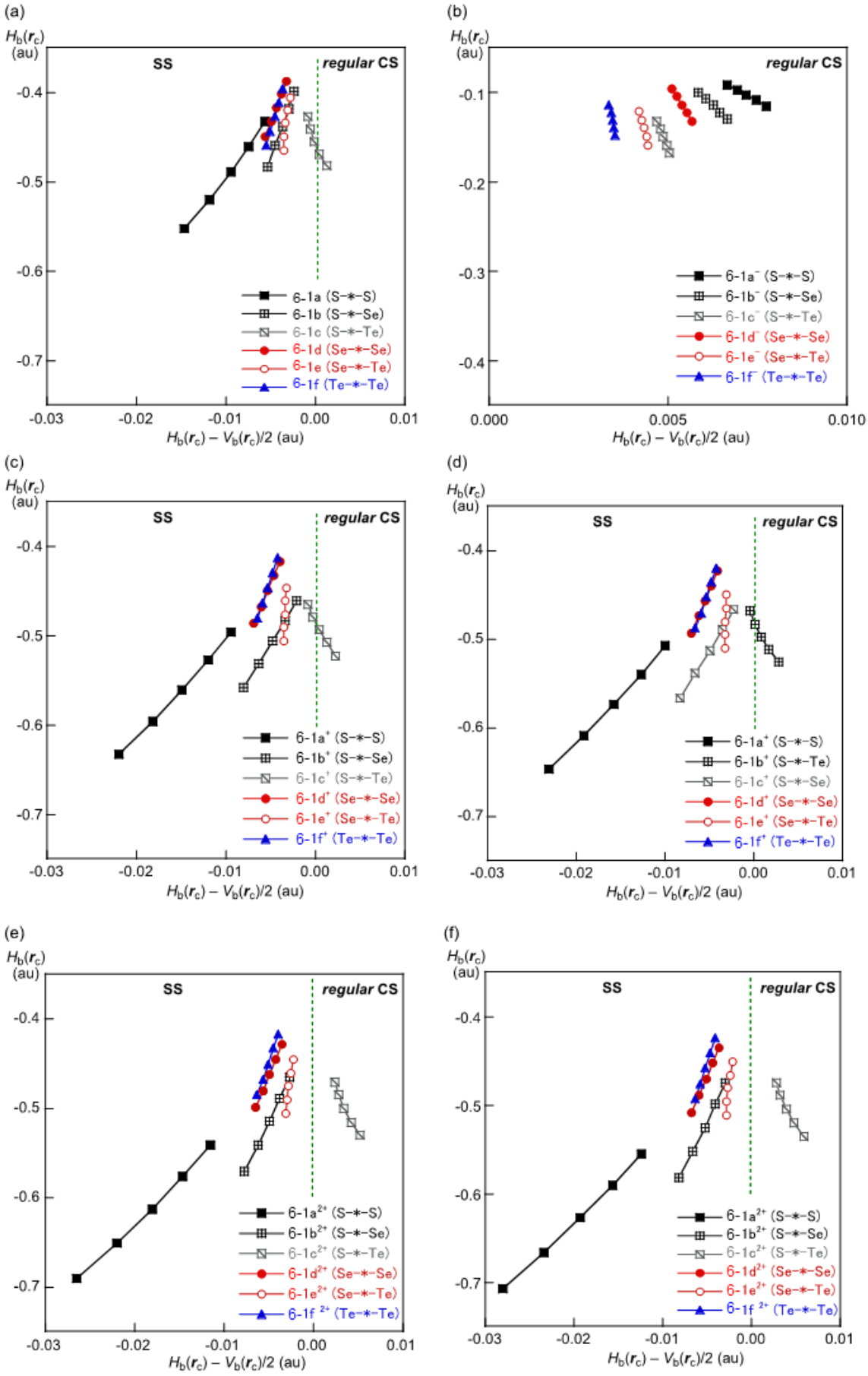

Figure 6-8. Plots of $H_b(\boldsymbol{r}_c)$ versus $H_b(\boldsymbol{r}_c) - V_b(\boldsymbol{r}_c)/2$ for (a) HEE'H (**6-1** ($C_{2:np}$-type)), (b) **6-1**$^-$ ($C_{2:np}$-type), (c) **6-1**$^+$ (*cis*-type), (d) **6-1**$^+$ (*trans*-type), (e) **6-1**$^{2+}$ (*cis*-type), and (f) **6-1**$^{2+}$ (*trans*-type).

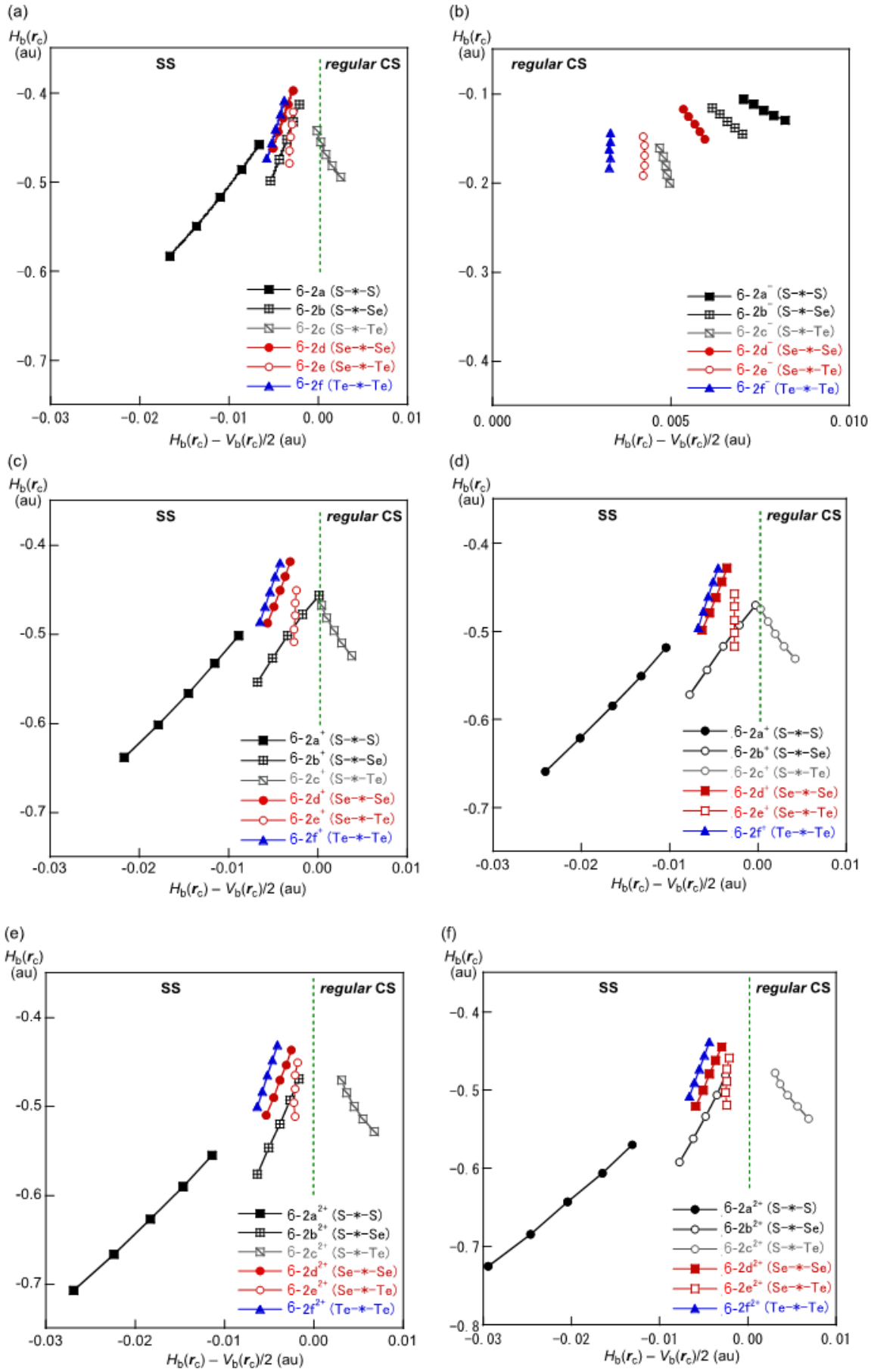

Figure 6-9. Plots of $H_b(\boldsymbol{r}_c)$ versus $H_b(\boldsymbol{r}_c) - V_b(\boldsymbol{r}_c)/2$ for (a) MeEE'Me (**6-2** ($C_{2:np}$-type)), (b) **6-2**$^-$ ($C_{2:np}$-type), (c) **6-2**$^+$ (*cis*-type), (d) **6-2**$^+$ (*trans*-type), (e) **6-2**$^{2+}$ (*cis*-type), and (f) **6-2**$^{2+}$ (*trans*-type).

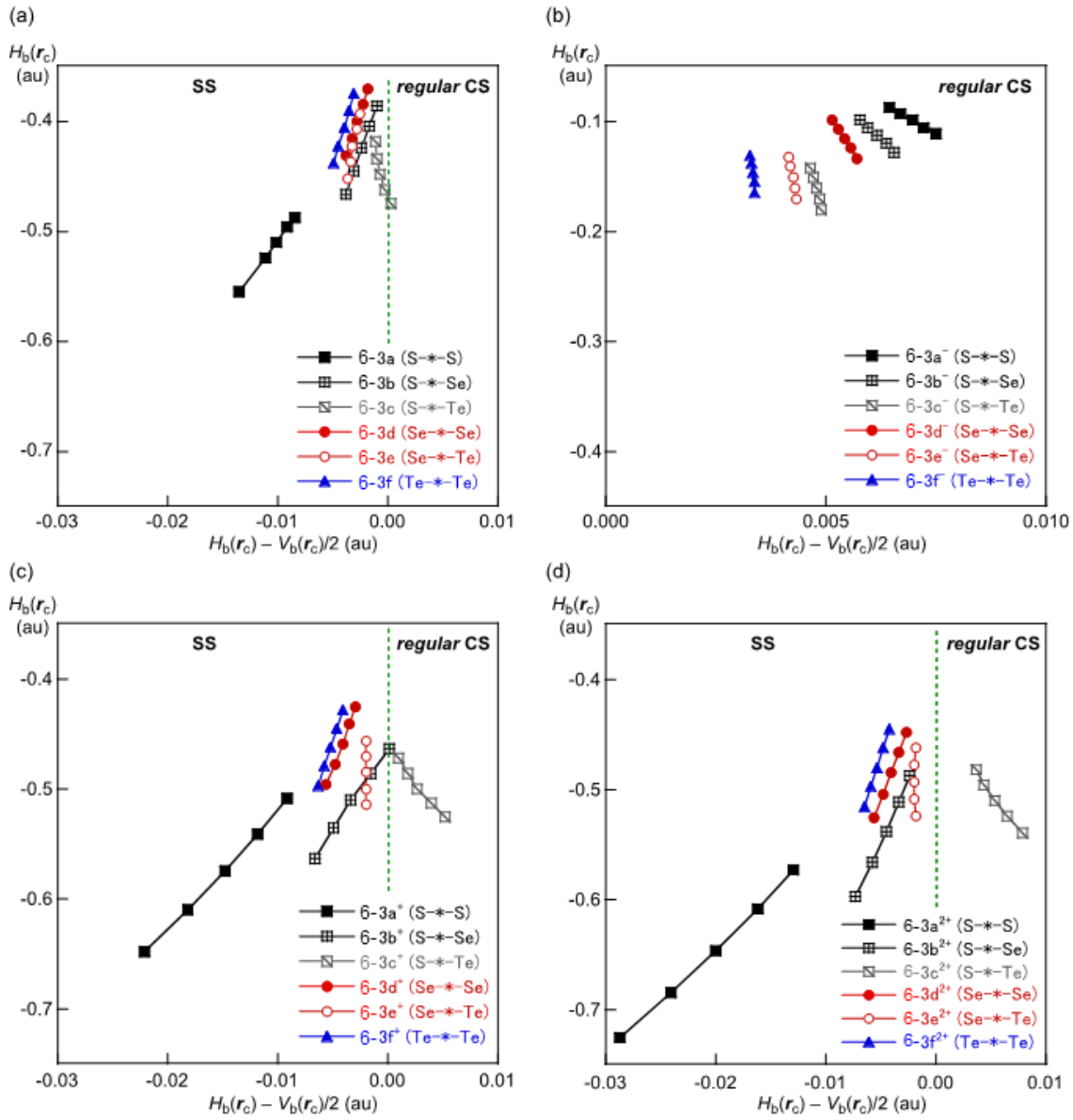

Figure 6-10. Plots of $H_b(\boldsymbol{r}_c)$ versus $H_b(\boldsymbol{r}_c) - V_b(\boldsymbol{r}_c)/2$ for (a) *cyclo*-1,2-EE'$(CH_2)_3$ (**6-3** (*cis*-type)), (b) **6-3**$^-$ (*cis*-type), (c) **6-3**$^+$ (*cis*-type), and (d) **6-3**$^{2+}$ (*cis*-type).

Table 6-5. QTAIM functions and parameters evaluated for the neutral, cationic and anionic forms in HEE'H (**6-1**) calculated with NIV at the MP2 level[a]

Interaction (E-∗-E')	$\rho_b(\boldsymbol{r}_c)$ (au)	$c\nabla^2\rho_b(\boldsymbol{r}_c)^b$ (au)	$H_b(\boldsymbol{r}_c)$ (au)	$k_b(\boldsymbol{r}_c)^c$	R (au)	θ (º)	ν_n $(n)^d$ (cm^{-1})	$k_f{}^d$ (unit[e])	$\theta_{p:NIV}$ (º)	$\kappa_{p:NIV}$ (au^{-1})
Neutral: $C_{2:np}$-type										
S-∗-S/**6-1a**	0.1329	–0.0095	–0.0651	–2.412	0.0658	188.3	508.3 (2)	4.049	197.4	1.0
S-∗-Se/**6-1b**	0.1103	–0.0037	–0.0484	–2.179	0.0486	184.3	411.1 (2)	2.457	189.5	0.5
S-∗-Te/**6-1c**	0.0950	–0.0001	–0.0433	–2.004	0.0433	180.1	374.3 (2)	2.492	171.1	17.0
Se-∗-Se/**6-1d**	0.0970	–0.0043	–0.0405	–2.274	0.0407	186.1	297.3 (1)	3.763	190.2	0.6
Se-∗-Te/**6-1e**	0.0861	–0.0033	–0.0375	–2.214	0.0376	185.0	258.4 (1)	3.232	183.8	14.2
Te-∗-Te/**6-1f**	0.0777	–0.0045	–0.0332	–2.373	0.0335	187.7	213.7 (1)	3.257	190.9	1.6
Mono-anionic: $C_{2:np}$-type										
S-∗-S/**6-1a**$^-$	0.0373	0.0072	–0.0039	–1.216	0.0082	118.2	217.6 (2)	0.067	145.0	46.5
S-∗-Se/**6-1b**$^-$	0.0358	0.0063	–0.0041	–1.248	0.0075	123.4	177.6 (1)	0.484	155.6	61.1
S-∗-Te/**6-1c**$^-$	0.0365	0.0049	–0.0055	–1.360	0.0073	138.4	166.0 (1)	0.432	170.6	50.6
Se-∗-Se/**6-1d**$^-$	0.0335	0.0054	–0.0038	–1.262	0.0066	125.4	130.6 (1)	0.693	163.2	63.8
Se-∗-Te/**6-1e**$^-$	0.0341	0.0043	–0.0048	–1.356	0.0065	137.9	118.1 (1)	0.560	172.7	55.8
Te-∗-Te/**6-1f**$^-$	0.0301	0.0035	–0.0041	–1.370	0.0053	139.6	100.6 (1)	0.507	173.7	79.3
Mono-cationic: *cis*-type										
S-∗-S/**6-1a**$^+$	0.1507	–0.0149	–0.0846	–2.544	0.0859	189.0	566.8 (2)	5.784	198.4	0.6
S-∗-Se/**6-1b**$^+$	0.1258	–0.0048	–0.0637	–2.177	0.0639	184.3	528.7 (2)	2.995	194.2	0.4
S-∗-Te/**6-1c**$^+$	0.1064	0.0004	–0.0526	–1.986	0.0526	179.6	438.9 (2)	2.738	168.3	10.3
Se-∗-Se/**6-1d**$^+$	0.1062	–0.0053	–0.0478	–2.288	0.0481	186.4	321.0 (1)	4.552	190.7	0.3
Se-∗-Te/**6-1e**$^+$	0.0959	–0.0034	–0.0457	–2.176	0.0458	184.3	316.0 (1)	4.639	181.7	8.2
Te-∗-Te/**6-1f**$^+$	0.0821	–0.0053	–0.0366	–2.405	0.0370	188.2	226.8 (1)	3.742	191.8	1.5
Mono-cationic: *trans*-type										
S-∗-S/**6-1a**$^+$	0.1529	–0.0158	–0.0876	–2.561	0.0891	190.2	577.7 (2)	4.668	198.4	0.5
S-∗-Se/**6-1b**$^+$	0.1271	–0.0050	–0.0652	–2.180	0.0654	184.4	531.3 (2)	2.403	194.0	0.4
S-∗-Te/**6-1c**$^+$	0.1073	0.0009	–0.0534	–1.969	0.0534	179.1	444.0 (2)	2.273	167.7	9.3
Se-∗-Se/**6-1d**$^+$	0.1075	–0.0054	–0.0491	–2.285	0.0494	186.7	326.5 (1)	3.685	190.6	0.3
Se-∗-Te/**6-1e**$^+$	0.0966	–0.0053	–0.0464	–2.160	0.0465	183.9	319.4 (1)	3.693	181.3	3.1
Te-∗-Te/**6-1f**$^+$	0.0830	–0.0054	–0.0376	–2.400	0.0380	188.1	230.6 (1)	2.875	191.6	1.6
Di-cationic: *cis*-type										
S-∗-S/**6-1a**$^{2+}$	0.1646	–0.0181	–0.1009	–2.559	0.1025	190.2	542.0 (1)	5.297	198.4	0.4
S-∗-Se/**6-1b**$^{2+}$	0.1304	–0.0049	–0.0671	–2.172	0.0673	184.2	419.1 (1)	2.863	190.9	0.1
S-∗-Te/**6-1c**$^{2+}$	0.1098	0.0034	–0.0550	–1.890	0.0551	176.5	407.9 (1)	1.949	159.8	8.9
Se-∗-Se/**6-1d**$^{2+}$	0.1104	–0.0049	–0.0510	–2.236	0.0513	185.5	289.8 (1)	3.651	190.4	0.2
Se-∗-Te/**6-1e**$^{2+}$	0.0964	–0.0028	–0.0459	–2.140	0.0460	183.5	265.7 (1)	2.993	183.4	8.2
Te-∗-Te/**6-1f**$^{2+}$	0.0840	–0.0051	–0.0378	–2.366	0.0382	187.6	208.9 (1)	3.213	191.5	1.5
Di-cationic: *trans*-type										
S-∗-S/**6-1a**$^{2+}$	0.1674	–0.0193	–0.1050	–2.581	0.1068	190.4	558.1 (1)	4.552	198.4	0.4
S-∗-Se/**6-1b**$^{2+}$	0.1324	–0.0053	–0.0696	–2.178	0.0698	184.3	430.6 (1)	2.546	190.9	0.2
S-∗-Te/**6-1c**$^{2+}$	0.1109	0.0039	–0.0560	–1.877	0.0561	176.0	416.2 (1)	1.766	159.1	4.0
Se-∗-Se/**6-1d**$^{2+}$	0.1121	–0.0051	–0.0528	–2.237	0.0530	185.5	298.2 (1)	3.145	190.2	0.1
Se-∗-Te/**6-1e**$^{2+}$	0.0975	–0.0026	–0.0469	–2.126	0.0470	183.2	271.7 (1)	2.712	182.8	8.2
Te-∗-Te/**6-1f**$^{2+}$	0.0851	–0.0052	–0.0390	–2.361	0.0394	187.6	214.8 (1)	2.602	191.3	1.5

[a] The 6-311+G(3d,p) basis set for H, S, and Se and that of the (7433111/743111/7411/2 + 1s1p1d1f) type for Te. [b] $c = \hbar^2/8m$. [c] $k = V_b(\boldsymbol{r}_c)/G_b(\boldsymbol{r}_c)$. [d] Corresponding to the E–E' bond in question. [e] mdyn $Å^{-1}$.

Table 6-6. QTAIM functions and parameters for the neutral, cationic and anionic forms of MeEE'Me (**6-2**) calculated with NIV method at the MP2 level[a]

Interaction (E-∗-E')	$\rho_b(\boldsymbol{r}_c)$ (au)	$c\nabla^2\rho_b(\boldsymbol{r}_c)$[b] (au)	$H_b(\boldsymbol{r}_c)$ (au)	k[c]	R (au)	θ (º)	$\nu_n\,(n)$[d] (cm^{-1})	k_f[d] (unit[e])	$\theta_{p:NIV}$ (º)	$\kappa_{p:NIV}$ (au^{-1})
Neutral: $C_{2:np}$-type										
S-∗-S/**6-2a**	0.1400	–0.0110	–0.0724	–2.435	0.0732	188.6	505.6 (6)	2.596	197.6	0.7
S-∗-Se/**6-2b**	0.1159	–0.0036	–0.0526	–2.157	0.0527	183.9	412.5 (6)	2.002	189.2	0.5
S-∗-Te/**6-2c**	0.0988	0.0008	–0.0464	–1.966	0.0464	179.0	377.4 (6)	1.558	167.9	16.5
Se-∗-Se/**6-2d**	0.1018	–0.0039	–0.0436	–2.217	0.0438	185.1	302.4 (6)	2.732	189.1	0.6
Se-∗-Te/**6-2e**	0.0894	–0.0031	–0.0403	–2.185	0.0404	184.5	261.9 (6)	2.178	181.9	9.3
Te-∗-Te/**6-2f**	0.0805	–0.0047	–0.0355	–2.363	0.0358	187.6	217.4 (6)	2.358	190.4	1.8
Mono-anionic: $C_{2:np}$-type										
S-∗-S/**6-2a**$^-$	0.0405	0.0076	–0.0047	–1.240	0.0090	122.2	221.3 (6)	0.491	146.1	49.9
S-∗-Se/**6-2b**$^-$	0.0389	0.0066	–0.0051	–1.279	0.0083	127.8	186.6 (6)	0.279	156.9	50.3
S-∗-Te/**6-2c**$^-$	0.0410	0.0048	–0.0074	–1.432	0.0088	146.7	174.8 (6)	0.184	174.6	36.3
Se-∗-Se/**6-2d**$^-$	0.0367	0.0057	–0.0049	–1.302	0.0075	130.9	136.6 (6)	0.199	163.6	46.9
Se-∗-Te/**6-2e**$^-$	0.0380	0.0043	–0.0064	–1.431	0.0077	146.6	108.4 (4)	0.031	180.2	30.5
Te-∗-Te/**6-2f**$^-$	0.0353	0.0033	–0.0058	–1.467	0.0066	150.3	97.5 (4)	0.042	182.0	76.9
Mono-anionic: *trans*-type										
S-∗-S/**6-2a**$^-$	0.0415	0.0076	–0.0050	–1.249	0.0091	123.5	247.0 (6)	0.283	148.1	51.1
S-∗-Se/**6-2b**$^-$	0.0401	0.0064	–0.0055	–1.300	0.0085	130.6	210.5 (6)	0.180	160.1	40.0
S-∗-Te/**6-2c**$^-$	0.0429	0.0045	–0.0083	–1.478	0.0094	151.4	206.7 (6)	0.141	176.5	23.4
Se-∗-Se/**6-2d**$^-$	0.0378	0.0055	–0.0054	–1.330	0.0077	134.5	119.0 (5)	0.077	171.3	47.0
Se-∗-Te/**6-2e**$^-$	0.0399	0.0039	–0.0073	–1.484	0.0083	151.9	113.0 (5)	0.090	181.6	25.0
Te-∗-Te/**6-2f**$^-$	0.0377	0.0029	–0.0068	–1.538	0.0074	156.8	98.6 (3)	0.123	184.3	14.9
Mono-cationic: *cis*-type										
S-∗-S/**6-2a**$^+$	0.1524	–0.0145	–0.0864	–2.504	0.0876	189.5	536.4 (6)	2.344	198.4	0.6
S-∗-Se/**6-2b**$^+$	0.1268	–0.0034	–0.0636	–2.121	0.0637	183.1	495.5 (6)	1.587	195.1	5.3
S-∗-Te/**6-2c**$^+$	0.1077	0.0018	–0.0534	–1.937	0.0535	178.1	438.5 (6)	1.944	167.0	7.8
Se-∗-Se/**6-2d**$^+$	0.1086	–0.0043	–0.0491	–2.210	0.0493	185.0	317.1 (6)	2.676	189.6	0.3
Se-∗-Te/**6-2e**$^+$	0.0969	–0.0026	–0.0465	–2.126	0.0466	183.2	317.0 (6)	2.799	181.7	2.3
Te-∗-Te/**6-2f**$^+$	0.0835	–0.0053	–0.0378	–2.388	0.0382	188.0	225.3 (6)	2.387	191.3	1.7
Mono-cationic: *trans*-type										
S-∗-S/**6-2a**$^+$	0.1567	–0.0165	–0.0917	–2.560	0.0932	190.2	571.1 (6)	2.183	198.6	0.5
S-∗-Se/**6-2b**$^+$	0.1303	–0.0040	–0.0675	–2.135	0.0676	183.4	533.6 (6)	1.786	195.7	4.3
S-∗-Te/**6-2c**$^+$	0.1097	0.0020	–0.0552	–1.934	0.0553	178.0	453.8 (6)	1.916	165.6	7.0
Se-∗-Se/**6-2d**$^+$	0.1109	–0.0048	–0.0513	–2.231	0.0515	185.4	333.8 (6)	1.961	189.8	0.3
Se-∗-Te/**6-2e**$^+$	0.0988	–0.0027	–0.0482	–2.126	0.0482	183.2	329.2 (6)	2.196	180.6	1.6
Te-∗-Te/**6-2f**$^+$	0.0849	–0.0056	–0.0392	–2.398	0.0396	188.1	235.3 (6)	1.281	191.3	1.9
Di-cationic: *cis*-type										
S-∗-S/**6-2a**$^{2+}$	0.1675	–0.0182	–0.1051	–2.531	0.1067	189.8	521.2 (6)	2.033	198.4	0.4
S-∗-Se/**6-2b**$^{2+}$	0.1331	–0.0038	–0.0692	–2.122	0.0693	183.1	409.9 (6)	1.481	189.9	0.3
S-∗-Te/**6-2c**$^{2+}$	0.1103	0.0045	–0.0551	–1.859	0.0554	175.3	391.3 (6)	1.361	166.9	14.5
Se-∗-Se/**6-2d**$^{2+}$	0.1146	–0.0038	–0.0541	–2.163	0.0542	184.0	296.5 (6)	2.269	189.1	0.2
Se-∗-Te/**6-2e**$^{2+}$	0.0982	–0.0022	–0.0472	–2.101	0.0473	182.6	262.9 (6)	1.747	181.1	8.9
Te-∗-Te/**6-2f**$^{2+}$	0.0869	–0.0052	–0.0405	–2.346	0.0408	187.3	213.8 (6)	2.206	190.7	1.9
Di-cationic: *trans*-type										
S-∗-S/**6-2a**$^{2+}$	0.1713	–0.0204	–0.1103	–2.585	0.1122	190.5	558.5 (6)	1.739	198.6	0.3
S-∗-Se/**6-2b**$^{2+}$	0.1363	–0.0048	–0.0727	–2.152	0.0729	183.8	438.6 (6)	1.548	190.3	0.3
S-∗-Te/**6-2c**$^{2+}$	0.1122	0.0046	–0.0569	–1.862	0.0571	175.4	411.3 (6)	1.488	166.8	13.6
Se-∗-Se/**6-2d**$^{2+}$	0.1168	–0.0043	–0.0561	–2.182	0.0563	184.4	316.7 (6)	1.466	189.3	0.2
Se-∗-Te/**6-2e**$^{2+}$	0.1000	–0.0025	–0.0489	–2.111	0.0490	182.9	278.2 (6)	1.356	181.0	8.9
Te-∗-Te/**6-2f**$^{2+}$	0.0882	–0.0055	–0.0418	–2.355	0.0421	187.5	226.2 (6)	0.959	190.7	2.0

[a] The 6-311+G(3d,p) basis set for H, C, S, and Se and that of the (7433111/743111/7411/2 + 1s1p1d1f) type for Te. [b] $c = \hbar^2/8m$. [c] $k = V_b(\boldsymbol{r}_c)/G_b(\boldsymbol{r}_c)$. [d] Corresponding to the E–E' bond in question. [e] mdyn Å^{-1}.

Table 6-7. QTAIM functions and parameters evaluated for the neutral, cationic and anionic forms in *Cyclo*-1,2-EE'$(CH_2)_3$ (**6-3**) calculated with NIV method at the MP2 level[a]

Interaction (E-∗-E')	$\rho_b(\boldsymbol{r}_c)$ (au)	$c\nabla^2\rho_b(\boldsymbol{r}_c)^b$ (au)	$H_b(\boldsymbol{r}_c)$ (au)	$k_b(\boldsymbol{r}_c)^c$	R (au)	θ (°)	$\nu_n\,(n)^d$ (cm^{-1})	$k_f{}^d$ (unit[e])	$\theta_{p:NIV}$ (°)	$\kappa_{p:NIV}$ (au^{-1})
Neutral: *cis*-type										
S-∗-S/**6-3a**	0.1348	–0.0091	–0.0669	–2.375	0.0675	187.8	501.1 (4)	2.175	197.1	9.7
S-∗-Se/**6-3b**	0.1093	–0.0024	–0.0464	–2.114	0.0465	182.9	403.4 (4)	1.859	189.3	1.4
S-∗-Te/**6-3c**	0.0930	–0.0008	–0.0417	–2.038	0.0417	181.0	369.3 (4)	1.257	174.3	23.2
Se-∗-Se/**6-3d**	0.0946	–0.0028	–0.0378	–2.170	0.0379	184.2	299.0 (4)	0.467	189.5	0.5
Se-∗-Te/**6-3e**	0.0835	–0.0032	–0.0353	–2.218	0.0355	185.1	253.1 (3)	0.592	185.9	12.6
Te-∗-Te/**6-3f**	0.0738	–0.0039	–0.0300	–2.356	0.0303	187.5	207.2 (3)	1.208	191.9	0.9
Mono-anionic: *cis*-type										
S-∗-S/**6-3a**$^-$	0.0356	0.0070	–0.0036	–1.203	0.0078	117.1	210.5 (2)	0.387	143.5	51.6
S-∗-Se/**6-3b**$^-$	0.0349	0.0062	–0.0040	–1.243	0.0073	122.7	173.8 (2)	0.355	155.3	57.0
S-∗-Te/**6-3c**$^-$	0.0377	0.0048	–0.0061	–1.388	0.0077	141.8	167.1 (2)	0.350	173.9	43.5
Se-∗-Se/**6-3d**$^-$	0.0333	0.0054	–0.0039	–1.262	0.0067	125.4	135.2 (2)	0.481	162.8	61.1
Se-∗-Te/**6-3e**$^-$	0.0351	0.0042	–0.0053	–1.384	0.0068	141.3	123.4 (2)	0.391	175.4	55.1
Te-∗-Te/**6-3f**$^-$	0.0327	0.0034	–0.0048	–1.418	0.0059	145.2	108.6 (2)	0.360	177.0	82.2
Mono-cationic: *cis*-type										
S-∗-S/**6-3a**$^+$	0.1540	–0.0148	–0.0886	–2.501	0.0898	189.5	564.9 (5)	2.463	198.3	0.5
S-∗-Se/**6-3b**$^+$	0.1285	–0.0033	–0.0655	–2.113	0.0066	182.9	534.1 (5)	1.209	194.7	4.2
S-∗-Te/**6-3c**$^+$	0.1089	0.0027	–0.0545	–1.909	0.0545	177.1	432.0 (4)	0.526	163.6	13.4
Se-∗-Se/**6-3d**$^+$	0.1102	–0.0042	–0.0506	–2.197	0.0508	184.7	330.1 (4)	1.057	189.4	0.3
Se-∗-Te/**6-3e**$^+$	0.0982	–0.0020	–0.0477	–2.093	0.0477	182.4	328.3 (4)	1.566	180.3	4.5
Te-∗-Te/**6-3f**$^+$	0.0849	–0.0052	–0.0393	–2.361	0.0396	187.6	230.4 (3)	0.696	190.9	1.9
Di-cationic: *cis*-type										
S-∗-S/**6-3a**$^{2+}$	0.1718	–0.0200	–0.1111	–2.561	0.1129	190.2	549.1 (5)	0.862	198.1	0.3
S-∗-Se/**6-3b**$^{2+}$	0.1373	–0.0045	–0.0740	–2.140	0.0741	183.5	414.0 (4)	0.892	189.8	0.2
S-∗-Te/**6-3c**$^{2+}$	0.1134	0.0053	–0.0580	–1.845	0.0582	174.8	402.0 (4)	0.679	165.5	12.2
Se-∗-Se/**6-3d**$^{2+}$	0.1180	–0.0041	–0.0573	–2.165	0.0575	184.1	314.0 (4)	0.928	188.9	0.1
Se-∗-Te/**6-3e**$^{2+}$	0.1011	–0.0020	–0.0499	–2.087	0.0499	182.3	286.9 (4)	0.296	180.3	8.8
Te-∗-Te/**6-3f**$^{2+}$	0.0893	–0.0053	–0.0429	–2.332	0.0432	187.1	221.9 (3)	0.548	190.2	2.1

[a] The 6-311+G(3d) basis set for S and Se and that of the (7433111/743111/7411/2 + 1s1p1d1f) type for Te with the 6-311+G(d) basis set for C and H. [b] $c = \hbar^2/8m$. [c] $k = V_b(\boldsymbol{r}_c)/G_b(\boldsymbol{r}_c)$. [d] Corresponding to the E–E' bond in question. [e] mdyn $Å^{-1}$.

The plots are analyzed according to eqs (2-8)–(2-12) of Chapter 2, which give QTAIM parameters of (R, θ) and (θ_p, κ_p). The (R, θ) values correspond to the static nature of interactions, whereas (θ_p, κ_p) represent the dynamic nature of the interactions. Tables 6-5–6-7 also collect the (R, θ) and (θ_p, κ_p) values for **6-1**–**6-3**, respectively, separated by the neutral, anionic, mono-cationic, and di-cationic forms, together with the types. The frequencies (ν) and force constants (k_f) corresponding to the E-∗-E' interactions in question are also given in the Tables.

Behaviors of E-∗-E' Elucidated by (R, θ) and (θ_p, κ_p)

The θ_p values in Tables 6-5–6-7 are plotted versus θ, which is shown in Figure 6-11. Figure 6-11a shows the plots for all forms of **6-1**–**6-3**. Figures 6-11b–6-11d depict those for neutral, mono-anionic, mono-cationic, and di-cationic forms, respectively. Some of the interactions are on the border area, therefore, the classification would be tentative. Nevertheless, the classification supplies useful insights into the nature of the chalcogen-chalcogen interactions. Table 6-8 collects the classified results.

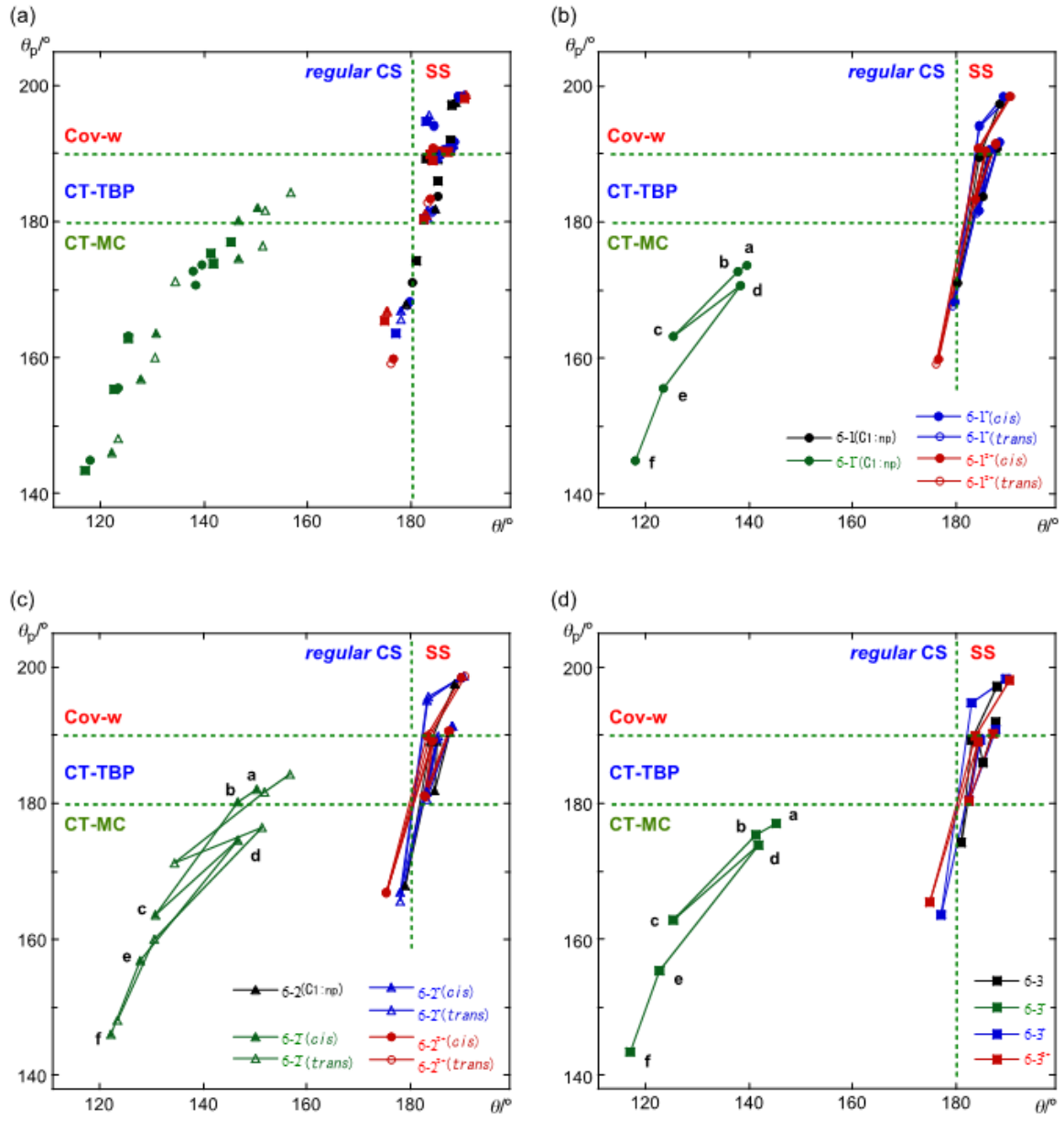

Figure 6-11. Plots of θ_p versus θ: (a) for all species shown in Tables 6-5–6-7, (b) for the neutral and charged species of **6-1**, **6-1**$^{-}$, **6-1**$^{+}$, and **6-1**$^{2+}$, (c) for the neutral and charged species of **6-2**, **6-2**$^{-}$, **6-2**$^{+}$, and **6-2**$^{2+}$, and (d) for the neutral and charged species of **6-3**, **6-3**$^{-}$, **6-3**$^{+}$, and **6-3**$^{2+}$.

Table 6-8. Classification of the E–E' bonds in neutral and charged species of **6-1**–**6-3**

Compd	HEE'H (**6-1**)			MeEE'Me (**6-2**)			*Cyclo*-1,2-EE'$(CH_2)_3$ (**6-3**)		
E-∗-E'	θ/º	θ_p/º	Character	θ/º	θ_p/º	Character	θ/º	θ_p/º	Character
Neutral									
S-∗-S	188.3	197.4	SS/Cov-w	188.6	197.6	SS/Cov-w	187.8	197.1	SS/Cov-w
S-∗-Se	184.3	189.5	SS/CT-TBP	183.9	189.2	SS/CT-TBP	182.9	189.3	SS/CT-TBP
S-∗-Te	180.1	171.1	SS/CT-MC	179.0	167.9	*r*-CS/CT-MC	181.0	174.3	SS/CT-MC
Se-∗-Se	186.1	190.2	SS/Cov-w	185.1	189.1	SS/CT-TBP	184.2	189.5	SS/CT-TBP
Se-∗-Te	185.0	183.8	SS/CT-TBP	184.5	181.9	SS/CT-TBP	185.1	185.9	SS/CT-TBP
Te-∗-Te	187.7	190.9	SS/Cov-w	187.6	190.4	SS/Cov-w	187.5	191.9	SS/Cov-w
Mono-anionic									
S-∗-S	118.2	145.0	*r*-CS/CT-MC	122.2	146.1	*r*-CS/CT-MC	117.1	143.5	*r*-CS/CT-MC
S-∗-Se	123.4	155.6	*r*-CS/CT-MC	127.8	156.9	*r*-CS/CT-MC	122.7	155.3	*r*-CS/CT-MC
S-∗-Te	138.4	170.6	*r*-CS/CT-MC	146.7	174.6	*r*-CS/CT-MC	141.8	173.9	*r*-CS/CT-MC
Se-∗-Se	125.4	163.2	*r*-CS/CT-MC	130.9	163.6	*r*-CS/CT-MC	125.4	162.8	*r*-CS/CT-MC
Se-∗-Te	137.9	172.7	*r*-CS/CT-MC	146.6	180.2	*r*-CS/CT-TBP	141.3	175.4	*r*-CS/CT-MC
Te-∗-Te	139.6	173.7	*r*-CS/CT-MC	150.3	182.0	*r*-CS/CT-TBP	145.2	177.0	*r*-CS/CT-MC
Mono-anionic: *trans*-type									
S-∗-S				123.5	148.1	*r*-CS/CT-MC			
S-∗-Se				130.6	160.1	*r*-CS/CT-MC			
S-∗-Te				151.4	176.5	*r*-CS/CT-MC			
Se-∗-Se				134.5	171.3	*r*-CS/CT-MC			
Se-∗-Te				151.9	181.6	*r*-CS/CT-TBP			
Te-∗-Te				156.8	184.3	*r*-CS/CT-TBP			
Mono-cationic: *cis*-type									
S-∗-S	189.0	198.4	SS/Cov-w	189.5	198.4	SS/Cov-w	189.5	198.3	SS/Cov-w
S-∗-Se	184.3	194.2	SS/Cov-w	183.1	195.1	SS/Cov-w	182.9	194.7	SS/Cov-w
S-∗-Te	179.6	168.3	*r*-CS/CT-MC	178.1	167.0	*r*-CS/CT-MC	177.1	163.6	*r*-CS/CT-MC
Se-∗-Se	186.4	190.7	SS/Cov-w	185.0	189.6	SS/CT-TBP	184.7	189.4	SS/CT-TBP
Se-∗-Te	184.3	181.7	SS/CT-TBP	183.2	181.7	SS/CT-TBP	182.4	180.3	SS/CT-TBP
Te-∗-Te	188.2	191.8	SS/Cov-w	188.0	191.3	SS/Cov-w	187.6	190.9	SS/Cov
Mono-cationic: *trans*-type									
S-∗-S	190.2	198.4	SS/Cov-w	190.2	198.6	SS/Cov-w			
S-∗-Se	184.4	194.0	SS/Cov-w	183.4	195.7	SS/Cov-w			
S-∗-Te	179.1	167.7	*r*-CS/CT-MC	178.0	165.6	*r*-CS/CT-MC			
Se-∗-Se	186.7	190.6	SS/Cov-w	185.4	189.8	SS/CT-TBP			
Se-∗-Te	183.9	181.3	SS/CT-TBP	183.2	180.6	SS/CT-TBP			
Te-∗-Te	188.1	191.6	SS/Cov-w	188.1	191.3	SS/Cov-w			

(continues)

Compd	HEE'H (**6-1**)			MeEE'Me (**6-2**)			*Cyclo*-1,2-EE'$(CH_2)_3$ (**6-3**)		
E-∗-E'	θ/º	θ_p/º	Character	θ/º	θ_p/º	Character	θ/º	θ_p/º	Character
Di-cationic: *cis*-type									
S-∗-S	190.2	198.4	SS/Cov-w	189.8	198.4	SS/Cov-w	190.2	198.1	SS/Cov-w
S-∗-Se	184.2	190.9	SS/Cov-w	183.1	189.9	SS/CT-TBP	183.5	189.8	SS/CT-TBP
S-∗-Te	176.5	159.8	*r*-CS/CT-MC	175.3	166.9	*r*-CS/CT-MC	174.8	165.5	*r*-CS/CT-MC
Se-∗-Se	185.5	190.4	SS/Cov-w	184.0	189.1	SS/CT-TBP	184.1	188.9	SS/CT-TBP
Se-∗-Te	183.5	183.4	SS/CT-TBP	182.6	181.1	SS/CT-TBP	182.3	180.3	SS/CT-TBP
Te-∗-Te	187.6	191.5	SS/Cov-w	187.3	190.7	SS/Cov-w	187.1	190.2	SS/Cov-w
Di-cationic: *trans*-type									
S-∗-S	190.4	198.4	SS/Cov-w	190.5	198.6	SS/Cov-w			
S-∗-Se	184.3	190.9	SS/Cov-w	183.8	190.3	SS/Cov-w			
S-∗-Te	176.0	159.1	*r*-CS/CT-MC	175.4	166.8	*r*-CS/CT-MC			
Se-∗-Se	185.5	190.2	SS/Cov-w	184.4	189.3	SS/CT-TBP			
Se-∗-Te	183.2	182.8	SS/CT-TBP	182.9	181.0	SS/CT-TBP			
Te-∗-Te	187.6	191.3	SS/Cov-w	187.5	190.7	SS/Cov-w			

The behaviors of E-∗-E' in the neutral and charged forms of **6-1**–**6-3** are discussed on the basis of the θ and θ_p values, using those in Scheme 2-3 of Chapter 2 as a reference. Data for E-∗-E' in the neutral forms of **6-1**–**6-3** appear in the SS region ($180^o < \theta$), except for MeS-∗-TeMe (**6-2c**), which does in the *regular* CS region ($\theta < 180^o$), showing the CT-MC character ($125^o < \theta_p < 180^o$). Data for S-∗-Te in **6-1** and **6-3** also show the CT-MC character, although they appear in the SS region. The SS/CT-MC character is not observed in the typical interactions shown in Figure 2-3 of Chapter 2 (see also Table 2-2 of Chapter 2). As confirmed in Figures 6-8–6-10, the direction of the plots for **6-1c**, **6-2c**, and **6-3c** seems very different from others in the neutral forms. On the other hand, data of all E-∗-E' in the monoanionic forms of **6-1**–**6-3** appear in the *regular* CS region. The bonds become weaker in the formation of the monoanionic forms of **6-1**–**6-3** by the QTAIM-DFA, which must be the reflection of largely elongated E–E' bonds by the addition of an electron for each. The directions of the plots seem to change gradually from S-∗-S to Te-∗-Te in the mono-anionic forms for **6-1**–**6-3**. As a result, the trend observed for S-∗-Te in the neutral forms seems to disappear in the mono-anionic forms in **6-1**–**6-3**.

The E–E' bonds become shorter in the formation of mono-cationic forms by 0.025–0.070 Å for **6-1**$^+$, 0.015–0.051 Å for **6-2**$^+$, and 0.087–0.109 Å for **6-3**$^+$, relative to those of the corresponding

neutral forms, if *cis*-forms are compared. The distances shorten further in the formation of di-cationic forms from the corresponding mono-cationic forms by 0.006–0.040 Å for **6-1**$^{2+}$, 0.004–0.047 Å for **6-2**$^{2+}$, and 0.010–0.053 Å for **6-3**$^{2+}$ in the *cis*-forms. The plots of $H_b(\boldsymbol{r}_c)$ versus $H_b(\boldsymbol{r}_c) - V_b(\boldsymbol{r}_c)/2$ for the mono-cationic forms seem to move stronger area, relative to the case of neutral case. The results can be understood by the image of the shorter E–E' bond lengths of the mono-cationic forms relative to the case of the neutral forms. While the larger magnitudes correspond to the S–S bonds, smaller ones to Se–Te. The plots for the di-cationic forms clarify an interesting feature of the bonds. Data for S–S move substantially to stronger area in the plot and those for S–Se, Se–Se, Te–Te do slightly. However, data for S–Te shift to weaker direction and those for Se–Te remain almost the same position in the plot, irrespective of the shortened bond distances. The results may suggest that factors, other than the E–E' distances, operate to control the strength of the bonds, if the strengths are evaluated with the QTAIM dual functional analysis. The factors apparently operate in S–Te and Se–Te and they must also do in other bonds. The numbers of electrons are decreased in the di-cations, relative to the case of the mono-cationic forms, which could be a candidate for the factor, although they are not clear now.

Summary

The behavior of E-∗-E' in neutral, mono-anionic, mono-cationic, and di-cationic forms of HEE'H (**6-1**), MeEE'Me (**6-1**), and *cyclo*-1,2-EE'$(CH_2)_3$ (**6-3**) (E, E' = O, S, Se, Te) are investigated by applying QTAIM dual functional analysis. The optimized structures of mono-anionic forms are similar to those of corresponding neutral species in **6-1**, which are called $C_{2:np}$–type, although the E–E' distances of the former are much longer than those of the latter. The *trans*-forms are optimized, in addition to the $C_{2:np}$–type in the mono-anionic forms of **6-2**. Both *cis*- and *trans*-forms are optimized for mono-cationic and di-cationic forms of **6-1** and **6-2**. Only *cis*-forms correspond to **6-3**, as expected. While the mono-anionic forms are characterized as EE' σ(2c–3e), where two are in σ with one in σ*, the mono- and di-cationic forms are as EE' π(2c–3e) and π(2c–2e), respectively. The structures are

well explained by the characters.

$H_b(\boldsymbol{r}_c)$ are plotted versus $H_b(\boldsymbol{r}_c) - V_b(\boldsymbol{r}_c)/2$ for the data of E-∗-E' at BCPs of the fully-optimized structures and the perturbed structures around the fully-optimized ones for **6-1**–**6-3**. The perturbed structures are generated employing NIV (normal coordinates of internal vibrations). QTAIM parameters of (R, θ) and (θ_p, κ_p) are obtained by analyzing according to eqs (2-8)–(2-12) of Chapter 2. While (R, θ) correspond to the static nature, (θ_p, κ_p) represent the dynamic nature of interactions. The natures of E-∗-E' in the neutral and charged species of **6-1**–**6-3** are classified using θ and θ_p of the standard bonds/interactions as a reference. Some interactions are on the border area, therefore, the classification would be tentative. Data for E-∗-E' in the neutral forms of **6-1**–**6-3** appear in the SS region ($180^o < \theta$), except for MeS-∗-TeMe (**6-2c**), which does in the *regular* CS region ($\theta < 180^o$) with the CT-MC character ($125^o < \theta_p < 180^o$). The direction of the plots for **6-1c**, **6-2c**, and **6-3c** seems very different from those of as the standard bonds/interactions, as specified by θ_p. On the other hand, data of all E-∗-E' in the mono-anionic forms of **6-1**–**6-3** appear in the *regular* CS region, which must be the reflection of largely elongated E–E' bonds by the addition of an electron for each. The directions of the plots change gradually from S-∗-S to Te-∗-Te in the mono-anionic forms for **6-1**–**6-3**. Plots of $H_b(\boldsymbol{r}_c)$ versus $H_b(\boldsymbol{r}_c) - V_b(\boldsymbol{r}_c)/2$ for the mono-cationic forms move to stronger area, relative to the neutral case. The results can be understood by the image of the shorter E–E' bond lengths of the mono-cationic forms. The plots for the di-cationic forms clarify an interesting feature of the bonds. Data for S–S move substantially to stronger area in the plot and those for S–Se, Se–Se, Te–Te do slightly. However, data for S–Te shift to weaker direction and those for Se–Te remain almost the same position in the plot, irrespective of the shortened bond distances. The results may suggest that factors, other than the E–E' distances, operate to control the strength of the bonds. The factors apparently operate in S–Te and Se–Te bonds. Factors other than the bond lengths are suggested for the mechanism.

Appendix

Table 6-A1. Distances, angles, and torsional angles for neutral and charged forms of HEE'H (**6-1**), together with relative energies, optimized at the MP2 level[a]

Compd	r_o(E, E') (Å)	Δr_o(E, E') (Å)	ϕ(CEE'C) (º)	r_o(E, H) (Å)	∠E'EH (º)	r_o(E', H) (Å)	∠EE'H (º)	ΔE^b (eV)	Sym-metry
Neutral form: $C_{2:np}$-type									
6-1g	1.4551	0.0000	111.1	0.9688	99.8	0.9688	99.8	0.00	$C_{2:np}$
6-1h	1.6870	0.0000	92.0	0.9671	106.9	1.3385	97.9	0.00	$C_{1:np}$
6-1i	1.8285	0.0000	91.2	0.9677	106.1	1.4660	96.2	0.00	$C_{1:np}$
6-1j	1.9815	0.0000	89.9	0.9675	107.8	1.6634	95.3	0.00	$C_{2:np}$
Mono-anionic form: $C_{2:np}$-type									
6-1g$^-$	2.2338	0.7787	133.2	0.9689	64.3	0.9689	64.3	–0.52	$C_{2:np}$
6-1h$^-$	1.7144	0.0274	81.2	0.9907	106.7	1.3502	95.5	0.74	$C_{1:np}$
6-1i$^-$	2.2302	0.4017	96.1	0.9684	101.9	1.4572	84.6	–0.32	$C_{1:np}$
6-1j$^-$	2.2580	0.2765	100.3	0.9697	101.1	1.6642	82.6	–0.50	$C_{2:np}$
Mono-cationic: *cis*-type									
6-1g$^+$	1.3247	–0.1304	0.0	0.9966	110.0	0.9966	110.0	10.81	C_{2v}
6-1h$^+$	1.5749	–0.1121	0.0	0.9817	116.8	1.3523	101.4	9.30	C_s
6-1i$^+$	1.7281	–0.1004	0.0	0.9796	114.9	1.4784	99.2	9.03	C_s
6-1j$^+$	1.9021	–0.0794	0.0	0.9766	115.9	1.6701	97.9	8.55	C_{2v}
Mono-cationic: *trans*-type									
6-1g$^+$	1.3290	–0.1261	180.0	0.9974	103.0	0.9974	103.0	10.44	C_s
6-1h$^+$	1.5823	–0.1047	180.0	0.9841	111.9	1.3483	93.9	9.19	C_s
6-1i$^+$	1.7337	–0.0948	180.0	0.9815	111.4	1.4728	91.3	8.94	C_s
6-1j$^+$	1.9070	–0.0745	180.0	0.9775	113.6	1.6639	90.1	8.50	C_{2h}
Di-cationic: *cis*-type									
6-1g^{2+}	1.2770	–0.1781	0.0	1.0813	115.5	1.0813	115.5	32.11	C_{2v}
6-1h^{2+}	1.5120	–0.1750	0.0	1.0297	125.3	1.3936	102.7	27.41	C_s
6-1i^{2+}	1.6752	–0.1533	0.0	1.0189	122.7	1.5143	99.6	26.41	C_s
6-1j^{2+}	1.8473	–0.1342	0.0	1.0036	124.3	1.69599	98.2	24.92	C_{2v}
Di-cationic: *trans*-type									
6-1g^{2+}	1.2849	–0.1702	180.0	1.0844	107.1	1.0844	107.1	31.66	C_{2h}
6-1h^{2+}	1.5227	–0.1643	180.0	1.0319	118.5	1.3912	94.7	27.28	C_s
6-1i^{2+}	1.6826	–0.1459	180.0	1.0211	117.7	1.5100	91.3	26.29	C_s
6-1j^{2+}	1.8537	–0.278	180.0	1.0036	124.3	1.6960	98.2	24.92	C_{2h}

[a] The 6-311++G(3d,p) basis set for H, O, S, and Se and that of the (7433111/743111/7411/2 + 1s1p1d1f) type for Te. [b] E(**6-1g**) = –151.2850531 au, E(**6-1h**) = –473.9386825 au, E(**6-1i**) = –2476.1907191 au, and E(**6-1j**) = –6688.135598 au.

Table 6-A2. Distances, angles, and torsional angles for neutral and charged forms of MeEE'Me (**6-2**), together with relative energies, optimized at the MP2 level[a]

Compd	r_o(E, E') (Å)	Δr_o(E, E') (Å)	ϕ(CEE'C) (º)	r_o(E, C) (Å)	∠E'EC (º)	r_o(E', C) (Å)	∠EE'C (º)	ΔE (eV)	Sym-metry
Neutral forms: $C_{2:np}$-type									
6-2h	1.6755	0.0000	88.6	1.4374	113.7	1.7942	100.3	0.00	$C_{1:np}$
6-2i	1.8183	0.0000	87.4	1.4354	113.8	1.9354	97.4	0.00	$C_{1:np}$
6-2j	1.9745	0.0000	84.5	1.4366	116.1	2.1270	95.3	0.00	$C_{2:np}$
Mono-anionic forms: $C_{2:np}$-type									
6-2h$^-$	2.3166	0.6411	97.3	1.3735	107.0	1.8049	81.4	0.27	$C_{1:np}$
6-2i$^-$	2.3492	0.5309	96.4	1.3797	108.5	1.9481	79.6	–0.04	$C_{1:np}$
6-2j$^-$	2.2881	0.3136	95.8	1.3964	112.1	2.1567	77.9	–0.28	$C_{2:np}$
Mono-cationic forms: *cis*-type									
6-2h$^+$	1.5711	–0.1044	0.1	1.4814	125.5	1.7754	108.0	8.21	C_1
6-2i$^+$	1.7226	–0.0957	–0.9	1.4733	124.2	1.9198	104.7	8.13	C_1
6-2j$^+$	1.8977	–0.0768	0.0	1.4690	125.1	2.1038	101.2	7.84	C_2
Mono-cationic: *trans*-type									
6-2h$^+$	1.5767	–0.0988	180.0	1.4921	117.4	1.7695	99.4	8.04	C_1
6-2i$^+$	1.7268	–0.0915	180.0	1.4832	118.4	1.9124	95.3	8.00	C_1
6-2j$^+$	1.9029	–0.0716	180.0	1.4764	121.1	2.0938	91.7	7.72	C_2
Di-cationic: *cis*-type									
6-2h^{2+}	1.5012	–0.1743	0.0	1.6130	139.3	1.7071	114.6	23.49	C_s
6-2i^{2+}	1.6823	–0.1360	0.0	1.5323	134.0	1.8852	107.8	23.20	C_s
6-2j^{2+}	1.8524	–0.1221	0.0	1.5232	137.1	2.0718	103.9	22.24	C_2
Di-cationic: *trans*-type									
6-2h^{2+}	1.5139	–0.1616	180.0	1.6305	125.0	1.7054	106.2	23.29	C_1
6-2i^{2+}	1.6868	–0.1315	180.0	1.5595	125.5	1.8751	99.8	23.01	C_1
6-2j^{2+}	1.8594	–0.1151	180.0	1.5371	130.3	2.0635	95.9	22.10	C_2

[a] The 6-311++G(3d,p) basis set for H, C, O, S, and Se and that of the (7433111/743111/7411/2 + 1s1p1d1f) type for Te. [b] E(**6-2h**) = –552.3049239 au, E(**6-2i**) = –2554.7239884 au, and E(**6-2j**) = –6766.5267503 au.

Table 6-A3. Distances, angles, and torsional angles for neutral and charged forms of *cyclo*-1,2-EE'$(CH_2)_3$ (**6-3**), together with relative energies, optimized at the MP2 level[a]

Compd	r_o(E, E') (Å)	Δr_o(E, E') (Å)	ϕ(CEE'C) (º)	r_o(E, C) (Å)	∠E'EC (º)	r_o(E', C) (Å)	∠EE'C (º)	ΔE (eV)	Sym-metry
Neutral: *cis*-type									
6-3g	1.4616	0.0000	–52.9	1.4318	101.2	1.4318	101.2	0.00	C_1
6-3h	1.7000	0.0000	–33.2	1.4338	106.4	1.8298	94.1	0.00	C_1
6-3i	1.8448	0.0000	–24.3	1.4314	107.0	1.9669	90.6	0.00	C_1
6-3j	1.9978	0.0000	–21.9	1.4351	108.0	2.1548	85.8	0.00	C_1
Mono-anionic: *cis*-type									
6-3g$^-$	1.4673	0.0057	–50.4	1.4363	101.7	1.4363	101.7	0.87	C_1
6-3h$^-$	1.7084	0.0084	–24.2	1.4427	107.2	1.8255	95.2	0.80	C_1
6-3i$^-$	2.4329	0.5881	–1.7	1.3690	104.6	1.9588	79.1	–0.27	C_1
6-3j$^-$	2.3235	0.3257	–17.4	1.3865	107.7	2.1825	78.0	–0.48	C_1
Mono-cationic: *cis*-type									
6-3h$^+$	1.5790	–0.1210	–1.0	1.5058	113.9	1.8033	92.9	7.86	C_1
6-3i$^+$	1.7287	–0.1161	–3.0	1.4930	113.4	1.9451	92.0	7.85	C_1
6-3j$^+$	1.9076	–0.0902	–5.1	1.4850	113.3	2.1269	86.7	7.62	C_1
Di-cationic: *cis*-type									
6-3h^{2+}	1.5150	–0.1850	–2.0	1.6543	113.6	1.7424	99.5	23.14	C_1
6-3i^{2+}	1.6821	–0.1627	–0.6	1.5967	114.5	1.9173	93.0	22.88	C_1
6-3j^{2+}	1.8602	–0.1375	–0.2	1.5648	115.5	2.1049	87.0	22.03	C_1

[a] The 6-311+G(3d) basis set for O, S, and Se and that of the (7433111/743111/7411/2 + 1s1p1d1f) type for Te with the 6-311++G(d) basis set for C and H. [b] E(**6-3g**) = –267.6655442 au, E(**6-3h**) = –590.3241482 au, E(**6-3i**) = –2592.7351573 au, and E(**6-3j**) = –6804.5281517 au.

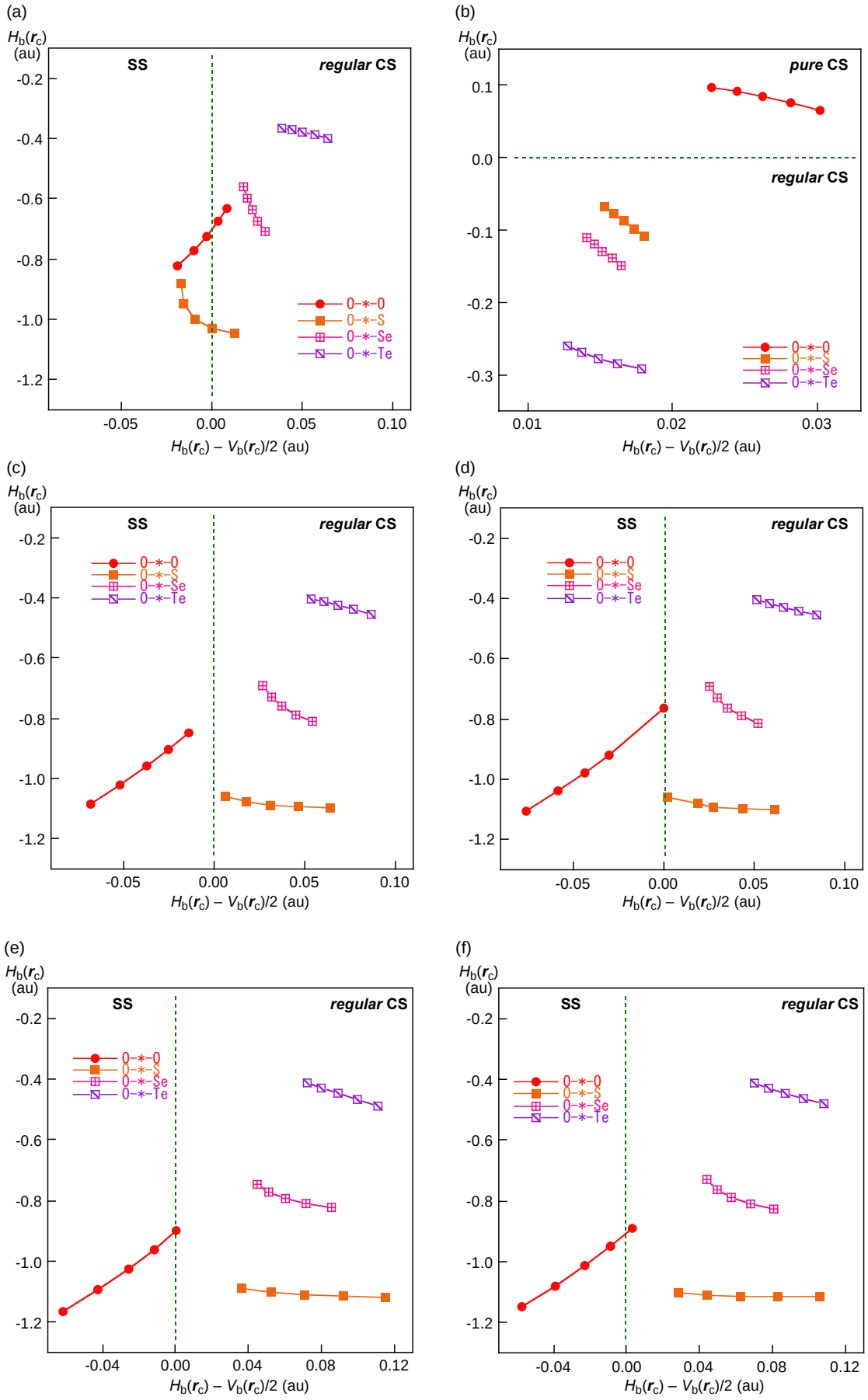

Figure 6-A1. Plots of $H_b(\boldsymbol{r}_c)$ versus $H_b(\boldsymbol{r}_c) - V_b(\boldsymbol{r}_c)/2$ for (a) HEE'H (**6-1** ($C_{2:np}$-type)), (b) **6-1**$^-$ ($C_{2:np}$-type), (c) **6-1**$^+$ (*cis*-type), (d) **6-1**$^+$ (*trans*-type), (e) **6-1**$^{2+}$ (*cis*-type), and (f) **6-1**$^{2+}$ (*trans*-type).

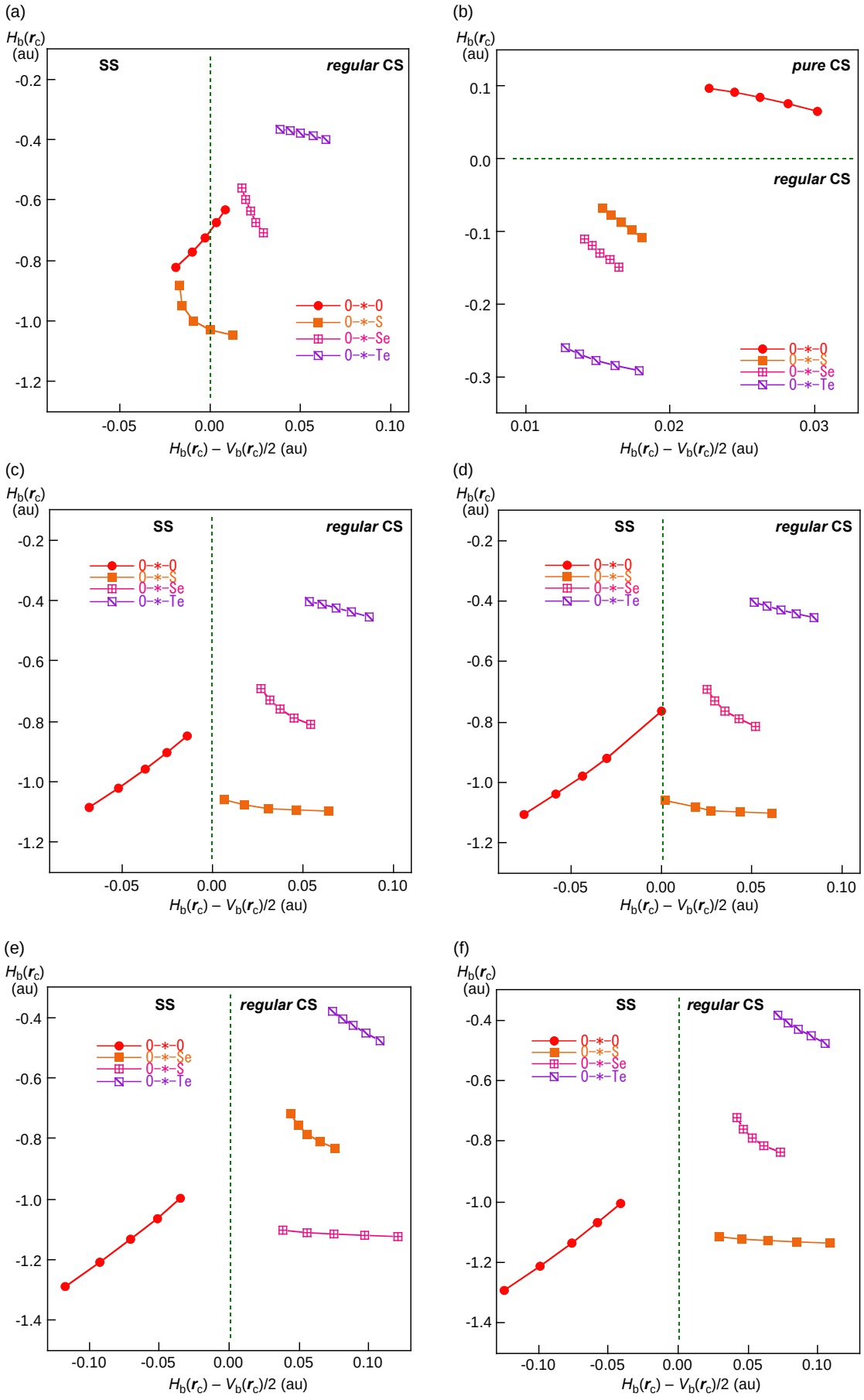

Figure 6-A2. Plots of $H_b(\boldsymbol{r}_c)$ versus $H_b(\boldsymbol{r}_c) - V_b(\boldsymbol{r}_c)/2$ for (a) MeEE'Me (**6-2** ($C_{2:np}$-type)), (b) **6-2**$^-$ ($C_{2:np}$-type), (c) **6-2**$^+$ (*cis*-type), (d) **6-2**$^+$ (*trans*-type), (e) **6-2**$^{2+}$ (*cis*-type), and (f) **6-2**$^{2+}$ (*trans*-type).

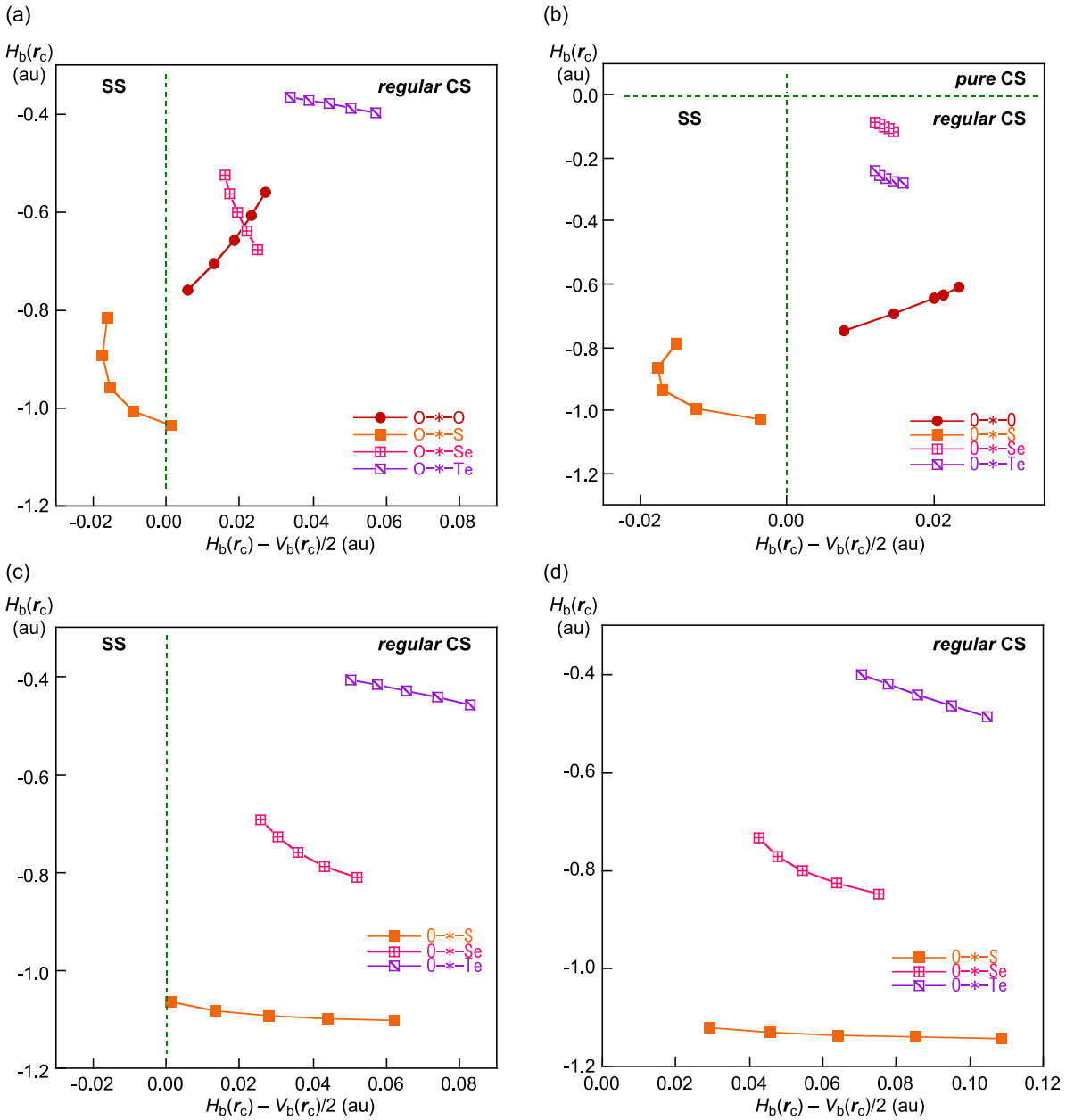

Figure 6-A3. Plots of $H_b(\boldsymbol{r}_c)$ versus $H_b(\boldsymbol{r}_c) - V_b(\boldsymbol{r}_c)/2$ for (a) *cyclo*-1,2-EE'$(CH_2)_3$ (**6-3** (*cis*-type)), (b) **6-3**$^-$ (*cis*-type), (c) **6-3**$^+$ (*cis*-type), and (d) **6-3**$^{2+}$ (*cis*-type).

Table 6-A4. AIM Functions and parameters evaluated for the neutral, cationic and anionic forms in HEE'H (**6-1**) calculated with NIV at the MP2 level[a]

Interaction (E-∗-E')	$\rho_b(\boldsymbol{r}_c)$ (au)	$c\nabla^2\rho_b(\boldsymbol{r}_c)$[b] (au)	$H_b(\boldsymbol{r}_c)$ (au)	$k_b(\boldsymbol{r}_c)$[c]	R (au)	θ (º)	ν_n (n)[d] (cm^{-1})	k_f[d] (unit[e])	$\theta_{p:NIV}$ (º)	$\kappa_{p:NIV}$ (au^{-1})
Neutral: $C_{2:np}$-type										
O-∗-O/**6-1g**	0.2678	0.0118	–0.1789	–1.884	0.1793	176.2	902.7 (2)	6.731	192.5	0.5
O-∗-S/**6-1h**	0.1778	–0.0114	–0.1747	–2.151	0.1751	183.7	747.8 (2)	5.371	156.2	16.0
O-∗-Se/**6-1i**	0.1439	0.0214	–0.0906	–1.679	0.0931	166.7	633.5 (2)	2.969	164.1	6.1
O-∗-Te/**6-1j**	0.1201	0.0487	–0.0449	–1.316	0.0662	132.7	615.3 (2)	2.358	118.4	1.7
Mono-anionic: $C_{2:np}$-type										
O-∗-S/**6-1g**$^-$	0.0427	0.0231	0.0054	–0.867	0.0237	76.8	322.6 (1)	0.143	87.8	65.0
O-∗-S/**6-1h**$^-$	0.1719	–0.0190	–0.1551	–2.325	0.1563	187.0	474.9 (2)	0.447	181.4	11.7
O-∗-Se/**6-1i**$^-$	0.0664	0.0174	–0.0123	–1.262	0.0213	125.3	387.2 (2)	0.393	158.7	32.8
O-∗-Te/**6-1j**$^-$	0.0725	0.0163	–0.0205	–1.386	0.0262	141.5	303.0 (2)	0.613	142.0	37.1
Mono-cationic: *cis*-type										
O-∗-O/**6-1g**$^+$	0.3840	–0.0194	–0.3549	–2.123	0.3555	183.1	1107.0 (2)	8.874	194.2	0.1
O-∗-S/**6-1h**$^+$	0.2185	0.0287	–0.2381	–1.806	0.2398	173.1	936.0 (2)	2.360	123.7	7.4
O-∗-Se/**6-1i**$^+$	0.1781	0.0360	–0.1359	–1.654	0.1405	165.2	782.1 (2)	2.685	148.2	9.1
O-∗-Te/**6-1j**$^+$	0.1419	0.0669	–0.0606	–1.316	0.0903	132.1	694.6 (2)	0.565	117.6	0.6
Mono-cationic: *trans*-type										
O-∗-O/**6-1g**$^+$	0.3810	–0.0175	–0.3505	–2.111	0.3510	182.9	1106.4 (2)	10.434	194.3	0.1
O-∗-S/**6-1h**$^+$	0.2163	0.0240	–0.2359	–1.831	0.2372	174.2	953.5 (2)	6.329	128.1	5.1
O-∗-Se/**6-1i**$^+$	0.1762	0.0348	–0.1334	–1.657	0.1378	165.4	783.1 (2)	2.491	151.5	8.5
O-∗-Te/**6-1j**$^+$	0.1406	0.0655	–0.0598	–1.313	0.0887	132.4	704.7 (2)	0.999	122.6	1.3
Di-cationic: *cis*-type										
O-∗-O/**6-1g**$^+$	0.4389	–0.0259	–0.4374	–2.115	0.4505	183.3	890.8 (1)	5.611	194.0	0.1
O-∗-S/**6-1h**$^+$	0.2448	0.0716	–0.2712	–1.656	0.2804	165.3	1052.7 (3)	1.423	129.1	1.5
O-∗-Se/**6-1i**$^{2+}$	0.1961	0.0604	–0.1556	–1.563	0.1669	158.8	799.3 (1)	1.051	140.5	10.1
O-∗-Te/**6-1j**$^{2+}$	0.1565	0.0895	–0.0700	–1.281	0.1136	128.0	799.9 (3)	1.611	124.6	0.0
Di-cationic: *trans*-type										
O-∗-O/**6-1g**$^{2+}$	0.4321	–0.0226	–0.4374	–2.115	0.4379	183.0	864.3 (1)	6.105	194.0	0.1
O-∗-S/**6-1h**$^{2+}$	0.2415	0.0625	–0.2687	–1.682	0.2759	166.9	972.8 (1)	4.125	124.0	2.0
O-∗-Se/**6-1i**$^{2+}$	0.1936	0.0577	–0.1528	–1.570	0.1634	159.3	813.4 (1)	1.386	147.0	7.5
O-∗-Te/**6-1j**$^{2+}$	0.1549	0.0871	–0.0689	–1.283	0.1111	128.3	800.9 (2)	1.311	122.4	0.4

[a] The 6-311+G(3d,p) basis set for H, O, S, and Se and that of the (7433111/743111/7411/2 + 1s1p1d1f) type for Te. [b] $c = \hbar^2/8m$. [c] $k = V_b(\boldsymbol{r}_c)/G_b(\boldsymbol{r}_c)$. [d] Corresponding to the E–E' bond in question. [e] mdyn $Å^{-1}$.

Table 6-A5. AIM functions and parameters for the neutral, cationic and anionic forms of MeEE'Me (**6-2**) calculated with NIV method at the MP2 level[a]

Interaction (E-∗-E')	$\rho_b(\boldsymbol{r}_c)$ (au)	$c\nabla^2\rho_b(\boldsymbol{r}_c)^b$ (au)	$H_b(\boldsymbol{r}_c)$ (au)	$k_b(\boldsymbol{r}_c)^c$	R (au)	θ (º)	ν_n $(n)^d$ (cm^{-1})	$k_f{}^d$ (unit[e])	$\theta_{p:NIV}$ (º)	$\kappa_{p:NIV}$ (au^{-1})
Neutral: $C_{2:np}$-type										
O-∗-S/**6-2h**	0.1823	–0.0092	–0.1823	–2.112	0.1825	182.9	692.8 (6)	1.859	151.4	15.8
O-∗-Se/**6-2i**	0.1489	0.0224	–0.0947	–1.679	0.0974	166.7	598.6 (6)	1.697	164.6	5.5
O-∗-Te/**6-2j**	0.1222	0.0504	–0.0464	–1.315	0.0684	132.6	573.2 (7)	1.524	117.3	1.6
Mono-anionic: $C_{2:np}$-type										
O-∗-O/**6-2g**$^-$	0.0516	0.0262	0.0044	–0.909	0.0266	80.5	384.0 (6)	0.685	94.9	30.5
O-∗-S/**6-2h**$^-$	0.0531	0.0166	–0.0046	–1.122	0.0172	105.6	325.1 (6)	0.327	138.4	27.5
O-∗-Se/**6-2i**$^-$	0.0545	0.0152	–0.0070	–1.188	0.0167	114.9	308.5 (6)	0.298	146.0	9.6
O-∗-Te/**6-2j**$^-$	0.0695	0.0148	–0.0192	–1.393	0.0243	142.4	290.9 (6)	0.253	136.5	50.5
Mono-cationic: *cis*-type										
O-∗-S/**6-2h**$^+$	0.2185	0.0311	–0.2376	–1.793	0.2396	172.5	1050.3 (10)	3.533	132.4	4.9
O-∗-Se/**6-2i**$^+$	0.1802	0.0374	–0.1370	–1.647	0.1420	164.7	676.3 (7)	2.022	152.0	8.4
O-∗-Te/**6-2j**$^+$	0.1422	0.0685	–0.0605	–1.306	0.0914	131.4	615.8 (7)	1.767	120.0	1.3
Mono-cationic: *trans*-type										
O-∗-S/**6-2h**$^+$	0.2183	0.0276	–0.2384	–1.812	0.2399	173.4	995.8 (9)	1.266	138.9	4.8
O-∗-Se/**6-2i**$^+$	0.1803	0.0356	–0.1373	–1.658	0.1418	165.5	698.4 (7)	1.919	153.0	8.0
O-∗-Te/**6-2j**$^+$	0.1416	0.0665	–0.0606	–1.313	0.0899	132.3	627.2 (7)	1.759	120.5	1.3
Di-cationic: *cis*-type										
O-∗-S/**6-2h**$^{2+}$	0.2486	0.0752	–0.2773	–1.648	0.2874	164.8	1022.6 (10)	3.717	126.1	1.3
O-∗-Se/**6-2i**$^{2+}$	0.1926	0.0559	–0.1513	–1.575	0.1613	159.7	755.9 (8)	3.397	151.7	7.8
O-∗-Te/**6-2j**$^{2+}$	0.1518	0.0893	–0.0650	–1.267	0.1104	126.0	811.4 (9)	1.588	130.9	0.8
Di-cationic: *trans*-type										
O-∗-S/**6-2h**$^{2+}$	0.2471	0.0644	–0.2790	–1.684	0.2863	167.0	976.8 (10)	3.918	126.8	1.7
O-∗-Se/**6-2i**$^{2+}$	0.1932	0.0530	–0.1527	–1.590	0.1616	160.9	779.3 (8)	3.778	153.0	8.7
O-∗-Te/**6-2j**$^{2+}$	0.1512	0.0864	–0.0650	–1.273	0.1081	127.0	805.9 (9)	2.414	130.0	0.8

[a] The 6-311+G(3d) basis set for H, C, O, S, and Se and that of the (7433111/743111/7411/2 + 1s1p1d1f) type for Te. [b] $c = \hbar^2/8m$. [c] $k = V_b(\boldsymbol{r}_c)/G_b(\boldsymbol{r}_c)$. [d] Corresponding to the E–E' bond in question. [e] mdyn $Å^{-1}$.

Table 6-A6. AIM functions and parameters evaluated for the neutral, cationic and anionic forms in *Cyclo*-1,2-EE'$(CH_2)_3$ (**6-3**) calculated with NIV method at the MP2 level[a]

Interaction (E-∗-E')	$\rho_b(\boldsymbol{r}_c)$ (au)	$c\nabla^2\rho_b(\boldsymbol{r}_c)^b$ (au)	$H_b(\boldsymbol{r}_c)$ (au)	$k_b(\boldsymbol{r}_c)^c$	R (au)	θ (º)	$\nu_n\,(n)^d$ (cm^{-1})	$k_f{}^d$ (unit[e])	$\theta_{p:NIV}$ (º)	$\kappa_{p:NIV}$ (au^{-1})
Neutral: *cis*-type										
O-∗-O/**6-3g**	0.2646	0.0186	–0.1738	–1.823	0.1748	173.9	813.5 (5)	2.794	191.5	0.6
O-∗-S/**6-3h**	0.1766	–0.0152	–0.1693	–2.218	0.1700	185.1	688.0 (5)	2.000	165.7	16.4
O-∗-Se/**6-3i**	0.1425	0.0194	–0.0857	–1.689	0.0879	167.3	599.7 (5)	0.658	167.8	4.7
O-∗-Te/**6-3j**	0.1183	0.0443	–0.0449	–1.337	0.0631	135.4	577.1 (5)	0.495	117.0	0.2
Mono-anionic: *cis*-type										
O-∗-O/**6-3g**$^-$	0.2602	0.0200	–0.1675	–1.808	0.1690	173.2	798.6 (5)	2.705	191.4	0.6
O-∗-S/**6-3h**$^-$	0.1744	–0.0170	–0.1634	–2.264	0.1642	186.0	669.4 (5)	2.027	172.1	14.3
O-∗-Se/**6-3i**$^-$	0.0471	0.0132	–0.0048	–1.153	0.0140	109.8	218.7 (2)	0.269	134.8	55.2
O-∗-Te/**6-3j**$^-$	0.0657	0.0135	–0.0173	–1.390	0.0219	142.0	236.5 (2)	0.315	145.2	41.3
Mono-cationic: *cis*-type										
O-∗-S/**6-3h**$^+$	0.2177	0.0280	–0.2378	–1.809	0.2394	173.3	968.8 (10)	3.717	129.0	4.2
O-∗-Se/**6-3i**$^+$	0.1798	0.0360	–0.1366	–1.655	0.1412	165.3	916.5 (9)	1.256	152.7	7.5
O-∗-Te/**6-3j**$^+$	0.1413	0.0655	–0.0607	–1.317	0.0893	132.9	936.5 (10)	1.353	119.9	2.0
Di-cationic: *cis*-type										
O-∗-S/**6-3h**$^{2+}$	0.2484	0.0644	–0.2819	–1.687	0.2892	167.1	965.8 (11)	4.443	126.6	2.1
O-∗-Se/**6-3i**$^{2+}$	0.1969	0.0545	–0.1577	–1.592	0.1669	161.0	815.4 (8)	1.701	151.7	9.0
O-∗-Te/**6-3j**$^{2+}$	0.1534	0.0858	–0.0679	–1.283	0.1094	128.3	795.4 (8)	2.240	129.4	0.6

[a] The 6-311+G(3d) basis set for O, S, and Se and that of the (7433111/743111/7411/2 + 1s1p1d1f) type for Te with the 6-311+G(d) basis set for C and H. [b] $c = \hbar^2/8m$. [c] $k = V_b(\boldsymbol{r}_c)/G_b(\boldsymbol{r}_c)$. [d] Corresponding to the E–E' bond in question. [e] mdyn $Å^{-1}$.

References

1 Preliminary discussion for the neutral form of HEE'H and MeEE'Me (E, E' = S, Se, and Te), see S. Hayashi, H. Miza, and W. Nakanishi, Invited Paper on 1st Electronic Symposium on Selenium Chemistry eSeS-1, dedicated to Prof. M. Tiecco, on his retirement on the site http://eses1.chimfarm.unipg.it (2011). The θ_p value of 198.3º for HS-∗-SeH in Table 6-2 of the reference should be read 189.3º.

2 a) *Their Chemistry and Biology* (Eds.: D. L. Klayman, W. H. H. Günther), Wiley: New York, 1973; b) *The Chemistry of Organic Selenium and Tellurium Compounds* (Eds.: S. Patai, Z. Rappoport), John-Wiley and Sons: New York, 1986*;* Vols. 1 and 2; c) *Organic Selenium Chemistry* (Ed. D. Liotta), Wiley-Interscience: New York, 1987; *Organoselenium Chemistry, A practical Approach* (Ed. T. G. Back), Oxford University Press: Oxford, 1999; *Organoselenium Chemistry Modern Developments in Organic Synthesis*, *Top Curr. Chem.* (Ed.: T. Wirth), Springer: Berlin, Heidelberg, New York, London, Paris, Tokyo, 2000.

3 *Chemistry of Hypervalent Compounds* (Ed.: K.-y. Akiba), Wiley-VCH, New York, 1999.

4 a) W. Nakanishi, *Hypervalent Chalcogen Compounds* In *Handbook of Chalcogen Chemistry: New Perspectives in Sulfur, Selenium and Tellurium* (Ed.: F. A. Devillanova), Royal Society of Chemistry, Cambridge, 2006, Chap. 10.3, pp. 644–668; b) W. Nakanishi, S. Hayashi, *Hypervalent Chalcogen Compounds* In *Handbook of Chalcogen Chemistry: New Perspectives in Sulfur, Selenium and Tellurium: 2nd Edition*, Vol. 2, (Eds.: F. A. Devillanova, W.-W. du Mont), Royal Society of Chemistry, Cambridge, 2013, Chap. 12.3, pp. 335–372.

5 A. J. Mukherjee, S. S. Zade, H. B. Singh, R. B. Sunoj, *Chem. Rev.* **2010**, *110*, 4357–4416.

6 *The Chemistry of Organic Selenium and Tellurium Compounds* (Eds.: S. Patai, Z. Rappoport), Vol. 1, Wiley, New York, 1986, Chap. 6.

7 A. Panda, G. Mugesh, H. B. Singh, R. J. Butcher, *Organometallics* **1999**, *18*, 1986–1993; M. Kulcsar, A. Beleaga, C. Silvestru, A. Nicolescu, C. Deleanu, C. Todasca, A. Silvestru, *Dalton*

Trans. **2007**, 2187–2196; A. Beleaga, M. Kulcsar, C. Deleanu, A. Nicolescu, C. Silvestru, A. Silvestru, *J. Organomet. Chem.* **2009**, *694*, 1308–1316.

8 J. C. Martin, M. M. Chau, *J. Am. Chem. Soc.* **1974**, *96*, 3319–3321.

9 W. Nakanishi, S. Hayashi, S. Morinaka, T. Sasamori, N. Tokitoh, *New J. Chem.* **2008**, *32*, 1881–1889.

10 The electronegativity proposed by Allred-Rochow was employed to discuss the structure of the adducts. See, A. L. Allred, E. G. Rochow, *J. Inorg. Nucl. Chem.* **1958**, *5*, 264–268; A. L. Allred, E. G. Rochow, *J. Inorg. Nucl. Chem.* **1958**, *5*, 269–288.

11 H. Fujihara, T. Nakahodo, N. Furukawa, *Chem. Commun.* **1996**, 311; H. Fujihara, H. Ishitani, Y. Takaguchi, N. Furukawa, *Chem. Lett.* **1995**, 571–572; N. Furukawa, T. Fujii, T. Kimura, H. Fujihara, *Chem. Lett.* **1994**, 1007–1010; H. Fujihara, R. Saito, M. Yabe, N. Furukawa, *Chem. Lett.* **1992**, 1437–1440; H. Fujihara, M. Yabe, J.-J. Chiu, N. Furukawa, *Tetrahedron Lett.* **1991**, *32*, 4345–4348.

12 R. S. Glass, L. Adamowicz, J. L. Broeker, *J. Am. Chem. Soc.* **1991**, *113*, 1065–1072; R. S. Glass, S. W. Andruski, J. L. Broeker, H. Firouzabadi, L. K. Steffen, G. S. Wilson, *J. Am. Chem. Soc.* **1989**, *111*, 4036–4045.

13 *Atoms in Molecules. A Quantum Theory*, (Ed.; R. F. W. Bader), Oxford University Press, Oxford, UK, **1990**.

14 C. F. Matta, R. J. Boyd, *An Introduction to the Quantum Theory of Atoms in Molecules* In *The Quantum Theory of Atoms in Molecules: From Solid State to DNA and Drug Design* (Eds.: C. F. Matta, R. J. Boyd), WILEY-VCH, Weinheim, Germany, **2007**, Chap. 1.

15 a) F. Biegler-König, J. Schönbohm, *J. Comput. Chem.* **2002**, *23*, 1489–1494; b) F. Biegler-König, J. Schönbohm, D. Bayles, *J. Comput. Chem.* **2001**, *22*, 545–559; c) R. F. W. Bader, *J. Phys. Chem. A* **1998**, *102*, 7314–7323; d) R. F. W. Bader, *Chem. Res.* **1991**, *91*, 893–926; e) R. F. W. Bader, *Acc. Chem. Res.* **1985**, *18*, 9–15; f) T. H. Tang, R. F. W. Bader, P. MacDougall, *Inorg. Chem.* **1985**, *24*, 2047–2053; g) R. F. W. Bader, T. S. Slee, D. Cremer, E. Kraka, *J. Am. Chem.*

Soc. **1983**, *105*, 5061–5068; h) F. Biegler-König, R. F. W. Bader, T. H. Tang, *J. Comput. Chem.* **1982**, *3*, 317–328.

16 J. A. Dobado, H. Martînez-Garcîa, J. Molina, M. R. Sundberg, *J. Am. Chem. Soc.* **2000**, *122*, 1144–1149.

17 J. Molina, J. A. Dobado, *Theor. Chem. Acc.* **2001**, *105*, 328–337.

18 S. K. Ignatov, N. H. Rees, B. R. Tyrrell, S. R. Dubberley, A. G. Razuvaev, P. Mountford, G. I. Nikonov, *Chem. Eur. J.* **2004**, *10*, 4991–4999.

19 S. K. Tripathi, U. Patel, D. Roy, R. B. Sunoj, H. B. Singh, G. Wolmershäuser, R. J. Butcher, *J. Org. Chem.* **2005**, *70*, 9237–9247.

20 a) M. Yamashita, Y. Yamamoto, K.-y. Akiba, D. Hashizume, F. Iwasaki, N. Takagi, S. Nagase, *J. Am. Chem. Soc.* **2005**, *127*, 435–4371; b) Y. Yamamoto, K.-y. Akiba, *J. Syn. Org. Chem. Jpn.* **2004**, *62*, 1128–1137.

21 W. Nakanishi, T. Nakamoto, S. Hayashi, T. Sasamori, N. Tokitoh, *Chem. Eur. J.* **2007**, *13*, 255–268.

22 a) W. Nakanishi, S. Hayashi, K. Narahara, *J. Phys. Chem. A* **2009**, *113*, 10050–10057; b) W. Nakanishi, S. Hayashi, K. Narahara, *J. Phys. Chem. A* **2008**, *112*, 13593–13599.

23 W. Nakanishi, S. Hayashi, *Curr. Org. Chem.* **2010**, *14*, 181–197.

24 W. Nakanishi, S. Hayashi, *J. Phys. Chem. A* **2010**, *114*, 7423–7430.

25 W. Nakanishi, S. Hayashi, K. Matsuiwa, M. Kitamoto, *Bull. Chem. Soc. Jpn.* **2012**, *85*, 1293–1305.

26 QTAIM-DFA is successfully applied to analyze weak to strong interactions in gas phase. It could also be applied to the interactions in crystals and to those in larger systems, containing bioactive materials. The methodological improvement is inevitable to generate the perturbed structures suitable for the systems.

27 *Gaussian 03 (Revision D.02)*, M. J. Frisch, G. W. Trucks, H. B. Schlegel, G. E. Scuseria, M. A. Robb, J. R. Cheeseman, J. A. Montgomery, Jr., T. Vreven, K. N. Kudin, J. C. Burant, J. M.

Millam, S. S. Iyengar, J. Tomasi, V. Barone, B. Mennucci, M. Cossi, G. Scalmani, N. Rega, G. A. Petersson, H. Nakatsuji, M. Hada, M. Ehara, K. Toyota, R. Fukuda, J. Hasegawa, M. Ishida, T. Nakajima, Y. Honda, O. Kitao, H. Nakai, M. Klene, X. Li, J. E. Knox, H. P. Hratchian, J. B. Cross, V. Bakken, C. Adamo, J. Jaramillo, R. Gomperts, R. E. Stratmann, O. Yazyev, A. J. Austin, R. Cammi, C. Pomelli, J. W. Ochterski, P. Y. Ayala, K. Morokuma, G. A. Voth, P. Salvador, J. J. Dannenberg, V. G. Zakrzewski, S. Dapprich, A. D. Daniels, M. C. Strain, O. Farkas, D. K. Malick, A. D. Rabuck, K. Raghavachari, J. B. Foresman, J. V. Ortiz, Q. Cui, A. G. Baboul, S. Clifford, J. Cioslowski, B. B. Stefanov, G. Liu, A. Liashenko, P. Piskorz, I. Komaromi, R. L. Martin, D. J. Fox, T. Keith, M. A. Al-Laham, C. Y. Peng, A. Nanayakkara, M. Challacombe, P. M. W. Gill, B. Johnson, W. Chen, M. W. Wong, C. Gonzalez, J. A. Pople, Gaussian, Inc.; Wallingford CT, **2004**.

28 a) C. Møller, M. S. Plesset, *Phys. Rev.* **1934**, *46*, 618–622; b) J. Gauss, *J. Chem. Phys.* **1993**, *99*, 3629–3643; c) J. Gauss, *Ber. Bunsen-Ges. Phys. Chem.* **1995**, *99*, 1001–1008.

29 For the 6-311G(3d) basis sets, see: a) R. C, Binning Jr. L. A. Curtiss, *J. Comput. Chem.* **1990**, *11*, 1206−1216; b) L. A. Curtiss, M. P. McGrath, J.-P. Blaudeau, N. E. Davis, R. C. Binning Jr. L. Radom, *J. Chem. Phys.* **1995**, *103*, 6104−6113; c) M. P. McGrath, L. Radom, *J. Chem. Phys.* **1991**, *94*, 511−516; d) For the diffuse functions (+ and + +), see: T. Clark, J. Chandrasekhar, G. W. Spitznagel, P. v. R. Schleyer, *J. Comput. Chem.* **1983**, *4*, 294−301.

30 For inner and valence shells: T. Koga, S. Yamamoto, T. Shimazaki, H. Tatewaki, *Theor. Chem. Acc.* **2002**, *108*, 41–45. For valence correlated set: M. Sekiya, T. Noro, Y. Osanai, T. Koga, *Theor. Chem. Acc.* **2001**, *106*, 297–300.

31 The AIM2000 program (Version 2.0) is employed to analyze and visualize atoms-in-molecules: F. Biegler-König, *J. Comput. Chem.* **2000**, *21*, 1040–1048. See also ref. 13.

Chapter 7

Transannular E---E' Interactions in Neutral, Radical Cationic, and Dicationic Forms of *cyclo*-[E($CH_2CH_2CH_2$)$_2$E'] (E, E' = S, Se, Te, and O) with Structural Feature: Dynamic and Static Behavior of E---E' Elucidated by QTAIM Dual Functional Analysis

Abstract

The nature of the transannular E-∗-E' interactions in neutral, radical cationic, and dicationic forms of *cyclo*-E($CH_2CH_2CH_2$)$_2$E' (**7-1**) (E, E' = S, Se, Te, and O) (**7-1**, **7-1**$^{\bullet+}$, and **7-1**$^{2+}$, respectively) is elucidated by applying QTAIM dual functional analysis (QTAIM-DFA). $H_b(\boldsymbol{r}_c)$ are plotted versus $H_b(\boldsymbol{r}_c) - V_b(\boldsymbol{r}_c)/2$ for the data of E-∗-E' at BCPs in QTAIM-DFA, where ∗ emphasizes the existence of BCP. Plots for the fully-optimized structures are analyzed by the polar coordinate (R, θ) representation. Those containing the perturbed structures are analyzed by (θ_p, κ_p): θ_p corresponds to the tangent line of the plot and κ_p is the curvature. While (R, θ) describes to the static nature, (θ_p, κ_p) represent the dynamic nature of interactions. The nature is well specified by (R, θ) and (θ_p, κ_p). E-∗-E' becomes stronger in the order of **7-1** < **7-1**$^{\bullet+}$ < **7-1**$^{2+}$, except for O-∗-O. While E-∗-E' (E, E' = S, Se, and Te) in **7-1**$^{2+}$ are characterized as weak covalent bonds, except for S-∗-Te (MC nature through CT) and Se-∗-Te (TBP nature through CT), O-∗-E' seems more complex. The behavior of E-∗-E' in **7-1**$^{2+}$ is very close to that of *cyclo*-E($CH_2CH_2CH_2$)$_2$E' (E, E' = S, Se, Te, and O), except for O-∗-O.

Introduction

Chalcogen-chalcogen interactions (E–E' and E---E': E, E' = S, Se, and Te, together with O) are of current and continuous interest, not only those of the shared-shell (SS) type (E–E') but also of the closed-shell (CS) type (E---E').[1-6] The E–E' bonds play an important role in all field of chemical and biological sciences. They maintain the peptide structures and in biological activities containing enzymes, especially for E, E' = S, Se.[7-11] The E–E' bonds in dichalcogenides (RE–E'R') supply low-lying vacant orbitals of the σ-type (σ*(E–E')), where the E/E' atoms contain lone pair orbitals of s- and p-types (n_s(E/E') and n_p(E/E'), respectively) of relatively high energy levels. Consequently, the E–E' bonds in RE–E'R' are easily oxidized and reduced, which is important to develop the highly functionalized materials. On the other hand, the intermolecular E---E' interactions of the CS type are often encountered in crystals of organic compounds containing chalcogen atoms, which must be the important driving force to grow the crystals and they create useful properties of materials. 1,8-(Dichalcogena)naphthalenes and the related species must be the typical systems for the intramolecular E---E' interactions.[12]

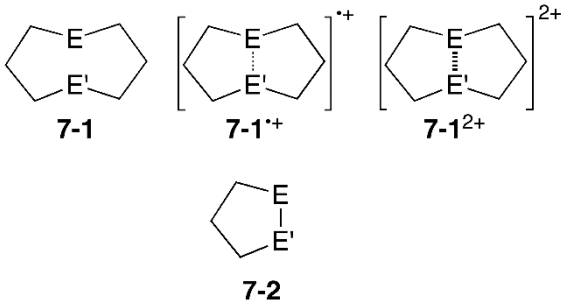

Chart 7-1. 1,5-(Dichalcogena)canes and the related species

1,5-(Dichalcogena)canes and the related species also supply a typical system to study the E---E' interactions. Research groups of Furukawa[13-22] and Glass[23-27] have investigated the transannular E---E' interactions in *cyclo*-E($CH_2CH_2CH_2$)$_2$E' (**7-1**) with some (E, E') of (S, S: **a**), (S, Se: **b**), (S, Te: **c**),

(Se, Se: **d**), (Se, Te: **e**), (Te, Te: **f**), (O, O: **g**), (O, S: **h**), (O, Se: **i**), and (O, Te: **j**) (Chart 7-1). E and E' are chosen so as to the electronegativity of E (χ_E) is larger than or equal to that of E' ($\chi_{E'}$) ($\chi_E \geq \chi_{E'}$).[28] The transannular E---E' interactions at the 1,5-positions of the eight-membered ring in **7-1** are expected to be highly advantageous due to the formation of two fused five-membered rings. One-electron oxidation of 1,5-dithiocane (**7-1a**) will give a radical cation **7-1a**$^{\bullet+}$, which can be described as a rather stable species. Its EPR spectrum persists for at least 72 hrs at room temperature.[29] Two fused five-membered rings through the transannular S–S interaction in **7-1a**$^{\bullet+}$ must be responsible for the remarkable stability of **7-1a**$^{\bullet+}$.[29,30] Three energetically favoured *cis*-fused conformers are predicted through the conformational analysis, which are chair-boat (**CB**), chair-chair (**CC**), boat-boat (**BB**) conformers. The **CB** conformer is shown to be the global minimum, which is more stable than **CC** and **BB** by about 8 kJ mol^{-1}.[27,31] **7-1a**$^{\bullet+}$ is further oxidized to give a dication **7-1a**$^{2+}$, of which structure is determined by the X-ray crystallographic analysis.[13] The transannular interactions are also investigated for **7-1b**–**7-1f**. Among the species, the structure of **7-1d**$^{2+}$ is reported,[14] together with those of [**7-1b**–**7-1b**]$^{2+}$ and **7-1c**$^{2+}$.[26] Dimer dications could be produced in the dimerization of the corresponding monomer radical cations or the reaction of the monomer dications with the corresponding neutral monomers.

Figure 7-1 shows the structures of **7-1a**$^{2+}$, **7-1c**$^{2+}$, and **7-1d**$^{2+}$, determined by the X-ray analysis,[13,14] where the counter anions are neglected. Figure 7-2 draws the structures of **7-1a**$^{\bullet+}$ (**CB**), **7-1a**$^{\bullet+}$ (**CC**), and **7-1a**$^{\bullet+}$ (**BB**), optimized at the MP2 level as a beginning of this work. **7-1a**$^{\bullet+}$ (**CB**) is shown to have the C_s symmetry and to be more stable than **7-1a**$^{\bullet+}$ (**CC**) and **7-1a**$^{\bullet+}$ (**BB**) by 12.0 and 10.1 kJ mol^{-1}, respectively, under the calculation conditions employed in this chapter. The optimized structure of **7-1a**$^{\bullet+}$ (**BB**) has the C_2 symmetry, which is somewhat twisted from the C_{2v} symmetry. That of **7-1a**$^{\bullet+}$ (**CC**) also has the C_2 symmetry. The results of the calculations on **7-1a**$^{\bullet+}$ supported the previous observations. While the observed structure of **7-1a**$^{2+}$ is the **CC** type with substantial deformation (twisted: KAGHOP),[13] those of **7-1d**$^{2+}$ (KIVHIG) and **7-1c**$^{2+}$ (**CB**) (GUYSID)[26] are the **CB** type without substantial deformation.[14] The structure of **7-1b**$^{\bullet+}$ (GUYRUO)[26] is also the **CB** type

as shown in Figure 7-1, although the half structure of [**7-1b**–**7-1b**]$^{2+}$ is drawn for **7-1b**$^{\bullet+}$. Substantial deformations are not found in the components, although the environmental conditions must be different for the head and tail positions in the components when dimers are formed from the corresponding monomers. As a result, the **CB** type must be most important for the structures of **7-1**$^{\bullet+}$ and **7-1**$^{2+}$. The **CC** structure should also be taken into account in some cases, since the structure of **7-1a**$^{2+}$ is observed as **CC**. Figure 7-3 illustrates MO descriptions for the chalcogen-chalcogen interactions in **7-1**, **7-1**$^{\bullet+}$, and **7-1**$^{2+}$, which are to be clarified in this chapter.

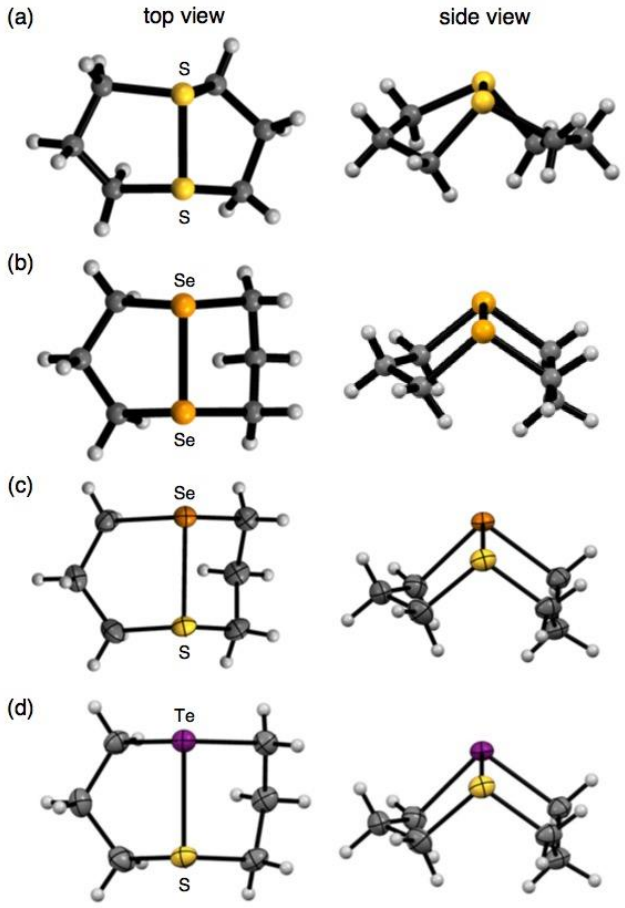

Figure 7-1. Observed structures of **7-1a**$^{2+}$ (**CC**: KAGHOP)[13] (a) and **7-1d**$^{2+}$ (**CB**: KIVHIG)[14] (b), together with **7-1b**$^{\bullet+}$ (**CB**, half structure of [**7-1b**–**7-1b**]$^{2+}$: GUYRUO)[26] (c) and **7-1c**$^{2+}$ (**CB**: GUYSID)[26] (d).

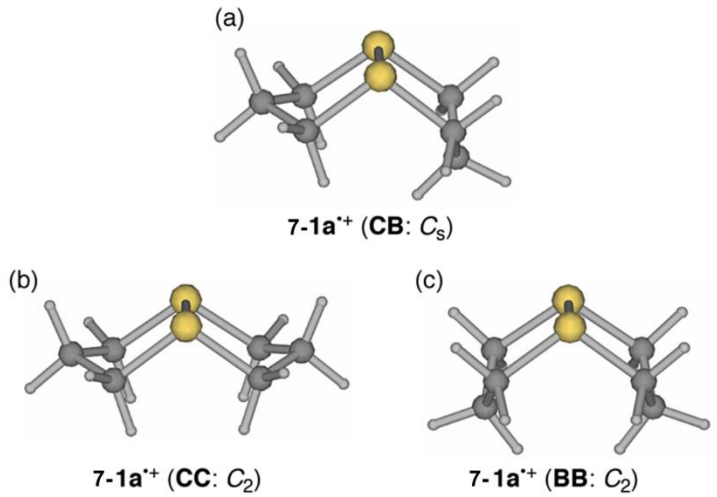

Figure 7-2. Optimized structures of **7-1a**$^{\bullet+}$ (**CB**: C_s) (a), **7-1a**$^{\bullet+}$ (**CC**: C_2) (b), and **7-1a**$^{\bullet+}$ (**BB**: C_2) (c).

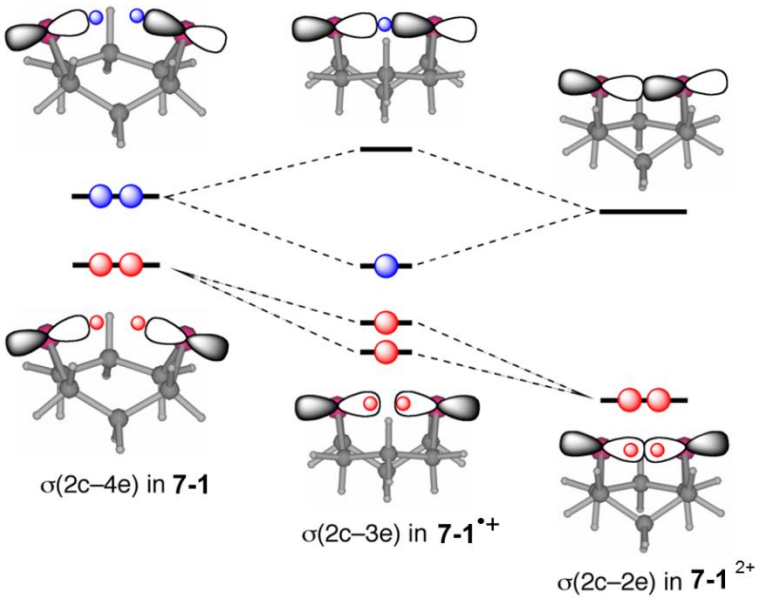

Figure 7-3. MO descriptions for the chalcogen-chalcogen interactions in **7-1**, **7-1**$^{\bullet+}$, and **7-1**$^{2+}$ of the **CB** type (*cf*: Figure 7-7).

QTAIM (the quantum theory of atoms-in-molecules) approach, introduced by Bader,[32,33] enables us to analyze the nature of chemical bonds and interactions.[34-38] Lots of QTAIM investigations have been reported so far,[39-46] however, those from a viewpoint of experimental chemists seem not so many. His research group searched for such methods that enable experimental chemists to analyze their own results, concerning chemical bonds and interactions, by their own image and proposed QTAIM dual functional analysis (QTAIM-DFA),[47-49] recently. QTAIM-DFA will provide an excellent possibility to evaluate, understand, and classify weak to strong interactions in a unified form.

He considers QTAIM-DFA to be well-suited to clarify the dynamic and static behavior of the E–E' and E---E' interactions (E, E' = S, Se, Te, and O). The structures of **7-1**$^{\bullet+}$ and **7-1**$^{2+}$ are investigated and some pictures for the E---E' interactions are proposed, so far. However, the nature of the E---E' interactions must be clarified further for the better understanding of the phenomena derived from the interactions with physical necessity. Here he reports the behavior of the E---E' interactions in **7-1**$^{\bullet+}$ and **7-1**$^{2+}$, together with **7-1**, by applying QTAIM-DFA. The behavior of E---E' in **7-1**$^{\bullet+}$ and **7-1**$^{2+}$ must be closely related to that of E–E' in the neutral and ionic forms of *cyclo*-1,2-EE'$(CH_2)_3$ (**7-2**: E, E' = S, Se, Te, and O), together with HEE'H and MeEE'Me, reported recently by applying QTAIM-DFA.[50]

His research group also proposed the concept of "the dynamic nature of interactions" originated from the data containing the perturbed structures.[47a,48,49] Data from the fully optimized structures correspond to the static nature of interactions. QTAIM-DFA is applied to typical chemical bonds and interactions, and rough criteria have been established, which can distinguish the chemical bonds and interactions in question from others. QTAIM-DFA and the criteria are explained in Chapter 2, employing Schemes 2-1–2-3, Figure 2-1 and eqs (2-8)–(2-12). The basic concept of the QTAIM approach is also surveyed in Chapter 2.

Methodological Details in Calculations

Neutral, radical cationic, and dicationic forms of **7-1** (**7-1**, **7-1**$^{\bullet+}$, and **7-1**$^{2+}$, respectively) were optimized using the Gaussian 09 program package.[51] Calculations are performed employing the 6-311+G(3df)[52] basis sets for O, S, and Se, that of the (7433111/743111/7411/2 + 1s1p1d1f) type[53] for Te, and the 6-311G+(d,p) basis sets for C and H at the Møller-Plesset second order energy correlation level (MP2),[54] after examination of the calculation method. Applicability of the basis set systems and levels was examined, employing the observed E---E distances of **7-1a**$^{2+}$ (E = S) and **7-1d**$^{2+}$ (E = Se), of which structures were determined by the X-ray crystallographic analysis. They were the **CB** form[13] and the **CC** form with substantial deformations,[14] respectively. Two basis set systems (BSSs) were

examined. One is called BSS-A, which are the 6-311+G(3d) basis set for O, S, and Se with the 6-311+G(d,p) basis set for C and H (BSS-A). Another is BSS-B, which are the 6-311+G(3df) basis set for O, S, and Se with the 6-311+G(d,p) basis set for C and H. Various levels were also examined for MP2,[54] M06-2X,[55] M06,[55] LC-wPBE,[56] CAM-B3LYP,[57,58] and B3LYP.[59,60] The results for **7-1a**$^{2+}$ and **7-1d**$^{2+}$ are given in Tables 7-A1 and 7-A2 of the Appendix, respectively. Calculation method with BSS-B at the MP2 level is selected for the evaluations as mentioned above, since the magnitudes between the predicted and observed E---E' distances seem less than 0.01 Å or around the value, although the counter ions near the cationic species and/or the crystal packing effect are not considered in the examinations.[13,14,26] Unrestricted MP2 method (UMP2)[61] is applied to the odd electron system of **7-1**$^{\bullet+}$. The structures were confirmed by the frequency analysis performed on the optimized structures.

QTAIM functions were calculated using the Gaussian 09 program package[51] with the same method of the optimizations. The results were analyzed with the AIM2000 program.[62] Normal coordinates of internal vibrations (NIV) obtained by the frequency analysis were employed to generate the perturbed structures.[49] The method is explained in Chapter 2.

Results and Discussion

Structural Feature in Neutral and Charged Forms of 1,5-Di(chalcogena)canes, 7-1, 7-1$^{\bullet+}$, and 7-1^{2+}

1,5-Di(chalcogena)canes of the neutral, radical cationic, and dicationic forms, **7-1a**–**7-1j**, **7-1a**$^{\bullet+}$–**7-1j**$^{\bullet+}$, and **7-1a**$^{2+}$–**7-1j**$^{2+}$, are optimized with BSS-B at the MP2 level. Table 7-1 collects the E---E', E–C_C, and E'–$C_{C'}$ distances (r(E, E'), r(E, C_C), r(E', $C_{C'}$), respectively) for the **CB** forms of the optimized structures of **7-1a**–**1j**, **7-1a**$^{\bullet+}$–**7-1j**$^{\bullet+}$, and **7-1a**$^{2+}$–**7-1j**$^{2+}$, where C_C stands for the carbon atoms adjacent to E and E' in the chair ring. The notation, containing points M and M', is illustrated in the footenote of Table 7-1, modeled by **7-1**$^{2+}$.

It would be instructive to compare the *r*(E, E') values of **7-1a**–**7-1j**, **7-1a**$^{\bullet+}$–**7-1j**$^{\bullet+}$, and **7-1a**$^{2+}$–**7-1j**$^{2+}$ with the corresponding values of **7-2a**–**7-2j**. Therefore, the Δ*r*(E, E') values [= *r*(E, E': **7-1*x****) – *r*(E, E': **7-2*x***); ***x*** = **a**–**j** and * = null, •+, and 2+] are also shown in Table 7-1, where *r*(E, E': **7-2*x***) are expected to be very close to the sum of covalent radii of E and E' (r_{cov}(E) + r_{cov}(E')). Table 7-1 also collects the angles (∠E'EM and ∠EE'M') and torsional angles (ϕ(MEE'M')) for **7-1a**–**7-1j**, **7-1a**$^{\bullet+}$–**7-1j**$^{\bullet+}$, and **7-1a**$^{2+}$–**7-1j**$^{2+}$, where a point M is put at the midpoint between C_C and C_B, adjacent to E and a point M' at the midpoint between $C_{C'}$ and $C_{B'}$, adjacent to E' (see footnote of Table 7-1).

Table 7-1. Distances, angles, and torsional angles for neutral and charged forms of *cyclo*-E($CH_2CH_2CH_2$)$_2$E' (**7-1**) (**CB**), together with relative energies, optimized with BSS-B at the MP2 level[a]

species (E, E')	r(E, E') (Å)	Δr(E, E')[b] (Å)	r(E, C_C)[c] (Å)	r(E', C_C')[d] (Å)	∠E'EM (°)	∠EE'M' (°)	ϕ(MEE'M') (°)	ΔE[e] (eV)	sym-metry
neutral species									
1a (S, S)	3.4093	1.3270	1.8172	1.8172	69.7	69.7	0.0	as 0.00	C_s
1b (S, Se)	3.7499	1.5081	1.8160	1.9510	72.1	39.5	11.4	as 0.00	C_1
1c (S, Te)	3.7372	1.3243	1.8185	2.1495	78.3	41.4	11.3	as 0.00	C_1
1d (Se, Se)	3.5740	1.0422	1.9555	1.9555	67.5	67.5	0.0	as 0.00	C_s
1e (Se, Te)	3.8176	1.2769	1.9808	2.2062	78.5	45.0	11.9	as 0.00	C_1
1f (Te, Te)	3.8244	1.0946	2.1541	2.1541	47.4	46.4	0.0	as 0.00	C_s
1g (O, O)	2.8557	1.3941	1.4211	1.4211	79.6	79.6	0.0	as 0.00	C_s
1h (O, S)	3.0965	1.3965	1.4206	1.8172	91.3	61.2	–0.5	as 0.00	C_1
1i (O, Se)	3.1740	1.3292	1.4209	1.9546	96.1	54.8	1.8	as 0.00	C_1
1j (O, Te)	3.2475	1.2497	1.4216	2.1511	103.8	47.4	2.8	as 0.00	C_1
radical cationic species									
1a$^{\bullet+}$ (S, S)	2.7049	0.6226	1.8145	1.8145	85.8	85.8	0.0	6.81	C_s
1b$^{\bullet+}$ (S, Se)	2.7783	0.5365	1.8180	1.9522	88.3	80.7	–0.4	6.69	C_1
1c$^{\bullet+}$ (S, Te)	2.9068	0.4939	1.8216	2.1439	92.4	72.7	–0.5	6.47	C_1
1d$^{\bullet+}$ (Se, Se)	2.8730	0.5059	1.9552	1.9552	82.7	82.7	0.0	6.53	C_s
1e$^{\bullet+}$ (Se, Te)	3.0094	0.4687	1.9587	2.1465	86.3	74.6	–0.1	6.26	C_1
1f$^{\bullet+}$ (Te, Te)	3.1814	0.4516	2.1504	2.1504	77.6	77.6	0.0	6.09	C_s
1g$^{\bullet+}$ (O, O)	2.3546	0.8930	1.4118	1.4118	95.1	95.1	0.0	8.35	C_s
1h$^{\bullet+}$ (O, S)	2.3410	0.6410	1.4470	1.8014	115.1	78.7	–3.0	7.49	C_1
1i$^{\bullet+}$ (O, Se)	2.4232	0.5784	1.4462	1.9419	118.2	73.1	–3.6	7.25	C_1
1j$^{\bullet+}$ (O, Te)	2.5096	0.5118	1.4479	2.1333	124.3	66.0	–5.8	6.80	C_1
dicationic species									
1a^{2+} (S, S)	2.1373	0.0550	1.8353	1.8353	99.0	99.0	0.0	18.16	C_s
1b^{2+} (S, Se)	2.2619	0.0201	1.8398	1.9712	99.5	92.4	–1.3	17.87	C_1
1c^{2+} (S, Te)	2.4513	0.0384	1.8482	2.1476	99.7	84.5	–2.2	17.36	C_1
1d^{2+} (Se, Se)	2.3770	0.0099	1.9768	1.9768	93.3	93.3	0.0	17.54	C_s
1e^{2+} (Se, Te)	2.5592	0.0185	1.9856	2.1536	93.7	85.7	–1.2	16.97	C_1
1f^{2+} (Te, Te)	2.7504	0.0206	2.1639	2.1639	86.1	86.1	0.0	16.53	C_s
1g^{2+} (O, O)	2.3257	0.8641	1.4054	1.4054	95.2	95.2	0.0	21.72	C_s
1h^{2+} (O, S)	1.7271	0.0271	1.5616	1.8030	131.2	97.0	–0.7	19.62	C_1
1i^{2+} (O, Se)	1.8690	0.0242	1.5479	1.9419	130.0	89.7	–3.9	19.26	C_1
1j^{2+} (O, Te)	2.0396	0.0418	1.5373	2.1199	131.5	80.9	–5.4	18.42	C_1

[a] For BSS-B: The 6-311+G(3df) basis set for O, S, and Se and that of the (7433111/743111/7411/2 + 1s1p1d1f) type for Te with the 6-311+G(d,p) basis set for C and H. [b] Δr(E, E') = r(E, E': **7-1*x****) – r(E, E': **7-2*x***), where ***x*** = **a**–**j** and * = null, •+, and 2+. [c] r(E, C_C) = r(E', $C_{C'}$). [d] r(E, C_B) = r(E', $C_{B'}$). [e] ΔE = E (**7-1*x****) – E (**7-1*x***), where ***x*** = **a**–**j** and * = •+ and 2+.

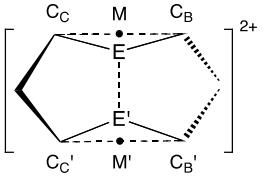

Figure 7-4 shows the plot of r(E, E') for **7-1a**–**7-1j**, **7-1a**$^{\bullet+}$–**7-1j**$^{\bullet+}$, and **7-1a**$^{2+}$–**7-1j**$^{2+}$, together with **7-2a**–**7-2j**. The r(E, E') values for **7-2a**–**7-2j** increase in the order of **7-2g** < **7-2h** < **7-2i** < **7-2j** < **7-2a** < **7-2b** < **7-2d** < **7-2c** < **7-2e** < **7-2f**, where the order seems irregular around **7-2d** and **7-2c** (see, Figure 7-5 and Table 7-1). The r(E, E') values of **7-1a**$^{2+}$–**7-1j**$^{2+}$ are very close to the corresponding values of **7-2a**–**7-2j**, except for **7-1g**$^{2+}$ (O, O). The Δr(O, O) value of 0.86 Å for **7-1g**$^{2+}$ is only slightly less than Δr(O, O) for **7-1g**$^{\bullet+}$ (0.89 Å), where Δr(E, E') are 0.01–0.06 Å for **7-1a**$^{2+}$–**7-1j**$^{2+}$. The E---E' σ(2c–2e) interactions in **7-1a**$^{2+}$–**7-1j**$^{2+}$ must be very close to the corresponding interactions in **7-2a**–**7-2j**, respectively, except for that in **7-1g**$^{2+}$ (O, O) versus **7-2g** (O, O). The O---O interaction in **7-1g**$^{2+}$ (O, O) must be analyzed carefully. The plot for **7-1a**$^{\bullet+}$–**7-1j**$^{\bullet+}$ seems parallel to that of **7-2a**–**7-2j**, although the data for **7-1g**$^{\bullet+}$ (O, O) deviate somewhat upside from that expected (Figure 7-5). The Δr(E, E') values are 0.45–0.64 Å for **7-1a**$^{\bullet+}$–**7-1j**$^{\bullet+}$ and **7-1h**$^{\bullet+}$–**7-1j**$^{\bullet+}$, although Δr(E, E') = 0.89 Å for **7-1g**$^{\bullet+}$. The value for **7-1g**$^{\bullet+}$ is somewhat larger than the value of 0.78 Å for HOOH$^{\bullet-}$.[50]

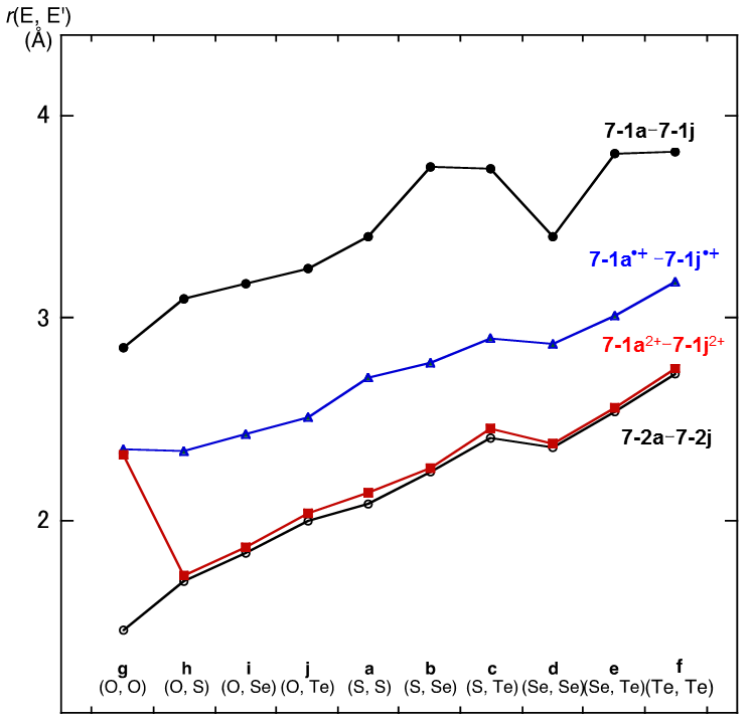

Figure 7-4. Plots of r(E, E') for **7-1a**–**7-1j**, **7-1a**$^{\bullet+}$–**7-1j**$^{\bullet+}$, and **7-1a**$^{2+}$–**7-1j**$^{2+}$, together with **7-2a**–**7-2j**.

The plot for **7-1a**–**7-1j** seems almost paralell to that of **7-2a**–**2j** (Figure 7-5). The Δ*r*(E, E') values are predicted to be 1.04–1.51 Å for σ(2c–4e) in **7-1a**–**7-1j**, where the values are small for **7-1d** (Se, Se) (1.04 Å) and **7-1f** (Te, Te) (1.10 Å) but large for **7-1b** (S, Se) (1.51 Å). The disadvantageous conditions are suggested for S---Se of **7-1b**. Indeed, the large values must be the reflection of the weak E---E' transannular interactions, but the some sterically disadvantageous conditions must also be important for the predicted values. The Δ*r*(E, E') values of σ(2c–4e) in **7-1a**–**7-1j (**1.04–1.51 Å**)** decrease in the formation of σ(2c–3e) in **7-1a**$^{\bullet+}$–**7-1f**$^{\bullet+}$, of which values are 0.45–0.64 Å with 0.89 Å for **7-1g**$^{\bullet+}$ (O, O). The values become much smaller for the formation of σ(2c–2e) in **7-1a**$^{2+}$–**7-1j**$^{2+}$ (0.01–0.06 Å), except for **7-1g**$^{2+}$ (O, O) (0.86 Å). The behavior of E---E' σ(2c–2e) in **7-1a**$^{2+}$–**7-1j**$^{2+}$ must be very close to that in **7-2a**–**7-2j**, except for **7-1g**$^{2+}$ (O, O) versus **7-2g** (O, O).

The ∠E'EM and ∠EE'M' values are closely related to the directions of n_p(E) and n_p(E') towards E' and E, respectively. They will overlap effectively if the angles are close to 90º. While ∠E'EM and ∠EE'M' in **7-1a**$^{2+}$–**7-1g**$^{2+}$ are 86º–100º and 85º–99º, respectively, those in **7-1h**$^{2+}$–**7-1j**$^{2+}$ are 130º–132º and 81º–97º, respectively. The values are the desirable range of around 90º, except for ∠E'EM in **7-1h**$^{2+}$–**7-1j**$^{2+}$. Similarly, ∠E'EM and ∠EE'M' in **7-1a**$^{\bullet+}$–**7-1g**$^{\bullet+}$ are 77º–95º and 72º–95º, respectively, whereas those in **7-1h**$^{\bullet+}$–**7-1j**$^{\bullet+}$ are 115º–125º and 66º–79º, respectively. The values seem acceptable. ∠E'EM in **7-1h**$^{2+}$–**7-1j**$^{2+}$ of 130º–132º are larger than 90º by over 40º, which seem too large to be accepted, at first glance, although the differences are less than 45º. While ∠E'EM (= ∠EE'M') for **7-1a** (S, S), **7-1d** (Se, Se), and **7-1g** (O, O) are close to 70º, 70º, and 80º, respectively, that for **1f** (Te, Te) is 47º in the average. On the other hand, ∠EE'M' for **7-1b** (S, Se) is close to 39.5º, which is the smallest as shown in Table 7-1. Some ∠E'EM and/or ∠EE'M' values seem smaller than the acceptable range for **7-1a**–**7-1j**. The disadvantageous geometry for the S---Se interaction in **7-1b** must decrease the effective overlap between the p-type lone pair orbitals of S and Se. On the other hand, the torsional angle ∅(MEE'M') is less than 12º for all the species.

How are the energies in the formation of the radical cations (**7-1a**$^{\bullet+}$–**7-1j**$^{\bullet+}$) and dications (**7-1a**$^{2+}$–**7-1j**$^{2+}$) from the corresponding neutral species (**7-1a**–**7-1j**)? The Δ*E* values are evaluated for **7-1a**$^{\bullet+}$–

7-1j$^{\bullet+}$ [ΔE (**7-1a**$^{\bullet+}$–**7-1j**$^{\bullet+}$) = E (**7-1a**$^{\bullet+}$–**7-1j**$^{\bullet+}$) – E (**7-1a**–**7-1j**)] and **7-1a**$^{2+}$–**7-1j**$^{2+}$ [ΔE (**7-1a**$^{2+}$–**7-1j**$^{2+}$) = E (**7-1a**$^{2+}$–**7-1j**$^{2+}$) – E (**7-1a**–**7-1j**)], using the E values in Table 7-1. Similarly, ΔE (**7-1a'**$^{\bullet+}$–**7-1j'**$^{\bullet+}$) [= E (**7-1a'**$^{\bullet+}$–**7-1j'**$^{\bullet+}$) – E (**7-1a**–**7-1j**)] and ΔE (**7-1a'**$^{2+}$–**7-1j'**$^{2+}$) [= E (**7-1a'**$^{2+}$–**7-1j'**$^{2+}$) – E (**7-1a**–**7-1j**)] are also evaluated, where E (**7-1a'**$^{\bullet+}$–**7-1j'**$^{\bullet+}$) and E (**7-1a'**$^{2+}$–**7-1j'**$^{2+}$) stand for the energies of the radical cations and dications evaluated employing the fully optimized structures of **7-1a**–**7-1j**. The ΔE (**7-1a**$^{\bullet+}$–**7-1j**$^{\bullet+}$), ΔE (**7-1a**$^{2+}$–**7-1j**$^{2+}$), ΔE (**7-1a'**$^{\bullet+}$–**7-1j'**$^{\bullet+}$), ΔE (**7-1a'**$^{2+}$–**7-1j'**$^{2+}$), and $-\varepsilon_{HOMO}$ (**7-1a**–**7-1j**) values are collected in Table 7-A3 in the Appendix, together with the differences between them. Figure 7-5 shows the plot of ΔE (**7-1a**$^{\bullet+}$–**7-1j**$^{\bullet+}$), ΔE (**7-1a**$^{2+}$–**7-1j**$^{2+}$), ΔE (**7-1a'**$^{\bullet+}$–**7-1j'**$^{\bullet+}$), ΔE (**7-1a'**$^{2+}$–**7-1j'**$^{2+}$), and $-\varepsilon_{HOMO}$ (**7-1a**–**7-1j**). The $\Delta\varepsilon_{HOMO}$ (**7-1a'**$^{\bullet+}$–**7-1j'**$^{\bullet+}$) values in Table 7-A3 correspond to the differences between $-\varepsilon_{HOMO}$ (**7-1a**–**7-1j**) and ΔE (**7-1a'**$^{\bullet+}$–**7-1j'**$^{\bullet+}$) in Figure 7-5 (for the longitudinal axis direction).

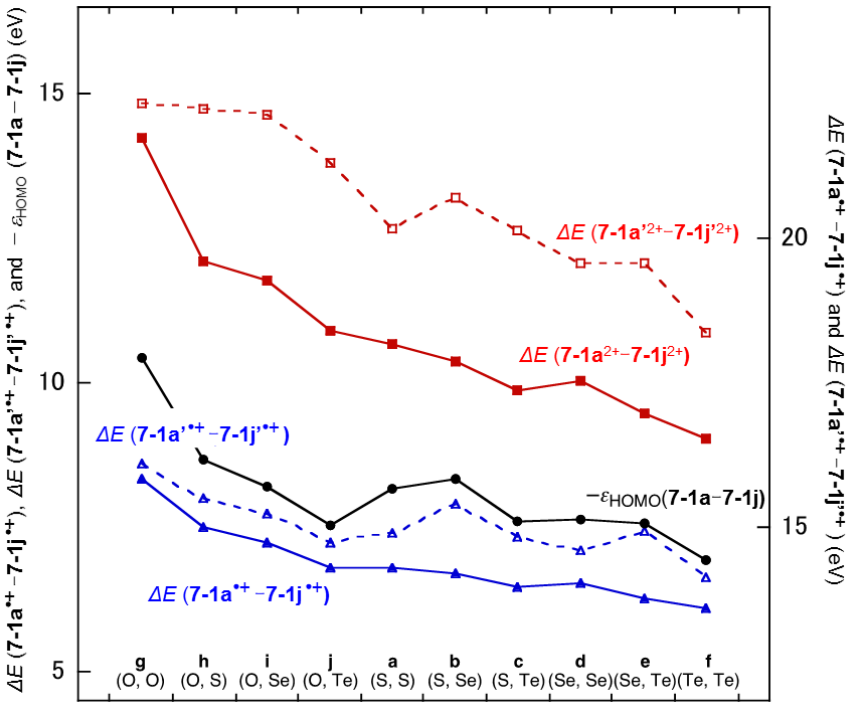

Figure 7-5. Plots of ΔE (**7-1a**$^{\bullet+}$–**7-1j**$^{\bullet+}$) (▲), ΔE (**7-1a'**$^{\bullet+}$–**7-1j'**$^{\bullet+}$) (△), ΔE (**7-1a**$^{2+}$–**7-1j**$^{2+}$) (■), ΔE (**7-1a'**$^{2+}$–**7-1j'**$^{2+}$) (□), and $-\varepsilon_{HOMO}$ (**7-1a**–**7-1j**) (●). The solid lines connect the energies or energy differences for the optimized structures, whereas the dotted lies do those evaluated employing the optimized structures of **7-1a**–**7-1j**.

Each of **7-1a''**$^{+}$–**7-1j''**$^{+}$ is stabilized through the redistribution of the remained electrons after the removal of an electron from each of **7-1a**–**7-1j**, in the same structure, which is estimated to be 0.13–1.83eV through $\Delta\varepsilon_{HOMO}$ (**7-1a''**$^{+}$–**7-1j''**$^{+}$) [= $-\varepsilon_{HOMO}$ (**7-1a**–**7-1j**) – ΔE (**7-1a''**$^{+}$–**7-1j''**$^{+}$)]. The stabilization energies for **7-1a**$^{\bullet+}$–**7-1j**$^{\bullet+}$ from **7-1a''**$^{+}$–**7-1j''**$^{+}$ through the structural change with the redistribution of the remained electrons after the one electron removal are also estimated by $\Delta\Delta E$ (**7-1a''**$^{+}$–**7-1j''**$^{+}$) of 0.25–1.21 eV. Similarly, the stabilization energies for **7-1a**$^{2+}$–**7-1j**$^{2+}$ from **7-1a'**$^{2+}$–**7-1j'**$^{2+}$ through the structural change with the redistribution of the remained electrons are estimated to be 0.61–2.89 eV by $\Delta\Delta E$ (**7-1a'**$^{2+}$–**7-1j'**$^{2+}$), which occur after two electron removal from each of **7-1a**–**7-1j**.

Figure 7-6 shows the plot of ΔE (**7-1a''**$^{+}$–**7-1j''**$^{+}$) versus $-\varepsilon_{HOMO}$, which is well analyzed by dividing the data into three groups. Data of **a** (S, S), **d** (Se, Se), and **f** (Te, Te) make Group **I** (G(**I**)), those of **b** (S, Se), **c** (S, Te), and **e** (Se, Te) do Group **II** (G(**II**)), and those of **g** (O, O), **h** (O, S), **i** (O, Se), and **j** (O, Te) belong to Group **III** (G(**III**)). The correlations are given in the figure. The removal of an electron and the redistribution of the remained electrons will occur equally on E and E' in G(**I**). The properties of E would be close to E' in G(**II**), therefore, the process is expected to occur not equally but not so differently on E and E'. As a result, the behavior would be different from those in G(**I**), although slightly. The mechanism in G(**III**) would be substantially different from those in G(**I**) and G(**II**). The process for the removal of an electron and the redistribution of the remained electrons would hardly occur on E = O in G(**III**), where (E, E') = (O, O) also belongs to G(**III**).

The plot of ΔE (**7-1a**$^{\bullet+}$–**7-1j**$^{\bullet+}$) versus $-\varepsilon_{HOMO}$ is drawn in Figure 7-A1 of the Appendix, which is very similar to that shown in Figure 7-6. The plot in Figure 7-A1 is similarly analyzed as three correlations. The correlations are shown in Table 7-A4 of the Appendix (entries 1–3). The plot of ΔE (**7-1a**$^{\bullet+}$–**7-1j**$^{\bullet+}$) versus ΔE (**7-1a''**$^{+}$–**7-1j''**$^{+}$) is similarly shown in Figure 7-A2 of the Appendix. A good correlation is obtained for G(**I**) + G(**III**), although data of G(**II**) deviate form the correlation. The correlation is given in Table 7-A4 (entry 4). The plot of ΔE (**7-1a**$^{2+}$–**7-1j**$^{2+}$) versus ΔE (**7-1a**$^{\bullet+}$–**7-1j**$^{\bullet+}$) is displayed in Figure 7-A3 of the Appendix. The plot is well analyzed as a correlation without

deviation, which is given in Table 7-A4 (entry 5). It is worthwhile to comment that ΔE (**7-1a**$^{2+}$–**7-1j**$^{2+}$) are well correlated to ΔE (**7-1a**$^{\bullet+}$–**7-1j**$^{\bullet+}$), irrespective of the irregular behavior of r(O, O) in **7-1g**$^{2+}$.

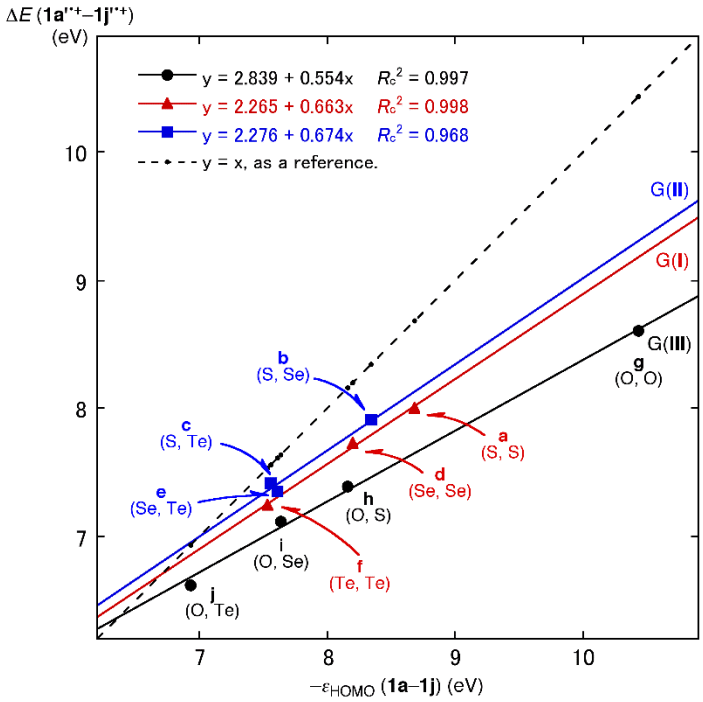

Figure 7-6. Plot of ΔE (**7-1a**$'^{\bullet+}$–**7-1j**$'^{\bullet+}$) versus $-\varepsilon_{HOMO}$ (**7-1a**–**7-1j**), which are analyzed as three correlations.

Survey of the E---E' Interactions in 7-1, 7-1$^{\bullet+}$, and 7-1^{2+}

The E---E' interactions are surveyed exemplified by E = E' = Se in the **CB** structures of **7-1**, **7-1**$^{\bullet+}$, and **7-1**$^{2+}$, which are denoted by **7-1d** (**CB**), **7-1d**$^{\bullet+}$ (**CB**), and **7-1d**$^{2+}$ (**CB**), respectively. The structures are optimized retaining the C_s symmetry, therefore, the E---E' interactions can be easily visualized. Figure 7-7 draws energy diagrams of ψ_{54}–ψ_{59} for **7-1d** (**CB**), **7-1d**$^{\bullet+}$ (**CB**), and **7-1d**$^{2+}$ (**CB**). HOMO-4, HOMO-3, HOMO-2, HOMO-1, HOMO, and LUMO correspond to **7-1d** (**CB**), $\psi_{54}(\alpha)$–$\psi_{59}(\alpha)$ and $\psi_{54}(\beta)$–$\psi_{59}(\beta)$ to **7-1d**$^{\bullet+}$ (**CB**), and HOMO-3, HOMO-2, HOMO-1, HOMO, LUMO, and LUMO+1 to **7-1d**$^{2+}$ (**CC**). Each $\psi_i(\alpha)$ is more stable than $\psi_i(\beta)$ in **7-1**$^{\bullet+}$, since the number of α-spin electrons is assumed to be larger than that of β-spin electrons by one, resulting in the larger

contribution from the exchange integrals between the α-spin electrons to the α-spin MO energies. Consequently, ψ_{58} (HOMO) of **7-1d** (**CB**) will split into $\psi_{58}(\alpha)$ and $\psi_{58}(\beta)$ in **7-1d**$^{\bullet+}$ (**CB**), after removal of an electron from **7-1d** (**CB**). In this case, $\psi_{58}(\alpha)$ and $\psi_{58}(\beta)$ have the characters of HOMO and LUMO, respectively, although $\psi_{58}(\alpha)$ should be called SOMO (singly occupied molecular orbital).

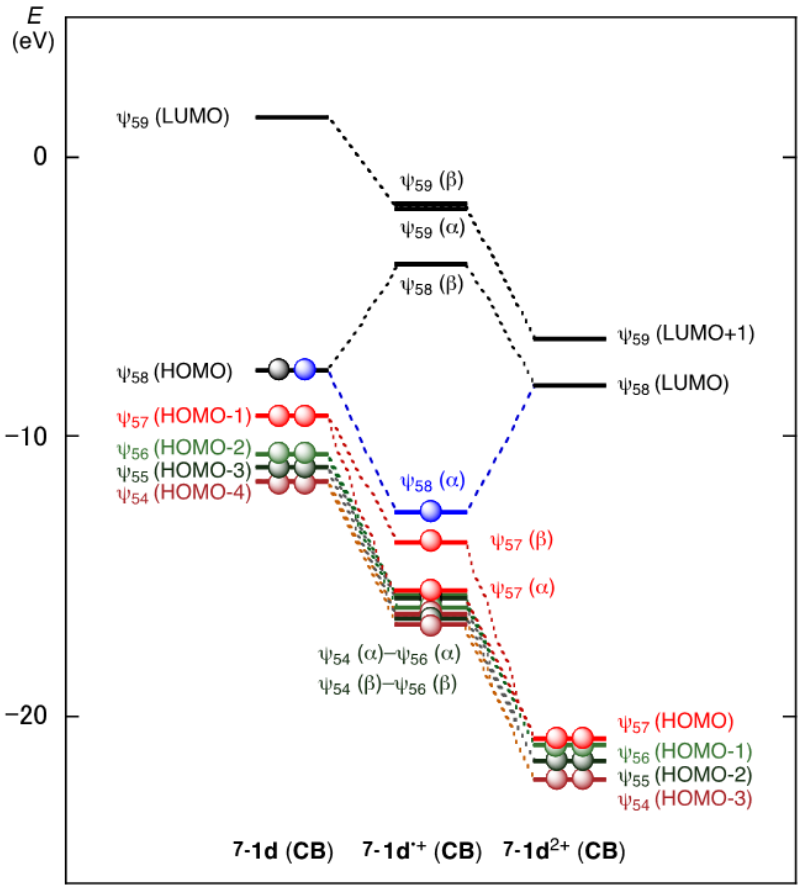

Figure 7-7. Energy diagram, drawn exemplified by **7-1d** (**CB**), **7-1d**$^{\bullet+}$ (**CB**), and **7-1d**$^{2+}$ (**CB**).

Figure 7-8 shows ψ_{57}(HOMO-1) and ψ_{58}(HOMO) of **7-1d** (**CB**), ψ_{57}(β: HOMO-1: SOMO) and ψ_{58}(α: HOMO: SOMO) of **7-1d**$^{\bullet+}$ (**CB**), and ψ_{54}(HOMO-3) and ψ_{58}(LUMO) of **7-1d**$^{2+}$ (**CB**). The Se---Se interactions in ψ_{58}(HOMO) of **7-1d** (**CB**), ψ_{58}(α: HOMO) of **7-1d**$^{\bullet+}$ (**CB**), and ψ_{58}(LUMO) of **7-1d**$^{2+}$ (**CB**) have the n_p(Se) – n_p(Se) character, whereas those in ψ_{57}(HOMO-1) of **7-1d** (**CB**), ψ_{57}(β: HOMO-1) of **7-1d**$^{\bullet+}$ (**CB**), and ψ_{54}(HOMO-3) of **7-1d**$^{2+}$ (**CB**) have the n_p(Se) + n_p(Se) character. One

may expect that the typical interactions of the n_p(Se) + n_p(Se) character should appear in HOMO for **7-1d**$^{2+}$ (**CB**), at first glance. However, the character in **7-1d**$^{2+}$ (**CB**) is not predicted for HOMO but mainly for HOMO-3 by the MP2 calculations. The n_p(Se) orbitals in **7-1d**$^{2+}$ (**CB**) is so stabilized, due to the high positive charge developed on each Se (*Qn*(Se) = 0.877), that they interact with MOs of the CH_2 groups. Consequently, the MO character of the n_p(Se) + n_p(Se) type will spread over not only HOMO-3 but also HOMO-2, and HOMO-1 in **7-1d**$^{2+}$ (**CB)**, although not shown.

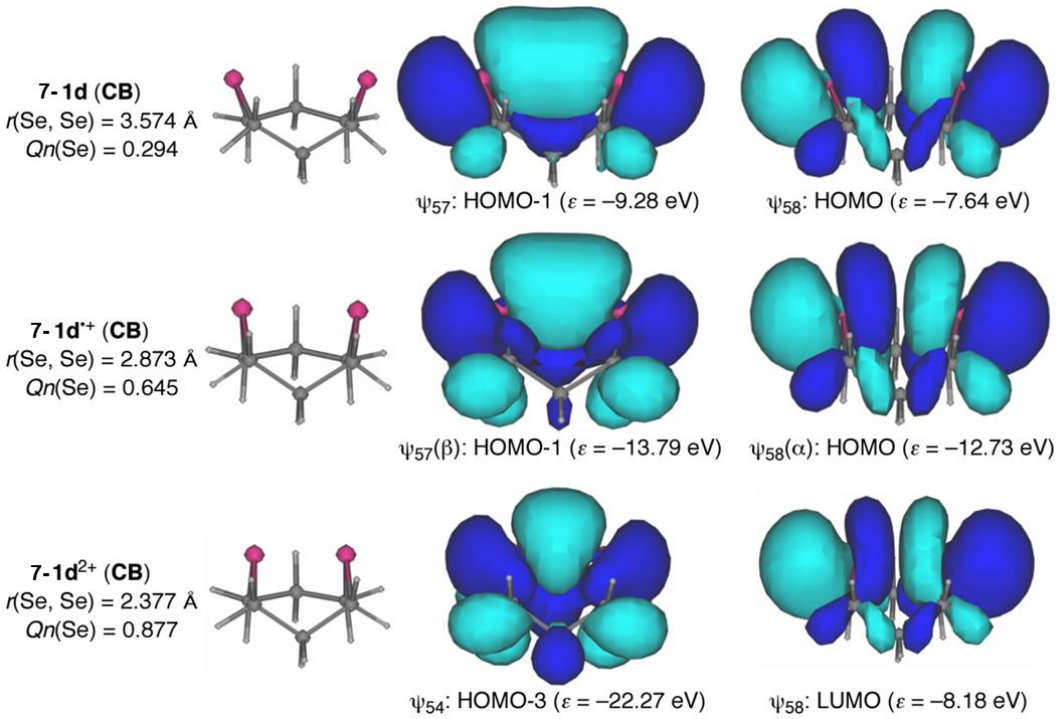

Figure 7-8. Typical n_p(Se)---n_p(Se) interactions in **7-1** (**CB**), **7-1**$^{\bullet+}$ (**CB**), and **7-1**$^{2+}$ (**CB**). Orbital energies, distances of Se---Se, and charges developed on Se are also given.

The Se-∗-Se interactions in **7-1d** (**CB**), **7-1d**$^{\bullet+}$ (**CB**), and **7-1d**$^{2+}$ (**CB**) can be explained by the σ(2c–4e), σ(2c–3e), and σ(2c–2e) models, respectively (*cf*: Figure 7-3 for the E---E' interactions in **7-1**, **7-1**$^{\bullet+}$, and **7-1**$^{2+}$). It must be difficult for the E---E' interactions in **7-1** to stabilize through the orbital overlaps, due to the high disadvantageous exchange repulsive factors of σ(2c–4e). On the other hand, the E---E' σ(2c–2e) interactions in **7-1**$^{2+}$ will be much stabilized through the orbital overlaps due to the advantageous exchange factors. The E---E' σ(2c–3e) interactions in **7-1**$^{\bullet+}$ must be

intermediate between σ(2c–4e) in **7-1** and σ(2c–2e) in **7-1**$^{2+}$.

After clarifying the basic structural feature, QTAIM-DFA is applied to the E---E' interactions in **7-1a**–**7-1j**, **7-1a**$^{\bullet+}$–**7-1j**$^{\bullet+}$, and **7-1a**$^{2+}$–**7-1j**$^{2+}$, next.

Molecular Graphs, Contour Plots, Negative Laplacians, and Trajectory Plots Around the E-∗-E' Interactions

Figure 7-9 shows the molecular graphs, exemplified by **7-1d** (**CB**), **7-1d**$^{\bullet+}$ (**CB**), and **7-1d**$^{2+}$ (**CB**). All BCPs expected are detected, containing those between the Se-∗-Se atoms. Figure 7-11 shows the contour plots, exemplified by **7-1d** (**CB**), **7-1d**$^{\bullet+}$ (**CB**), and **7-1d**$^{2+}$ (**CB**). The maps are drawn on the planes constructed by the C–Se–Se–C atoms in **7-1d** (**CB**), **7-1d**$^{\bullet+}$ (**CB**), and **7-1d**$^{2+}$ (**CB**), where two Se atoms, two C atoms, a BCP on the Se-∗-Se interaction, and two BCPs on the Se–C bonds are located on each plane. The contour plots for **7-1d** (**CB**), **7-1d**$^{\bullet+}$ (**CB**), and **7-1d**$^{2+}$ (**CB**) create the characteristic Se-∗-Se interactions of the σ(2c–4e), σ(2c–3e), and σ(2c–2e) types, respectively.

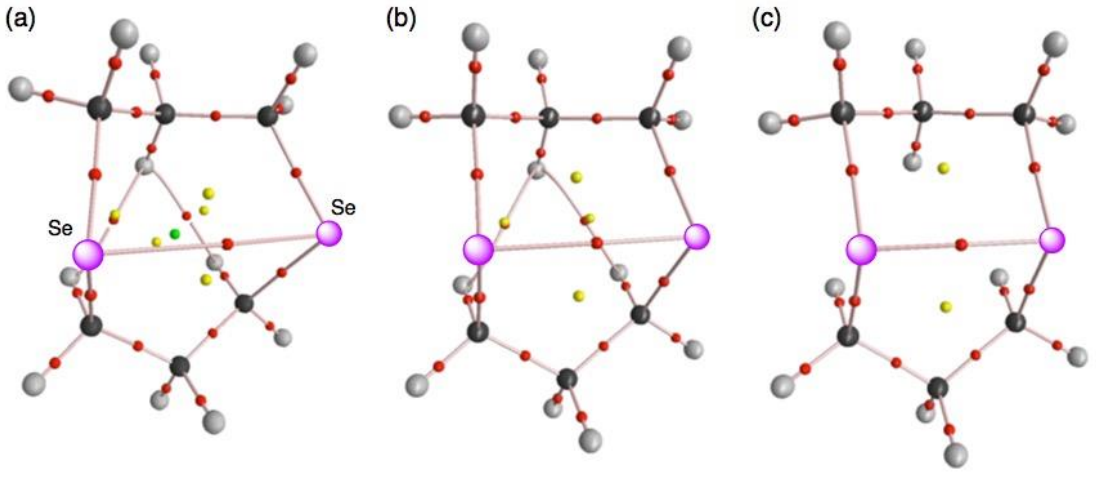

Figure 7-9. Molecular graphs for **7-1d** (**CB**) (a), **7-1d**$^{\bullet+}$ (**CB**) (b), and **7-1d**$^{2+}$ (**CB**) (c). Bond paths are denoted by solid lines, BCPs are denoted by small red balls on the bond path, together with ring critical points (small yellow balls) and cage critical points (small lime green balls).

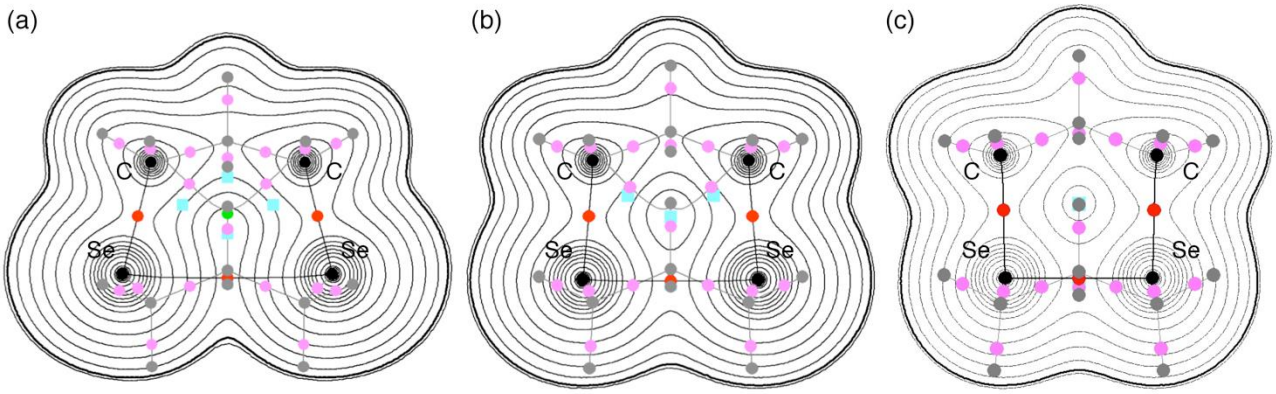

Figure 7-10. Contour plots of $\rho_b(\boldsymbol{r}_c)$ drawn on the C–Se–Se–C plane for **7-1d** (**CB**) (a), **7-1d**$^{\bullet+}$ (**CB**) (b), and **7-1d**$^{2+}$ (**CB**) (c), together with BCPs (red solid circles on the plane and pink solid circles out of the plane), ring critical points (cyan solid squares out of the plane), cage critical points (lime green solid circles), critical points (black solid circles on the plane and gray solid circles out of the plane), and bond paths. The contours ($e a_0^{-3}$) are at 2^l (l = 8, 7, ..., 0) and 0.0047 (heavy line).

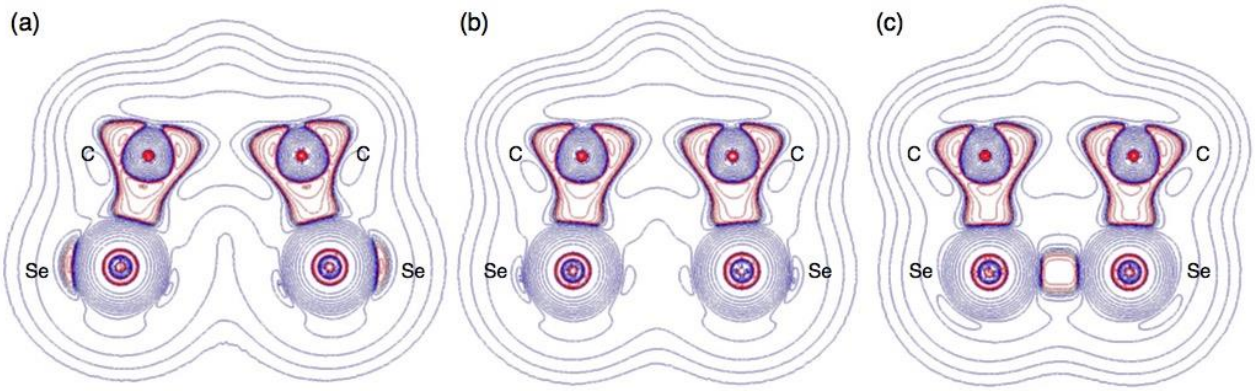

Figure 7-11. Negative Laplacians drawn on the C–Se–Se–C plane for **7-1d** (**CB**) (a), **7-1d**$^{\bullet+}$ (**CB**) (b), and **7-1d**$^{2+}$ (**CB**) (c), where the negative areas are shown in red and positive areas in blue.

Figure 7-11 draws negative Laplacians, exemplified by **7-1d** (**CB**), **7-1d**$^{\bullet+}$ (**CB**), and **7-1d**$^{2+}$ (**CB**). The BCPs between Se-∗-Se of **7-1d** (**CB**) and **7-1d**$^{\bullet+}$ (**CB**) exist in the blue area, whereas that of **7-1d**$^{2+}$ (**CB**) in the red area, which means that the Se-∗-Se interactions are classified as the CS interactions for the former two, whereas that of the latter as the SS interactions. Trajectory plots are similarly drawn for **7-1d** (**CB**), **7-1d**$^{\bullet+}$ (**CB**), and **7-1d**$^{2+}$ (**CB**) in Figures 7-A5 of the Appendix, where each space around the species are well fractionalized to the atoms. Figure 7-A6 of the Appendix depicts the Se---Se stretching modes of **7-1d** (**CB**), **7-1d**$^{\bullet+}$ (**CB**), and **7-1d**$^{2+}$ (**CB**), necessary to

generate the perturbed structures around the fully-optimized structures, for an example.

QTAIM-DFA Parameters of (R, θ) and (θ_p, κ_p), Evaluated for E-∗-E' in 7-1, 7-1$^{\bullet+}$, and 7-1^{2+}

QTAIM functions are calculated for $\rho_b(\boldsymbol{r}_c)$, $H_b(\boldsymbol{r}_c) - V_b(\boldsymbol{r}_c)/2$, $H_b(\boldsymbol{r}_c)$, and $k_b(\boldsymbol{r}_c)$ (=$V_b(\boldsymbol{r}_c)/G_b(\boldsymbol{r}_c)$) of E-∗-E' at BCP[63] in **7-1a**–**7-1j**, **7-1a**$^{\bullet+}$–**7-1j**$^{\bullet+}$, and **7-1a**$^{2+}$–**7-1j**$^{2+}$. Table 7-2 collects the values, although BCP of S-∗-Se is not detected for **7-1b**, maybe due to the disadvantageous steric reason. Figure 7-12 shows the plots of $H_b(\boldsymbol{r}_c) - V_b(\boldsymbol{r}_c)/2$ versus $H_b(\boldsymbol{r}_c)$ for the data of the fully-optimized structures, together with those of the perturbed structures around the fully-optimized ones. Figures 7-12a–7-12c correspond to the plots for **7-1a**–**7-1j**, **7-1a**$^{\bullet+}$–**7-1j**$^{\bullet+}$, and **7-1a**$^{2+}$–**7-1j**$^{2+}$, respectively. Data of a plot for each E-∗-E' interaction are connected by a regression curve, assuming the cubic function shown in eq (2-16), for **7-1a**–**7-1j**, **7-1a**$^{\bullet+}$–**7-1j**$^{\bullet+}$, and **7-1a**$^{2+}$–**7-1j**$^{2+}$. However, data of some plots are described as the line graph type if data cannot be connected as one-valued functions, such as those of **7-1h**$^{2+}$ (O-∗-S).[64] Figure 7-12d shows the similar plots for **7-2a**–**7-2j**, for convenience of comparison. Plots for **7-1a**$^{2+}$–**7-1j**$^{2+}$ in Figure 7-12c are very similar to those for **7-2a**–**7-2j** in Figure 7-12d, except for the plot for **7-1g**$^{2+}$ (O-∗-O) versus that **7-2g** (O-∗-O).

As shown in Figure 7-12a, all data of **7-1a**–**7-1j** appear in the *pure* CS region ($H_b(\boldsymbol{r}_c) - V_b(\boldsymbol{r}_c)/2 > 0$ and $H_b(\boldsymbol{r}_c) > 0$), except for those of **7-1f** (Te-∗-Te) and **7-1j** (O-∗-Te), which appear in the *regular* CS region ($H_b(\boldsymbol{r}_c) - V_b(\boldsymbol{r}_c)/2 > 0$ and $H_b(\boldsymbol{r}_c) < 0$). In the case of **7-1a**$^{\bullet+}$–**7-1j**$^{\bullet+}$, all data appear in the *regular* CS region, except for those of **7-1g**$^{\bullet+}$ (O-∗-O), which appear in the *pure* CS region (Figure 7-12b). On the other hand, data of **7-1a**$^{2+}$–**7-1f**$^{2+}$ and **7-1h**$^{2+}$ (O-∗-S) appear in the SS region ($H_b(\boldsymbol{r}_c) - V_b(\boldsymbol{r}_c)/2 < 0$ and $H_b(\boldsymbol{r}_c) > 0$), whereas those of **7-1i**$^{2+}$ (O-∗-Se) and **7-1j**$^{2+}$ (O-∗-Te) drop in the *regular* CS region with those of **7-1g**$^{2+}$ (O-∗-O) in the *pure* CS region.

QTAIM-DFA parameters of (R, θ) and (θ_p, κ_p) are obtained through analysis of the plots for **7-1a**–**7-1j**, **7-1a**$^{\bullet+}$–**7-1j**$^{\bullet+}$, and **7-1a**$^{2+}$–**7-1j**$^{2+}$, according to eqs (2-8)–(2-11) of Chapter 2. The (R, θ) and (θ_p, κ_p) values are collected in Table 7-2, together with the frequencies (ν) and force constants (k_f) corresponding to the E-∗-E' interactions in question.

The behavior of E-∗-E' in **7-1a**–**7-1j**, **7-1a**$^{\bullet+}$–**7-1j**$^{\bullet+}$, and **7-1a**$^{2+}$–**7-1j**$^{2+}$ is examined, next, employing the R, θ and θ_p values, mainly, together with those in Scheme 2-3 of Chapter 2, as a reference.

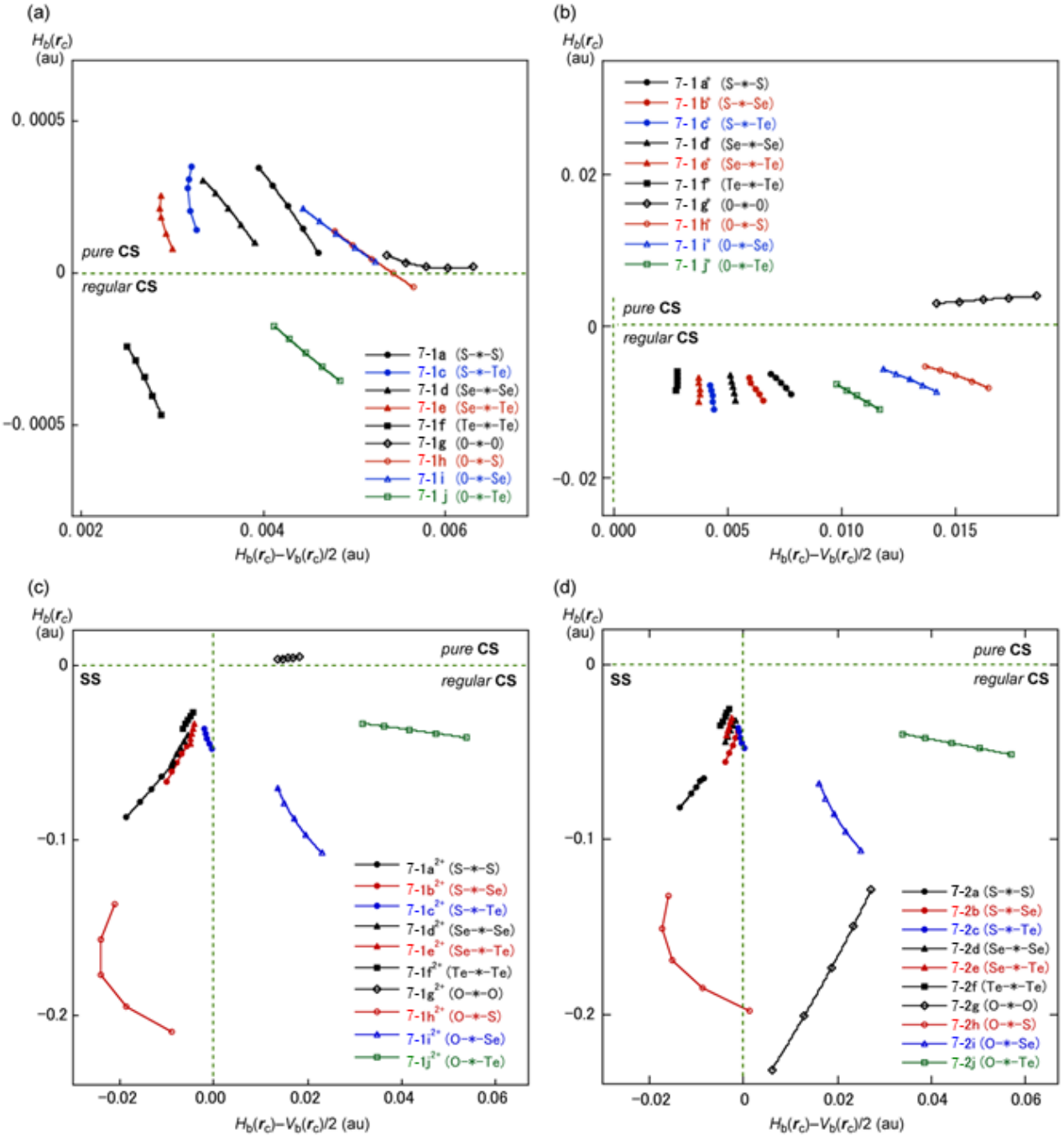

Figure 7-12. Plots of $H_b(\boldsymbol{r}_c)$ versus $H_b(\boldsymbol{r}_c) - V_b(\boldsymbol{r}_c)/2$ for **7-1** (a), **7-1**$^{\bullet+}$ (b), and **7-1**$^{2+}$ (c), together with **7-2** (d).

Table 7-2. QTAIM functions and parameters evaluated for the neutral, radical cationic and dicationic forms in *cyclo*-E($CH_2CH_2CH_2$)$_2$E' (**7-1**) calculated employing QTAIM-DFA with NIV at the MP2 level[a]

interaction (E-∗-E')	$\rho_b(\boldsymbol{r}_c)$ (au)	$c\nabla^2\rho_b(\boldsymbol{r}_c)$[b] (au)	$H_b(\boldsymbol{r}_c)$ (au)	$k_b(\boldsymbol{r}_c)$[c]	R (au)	θ (°)	ν_n (n)[d] (cm^{-1})	k_f[d] (unit[e])	θ_p (°)	κ_p (au^{-1})
neutral species										
S-∗-S/**7-1a**	0.0130	0.0043	0.0002	-0.973	0.0043	87.0	146.6 (2)	0.087	113.2	127
S-∗-Se/**7-1b**	*e*	*e*	*e*	*e*	*e*	*e*	*e*	*e*	*e*	*e*
S-∗-Te/**7-1c**	0.0106	0.0032	0.0003	-0.954	0.0032	84.9	59.7 (1)	0.009	170.8	0.0
Se-∗-Se/**7-1d**	0.0127	0.0036	0.0002	-0.969	0.0036	86.6	97.4 (2)	0.089	110.3	178
Se-∗-Te/**7-1e**	0.0106	0.0029	0.0002	-0.967	0.0029	86.4	54.9 (1)	0.014	142.1	0.0
Te-∗-Te/**7-1f**	0.0133	0.0027	-0.0003	-1.060	0.0027	97.3	77.8 (2)	0.077	121.0	259
O-∗-O/**7-1g**	0.0130	0.0058	0.0000	-0.998	0.0058	89.8	196.7 (2)	0.131	92.6	199
O-∗-S/**7-1h**	0.0135	0.0052	0.0000	-0.996	0.0052	89.5	190.9 (3)	0.111	101.8	38.3
O-∗-Se/**7-1i**	0.0130	0.0048	0.0001	-0.987	0.0048	88.5	169.5 (3)	0.076	102.5	21.1
O-∗-Te/**7-1j**	0.0138	0.0045	-0.0003	-1.029	0.0045	93.4	150.5 (3)	0.080	104.1	37.9
radical cationic species										
S-∗-S/**7-1a**$^{\bullet+}$	0.0472	0.0074	-0.0075	-1.338	0.0105	135.6	253.9 (4)	0.284	162.3	43.1
S-∗-Se/**7-1b**$^{\bullet+}$	0.0464	0.0062	-0.0083	-1.400	0.0103	143.1	222.8 (4)	0.231	165.8	89.7
S-∗-Te/**7-1c**$^{\bullet+}$	0.0441	0.0043	-0.0092	-1.516	0.0102	154.9	184.1 (3)	0.099	177.3	4.8
Se-∗-Se/**7-1d**$^{\bullet+}$	0.0439	0.0052	-0.0080	-1.434	0.0096	146.9	173.6 (3)	0.344	175.7	26.6
Se-∗-Te/**7-1e**$^{\bullet+}$	0.0417	0.0038	-0.0083	-1.524	0.0091	155.5	154.9 (3)	0.373	179.8	50.4
Te-∗-Te/**7-1f**$^{\bullet+}$	0.0385	0.0028	-0.0072	-1.563	0.0077	158.8	129.0 (2)	0.069	181.6	54.3
O-∗-O/**7-1g**$^{\bullet+}$	0.0323	0.0162	0.0035	-0.879	0.0166	77.8	176.9 (2)	0.125	77.6	24.5
O-∗-S/**7-1h**$^{\bullet+}$	0.0547	0.0150	-0.0065	-1.178	0.0164	113.4	295.1 (4)	0.138	135.6	60.9
O-∗-Se/**7-1i**$^{\bullet+}$	0.0500	0.0130	-0.0070	-1.213	0.0148	118.4	211.0 (3)	0.136	141.7	45.9
O-∗-Te/**7-1j**$^{\bullet+}$	0.0473	0.0106	-0.0092	-1.302	0.0141	130.9	187.7 (3)	0.127	151.1	4.4
dicationic species										
S-∗-S/**7-1a**$^{2+}$	0.1351	-0.0133	-0.0708	-2.601	0.0720	190.6	425.6 (8)	0.551	198.1	0.5
S-∗-Se/**7-1b**$^{2+}$	0.1155	-0.0078	-0.0558	-2.387	0.0563	187.9	377.0 (8)	0.565	192.0	0.8
S-∗-Te/**7-1c**$^{2+}$	0.0923	-0.0013	-0.0419	-2.067	0.0420	181.8	355.2 (8)	0.456	171.9	22.9
Se-∗-Se/**7-1d**$^{2+}$	0.1032	-0.0070	-0.0471	-2.427	0.0476	188.5	263.3 (5)	0.238	192.3	0.6
Se-∗-Te/**7-1e**$^{2+}$	0.0867	-0.0046	-0.0390	-2.313	0.0392	186.8	249.4 (6)	0.275	184.9	24.7
Te-∗-Te/**7-1f**$^{2+}$	0.0760	-0.0054	-0.0313	-2.530	0.0318	189.8	196.7 (4)	0.781	193.4	1.1
O-∗-O/**7-1g**$^{2+}$	0.0325	0.0158	0.0041	-0.850	0.0163	75.4	252.1 (3)	0.161	74.1	20.8
O-∗-S/**7-1h**$^{2+}$	0.1765	-0.0240	-0.1774	-2.370	0.1790	187.7	586.3 (10)	1.274	172.3	2.3
O-∗-Se/**7-1i**$^{2+}$	0.1407	0.0171	-0.0877	-1.720	0.0894	169.0	518.9 (9)	0.801	166.4	5.6
O-∗-Te/**7-1j**$^{2+}$	0.1079	0.0416	-0.0368	-1.307	0.0555	131.5	506.6 (9)	0.754	110.4	1.2

[a] For BSS-B: The 6-311+G(3df) basis set for O, S, and Se and that of the (7433111/743111/7411/2 + 1s1p1d1f) type for Te with the 6-311+G(d,p) basis set for C and H. [b] $c = \hbar^2/8m$. [c] $k_b(\boldsymbol{r}_c) = V_b(\boldsymbol{r}_c)/G_b(\boldsymbol{r}_c)$. [d] Corresponding to the E–E' bond in question. [e] BCP being not detected.

The Nature of E-∗-E' in 7-1, 7-1$^{\bullet+}$, and 7-1^{2+}, Elucidated with (R, θ) and (θ_p, κ_p)

It is instructive to survey the criteria, before detail discussion of the nature of E-∗-E'. Scheme 2-

3 of Chapter 2 tells us that $\theta < 180^{o}$ for the CS interactions, whereas $\theta > 180^{o}$ for the SS interactions. The CS and SS interactions correspond to $H_b(\boldsymbol{r}_c) - V_b(\boldsymbol{r}_c)/2 > 0$ and $H_b(\boldsymbol{r}_c) - V_b(\boldsymbol{r}_c)/2 < 0$, respectively. The CS interactions are divided into *pure* CS and *regular* CS interactions for $45^{o} < \theta < 90^{o}$ and $90^{o} < \theta < 180^{o}$, respectively, which correspond to $H_b(\boldsymbol{r}_c) > 0$ and $H_b(\boldsymbol{r}_c) < 0$, respectively, with $H_b(\boldsymbol{r}_c) - V_b(\boldsymbol{r}_c)/2 > 0$. The θ_p value will play an important role to determine the characters of the interactions. In the *pure* CS region of $45^{o} < \theta < 90^{o}$, the character of interactions will be the vdW type for $45^{o} < \theta_p < 90^{o}$ or the *typical*-HB type with no covalency for $90^{o} < \theta_p < 125^{o}$, although θ_p of 125^{o} tentatively corresponds to $\theta = 90^{o}$. The CT interactions will appear in the *regular* CS region of $90^{o} < \theta < 180^{o}$. Interactions of the CT-MC and CT-TBP types will appear in the ranges of $150^{o} \leq \theta_p < 180^{o}$ ($115^{o} \leq \theta < 150^{o}$) and $180^{o} \leq \theta_p < 190^{o}$ ($150^{o} \leq \theta < 180^{o}$), respectively. *Typical*-HB interactions with covalency will appear in the region of $125^{o} \leq \theta_p < 150^{o}$ ($90^{o} \leq \theta < 115^{o}$). CT will contribute to *typical*-HBs in this region. The value of R classifies SS, further. Classical chemical bonds of SS are strong when $R > 0.15$ au but they will be weak if $R < 0.15$ au.

Table 7-3 collects the characters of the E-∗-E' interactions in **7-1a**–**7-1j**, **7-1a**$^{\bullet+}$–**7-1j**$^{\bullet+}$, and **7-1a**$^{2+}$–**7-1j**$^{2+}$, determined using the R, θ and θ_p values, together with **7-2a**–**7-2j**, for convenience of comparison. The interactions become stronger in the order of **7-1a**–**7-1j** < **7-1a**$^{\bullet+}$–**7-1j**$^{\bullet+}$ < **7-1a**$^{2+}$–**7-1j**$^{2+}$, if the same E-∗-E' are compared, except for O-∗-O. The O-∗-O interaction seems weaker in the order of **7-1g** (O-∗-O) > **7-1g**$^{\bullet+}$ (O-∗-O) > **7-1g**$^{2+}$ (O-∗-O), judging from the θ and θ_p values. The trend is inverse, relative to the cases of other E-∗-E' interactions in Table 7-3. All E-∗-E' in **7-1a**–**7-1j** are characterized as typical-HB nature with no covalency appeared in the *pure* CS-region, except for Te-∗-Te in **7-1f** and O-∗-Te in **7-1j**, which are characterized as the typical-HB nature with covalency appeared in the *regular* CS-region. BCP is not detected for S-∗-Se in **7-1b**. Similarly, E-∗-E' in **7-1a**$^{\bullet+}$–**7-1j**$^{\bullet+}$ are all characterized as CT-MC appeared at the *regular* CS region, except for Te-∗-Te in **7-1f**$^{\bullet+}$ and O-∗-O in **7-1g**$^{\bullet+}$, which are characterized as CT-TBP appeared at the *regular* CS region and the vdW nature appeared at the *pure* CS-region, respectively.

Table 7-3. Classification and characterization of E---E' in the neutral, radical cationic, and dicationic forms in *cyclo*-1,5-E($CH_2CH_2CH_2$)$_2$E' (**7-1**), together with the neutral forms of *cyclo*-1,2-E($CH_2CH_2CH_2$)E' (**7-2**), evaluated with NIV at the MP2 level[a]

interaction (E-∗-E')	R (au)	θ (º)	θ_p (º)	classification /character	interaction (E-∗-E')	R (au)	θ (º)	θ_p (º)	classification /character
neutral species									
S-∗-S/**7-1a**	0.004	87.0	113.2	*p*-CS/*t*-HB	O-∗-O/**7-1g**	0.006	89.8	92.6	*p*-CS/*t*-HB
S-∗-Se/**7-1b**	*b*	*b*	*b*	*b*	O-∗-S/**7-1h**	0.005	89.5	101.8	*p*-CS/*t*-HB
S-∗-Te/**7-1c**	0.003	84.9	170.8	*p*-CS/*t*-HB	O-∗-Se/**7-1i**	0.005	88.5	102.5	*p*-CS/*t*-HB
Se-∗-Se/**7-1d**	0.004	86.6	110.3	*p*-CS/*t*-HB	O-∗-Te/**7-1j**	0.005	93.4	104.1	*r*-CS/*t*-HB
Se-∗-Te/**7-1e**	0.003	86.4	142.1	*p*-CS/*t*-HB					
Te-∗-Te/**7-1f**	0.003	97.3	121.0	*r*-CS/*t*-HB					
radical cationic species									
S-∗-S/**7-1a**$^{\bullet+}$	0.011	135.6	162.3	*r*-CS/CT-MC	O-∗-O/**7-1g**$^{\bullet+}$	0.017	77.8	77.6	*p*-CS/vdW
S-∗-Se/**7-1b**$^{\bullet+}$	0.010	143.1	165.8	*r*-CS/CT-MC	O-∗-S/**7-1h**$^{\bullet+}$	0.016	113.4	135.6	*r*-CS/CT-MC
S-∗-Te/**7-1c**$^{\bullet+}$	0.010	154.9	177.3	*r*-CS/CT-MC	O-∗-Se/**7-1i**$^{\bullet+}$	0.015	118.4	141.7	*r*-CS/CT-MC
Se-∗-Se/**7-1d**$^{\bullet+}$	0.010	146.9	175.7	*r*-CS/CT-MC	O-∗-Te/**7-1j**$^{\bullet+}$	0.014	130.9	151.1	*r*-CS/CT-MC
Se-∗-Te/**7-1e**$^{\bullet+}$	0.009	155.5	179.8	*r*-CS/CT-MC					
Te-∗-Te/**7-1f**$^{\bullet+}$	0.008	158.8	181.6	*r*-CS/CT-TBP					
dicationic species									
S-∗-S/**7-1a**$^{2+}$	0.072	190.6	198.1	SS/Cov-w	O-∗-O/**7-1g**$^{2+}$	0.016	75.4	74.1	*p*-CS/vdW
S-∗-Se/**7-1b**$^{2+}$	0.056	187.9	192.0	SS/Cov-w	O-∗-S/**7-1h**$^{2+}$	0.179	187.7	172.3	SS/CT-MC
S-∗-Te/**7-1c**$^{2+}$	0.042	181.8	171.9	SS/CT-MC	O-∗-Se/**7-1i**$^{2+}$	0.089	169.0	166.4	*r*-CS/CT-MC
Se-∗-Se/**7-1d**$^{2+}$	0.048	188.5	192.3	SS/Cov-w	O-∗-Te/**7-1j**$^{2+}$	0.056	131.5	110.4	*r*-CS/*t*-HB
Se-∗-Te/**7-1e**$^{2+}$	0.039	186.8	184.9	SS/CT-TBP					
Te-∗-Te/**7-1f**$^{2+}$	0.032	189.8	193.4	SS/Cov-w					
Neutral species									
S-∗-S/**7-2a**	0.068	190.2	198.1	SS/Cov-w	O-∗-O/**7-2g**	0.175	173.9	191.5	*p*-CS/CT-TBP
S-∗-Se/**7-2b**	0.047	183.5	189.8	SS/CT-TBP	O-∗-S/**7-2h**	0.170	185.1	165.9	SS/CT-MC
S-∗-Te/**7-2c**	0.042	174.8	165.5	*r*-CS/CT-MC	O-∗-Se/**7-2i**	0.088	167.3	167.8	*r*-CS/CT-MC
Se-∗-Se/**7-2d**	0.038	184.1	188.9	SS/CT-TBP	O-∗-Te/**7-2j**	0.063	135.4	117.0	*r*-CS/*t*-HB
Se-∗-Te/**7-2e**	0.036	182.3	180.3	SS/CT-TBP					
Te-∗-Te/**7-2f**	0.030	187.1	190.2	SS/Cov-w					

[a] Data from Table 7-2. [b] BCP being not detected.

In the case of E-∗-E' in **7-1a**$^{2+}$–**7-1f**$^{2+}$, they are all classified by the SS interactions (θ > 180º) and characterized to have the Cov-w nature (θ_p > 180º: R < 0.15 au), except for S-∗-Te in **7-1c**$^{2+}$ (θ_p = 172º) and Se-∗-Te in **7-1e**$^{2+}$ (θ_p = 185º), which should be characterized to have the CT-MC and CT-TBP nature, respectively (appeared in the SS region). On the other hand, the behavior of O-∗-E' in **7-1g**$^{2+}$–**7-1j**$^{2+}$ seems somewhat complex. The interactions of O-∗-O in **7-1g**$^{2+}$, O-∗-S in **7-1h**$^{2+}$, O-∗-Se in **7-1i**$^{2+}$, and O-∗-Te in **7-1j**$^{2+}$ are classified and characterized as (*pure* CS; vdW), (SS; CT-MC), (*regular* CS; CT-MC), and (*regular* CS; *typical* HB with covalent nature), respectively. Indeed, S-∗-

Te in **7-1c**$^{2+}$ and O-∗-S in **7-1h**$^{2+}$ are characterized as CT-MC with their θ_p values, but the interactions should be characterized as Cov-w and Cov-s, respectively, if θ are mainly considered. The dynamic behavior of S-∗-Te in **7-1c**$^{2+}$ and O-∗-S in **7-1h**$^{2+}$ seems very complex, which should be clarified further.

The (R, θ, θ_p) values for O-∗-S in **7-1h**$^{2+}$ are (0.179 au, 187.7º, 172.3º). The (R, θ) values seem to satisfy the requirements for O-∗-S in **7-1h**$^{2+}$ to be classified by Cov-s, of which data appear in the SS region. However, the θ_p value of 172.3º corresponds to the CT-MC region for O-∗-S in **7-1h**$^{2+}$. The O-∗-S in **7-1h**$^{2+}$ is characterized by CT-MC as shown in Table 7-3, so are other cases of interactions. However, the results strongly suggest that the O-∗-S interactions must be more complex than those clarified in this chapter. This discrepancy must be the reflection of the fact that θ_p is less than θ for O-∗-S in **7-1h**$^{2+}$, although θ_p are larger than θ for usual cases. The complex behavior in O-∗-S in **7-1h**$^{2+}$ (and **7-2h**) can be confirmed in the plot shown in Figure 7-12c (and Figure 7-12d). The reason and/or mechanisms should also be elucidated further.

As mentioned above, the behavior of E–E' in **7-1a**$^{2+}$–**7-1j**$^{2+}$ is very similar to that in **7-2a**–**7-2f**, respectively, except for **7-1g**$^{2+}$ (O-∗-O)/**7-2g** (O-∗-O). Figures 7-14a and 7-14b show the plot of θ and θ_p for **7-1a**$^{2+}$–**7-1j**$^{2+}$ versus those for **7-2a**–**7-2f**, respectively. The plot in Figure 7-13a gives a very good correlation, which is shown in the figure. The θ values of **7-1a**$^{2+}$–**7-1j**$^{2+}$ are linearly correlated well with those of **7-2a**–**7-2f**, although the correlation would be better to analyze as parabolic (y = –202.4 + 3.426x –0.007x^2: R_c^2 = 0.993, without data for **7-1g**$^{2+}$/**7-2g**). Similarly, the plot for θ_p in Figure 7-13b shows a very good correlation, which is given in the figure. The correlation would also be better to analyze as parabolic (y = –110.4 + 2.356x –0.004x^2: R_c^2 = 0.992, without data for **7-1g**$^{2+}$/**7-2g**). The θ and θ_p values for **7-1a**$^{2+}$–**7-1j**$^{2+}$ are demonstrated to be linearly correlated to those in **7-2a**–**7-2j**, respectively, as a whole. The R values in (R, θ) for **7-1a**$^{2+}$–**7-1j**$^{2+}$ are also plotted versus those of **7-2a**–**7-2f**, which is shown in Figure 7-A7 of the Appendix. The plot gives a very good correlation (y = 1.027x + 0.0017; R_c^2 = 0.986), where data for **7-g** (O-∗-O) are neglected from the correlation, again. The results clarify well the similarities in the behavior of E–E' between **7-1a**$^{2+}$–

7-1j^{2+} and **7-2a**–**7-2f**, except for **7-1g**$^{2+}$/**7-2g**. The E–E' interactions in **7-1**$^{2+}$ and **7-2** can be described by σ(2c–2e), which must be the main reason for the similarity, although n_p(E) and n_p(E') in **7-2** are replaced by E–C σ(2c–2e) and E'–C' σ(2c–2e) in **7-1**$^{2+}$, respectively.

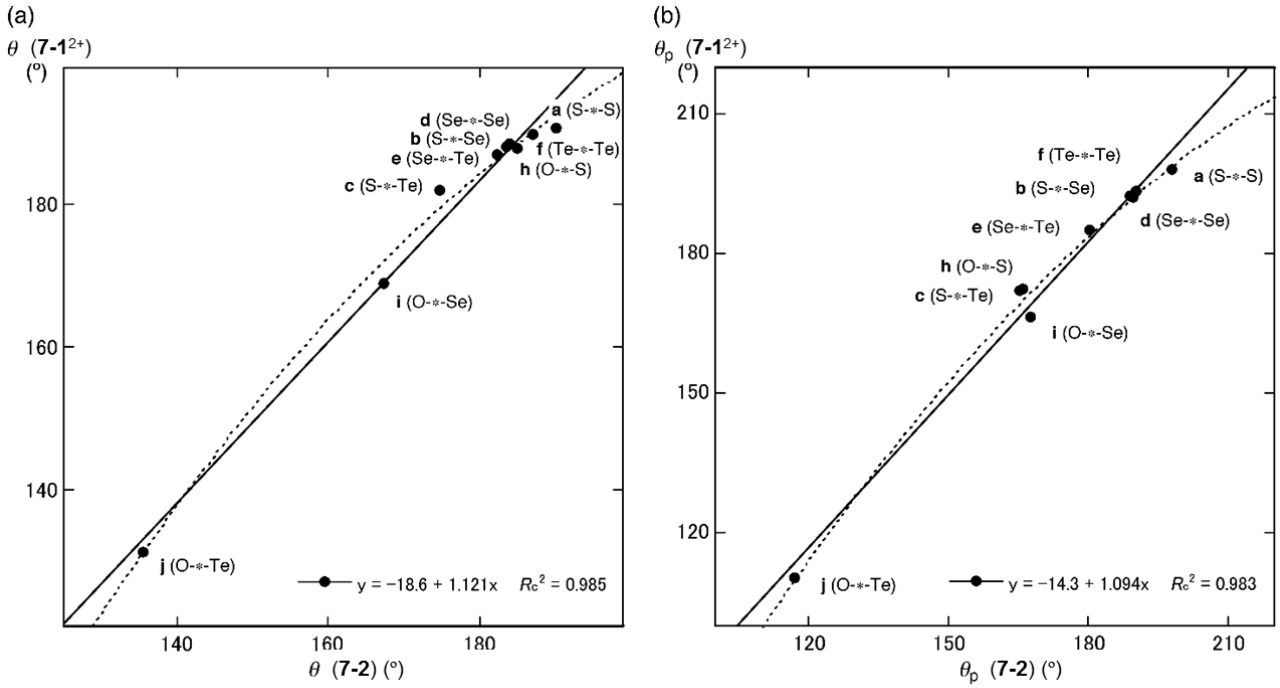

Figure 7-13. Plot of θ for **7-1a**$^{2+}$–**7-1j**$^{2+}$ versus those for **7-2a**–**7-2f** (a) and that of θ_p for **7-1a**$^{2+}$–**7-1j**$^{2+}$ versus those for **7-2a**–**7-2f** (b). Data for **7-1g**$^{2+}$ and **7-2g** are not shown in the plots.

The behavior of E–E' in **7-1**, **7-1**$^{\bullet+}$, and **7-1**$^{2+}$ is well clarified by QTAIM-DFA and the similarities in E–E' between **7-1**$^{2+}$ and **7-2** are confirmed by the QTAIM-DFA parameters, except for O-∗-O.

Summary

The nature of the E–E and E---E' interactions in neutral, radical cationic, and dicationic forms of 1,5-*cyclo*-E($CH_2CH_2CH_2$)$_2$E' (**7-1**) ((E, E') = **a** (S, S), **b** (S, Se), **c** (S, Te), **d** (Se, Se), **e** (Se, Te), **f** (Te, Te), **g** (O, O), **h** (O, S), **i** (O, Se), and **j** (O, Te)) (**7-1a**–**7-1j**, **7-1a**$^{\bullet+}$–**7-1j**$^{\bullet+}$, and **7-1a**$^{2+}$–**7-1j**$^{2+}$, respectively) are elucidated be applying QTAIM-DFA. Structures are optimized with BSS-B at the MP2 level for **7-1a**–**7-1j**, **7-1a**$^{\bullet+}$–**7-1j**$^{\bullet+}$, and **7-1a**$^{2+}$–**7-1j**$^{2+}$ of the chair-boat (**CB**) forms. QTAIM

functions are calculated with the same basis set system at the MP2 level. The molecular graphs, contour plots, negative Laplacians, and trajectory plots are drawn for the species, which depicts the basis nature of E-∗-E' in the species. $H_b(\boldsymbol{r}_c)$ are plotted versus $H_b(\boldsymbol{r}_c) - V_b(\boldsymbol{r}_c)/2$ for the data of E-∗-E' at BCPs of fully-optimized structures and perturbed structures around the fully-optimized ones. The plots are analyzed according to the definitions in QTAIM-DFA. Plots for the data of fully-optimized structures are analyzed by the polar coordinate (R, θ) representation. The (θ_p, κ_p) parameters are derived from those containing the perturbed structures: θ_p corresponds to the tangent line of each plot and κ_p is the curvature. While (R, θ) correspond to the static nature, (θ_p, κ_p) represent the dynamic nature of interactions.

QTAIM parameters of R, θ, and θ_p are mainly employed to clarify the nature of E-∗-E' in **7-1a**–**7-1j**, **7-1a**$^{\bullet+}$–**7-1j**$^{\bullet+}$, and **7-1a**$^{2+}$–**7-1j**$^{2+}$, using those of the standard values, as a reference. Each E-∗-E' becomes stronger in the order of **7-1a**–**7-1j** < **7-1a**$^{\bullet+}$–**7-1j**$^{\bullet+}$ < **7-1a**$^{2+}$–**7-1j**$^{2+}$, if the same E-∗-E' is compared, except for O-∗-O. The O-∗-O interactions become to weaken in the order of **7-1g** > **7-1g**$^{\bullet+}$ > **7-1g**$^{2+}$, judging from the θ and θ_p values. All E-∗-E' in **7-1a**–**7-1j** are characterized as *typical*-HB with no covalency appeared in the *pure* CS region, except for Te-∗-Te in **7-1f** and O-∗-Te in **7-1j**, which are characterized as the typical-HB with covalency appeared in the *regular* CS region. BCP is not detected for S-∗-Se in **7-1b**. Similarly, all E-∗-E' in **7-1a**$^{\bullet+}$–**7-1j**$^{\bullet+}$ are characterized as CT-MC appeared in the *regular* CS region, except for Te-∗-Te in **7-1f**$^{\bullet+}$ and O-∗-O in **7-1g**$^{\bullet+}$, which are characterized as CT-MC appeared in the *regular* CS region and the vdW type appeared in the *pure* CS-region, respectively. The E-∗-E' interactions in **7-1a**$^{2+}$–**7-1f**$^{2+}$ are all classified by SS (θ > 180º) and characterized to have the Cov-w nature (θ_p > 180º: R < 0.15 au), except for S-∗-Te in **7-1c**$^{2+}$ (θ_p = 172º) and Se-∗-Te in **7-1e**$^{2+}$ (θ_p = 185º), which should be characterized to have the CT-MC and CT-TBP nature, respectively (appeared in the SS region). On the other hand, the interactions of O-∗-O in **7-1g**$^{2+}$, O-∗-S in **7-1h**$^{2+}$, O-∗-Se in **7-1i**$^{2+}$, and O-∗-Te in **7-1j**$^{2+}$ are classified and characterized as (*pure* CS; vdW), (SS; CT-MC), (*regular* CS; CT-MC), and (*regular* CS; *typical* HB with covalent nature), respectively. The (R, θ, θ_p) values for O-∗-S in **7-1h**$^{2+}$ are (0.179 au, 187.7º, 172.3º). The (R,

θ) values satisfy the requirements for O-∗-S in **7-1h**$^{2+}$ to have the Cov-s nature appeared in the SS region. However, it should be classified to have the CT-MC nature, if θ_p of 172.3º is mainly considered. The O-∗-S interaction must be analyzed carefully. The behaviors of E–E' in **7-1a**$^{2+}$–**7-1j**$^{2+}$ are very similar to those in **7-2a**–**7-2j**, respectively, except for **7-1g**$^{2+}$/**7-2g** (O-∗-O). The E–E' in **7-1**$^{2+}$ and **7-2** can be described by E–E' σ(2c–2e), which must be the main reason for the similarity, although n_p(E) and n_p(E') in **7-2** are replaced by E–C σ(2c–2e) and E'–C' σ(2c–2e) in **7-1**$^{2+}$, respectively. Indeed, the nature of E–E' is well clarified with QTAIM-DFA, but some seem in the dark, which should be elucidated further.

Appendix

Table 7-A1. Observed[a] and evaluated S---S distances[b] for $[S(CH_2CH_2CH_2)_2S]^{2+}$ (**7-1a**$^{2+}$ (S_2))

Distance	Observed Values	Calculated at the Level of MP2	M062X	M06	LC-wPBE	CB-B3LYP	B3LYP	
☆ *With the 6-311+G(**3d**) basis set for S and the 6-311+G(d,p) basis set for C and H on* **1a**$^{2+}$ (S_2: C_s):								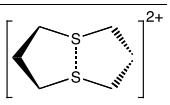
r(S, S)	2.124	2.1729	2.1579	2.1755	2.1259	2.1604	2.1913	
Δ*r*(S, S)	as **0.000**	0.0489	0.0339	0.0515	**0.0019**	0.0364	0.0673	
☆ *With the 6-311+G(**3df**) basis set for S and the 6-311+G(d,p) basis set for C and H on* **1a**$^{2+}$ (S_2: C_s):								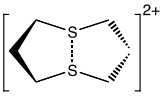
r(S, S)	2.124	2.1373	2.1451	2.1635	2.1144	2.1472	2.1764	
Δ*r*(S, S)	as **0.000**	**0.0133**	**0.0211**	0.0395	**-0.0096**	**0.0232**	0.0524	
☆ *With the **6-311+G(3d)** basis set for S and the 6-311+G(d,p) basis set for C and H on* **1a**$^{2+}$ (S_2: C_2):								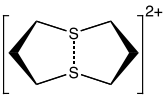
r(S, S)	2.124	2.1755	2.1561	2.1773	2.1254	2.1600	2.1911	
Δ*r*(S, S)	as **0.000**	0.0515	0.0321	0.0533	**0.0014**	0.0360	0.0671	
☆ *With the **6-311+G(3df)** basis set for S and the 6-311+G(d,p) basis set for C and H on* **1a**$^{2+}$ (S_2: C_2):								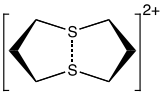
r(S, S)	2.124	2.1393	2.1442	2.1631	2.1136	2.1461	2.1765	
Δ*r*(S, S)	as **0.000**	**0.0153**	**0.0202**	0.0391	**-0.0104**	**0.0221**	0.0525	

[a] 2.126(3) Å and 2.122(3) Å, see Iwasaki, F.; Toyoda, Y.; Akaishi, R.; Fujihara, H.; Furukawa, N. *Bull. Chem. Soc. Jpn.* **1988**, *61*, 2563–2567. [b] In Å.

Table 7-A2. Observed[a] and evaluated Se---Se distances[b] for $[Se(CH_2CH_2CH_2)_2Se]^{2+}$ (**7-1d**$^{2+}$ (Se_2))

Distance	Observed Values	Calculated at the Level of MP2	M062X	M06	LC-wPBE	CB-B3LYP	B3LYP	
☆ *With the 6-311+G(3d) basis set for Se and the 6-311+G(d) basis set for C and H on* **1d**$^{2+}$ (Se_2: C_s):								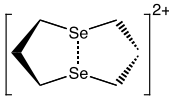
r(Se, Se)	2.382(2)	2.4075	2.4042	2.4234	2.3713	2.4080	2.4404	
Δ*r*(Se, Se)	as **0.000**	**0.0255**	**0.0222**	0.0414	**-0.0107**	**0.0260**	0.0584	
☆ *With the 6-311+G(3df) basis set for Se and the 6-311+G(d) basis set for C and H on* **1d**$^{2+}$ (Se_2: C_s):								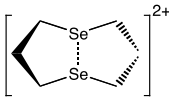
r(Se, Se)	2.382(2)	2.3770	2.3969	2.4170	2.3647	2.4011	2.4333	
Δ*r*(Se, Se)	as **0.000**	**-0.0050**	**0.0149**	0.0350	**-0.0173**	**0.0191**	0.0513	
☆ *With the **6-311+G(3d)** basis set for **Se** and the 6-311+G(d,p) basis set for C and H on* **1d**$^{2+}$ (Se_2: C_{2v}):								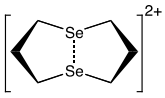
r(Se, Se)	2.382(2)	2.4085	2.4045	2.4231	2.3705	2.4068	2.4386	
Δ*r*(Se, Se)	as **0.000**	**0.0265**	**0.0225**	0.0411	**-0.0115**	**0.0248**	0.0566	
☆ *With the **6-311+G(3df)** basis set for **Se** and the 6-311+G(d,p) basis set for C and H on* **1d**$^{2+}$ (Se_2: C_{2v}):								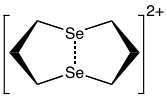
r(Se, Se)	2.382(2)	2.3783	2.3973	2.4169	2.3638	2.4000	2.4317	
Δ*r*(Se, Se)	as **0.000**	**-0.0037**	**0.0153**	0.0349	**-0.0182**	**0.0180**	0.0497	

[a] See Iwasaki, F.; Morimoto, M.; Yasui, M.; Akaishi, R.; Fujihara, H.; Furukawa, N. *Acta Cryst.* **1991**, *C47*, 1463–1466. [b] In Å.

Table 7-A3. Energy differences in **7-1a**–**7-1j**, **7-1a**$^{\bullet+}$–**7-1j**$^{\bullet+}$, and **7-1a**$^{2+}$–**7-1j**$^{2+}$, evaluated at the MP2 level[a,b]

x =	**a** (S, S)	**b** (S, Se)	**c** (S, Te)	**d** (Se, Se)	**e** (Se, Te)	**f** (Te, Te)	**g** (O, O)	**h** (O, S)	**i** (O, Se)	**j** (O, Te)
ΔE (**7-1*x***$^{\bullet+}$)[c,d]	6.809	6.694	6.469	6.528	6.265	6.085	8.349	7.490	7.249	6.802
	0.000	0.000	0.000	0.000	0.000	0.000	0.000	0.000	0.000	0.000
ΔE (**7-1*x*** **'**$^{\bullet+}$)[e]	7.391	7.905	7.351	7.118	7.420	6.621	8.597	8.008	7.722	7.247
$\Delta\Delta E$ (**7-1*x*'**$^{\bullet+}$)[f]	0.582	1.211	0.882	0.590	1.155	0.536	0.248	0.518	0.473	0.445
$-\varepsilon_{\mathrm{HOMO}}$ (**7-1*x***)	8.158	8.345	7.612	7.640	7.554	6.925	10.427	8.682	8.198	7.529
$\Delta\varepsilon_{\mathrm{HOMO}}$ (**7-1*x***$^{\bullet+}$)[g]	1.349	1.651	1.143	1.112	1.289	0.840	2.078	1.192	0.949	0.727
$\Delta\varepsilon_{\mathrm{HOMO}}$ (**7-1*x*'**$^{\bullet+}$)[h]	0.767	0.440	0.261	0.522	0.134	0.304	1.830	0.674	0.476	0.282
ΔE (**7-1*x***$^{2+}$)[d,i]	18.158	17.875	17.362	17.541	16.972	16.525	21.719	19.616	19.265	18.416
	0.000	0.000	0.000	0.000	0.000	0.000	0.000	0.000	0.000	0.000
ΔE (**7-1*x*'**$^{2+}$)[j]	20.175	20.692	20.149	19.584	19.576	18.355	22.329	22.224	22.150	21.307
$\Delta\Delta E$ (**7-1*x*'**$^{2+}$)[k]	2.017	2.817	2.787	2.043	2.604	1.830	0.610	2.608	2.885	2.891

[a] Evaluated using the energies (*E*) given in Table 2. [b] In kJ mol^{-1}. [c] ΔE (**7-1*x***$^{\bullet+}$) = *E* (**7-1*x***$^{\bullet+}$) – *E* (**7-1*x***). [d] Taken as a standard. [e] ΔE (**7-1*x*'**$^{\bullet+}$) = *E* (**7-1*x*'**$^{\bullet+}$) – *E* (**7-1*x***), where *E* (**7-1*x*'**$^{\bullet+}$) stand for the energies of the radical cations evaluated employing the fully optimized structures of **7-1*x***. [f] $\Delta\Delta E$ (**7-1*x*'**$^{\bullet+}$) = ΔE (**7-1*x*'**$^{\bullet+}$) – ΔE (**7-1*x***$^{\bullet+}$). [g] $\Delta\varepsilon_{\mathrm{HOMO}}$ (**7-1*x***$^{\bullet+}$) = $-\varepsilon_{\mathrm{HOMO}}$ (**7-1*x***) – ΔE (**7-1*x***$^{\bullet+}$). [h] $\Delta\varepsilon_{\mathrm{HOMO}}$ (**7-1*x*'**$^{\bullet+}$) = $-\varepsilon_{\mathrm{HOMO}}$ (**7-1*x***) – ΔE (**7-1*x*'**$^{\bullet+}$). [i] ΔE (**7-1*x***$^{2+}$) = *E* (**7-1*x***$^{2+}$) – *E* (**7-1*x***). [j] ΔE (**7-1*x*'**$^{2+}$) = *E* (**7-1*x*'**$^{2+}$) – *E* (**7-1*x***), where *E* (**7-1*x*'**$^{2+}$) stand for the energies of the dications evaluated employing the fully optimized structures of **7-1*x***. [k] $\Delta\Delta E$ (**7-1*x*'**$^{2+}$) =ΔE (**7-1*x*'**$^{2+}$) – ΔE (**7-1*x***$^{2+}$).

Table 7-A4. Correlations in ΔE and $-\varepsilon_{\mathrm{HOMO}}$ for **7-1a**–**7-1j**, **7-1a'**$^{\bullet+}$–**7-1j'**$^{\bullet+}$, **7-1a**$^{\bullet+}$–**7-1j**$^{\bullet+}$, and/or **7-1a**$^{2+}$–**7-1j**$^{2+}$

entry	correlation	*a*	*b*	R_c^2	comment
1	ΔE (**7-1a**$^{\bullet+}$–**7-1j**$^{\bullet+}$) *vs* $-\varepsilon_{\mathrm{HOMO}}$ (**7-1a**–**7-1j**)	0.590	2.008	0.999	G(**I**)
2	ΔE (**7-1a**$^{\bullet+}$–**7-1j**$^{\bullet+}$) *vs* $-\varepsilon_{\mathrm{HOMO}}$ (**7-1a**–**7-1j**)	0.444	3.000	0.827	G(**II**)
3	ΔE (**7-1a**$^{\bullet+}$–**7-1j**$^{\bullet+}$) *vs* $-\varepsilon_{\mathrm{HOMO}}$ (**7-1a**–**7-1j**)	0.523	2.914	0.995	G(**III**)
4	ΔE (**7-1a**$^{\bullet+}$–**7-1j**$^{\bullet+}$) *vs* ΔE (**7-1a'**$^{\bullet+}$–**7-1j'**$^{\bullet+}$)	1.132	1.480	0.988	G(**I**)+G(**III**)
5	ΔE (**7-1a**$^{2+}$–**7-1j**$^{2+}$) *vs* ΔE (**7-1a**$^{\bullet+}$–**7-1j**$^{\bullet+}$)	2.278	2.686	0.996	G(**I**)+G(**II**)+G(**III**)

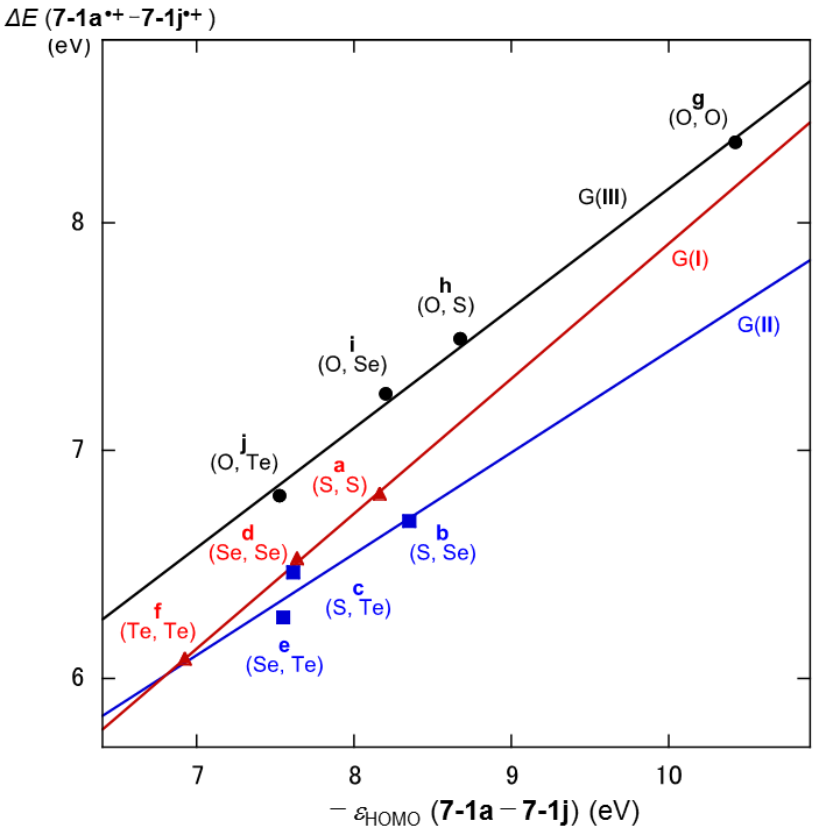

Figure 7-A1. Plot of ΔE (**7-1a**$^{\bullet+}$–**7-1j**$^{\bullet+}$) versus $-\varepsilon_{HOMO}$ (**7-1a**–**7-1j**), which are analyzed as three correlations. The correlations are given in Table 7-A4 of the Appendix (entries 1–3).

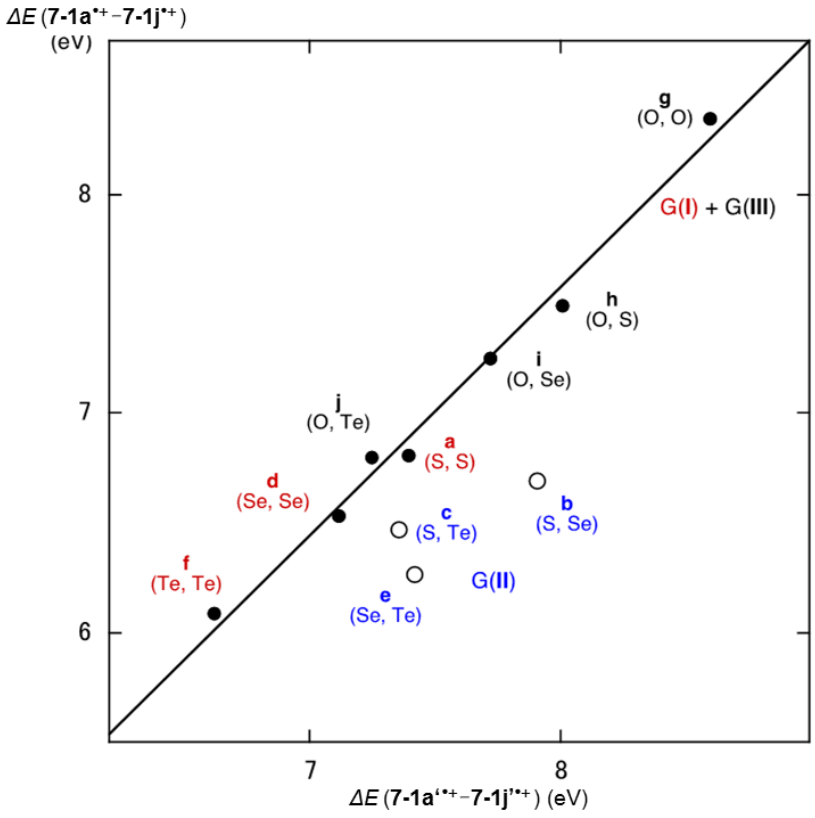

Figure 7-A2. Plot of ΔE (**7-1a**$^{\bullet+}$–**7-1j**$^{\bullet+}$) versus ΔE (**7-1a'**$^{\bullet+}$–**7-1j'**$^{\bullet+}$). The correlation is given in Table 7-A4 of the Appendix (entry 4).

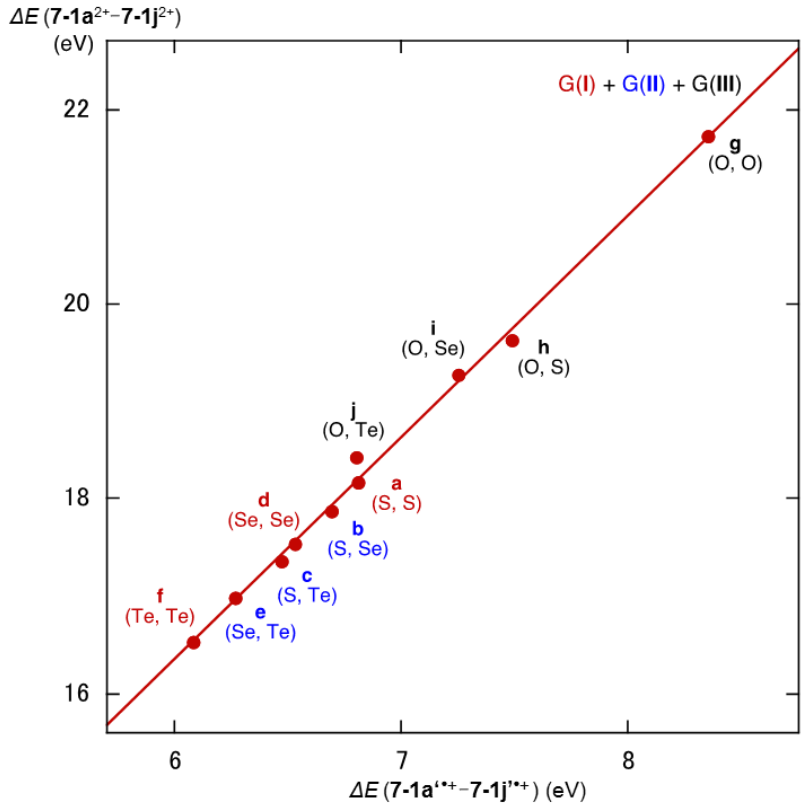

Figure 7-A3. Plot of ΔE (**7-1a**$^{2+}$–**7-1j**$^{2+}$) versus ΔE (**7-1a**$^{\bullet+}$–**7-1j**$^{\bullet+}$). The correlation is given in Table 7-A4 of the Appendix (entry 5).

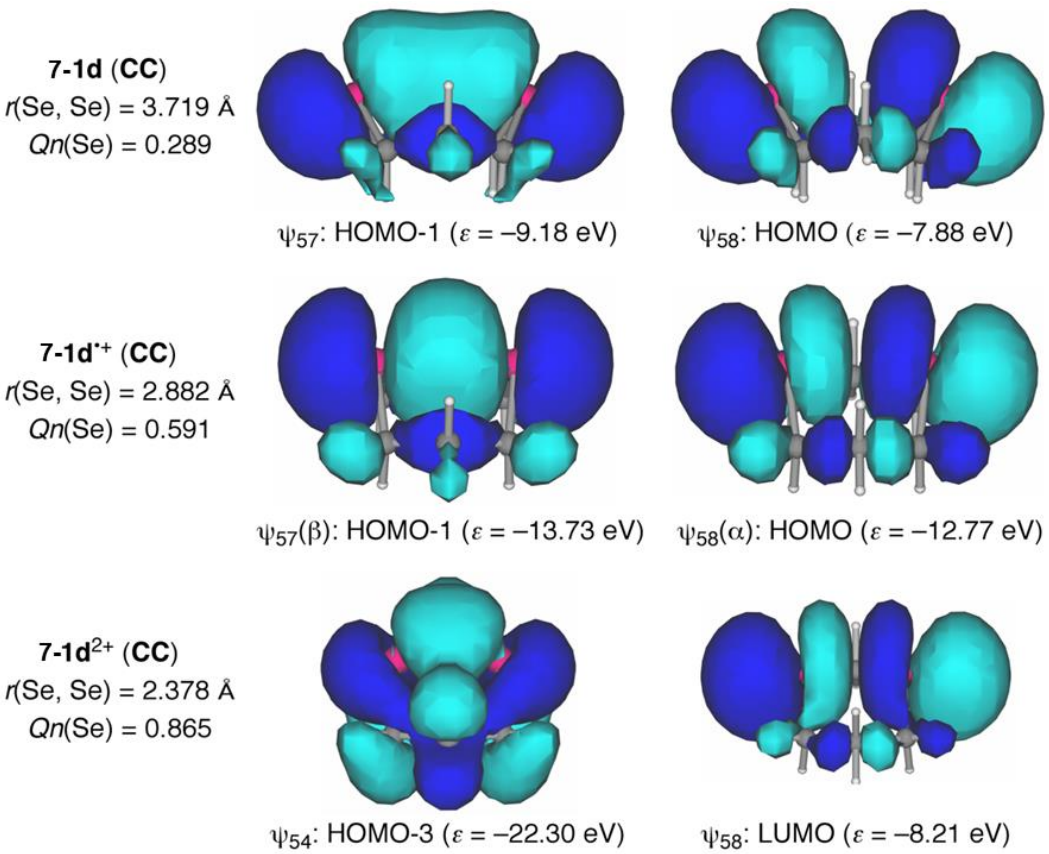

Figure 7-A4. Typical n_p(Se)---n_p(Se) interactions in **7-1** (**CC**), **7-1**$^{\bullet+}$ (**CC**), and **7-1**$^{2+}$ (**CC**). The orbital energies and the Se---Se distances are also given.

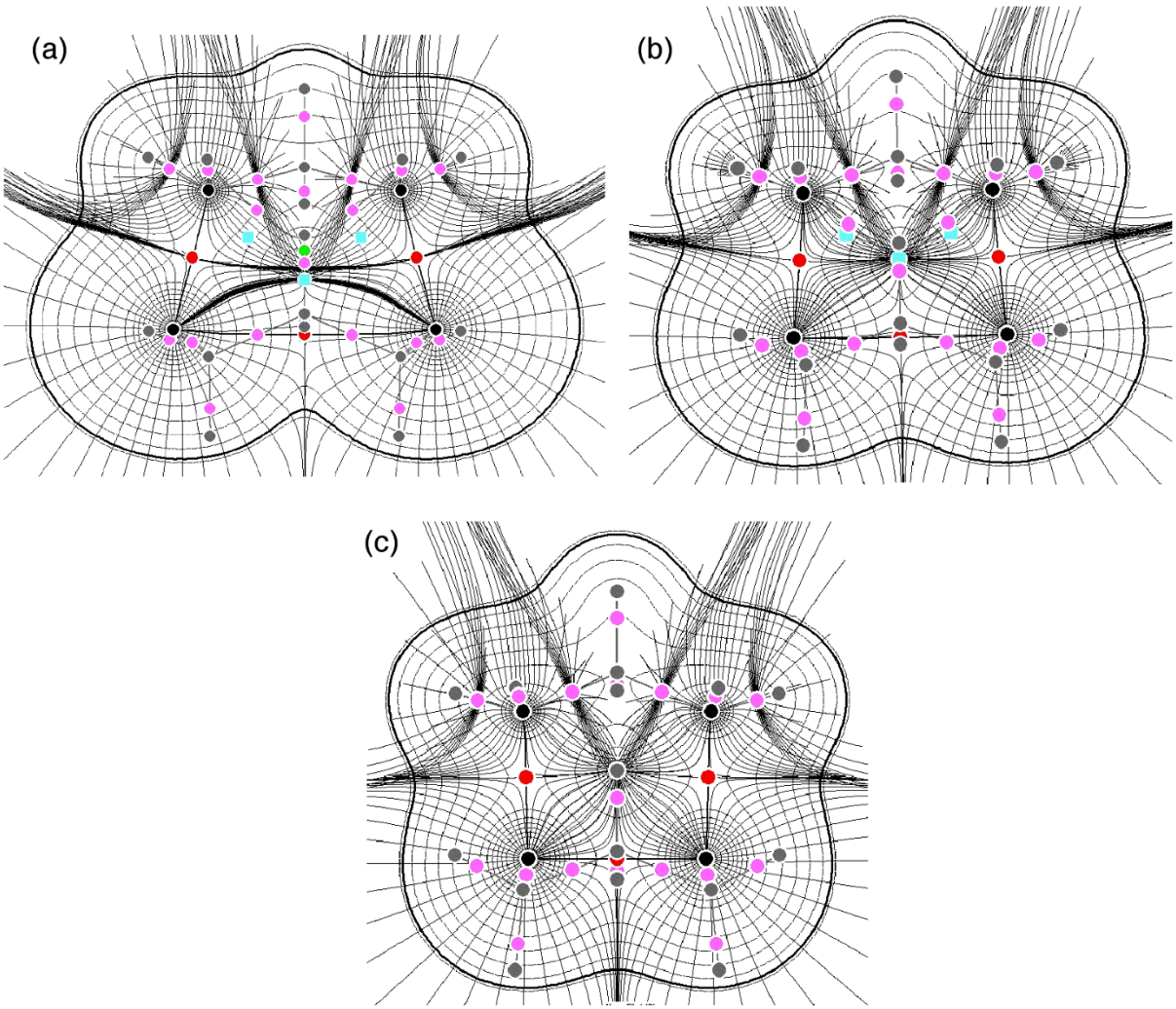

Figure 7-A5. Trajectory plots drawn on the C–Se–Se–C plane for **7-1d** (**CB**) (a), **7-1d**$^{\bullet+}$ (**CB**) (b), and **7-1d**$^{2+}$ (**CB**) (c), together with BCPs (red solid circles on the plane and pink solid circles out of the plane), ring critical points (cyan solid squares out of the plane), cage critical points (lime green solid circles), critical points (black solid circles on the plane and gray solid circles out of the plane), and bond paths.

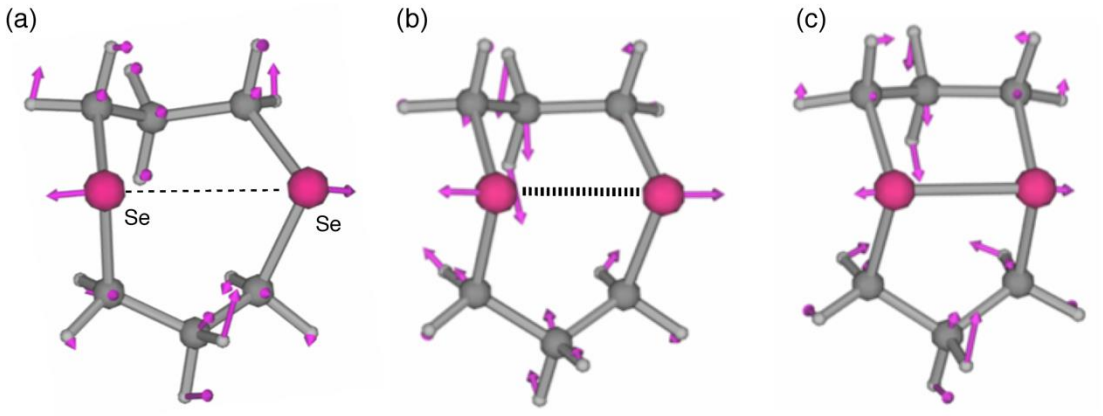

Figure 7-A6. The Se–Se stretching mode of **7-1d** (**CB**: ν_2) (a), **7-1d**$^{\bullet+}$ (**CB**: ν_3) (b), and **7-1d**$^{2+}$ (**CB**: ν_5) (c).

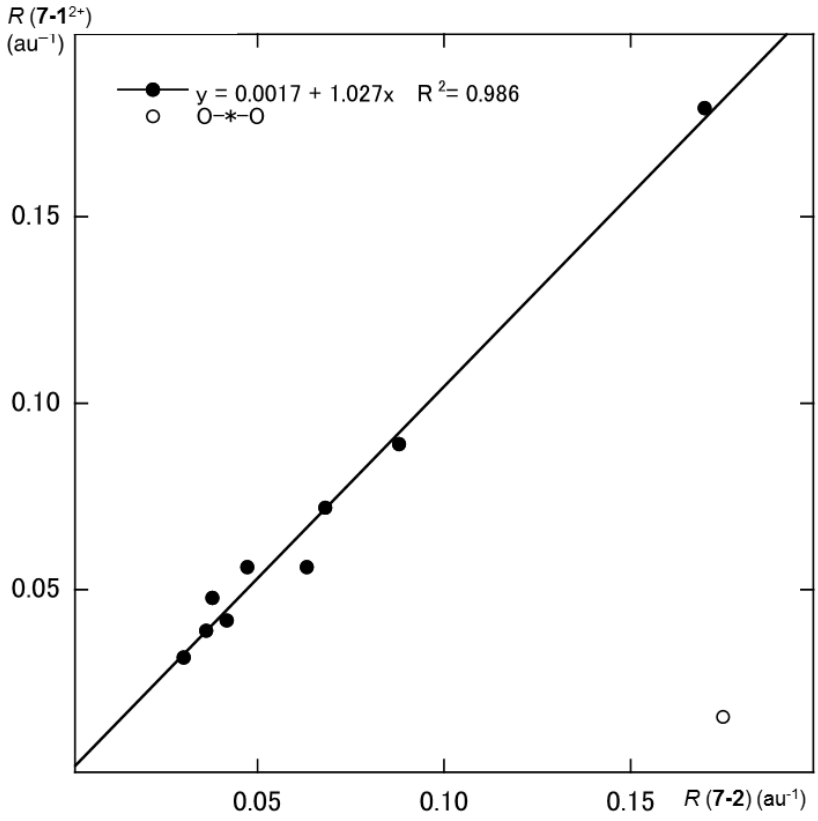

Figure 7-A7. Plot of *R* (**7-1a**$^{2+}$–**7-1j**$^{2+}$) versus *R* (**7-2a**–**7-2j**).

References

1 a) *Their Chemistry and Biology* (Eds.: D. L. Klayman, W. H. H. Günther), Wiley: New York, 1973; b) *The Chemistry of Organic Selenium and Tellurium Compounds* (Eds.: S. Patai, Z. Rappoport), John-Wiley and Sons: New York, 1986*;* Vols. 1 and 2; c) *Organic Selenium Chemistry* (Ed. D. Liotta), Wiley-Interscience: New York, 1987; *Organoselenium Chemistry, A practical Approach* (Ed. T. G. Back), Oxford University Press: Oxford, 1999; *Organoselenium Chemistry Modern Developments in Organic Synthesis*, *Top Curr. Chem.* (Ed.: T. Wirth), Springer: Berlin, Heidelberg, New York, London, Paris, Tokyo, 2000.

2 *Chemistry of Hypervalent Compounds* (Ed.: K.-y. Akiba), Wiley-VCH, New York, 1999.

3 a) W. Nakanishi, *Hypervalent Chalcogen Compounds* In *Handbook of Chalcogen Chemistry: New Perspectives in Sulfur, Selenium and Tellurium* (Ed.: F. A. Devillanova), Royal Society of Chemistry, Cambridge, 2006, Chap. 10.3, pp. 644–668; b) W. Nakanishi, S. Hayashi, *Hypervalent Chalcogen Compounds* In *Handbook of Chalcogen Chemistry: New Perspectives in Sulfur, Selenium and Tellurium: 2nd Edition*, Vol. 2, (Eds.: F. A. Devillanova, W.-W. du Mont), Royal Society of Chemistry, Cambridge, 2013, Chap. 12.3, pp. 335–372.

4 A. J. Mukherjee, S. S. Zade, H. B. Singh, R. B. Sunoj, *Chem. Rev.* **2010**, *110*, 4357–4416.

5 a) K. Morihashi, S. Kushihara, Y. Inadomi, O. Kikuchi, *J. Mol. Struct. (Theochem.)* **1997**, *418*, 171–178; b) B. Mueller, T. T. Takaluoma, R. S. Laitinen, K. Seppelt, *Eur. J. Inorg. Chem.* **2011**, 4970–4977; c) B. Mueller, H. Poleschner, K. Seppelt, *Dalton Trans.* **2008**, 4424–4427; d) A. Wakamiya, T. Nishinaga, K. Komatsu, *J. Am. Chem. Soc.* **2002**, *124*, 15038–15050; e) O. Mundt, G. Becker, J. Baumgarten, H. Riffel, A. Simon, *Z. Anorg. Allg. Chem.* **2006**, *632*, 1687–1709.

6 “Hard-shell” for E-E' interactions is used sometimes, but “Shard-shell” for ones is used in this Chapter.

7 B. J. Bhuyan, D. S. Lamani, G. Mugesh, T. Wirth, In *Handbook of Chalcogen Chemistry: New Perspectives in Sulfur, Selenium and Tellurium: 2nd Edition*, (Eds.: F. A. Devillanova, W.-W. du

Mont), Royal Society of Chemistry, Cambridge, 2013, Vol. 2, Chap. 10.2, pp. 25–46.

8 S. R. Jakka, G. Mugesh, In *Handbook of Chalcogen Chemistry: New Perspectives in Sulfur, Selenium and Tellurium: 2nd Edition*, (Eds.: F. A. Devillanova, W.-W. du Mont), Royal Society of Chemistry, Cambridge, 2013, Vol. 2, Chap. 10.3, pp. 46–65.

9 *The Chemistry of Organic Selenium and Tellurium Compounds*, (Eds.: S. Patai, Z. Rappoport), Wiley, New York, 1986, Vol. 1, Chap. 6.

10 *The Chemistry of Organic Selenium and Tellurium Compounds* (Ed.: Z. Rappoport), Wiley, New York, 2013, Vol. 4, Chaps. 13–16.

11 a) A. Panda, G. Mugesh, H. B. Singh, R. J. Butcher, *Organometallics* **1999**, *18*, 1986–1993; b) M. Kulcsar, A. Beleaga, C. Silvestru, A. Nicolescu, C. Deleanu, C. Todasca, A. Silvestru, *Dalton Trans.* **2007**, 2187–2196; c) A. Beleaga, M. Kulcsar, C. Deleanu, A. Nicolescu, C. Silvestru, A. Silvestru, *J. Organomet. Chem.* **2009**, *694*, 1308–1316.

12 W. Nakanishi, S. Hayashi, S. Morinaka, T. Sasamori, N. Tokitoh, *New J. Chem.* **2008**, *32*, 1881–1889.

13 a) F. Iwasaki, N. Toyoda, R. Akaishi, H. Fujihara, N. Furukawa, *Bull. Chem. Soc. Jpn.* **1988**, *61*, 2563–2567; b) H. Fujihara, A. Kawada, N. Furukawa, *J. Org. Chem.* **1987**, *52*, 4254–4257.

14 a) F. Iwasaki, M. Morimoto, M. Yasui, R. Akaishi, H. Fujihara, N. Furukawa, *Acta Cryst.* **1991**, *C47*, 1463–1466; b) H. Fujihara, N. Furukawa, *Phosphorus, Sulfur Silicon Rel. Elem.* **1992**, *67*, 131–134.

15 a) H. Fujihara, R. Akaishi, T. Erata, N. Furukawa, *Chem. Commun.* **1989**, 1789–1790; b) H. Fujihara, R. Akaishi, N. Furukawa, *Tetrahedron* **1993**, *49*, 1605–1618.

16 H. Fujihara, R. Akaishi, A. Nakamura, N. Furukawa, *Tetrahedron Lett.* **1990**, *31*, 6375–6378.

17 H. Fujihara, M. Yabe, J.-J. Chiu, N. Furukawa, *Tetrahedron Lett.* **1991**, *32*, 4345–4348.

18 H. Fujihara, T. Ninoi, R. Akaishi, T. Erata, N. Furukawa, *Tetrahedron Lett.* **1991**, *32*, 4537–4540.

19 H. Fujihara, Y. Takuguchi, T. Ninoi, T. Erata, N. Furukawa, *J. Chem. Soc., Perkin Trans. 1* **1992**, 2583–2584.

20 H. Fujihara, N. Furukawa, *J. Mol. Struct. (Theochem)* **1989**, *186*, 261–272.

21 N. Nakayama, O. Takahashi, O. Kikuchi, N. Furukawa, *Heteroatom Chem.* **2000**, *11*, 31–41.

22 N. Nakayama, O. Takahashi, O. Kikuchi, N. Furukawa, *J. Mol. Struct. (Theochem.)* **2001**, *542*, 215–226.

23 a) E. Block, E. V. Dikarev, R. S. Glass, J. Jin, B. Li, X. Li, S.-Z. Zhang, *J. Am. Chem. Soc.* **2006**, *128*, 14949–14961; b) E. Block, R. S. Glass, E. V. Dikarev, N. E. Gruhn, J. Jin, B. Li, E. Lorance, U. I. Zakai, S. Z. Zhang, *Heteroatom Chem.* **2007**, *18*, 509–515; c) C. Liao, S.-Z. Zhang, E. Block, E. L. Clennan, *J. Org. Chem.* **2008**, *73*, 8587–8590.

24 a) R. S. Glass, E. Block, E. Lorance, U. I. Zakai, N. E. Gruhn, J. Jin, S.-Z. Zhang, *J. Am. Chem. Soc.* **2006**, *128*, 12685–12692; b) R. S. Glass, E. Block, N. E. Gruhn, J. Jin, E. Lorance, U. I. Zakai, S.-Z. Zhang, *J. Org. Chem.* **2007**, *72*, 8290–8297.

25 a) R. S. Glass, L. Adamowicz, J. L. Broeker, *J. Am. Chem. Soc.* **1991**, *113*, 1065–1072; b) R. S. Glass, S. W. Andruski, J. L. Broeker, H. Firouzabadi, L. K. Steffen, G. S. Wilson, *J. Am. Chem. Soc.* **1989**, *111*, 4036–4045.

26 D. H. Evans, N. E. Gruhn, J. Jin, B. Li, E. Lorance, N. Okumura, N. A. Macias-Ruvalcaba, U. I. Zakai, S.-Z. Zhang, E. Block, R. S. Glass, *J. Org. Chem.* **2010**, *75*, 1997–2009.

27 R. Stowasser, R. S. Glass, R. Hoffmann, *J. Chem. Soc., Perkin Trans. 2* **1999**, 1559–1561.

28 The electronegativity proposed by Allred-Rochow was employed to discuss the structure of the adducts. See, A. L. Allred, E. G. Rochow, *J. Inorg. Nucl. Chem.* **1958**, *5*, 264–268; A. L. Allred, E. G. Rochow, *J. Inorg. Nucl. Chem.* **1958**, *5*, 269–288.

29 W. K. Musker, T. L. Wolford, *J. Am. Chem. Soc.* **1976**, *98*, 3055–3056.

30 a) W. K. Musker, T. L. Wolford, P. D. Roush, *J. Am. Chem. Soc.* **1978**, *100*, 6416–6421; b) W. K. Musker, *Acc. Chem. Res.* **1980**, *13*, 200–206.

31 a) K.-D. Asmus, *Acc. Chem. Res.* **1979**, *12*, 436–442; b) D. K. Maity, *J. Am. Chem. Soc.* **2002**, *124*, 8321–8328. See also ref. 22.

32 a) *Atoms in Molecules. A Quantum Theory*, (Ed.; R. F. W. Bader), Oxford University Press, Oxford, UK, **1990**; b) Matta, C. F.; Boyd, R. J. *An Introduction to the Quantum Theory of Atoms in Molecules* In *The Quantum Theory of Atoms in Molecules: From Solid State to DNA and Drug Design* (Eds.: C. F. Matta, R. J. Boyd), WILEY-VCH, Weinheim, Germany, **2007**, Chap. 1.

33 a) F. Biegler-König, J. Schönbohm, *J. Comput. Chem.* **2002**, *23*, 1489–1494; b) F. Biegler-König, J. Schönbohm, D. Bayles, *J. Comput. Chem.* **2001**, *22*, 545–559; c) R. F. W. Bader, *J. Phys. Chem. A* **1998**, *102*, 7314–7323; d) R. F. W. Bader, *Chem. Res.* **1991**, *91*, 893–926; e) R. F. W. Bader, *Acc. Chem. Res.* **1985**, *18*, 9–15; f) T. H. Tang, R. F. W. Bader, P. MacDougall, *Inorg. Chem.* **1985**, *24*, 2047–2053; g) R. F. W. Bader, T. S. Slee, D. Cremer, E. Kraka, *J. Am. Chem. Soc.* **1983**, *105*, 5061–5068; h) F. Biegler-König, R. F. W. Bader, T. H. Tang, *J. Comput. Chem.* **1982**, *3*, 317–328.

34 J. Molina, J. A. Dobado, *Theor. Chem. Acc.* **2001**, *105*, 328–337.

35 J. A. Dobado, H. Martînez-Garcîa, J. Molina, M. R. Sundberg, *J. Am. Chem. Soc.* **2000**, *122*, 1144–1149.

36 S. K. Ignatov, N. H. Rees, B. R. Tyrrell, S. R. Dubberley, A. G. Razuvaev, P. Mountford, G. I. Nikonov, *Chem. Eur. J.* **2004**, *10*, 4991–4999.

37 S. K. Tripathi, U. Patel, D. Roy, R. B. Sunoj, H. B. Singh, G. Wolmershäuser, R. J. Butcher, *J. Org. Chem.* **2005**, *70*, 9237–9247.

38 R. J. Boyd, S. C. Choi, *Chem. Phys. Lett.* **1986**, *129*, 62–65.

39 M. T. Carroll, R. F. W. Bader, *Mol. Phys.* **1988**, *65*, 695–722.

40 S. J. Grabowski, *J. Phys. Chem. A* **2001**, *105*, 10739–10746.

41 a) E. Espinosa, I. Alkorta, J. Elguero, E. Molins, *J. Chem. Phys.* **2002**, *117*, 5529–5542; b) I. Rozas, I. Alkorta, J. Elguero, *J. Am. Chem. Soc.* **2000**, *122*, 11154–11161; c) E. Espinosa, E. Molins, C. Lecomte. *Chem. Phys. Lett.* **1998**, *285*, 170–173.

42 M. Domagała, S. J. Grabowski, K. Urbaniak, G. Mloston, *J. Phys. Chem. A* **2003**, *107*, 2730–2736.

43 S. J. Grabowski, W. A. Sokalski, J. Leszczynski, *J. Phys. Chem. A* **2005**, *109*, 4331–4341.

44 M. Domagala, S. J. Grabowski, *J. Phys. Chem. A* **2005**, *109*, 5683–5688.

45 R. Parthasarathi, V. Subramanian, N. Sathyamurthy, *J. Phys. Chem. A* **2006**, *110*, 3349–3351

46 W. Nakanishi, T. Nakamoto, S. Hayashi, T. Sasamori, N. Tokitoh, *Chem. Eur. J.* **2007**, *13*, 255–268.

47 a) W. Nakanishi, S. Hayashi, K. Narahara, *J. Phys. Chem. A* **2009**, *113*, 10050–10057; b) W. Nakanishi, S. Hayashi, K. Narahara, *J. Phys. Chem. A* **2008**, *112*, 13593–13599.

48 W. Nakanishi, S. Hayashi, *Curr. Org. Chem.* **2010**, *14*, 181–197.

49 a) W. Nakanishi, S. Hayashi, *J. Phys. Chem. A* **2010**, *114*, 7423–7430; b) W. Nakanishi, S. Hayashi, K. Matsuiwa, M. Kitamoto, *Bull. Chem. Soc. Jpn.* **2012**, *85*, 1293–1305.

50 S. Hayashi, K. Matsuiwa, H. Miza, W. Nakanishi, *Heteroatom Chem.* **2014**, *25*, 449–472.

51 *Gaussian 09, Revision D.01*, M. J. Frisch, G. W. Trucks, H. B. Schlegel, G. E. Scuseria, M. A. Robb, J. R. Cheeseman, G. Scalmani, V. Barone, B. Mennucci, G. A. Petersson, H. Nakatsuji, M. Caricato, X. Li, H. P. Hratchian, A. F. Izmaylov, J. Bloino, G. Zheng, J. L. Sonnenberg, M. Hada, M. Ehara, K. Toyota, R. Fukuda, J. Hasegawa, M. Ishida, T. Nakajima, Y. Honda, O. Kitao, H. Nakai, T. Vreven, J. A. Montgomery, Jr., J. E. Peralta, F. Ogliaro, M. Bearpark, J. J. Heyd, E. Brothers, K. N. Kudin, V. N. Staroverov, R. Kobayashi, J. Normand, K. Raghavachari, A. Rendell, J. C. Burant, S. S. Iyengar, J. Tomasi, M. Cossi, N. Rega, J. M. Millam, M. Klene, J. E. Knox, J. B. Cross, V. Bakken, C. Adamo, J. Jaramillo, R. Gomperts, R. E. Stratmann, O. Yazyev, A. J. Austin, R. Cammi, C. Pomelli, J. W. Ochterski, R. L. Martin, K. Morokuma, V. G. Zakrzewski, G. A. Voth, P. Salvador, J. J. Dannenberg, S. Dapprich, A. D. Daniels, Ö. Farkas, J. B. Foresman, J. V. Ortiz, J. Cioslowski, D. J. Fox, Gaussian, Inc., Wallingford CT, 2009.

52 For the 6-311G(3d) basis sets, see: a) R. C, Binning Jr. L. A. Curtiss, *J. Comput. Chem.* **1990**, *11*, 1206−1216; b) L. A. Curtiss, M. P. McGrath, J.-P. Blaudeau, N. E. Davis, R. C. Binning Jr.

L. Radom, *J. Chem. Phys.* **1995**, *103*, 6104−6113; c) M. P. McGrath, L. Radom, *J. Chem. Phys.* **1991**, *94*, 511−516; d) For the diffuse functions (+ and + +), see: T. Clark, J. Chandrasekhar, G. W. Spitznagel, P. v. R. Schleyer, *J. Comput. Chem.* **1983**, *4*, 294−301.

53 a) For inner and valence shells: T. Koga, S. Yamamoto, T. Shimazaki, H. Tatewaki, *Theor. Chem. Acc.* **2002**, *108*, 41–45; b) For valence correlated set: M. Sekiya, T. Noro, Y. Osanai, T. Koga, *Theor. Chem. Acc.* **2001**, *106*, 297–300.

54 a) C. Møller, M. S. Plesset, *Phys. Rev.* **1934**, *46*, 618–622; b) J. Gauss, *J. Chem. Phys.* **1993**, *99*, 3629–3643; c) J. Gauss, *Ber. Bunsen-Ges. Phys. Chem.* **1995**, *99*, 1001–1008.

55 Y. Zhao, D. G. Truhlar, *Theor. Chem. Acc.* **2008**, *120*, 215−241.

56 O. A. Vydrov, G. E. Scuseria, *J. Chem. Phys.* **2006**, *125*, 234109/1–234109/9.

57 T. Yanai, D. P. Tew, N. C. Handy, *Chem. Phys. Lett.* **2004**, *393*, 51–57.

58 M. J. G. Peach, P. Benfield, T. Helgaker, D. J. Tozer, *J. Chem. Phys.* **2008**, *128*, 044118-1–044118-8.

59 A. D. Becke, *J. Chem. Phys*. **1993**, *98*, 5648–5652.

60 C. Lee, W. Yang, R. G. Parr, *Phys. Rev. B* **1988**, *37*, 785–789.

61 P. J. Knowles, J. S. Andrews, R. D. Amos, N. C. Handy, J. A. Pople, *Chem. Phys. Lett.* **1991**, *186*, 130–136.

62 The AIM2000 program (Version 2.0) is employed to analyze and visualize atoms-in-molecules: F. Biegler-König, *J. Comput. Chem.* **2000**, *21*, 1040–1048. See also ref. 32a.

63 A BCP will exist at the midpoint between E and E' in E–E', if E = E'. Where is BCP in E–E', when E ≠ E'? BCP will be closer to E than to E', where $\chi_E > \chi_{E'}$. The results are usually observed in QTAIM analysis, although the covalent radii of E' must be larger than that of E. The bond path between E and E' seems substantially straight along the E–E' bond.

64 In such cases, data are plotted inversely as $H_b(\boldsymbol{r}_c) - V_b(\boldsymbol{r}_c)/2$ versus $H_b(\boldsymbol{r}_c)$, although some modification in eq (7-5) is necessary to obtain the θ_p values.

Conclusions

Atoms construct molecules. The framework of molecules is constructed by the strong interactions in chemistry, which are usually called classical covalent bonds. Molecules assemble together to build up molecular aggregates. Weak interactions, such as van der Waals interactions (vdW), hydrogen bonds (HB), and/or charge-transfer interactions (CT), must be the driving force for the aggregation. Weak interactions play a crucial role in physical, chemical, and biological properties of materials, since they control fine details of the structures of molecules and create delicate properties of materials. It is inevitable to control such weak interactions to design new materials of high functionalities analogous to the vital activity. Investigations successfully utilizing weak interactions are increasing, however, it is still of high importance to clarify the cause-and-effect in the phenomena arising from weak interactions, with physical necessity.

To clarify the nature of the weak interactions must be the first step to control the whole picture of the weak interactions. QTAIM approach, introduced by Bader, enables us to analyze the nature of chemical bonds and interactions. A lot of QTAIM investigations have been reported so far, however, those from a viewpoint of experimental chemists seem not so many. Then such method enabled experimental chemists to analyze their own results, concerning chemical bonds and interactions, by their own image, and proposed QTAIM dual functional analysis (QTAIM-DFA), recently. Weak to strong interactions can be analyzed with QTAIM-DFA.

After confirmation of high applicability of NIV (normal coordinates of internal vibrations) to generate the perturbed structures for QTAIM-DFA, the weak interactions of the vdW, HB, and CT types are elucidated, exemplified by the intramolecular π–π interactions in diethanodihydronaphthalene, diethenodihydronaphthalene, and cyclophanes, together with the derivatives. The behaviors of the HB interactions are widely investigated from the *pure* closed shell to shared shell interactions, although not discussed explicitly in this thesis, instead, the *typical* HB nature is found in many interactions.

The chalcogen–chalcogen interactions from the closed shell interactions of the E---E' form to the shared shell interactions of the E–E' form (E, E' = S, Se, Te, and O) are exhaustively clarified employing the neutral, radical mono-anionic, radical mono-cationic, di-cationic forms of HEE'H, MeEE'Me and *cyclo*-1,2-EE'$(CH_2)_3$. After clarification of the basic behavior of the chalcogen-chalcogen interactions, the behavior of the transannular chalcogen–chalcogen interactions of the E---E' form is elucidated employing the neutral, radical cationic, and dicationic forms of *cyclo*-[E$(CH_2CH_2CH_2)_2$E'] (E, E' = S, Se, Te, and O).

All E-∗-E' in the neutral form are characterized as *typical* HB with no covalency appeared in the *pure* CS region, except for Te-∗-Te and O-∗-Te, which are characterized as the *typical* HB with covalency appeared in the *regular* CS region. BCP is not detected for S-∗-Se. Similarly, all E-∗-E' in the radical cationic form are characterized as CT-MC appeared in the *regular* CS region, except for Te-∗-Te and O-∗-O, which are characterized as CT-MC appeared in the *regular* CS region and the vdW type appeared in the *pure* CS-region, respectively. While the E---E' interactions (E, E' = S, Se, and Te) in the dicationic forms are characterized as Cov-w nature, except for S-∗-Te (CT-MC) and Se-∗-Te (CT-TBP), O-∗-E' seems more complex. The behavior of E-∗-E' in the dicationic forms is very close to that of *cyclo*-E$(CH_2CH_2CH_2)$E' (E, E' = S, Se, Te, and O), except for O-∗-O.

It is of further interest to clarify the behavior of the σ-type linear interactions constructed by the four chalcogen atoms of the ^{B}E---^{A}E–^{A}E---^{B}E form. The interaction is proposed to call the extended hypervalent interactions of *m* center–*n* electron bonds/interactions of the σ-type, which are described as σ(*m*c–*n*e) ($4 \leq m$; $m < n < 2m$). σ(4c–6e) is the first member of σ(*m*c–*n*e) ($4 \leq m$; $m < n < 2m$). The interactions will be formed in the reaction of the dication from *cyclo*-[E$(CH_2CH_2CH_2)_2$E'] with the neutral *cyclo*-[E$(CH_2CH_2CH_2)_2$E']. The behavior of σ(4c–6e) must be the next target to be elucidated employing QTAIM-DFA.

Chalcogen–chalcogen interactions (E–E' and E---E': E, E' = S, Se, and Te, together with O) are of current and continuous interest, not only those of the shard-shell (SS) type (E–E') but also of the closed-shell (CS) type (E---E'). The E–E' bonds play an important role in all field of chemical and

biological sciences. They maintain the peptide structures and biological activities containing enzymes, especially for E, E' = S, Se. The E–E' bonds in dichalcogenides (RE–E'R') supply low-lying vacant orbitals of the σ-type (σ*(E–E')), where the E/E' atoms contain lone pair orbitals of s- and p-types (n_s(E/E') and n_p(E/E'), respectively) of relatively high energy levels. Consequently, the E–E' bonds in RE–E'R' are easily oxidized and reduced, which is important to develop the highly functionalized materials. On the other hand, the intermolecular E---E' interactions of the CS type are often encountered in crystals of organic compounds containing chalcogen atoms, which must be the important driving force to grow the crystals and they create useful properties of materials. 1,8-(Dichalcogena)naphthalenes and the related species must be the typical systems for the intramolecular E---E' interactions.

List of Publications

1. Applications of Normal Coordinates of Internal Vibrations to Generate Perturbed Structures: Dynamic Behavior of Weak to Strong Interactions Elucidated by Atoms-in-Molecules Dual Functional Analysis, S. Hayashi, K. Matsuiwa, M. Kitamoto, and W. Nakanishi, *Bull. Chem. Soc. Jpn*, **85**, 1293–1305 (2012) (Chapter 2).

2. Intramolecular π–π Interactions in Diethanodihydronaphthalene and Derivatives: Dynamic and Static Behavior of the Interactions Elucidated by QTAIM Dual Functional Analysis, K. Matsuiwa, S. Hayashi, and W. Nakanishi, *Chemistry Select*, **1**, 2344–2353 (2016) (Chapter 3).

3. Behavior of Intramolecular π–π Interactions with Doubly Degenerated Bond Paths Between Carbon Atoms in Opposite Benzene Rings of Diethenodihydronaphthalenes by QTAIM Approach, K. Matsuiwa, Y. Sugibayashi, Y. Tsubomoto, S. Hayashi, and W. Nakanishi, *Chemistry Select*, **2**, 90–100 (2017) (Chapter 4).

4. Dynamic and Static Behavior of Intramolecular π–π Interactions in [2.2]- and [3.3]Cyclophanes, Elucidated by QTAIM Dual Functional Analysis with QC Calculations, K. Matsuiwa, S. Hayashi, and W. Nakanishi, *Chemistry Select*, **2**, 1774–1782 (2017) (Chapter 5).

5. Dynamic and Static Behavior of E–E' Bonds in Neutral and Charged Forms of HEE'H, MeEE'Me, and *cyclo*-1,2-EE'$(CH_2)_3$ (E, E' = O, S, Se, and Te) Elucidated by AIM Dual Functional Analysis, S. Hayashi, K. Matsuiwa, H. Miza, and W. Nakanishi, *Heteroatom Chem.*, **25**, 449–472 (2014) (Chapter 6).

6. Transannular E---E' Interactions in Neutral, Radical Cationic, and Dicationic Forms of *cyclo*-$[E(CH_2CH_2CH_2)_2E']$ (E, E' = S, Se, Te, and O) with Structural Feature: Dynamic and Static Behavior of E---E' Elucidated by QTAIM Dual Functional Analysis, S. Hayashi, K. Matsuiwa, N. Nishizawa, and W. Nakanishi, *J. Org. Chem.*, **80**, 11963−11976 (2015) (Chapter 7).

Other Publications

1. Dynamic Behavior of Hydrogen Bonds from Pure Closed Shell to Shared Shell Interaction Regions Elucidated by AIM Dual Functional Analysis, S. Hayashi, K. Matsuiwa, M. Kitamoto, and W. Nakanishi, *J. Phys. Chem. A*, **117**, 1804–1816 (2013).

2. Relativistic Effects on the ^{125}Te and ^{33}S NMR Chemical Shifts of Various Tellurium and Sulfur Species, Together with ^{77}Se of Selenium Congeners, in the Framework of a Zeroth-order Regular Approximation: Applicability to Tellurium Compounds, S. Hayashi, K. Matsuiwa, and W. Nakanishi, *RSC Advances*, **4**, 44795–44810 (2014).

List of International Conferences

1. Behavior of E---E' Interactions in Neutral and Charged 1,5-(Dichalcogena)canes, Elucidated by AIM-DFA, N. Nishizawa, K. Matsuiwa, S. Hayashi, and W. Nakanishi, *The 11th International Conference on Heteroatom Chemistry (ICHAC-11)*, June 14-19, 2015, the historic University of Caen Basse-Normandie in Caen (Normandy, France), P-14 (p. 126).

2. Behavior of Linear ^{1}E---^{2}E Interactions in Mono- and Di-cationic Dimers of 1,5-(Dichalcogena)canes: Theoretical Investigations, S. Otsuki, K. Matsuiwa, S. Hayashi, and W. Nakanishi, *The 11th International Conference on Heteroatom Chemistry (ICHAC-11)*, June 24-29, 2015, the historic University of Caen Basse-Normandie in Caen (Normandy, France), P-17 (p. 129).

3. Behavior of E---E' in Neutral and Charged Forms of *cyclo*-1,2-EE'$(CH_2)_3$ (E, E' = O, S, Se, and Te), Elucidated by AIM-DFA, K. Isoda, K. Matsuiwa, S. Hayashi, and W. Nakanishi, *The 11th International Conference on Heteroatom Chemistry (ICHAC-11)*, June 24-29, 2015, the historic University of Caen Basse-Normandie in Caen (Normandy, France), P-27 (p. 139).

4. Behavior of Hydrogen Bonds from Pure Closed Shell to Shared Shell Interaction Regions, Elucidated by AIM-DFA, W. Nakanishi, K. Matsuiwa, and S. Hayashi, *The 11th International Conference on Heteroatom Chemistry (ICHAC-11)*, June 24-29, 2015, the historic University of Caen Basse-Normandie in Caen (Normandy, France), KN16-70 (p. 77).

Acknowledgement

The author would like to express his hearty thanks to Emeritus Professor Waro Nakanishi and Associate Professor Satoko Hayashi at Wakayama University for their valuable and helpful suggestions, discussion, and encouragement during this work.

Acknowledgements are also extended to the members of Hayashi Laboratory for their kindness support for his research work.

Finally, the author would like to thank his parents for their continuous support and warm encouragement.

March 2017

Kohei Matsuiwa
Graduate School of Systems Engineering
Wakayama University